DEVELOPMENT OF SMALL PRODUCTION PLATFORM FOR CITRONELLAL PROCESSING

By

Lubabalo Rowan Mafu

A thesis submitted in fulfilment of the requirements for the degree of

Doctor of Philosophy
Chemistry

in the Faculty of Science at the
Nelson Mandela Metropolitan University.

Prof. Paul Watts **Date:** 10/03/2016

Prof. Ben Zeelie

PREFACE

The experimental work for this thesis was carried out between July 2012 to July 2015 in the North Campus Research Laboratory and InnoVenton, Institute of Chemical Technology under the promotion of Prof. Paul Watts and co-promotion of Prof. Ben Zeelie. The research was funded by the National Research Foundation (NRF) and by InnoVenton.

Lubabalo Rowan Mafu

DECLARATION

I **Lubabalo Rowan Mafu** hereby declare that this thesis is my own. It is being submitted for the degree of Doctor of Philosophy at the Nelson Mandela Metropolitan University, Port Elizabeth and it has not been previously submitted for assessment in any other Institution.

RESEARCH OUTPUT

Conference proceedings: Lecture presentations

- Development of a small production platform for citronellal processing, Catalysis Society of South Africa (CATSA) 24th annual conference, Wild Coast Sun, Port Edward, 17-20 Nov, 2013.

- Continuous flow synthesis of isopulegyl ethers using heterogeneous catalysts, IUPAC Green Chemistry Conference, Durban, 17-21st August 2014.

- Continuous-flow synthesis of di-ester derivatives, SELECTBIO Flow Chemistry Congress, San Diego, CA, USA, 15-16 September 2015.

Journal articles

- Lubabalo Mafu, Ben Zeelie and Paul Watts, "Batch-scale synthesis of novel *para*-Menthane-3,8-ester derivatives" *in preparation.*

- Lubabalo Mafu, Coos Bosma, Ben Zeelie and Paul Watts, "Continuous-flow synthesis of di-ester derivatives in milli-reactors using microwave heating" *in preparation*.

ACKNOWLEDGEMENTS

- Special thanks and appreciation to my promoters, Professor Paul Watts and Professor Ben Zeelie for their guidance and support throughout this work.
- To Mr. Coos Bosma, thank you for the intellectual support on experimental design and statistical analysis.
- To Dr. Gary Dugmore and Dr. Batsho Mpuhlu, thanks for the valuable discussion and support in this project.
- Many thanks to the University of Cape Town team for their assistance and their input in this work, especially in continuous-flow synthesis of isopulegol.
- I acknowledge InnoVenton: Institute of Chemical Technology and National Research Fund (NRF SARChI research grant) for their financial support, without which this program would not have been successful.
- To the InnoVenton staff and students for support and encouragement through my research work, thank you very much.
- To my family for the support, love, encouragement and prayers at all times.
- Lastly, a word of thanks to the Almighty for strength and resilience he gave me during the course of my studies.

EXECUTIVE SUMMARY

The aim of the project was to develop a small production platform for citronellal processing. The objective of the study was to develop a single continuous flow reactor system for the synthesis of novel derivatives of citronellal and isopulegol. The first step was to develop a continuous flow reactor system for the isopulegol synthesis. The stainless steel tubular fixed-bed reactor equipped with a reaction column (I.D: 9.53 mm and length: 120 mm) was used for the study. The reactor column was packed with H-ZMS-5 zeolite extrusion catalyst. The solvent-free cyclisation reaction of citronellal was investigated and at optimum conditions, 100% of citronellal conversion and almost 100% selectivity towards isopulegol was achieved. A good catalytic performance was observed from the H-ZSM-5 catalyst and proved to be stable for a prolonged reaction time.

The second reaction step was to develop a continuous flow reactor system for the synthesis of isopulegyl-ether derivatives. A UniQsis FlowSyn reactor system equipped with a stainless steel reactor column was used for the study. The reactor column was packed with amberlyst-15 dry catalyst. Wherein, *n*-propanol was employed as a model etherifying agent and as a reaction solvent. At optimum reaction condition, only 30% selectivity of isopulegyl propoxy-ether was achieved. The reaction was found to depend highly on temperature and residence time. The increase of these parameters was found to increase the side reactions and reduced the selectivity of the desired product.

Other heterogeneous catalysts such as H-beta zeolite, aluminium pillared clay, Aluminium oxide and H-ZSM-5 were also evaluated in the reaction. Among these catalysts, a catalytic activity was observed with H-beta zeolite (19%) and aluminium pillared clay (5%). Based on these results, none of the evaluated catalysts provided the desired selectivity (greater than 70%) towards the isopulegyl propoxy-ether, therefore the process was not investigated further. In light of this, the isopulegol etherification synthetic route was terminated. Consequently, another analogue of citronellal was used as an alternative intermediate in place of isopulegol, namely *para*-menthane-3,8-diol (PMD).

The initial studies for the synthesis of the novel PMD di-esters from isopulegol were performed in the batch-scale reactor. In a solvent-free reaction, acetic anhydride was initially used as a model acetylating agent. The reaction was performed using polymer-bound scandium triflate (PS-Sc(OTf)$_3$) catalyst. The effect of reaction parameters such as

temperature, molar ratio, and reaction time were studied towards the PMD conversion and di-esters selectivity. At optimum reaction conditions, PMD conversion of 70% and di-acetate selectivity of 67% were observed. The reaction was found to follow the zeroth-order kinetics with respect to PMD conversion and obeyed the Arrhenius equation. Other types of di-ester derivatives were synthesized from PMD by varying the carbon chain length of the acetylating agent. The prepared compounds were separated from the product mixtures by vacuum distillation, purified on a column chromatography and characterised by FT-IR, GC-MS, and ^{1}H-NMR, ^{13}C-NMR.

The developed methodology was optimised in flow by using an ArrheniumOne microwave-assisted continuous-flow fixed-bed reactor system. A detailed experimental design was used to carry-out the reactions. The reaction parameters such as temperature and flow-rate were studied towards the PMD conversion and di-ester selectivity. From the experimental design analysis, the di-ester selectivity was found to depend highly on the residence time (flow-rate) and significantly on temperature. The PMD conversion and di-ester selectivity were found to increase with decrease in the flow-rate. The conversion and selectivity achieved in the continuous flow process were significantly higher than the achieved in the batch-scale process with respect to the residence time.

Keywords*: Acetylation, esterification, packed-bed reactor, microwave-assisted, para-Menthane-3,8-diol, para-menthane-3,8-diester, selectivity, conversion, space velocity,*

TABLE OF CONTENTS

LIST OF ABBREVIATIONS

Al_2O_3	Aluminium oxide
BBP	Benzyl butyl phthalate
CCD	Central composite design
CPO	Crude palm oil
d	Doublet
DEP	Di-ethyl phthalate
DEHP	Di-2-ethylhexyl phthalate
DEET	Diethyl-*m*-toluamide
DIDP	Di-*iso*-decyl phthalate
DINP	Di-*iso*-nonyl phthalate
DMSO	Dimethyl sulfoxide
DPP	Di-propyl phthalate
FDA	Food and drug administration
FFMSR	Falling film micro-structured reactor
FFA	Free fatty acid
FPA	Focal plane array
FT-IR	Fourier transform infrared
GC	Gas chromatography
GC-MS	Gas chromatography-mass spectrometry
GRAS	General regarded as safe
J	Coupling constant
KOH	Potassium hydroxide
KOH/Jc	Potassium hydroxide supported on jatropha curcas
m	Multiplet
MSR	Micro-structured reactor
NMR	Nuclear magnetic resonance
PC	Polycondensation
PLA	Polylactic acid
PMD	*para*-Menthane-3, 8-diol
Ps-Sc$(OTf)_3$	Polymer-supported scandium triflate
PVC	Polyvinyl chloride
PVC-P	Polyvinyl chloride plasticiser

ROP	Ring opening polymerisation
RSD	Relative standard deviation
RTD	Residence time distribution
S	Standard deviation
s	Singlet
t	T-test
t	Triplet

CHAPTER 1

Literature Review

1. General introduction

1.1. What are plasticizers?

Plasticizers are defined as substances or materials that are incorporated into a plastic or elastomer to improve their flexibility, durability and transparency. Consumer products such as wires, cables, insulators, wall covering and packing materials are all manufactured from polyvinyl chloride (PVC) and in order to achieve desirable flexibility, a suitable plasticizer is required as a blender.[1] Globally, over 80-90% of all plasticizers are used in PVC manufacturing industries.[2] Currently, over 90% of all PVC plasticizers (PVC-P) are prepared from phthalic acid or phthalic anhydride. During the synthesis of phthalate esters, both reagents are reacted with the appropriate alcohol to yield a mono or dialkyl phthalate ester.[3] In particular, the commercially produced dialkyl phthalate esters contribute more than 51% of the global plasticizer market.[4]

In general, plasticizers are synthetic organic additives that are added as blenders to the polyvinyl chloride (PVC).[5] Several types of plasticizers are prepared from different classes of organic compounds such as phthalate esters **1**, maleate **2**, phosphates **3**, ethers **4,** epoxides **5** and ionic liquids **6** (Scheme 1).[4,6]

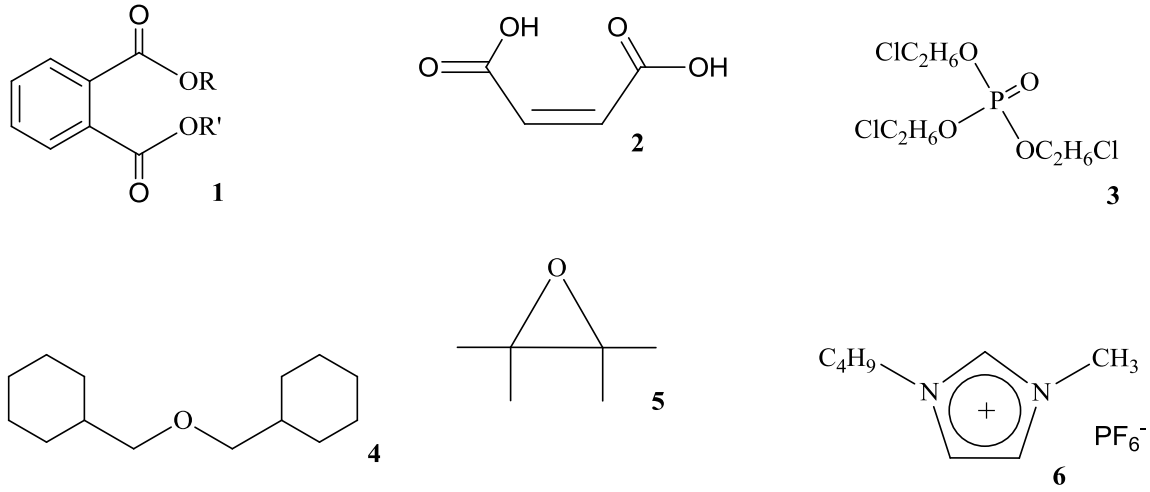

Scheme 1: General classes of plasticisers

When a plasticizer is blended to the PVC material, it is expected to reduce the following polymer properties; namely tensile strength, electrostatic chargeability, glass transition temperature, melt viscosity, hardness and density. However, other properties such as polymer flexibility, longevity and elongation at break point are expected to improve.[4]

1.1.1. History

For many years, plasticizers have been used in food contact material to produce flexible plastics. As early as 1862, Alexander Parkes in London introduced the first man-made plastic.[7] In the 19th century, the concept of plasticizers was adopted. In the early days, a natural camphor and castor oil mixture was used to manufacture a celluloid or celluloid lacquer for the plasticization purpose. However, the plasticization results from these compounds were unsatisfactory for many end-user products.[4,8] In the 1930s, phthalate plasticizers were then introduced and were successfully blended in PVC materials. Consequently, a rapid increase in their use was observed even in the rubber industry.[4,8] Kyrides *et al.*, patented a work on dioctyl phthalate plasticizer; the latter was adopted in North America and it was produced in large volumes.[9] The interest in phthalate plasticizers continued to grow even to other candidates such as di-2-ethyl hexyl phthalate (DEHP) and di-*iso*-nonyl phthalate (DINP).[10] Moreover, these plasticizers are currently produced and blended to the PVC to prepare a wide range of end-user products.[11]

1.1.2. Chemistry

Different classes of organic compounds are used as PVC-plasticizers (PVC-Ps). As mentioned earlier, dialkyl phthalate esters **1** are the most commonly used substances and are produced in large volumes commercially. Phthalate esters are synthesised from a straightforward esterification reaction of phthalic anhydride **7** or phthalic acid **8** with an alcohol under acidic conditions (Scheme 2). Usually, inorganic acid like sulphuric acid or HCl are used as the homogeneous catalyst.[12]

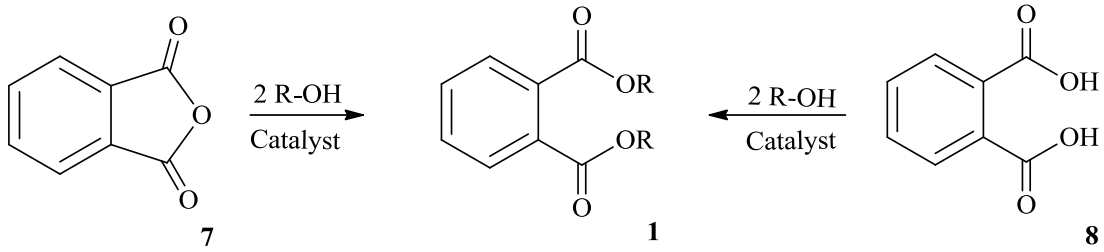

7 **1** **8**

Where, R is the straight or branched hydrocarbon chain

Scheme 2: Dialkyl phthalate synthesis routes

Considering their physical properties, phthalates are colourless liquids with a faint odor. The oil is insoluble in water, however is miscible with many non-polar organic solvents like hexane, tetrahydrofuran, toluene and mineral oil.[5] Typical examples of such oils include di-2-ethyl hexyl phthalate (DEHP) **9**, di-*iso*-decyl phthalate (DIDP) **10**, benzyl butyl phthalate (BBP) **11** and di-*iso*-nonyl phthalate (DINP) **12** (Scheme 3). Among these, DEHP has been a common choice for the application in many end-user products. Note that the majority of the plasticizers are symmetrical, containing two of the same ester groups, **11** being one exception to this general trend.

For the preparation of unsymmetrical phthalates such as **11**, the phthalic acid is first reacted with benzyl alcohol in the presence of catalyst (boron trifluoride etherate) and the reaction is allowed to stand for few minutes (10 min). Then, this is followed by the slow addition of *n*-butanol and the reaction mixture is allowed to reflux for an hour. The di-butyl phthalate is observed as a minor product of the reaction. Both compounds are separated by the solvent extraction method as indicated in the literature.[13]

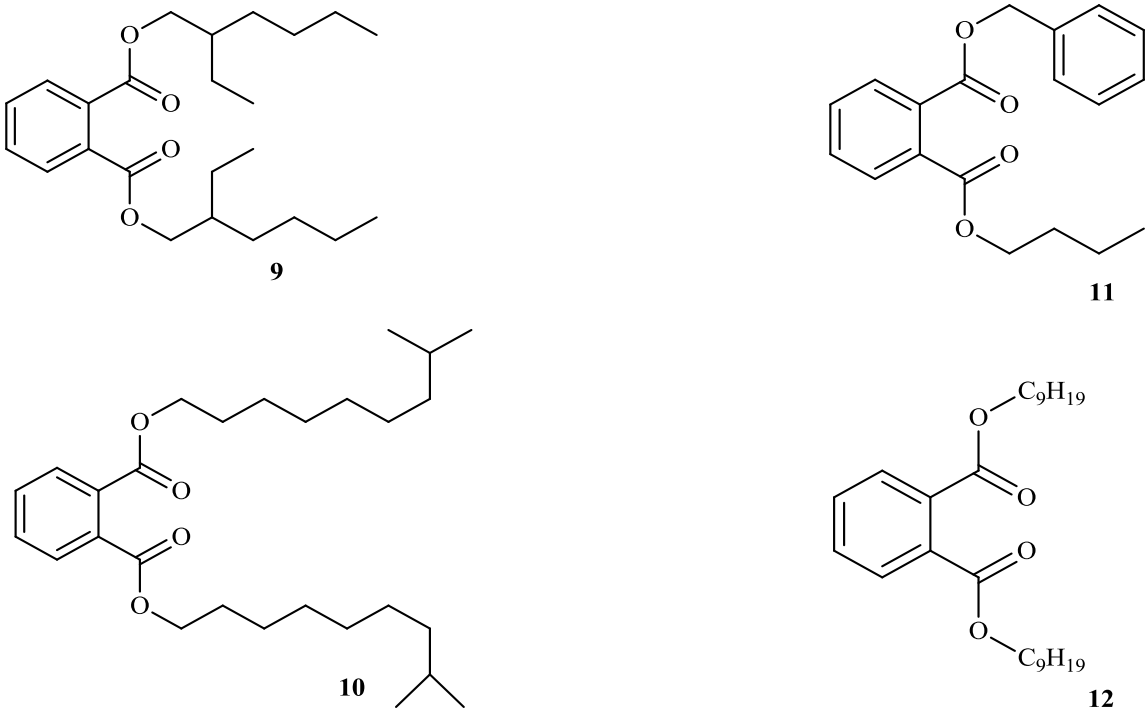

Scheme 3: Phthalate ester derivatives

The application of DEHP in many formulations has dropped significantly over the past few years. This is due to its related carcinogenic effects, which were observed from its toxicology study that was conducted on mice and rats.[14,15] DINP was subsequently introduced as a less toxic replacement for the DEHP.

When plasticizers are blended with a polymer, they are expected to lower the second order transition temperature of the polymer. However, other polymer properties such as flexibility and processability are expected to improve.[16,17] As plasticizers are of low molecular weight, they result in the second bond formation with the polymer, which is known as polymer-plasticizer bonding (Figure 1.1).

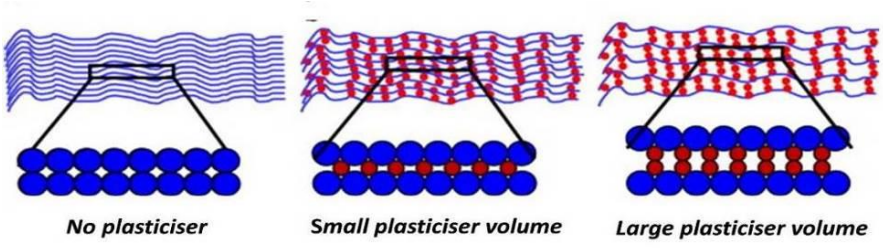

Figure 1. 1: Plasticization process of polyvinyl chloride[16]

The effect of this bond is designed to reduce the rigidity of the original polymer-polymer chain. As a result, the macro-molecules on the polymer gain extra mobility and yield a softer and more easily deformable mass.[4,16]

As mentioned earlier, the most frequently used phthalate plasticizer is the di-2-ethyl hexyl phthalate (DEHP). The latter comprises up 50% by weight of plasticizer content in many end-user products.[18] The recent studies also reveal that the phthalate esters are ubiquitous environmental pollutants. Moreover, they are also regarded as environmental endocrine disrupters.[5] As a consequence, countries like the USA, Canada and the European Union have developed new and restrictive regulations on the use of these compounds.[3] This initiative has resulted in a drastic change in this chemical research field. Based on the recent reports, it can be observed that researchers are now exploring new natural ways to prepare these types of compounds.

In light of the change in the conventional plasticizers, the concept of biodegradable plastics has received a close attention. These compounds are derived from renewable materials, hence are classified as bio-based organic compounds. Upon the evaluation of these compounds, they have been found to serve the same purpose as the conventional plasticizers. Typical examples of such compounds include the tetrabutyl acetyl citrate **13**, polylactic acid **14**, sorbitol acetate **15**, triglyceride **16**, cellulose acetate **17** and 1,2-propanediol **18**, *etc*. (Scheme 4).

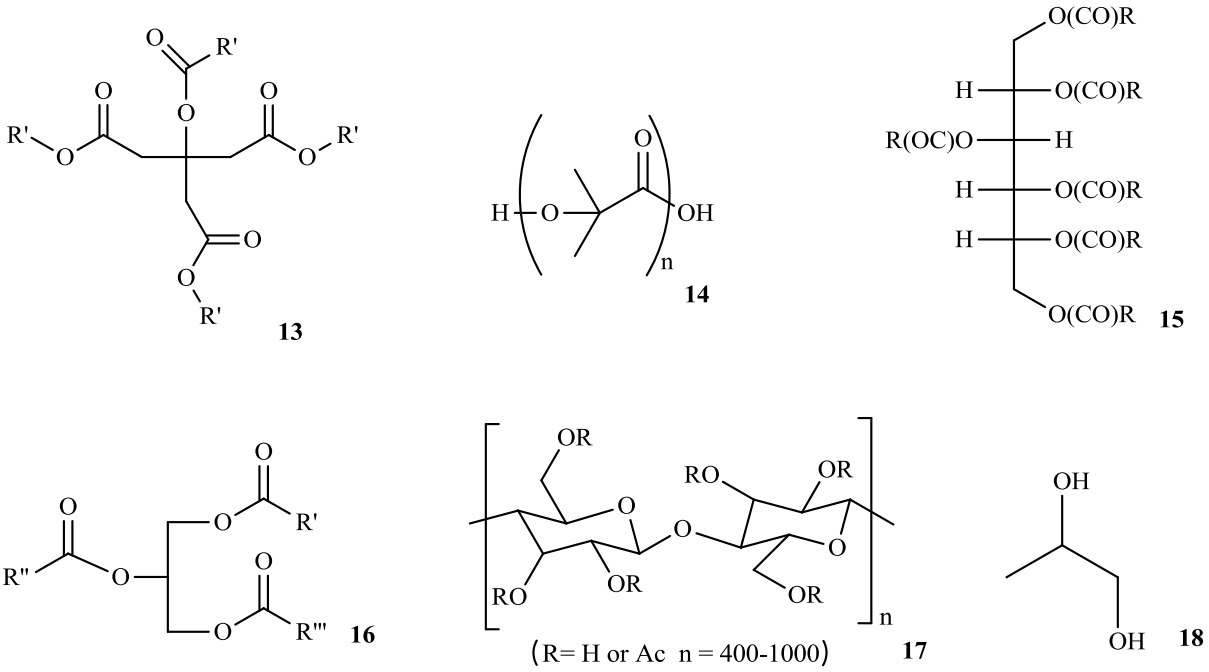

Scheme 4: Different classes of biodegradable plasticizers

Among these compounds, polylactic acid **14** is one of the preferred choices in many formulations, as its synthesis route is regarded as green and safe.[19]

1.1.3. Uses

Plasticizers are mainly used as additives in the production of flexible customer products such as children's toys, childcare articles, medical devices, drug containers and household products. The industrial hardware application includes electrical cables, PVC flooring and water pipes *etc*.[12] Various types of plasticizers are used in the manufacturing of many end-user products. Phthalate plasticizers have been the preferred PVC blenders for many years as compared to their counterparts (Figure 1.2).

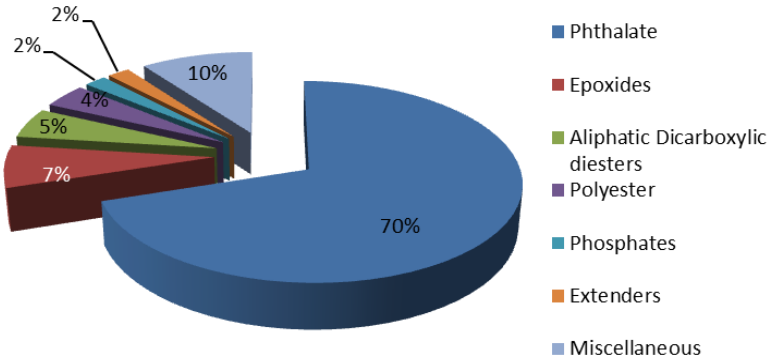

Figure 1. 2: Types of common plasticizers

When plasticizers are blended to the PVC, various plasticizer proportions are used. The plasticizer content is measured based on the rigidity of the polymer. This means rigid PVC contains a very low percentage of plasticizer content. Whereas flexible consumer products contain large volumes of plasticizer content (see Figure 1.1). The plasticizer content in PVC ranges as follows: rigid PVC contains less than 10%, semi-rigid PVC contains about 10-30% and highly flexible PVC contains up to 50% plasticizer content.[4,20]

Considering medical devices as an example, rigid-PVC is used to manufacture products like connectors, containers, syringes and hospital disposals, whereas semi-rigid or semi-flexible PVC is used to manufacture products like chambers, trays, blister packing *etc*. Soft consumer products such as gloves, blood tubing and blood bags are all manufactured from highly-flexible PVC.[3,21]

1.1.4. Economic and market analysis

When considering the global plastic additive market, plasticizers account for about one third of the chemical ingredients in terms of consumption.[4] When the plastic industry continues to grow, the plasticizer industry grows proportionally. In the last decade, the annual production volume of the global phthalate plasticizers was around 5 million tons per annum. The produced phthalate plasticizer has been used in more than 30 different groups of products and applied in about 60 polymer materials.[8] The commonly used plasticizer is the dioctyl phthalate, which was introduced in 1993 and show a current contribution quantity of 500 000 tonnes per year in North America alone.[9]

In 2003, a rapid growth in the global plasticizer market was observed, and it is expected to grow above 5 million metric tons, worth more than 10 billion pounds per annum. The PVC industry consumed approximately 90% of the production volume.[7] Countries like North America, Japan, Europe and Middle East countries have been declared as leading plasticizer producers.[22] In 2010, phthalate plasticizer global production was 5.0 million tonnes, which then accounts for 84% of the total plasticizer production globally.[5] When considering the global plasticizer breakdown, flexible consumer products account for the highest plasticizer demand more than any other product (Figure 1.3).

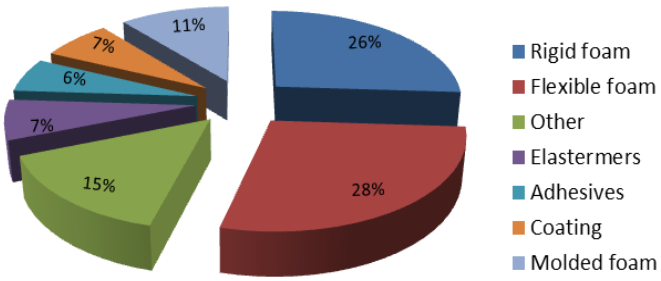

Figure 1. 3: Global breakdown of plasticizer end use

Recent studies reveals that many countries have lost interest in phthalate plasticizers, because of their potential to stimulate reproductive and developmental toxicity.[5] Other disadvantages of phthalate plasticizer are related to their leaching, migration and evaporation from the end-user products. On the other hand, the increasing demand for bio-based plasticizer is observed in many countries. Recent studies indicate that, 50 000 tonnes per year of bio-polymer based packaging is currently produced in Europe. This new development reveals an estimated contribution of 5-10% of green packaging material in the current plastic market.[23] Based on the study which was

conducted by the Pfizer Drug Safety Evolution Department, the citrate bio-based plasticisers have been proven to be safe through acute skin toxicity and ocular irritation tests in rabbits. Moreover, it was shown to be less toxic through acute oral toxicity tests in mice and rabbits.[24]

Malaysia in-particular, is known as a huge crude palm oil producer (CPO). Their oil is mainly used for the plasticization applications. The studies reveal an estimate of 8.4 million tonnes of CPO, which is reported annually from their production. As for the latest report, this work contributes up to 51% of the world palm oil production.[25]

The growing interest in bio-based plasticizer use has also extended to the essential oils such as epoxidized triglyceride (vegetable oil from soyabean), linseed oil, castor oil, sunflower oil and fatty acid esters (FAEs).[8] These natural-based compounds are characterised by low toxicity and low migration properties. Moreover, they are natural derivatives of renewable and biodegradable materials. Based on our recent studies, it has been observed that the modified eucalyptus citriodora oil component (*e.g.* citronellal) also has a great potential as a natural feedstock material to synthesize a wide range of bio-based plasticizers.[26]

1.2. Overview of citriodora oil

Citriodora oil is a natural plant extract from the indigenous plant known as *Eucalyptus citriodora* tree, which is common in many countries including the Southern Africa.[27] The oil constitutes of different organic compounds like citronellal **19 (**70-87%), citronellol **20** (5-9%), linalool **21** (2-6 %), isopulegol **22** (0.9-3%) and citronellyl acetate **23** (0.4-1%) *etc* (Scheme 5).[28]

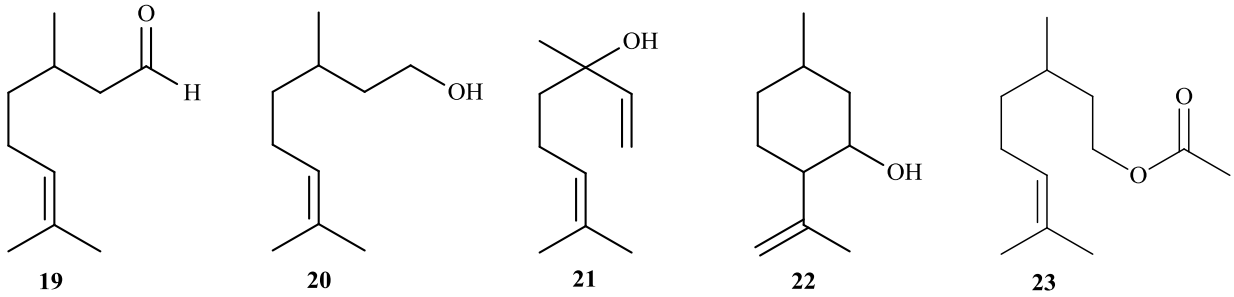

19 **20** **21** **22** **23**

Scheme 5: Citriodora oil components

Among these oil components, citronellal **19** (3,7-dimethyl-6-octenal) is obtained as a major constituent. It is extracted from the oil as a racemic mixture of *R* and *S* enantiomers through steam or hydro-distillation.[29] In other cases, a solvent extraction method is used (Scheme 6).[30]

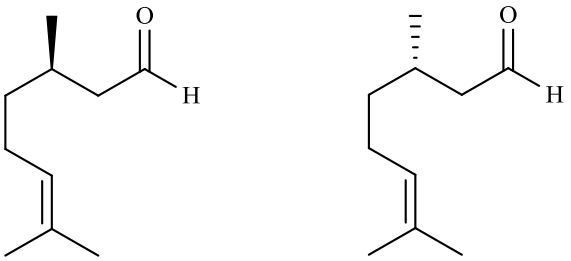

(*R*)-19 (*S*)-19

Scheme 6: Citronellal enantiomers

1.2.1. Properties of citronellal

Citronellal is a clear to pale-yellow viscous liquid and is widely used in a number of cheap perfumery formulations, fragrance soaps, toiletries and in disinfectant agents. It is best known for its insect repellent and antiseptic properties. It is soluble in alcohol and other oils, however is insoluble in water and oils such as glycerine.[28]

1.2.2. Production of citronellal

Common plants containing citronellal oil include Tasmanian blue gum (*Eucalyptus globulus Labill.*), river red gum (*Eucalyptus camaldulensis Dehn h.*), forest red gum (*Eucalyptus tereticornis Sm.*) and lemon scent eucalyptus (*Eucalyptus citriodora species*) are planted across the world, especially in North India.[31] In South Africa, the *E. carnaldulensis* plant species contain citriodora oil. The latter is dominant in the sub-Saharan Africa and contains a high concentration of citronellal oil.[28,32]

The citronellal market trend indicates that more than 2300 metric tonnes of citriodora oil is produced across the world, while 40-50% of citronellal is chemically produced.[30] An annual production of 2000 tons of (*R*)-citronellal is reported by Takasago International Co-operation. The produced citronellal is used to prepare the stable commercial isopulegol intermediate, which is used as a feedstock in the synthesis of menthol.[33]

In subtropical and tropical countries, citronellal is extracted from plants, seeds, leaves and from the resin of the trees. The resultant oil extract is mainly used as an active ingredient in the formulation of repellents, which are the main interest for the local target market.[34]

1.2.3. Uses of citronellal

As mentioned earlier, citronellal is mainly used for the production of menthol, an important compound that is widely used as an additive in pharmaceuticals, flavour and fragrance applications. In the food and beverage industry, citronellal is used as flavour additive. The household products such as detergents, soaps, air-fresheners and insect repellents also contain citronellal as the scenting agent.[35-37]

Citronellal is regarded as an antiseptic essential oil, normally used as a bio-herbicide treatment for various infections. The antibacterial, antifungal, ascaricidal and insect repellent activities are the main antiseptic properties that have been identified from its various uses. Its antimicrobial activities are widely used in the formulation of medicine, food, beverages and pharmaceutical products.[28,36,38] In sub-Saharan Africa, many cases of malaria disease are reported annually, over a million people per year die because of anopheline mosquito bites.[34] Citronellal oil is used as a mosquito-repellent to control the spread of malaria. Additionally, countries like the United States of America and many other countries, retail candles and incense containing citronellal as insect repellent.[39]

1.2.4. Reactions of citronellal

The intramolecular cyclisation reaction of citronellal **19** is a common synthetic route used to prepare isopulegol **22**. It is also used extensively in the synthesis of other value added chemical derivatives such as citronellol **20**, 3-hydrocyclocitral **24**, (*R*)-(-)muscone **25**, octahydroacridine **26** *etc.* (Scheme 7).[40- 43]

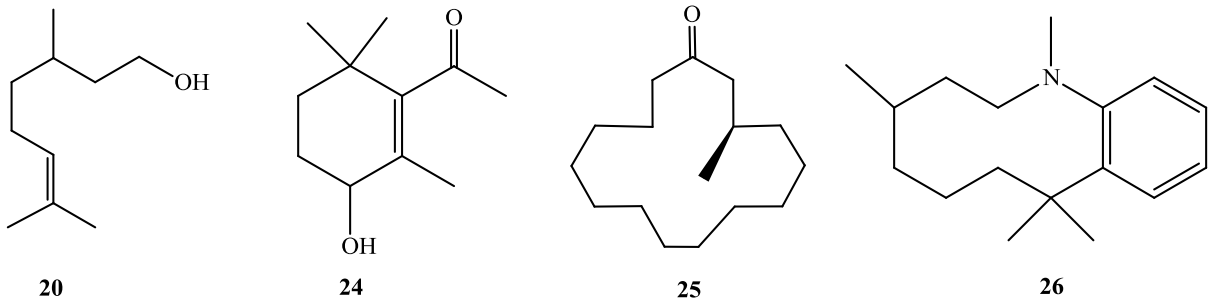

20 **24** **25** **26**

Scheme 7: Citronellal value added derivatives

In this section, special attention will be given to the chemical routes that involve the isopulegol intermediate. These synthetic routes include the citronellal cyclisation, *para*-menthane-3,8-diol (PMD) and menthol synthesis.

1.2.4.1. Citronellal isomerisation

In the citronellal cyclisation process, a strong acid catalyst plays a vital role in transforming the molecule. When an acidic catalyst is introduced in the reaction, it protonates the carbonyl oxygen of citronellal **19**. This helps to increase the electrophilicity of the carbonyl carbon atom. As a result, this renders the carbonyl carbon even more susceptible to nucleophilic attack. The alkene in the molecule acts as a nucleophile and undergoes an intramolecular cyclisation. This is followed by the molecular rearrangement and results in the formation of isopulegol (Scheme 8).[44,45]

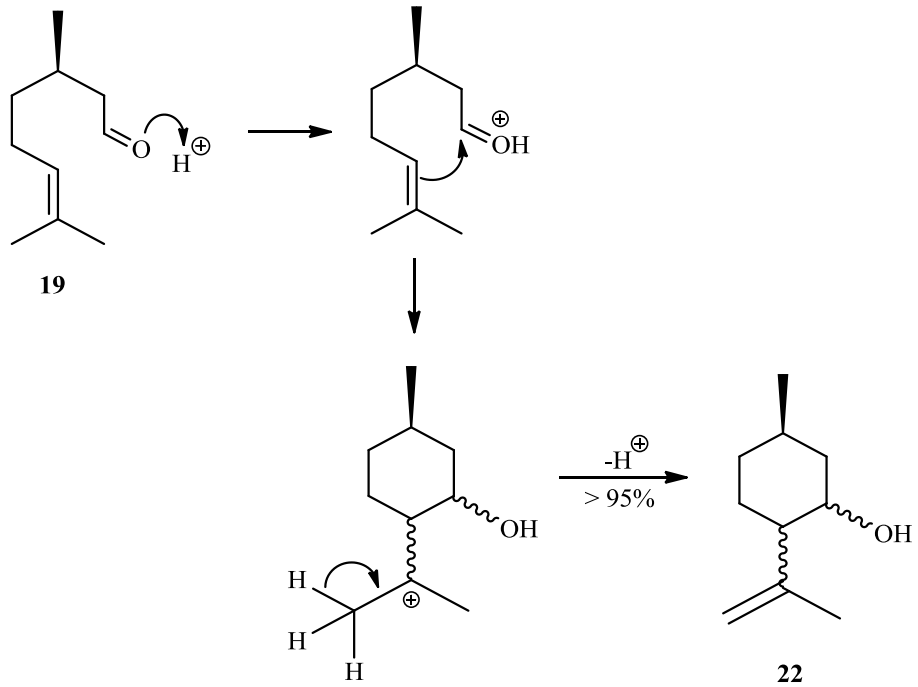

Scheme 8: Intramolecular cyclisation reaction

Assume starting from chiral molecule **19** (as drawn in Scheme 8), the isopulegol exist as four pairs of isomers, namely (±)-isopulegol **22a**, (±)-neo-isopulegol **22b**, (±)-iso-isopulegol **22c** and (±)-neoiso-isopulegol **22d** (Scheme 9).[46,47]

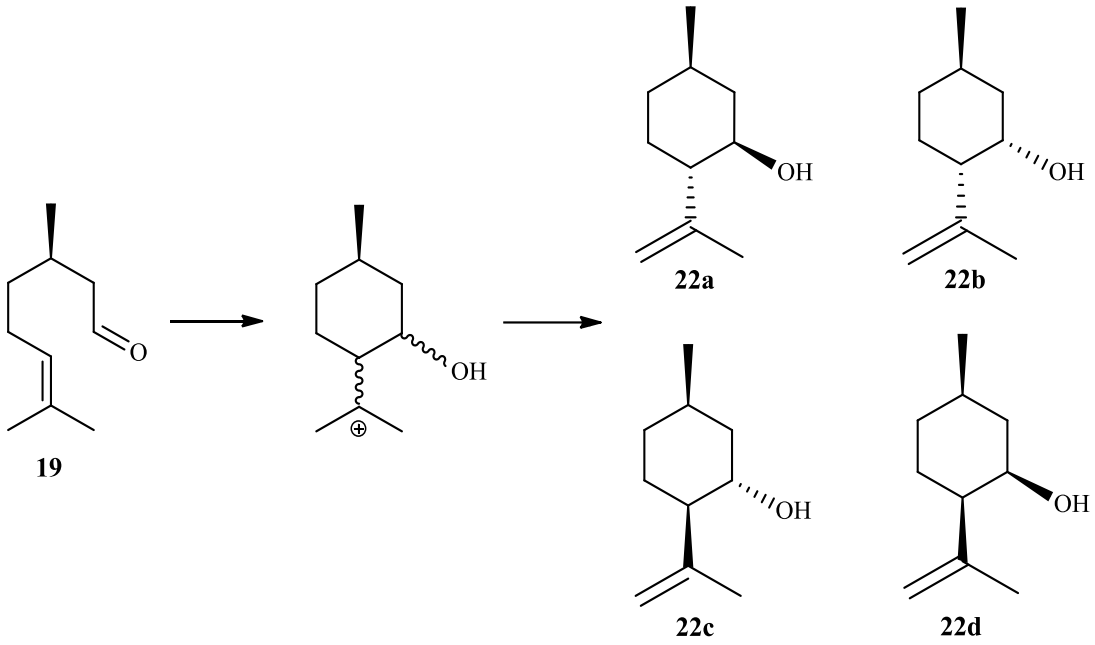

Scheme 9: Isopulegol isomers

Among these stereoisomers, (-)-isopulegol **22a** is desirable in high yields as it is used effectively in (-)-menthol synthesis.

The citronellal cyclisation reaction is 100% atom efficient, meaning all the atoms present in the substrate react completely and yield the isopulegol. Such atom efficient reactions are preferred in organic synthesis, because they avoid waste generation and are regarded as environmentally friendly green reactions.[48]

1.2.4.2. *para*-Menthane-3, 8-diol (PMD) synthesis

para-Methane-3,8-diol (PMD) **27** is also known as *p*-menthane-3,8-diol or menthoglycol. It is obtained naturally as one of the citriodora oil components, even though it occurs in a small quantity. Synthetically, it is prepared from the reaction of citronellal in aqueous acidic solution. The resultant product consists of its *cis* and *trans* isomers (Scheme 10). Among these isomers, the *trans* isomers exist in a higher concentration than the *cis* isomer. From an industrial interest, a mixture of these isomers is used as the active ingredient in the formulation of insect repellents.[34]

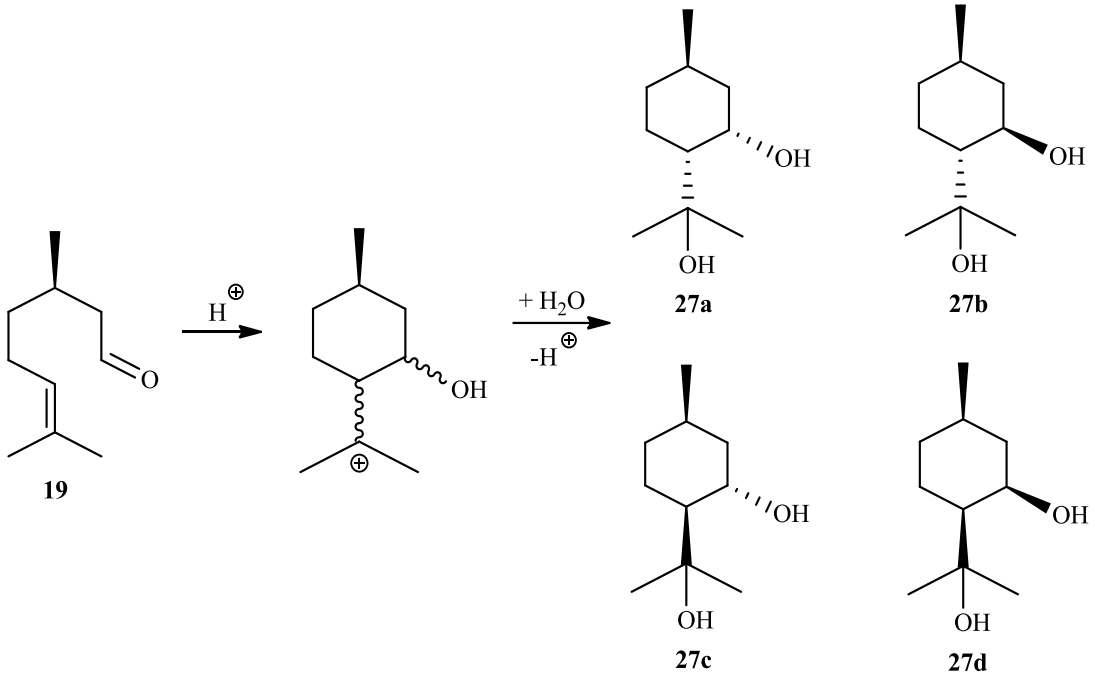

Scheme 10: *para*-Menthane-3,8-diol isomers

Most repellents often contain synthetic chemicals such as diethyl-*m*-toluamide (DEET), picaridin, *para*-menthane-3,8-diol (PMD) *etc*. Among these, PMD is preferred to be used, because it's a natural derived chemical, unlike other synthetic chemicals. Moreover, its synthesis route is based on natural oil upgrade.[34]

1.2.4.3. Menthol synthesis

During the manufacturing of menthol **28**, the industrial process consists of two reaction steps, when starting from (+)-citronellal **19**. The first reaction step is based on the synthesis of (-)-isopulegol **22a** *via* a citronellal cyclisation. The (-)-isopulegol so-formed further undergo a hydrogenation reaction over a Ni metal-supported catalyst. The reaction leads to (-)-menthol **28a** (Scheme 11).[49] The latter has a wide range of application in a variety of products such as cosmetics, personal care products, pharmaceuticals *etc*.[46]

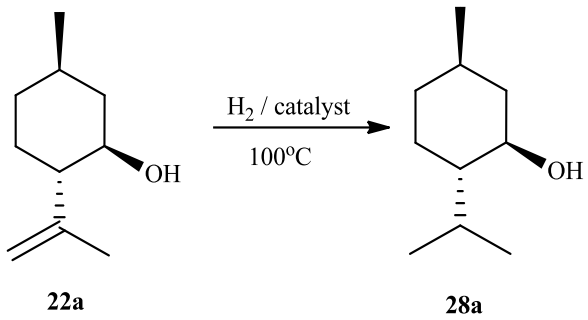

Scheme 11: Menthol synthesis route

The most competitive industrial process for (-)-menthol **28a** synthesis is the Takasago process.[47] In this manufacturing process, all isopulegol stereoisomers are hydrogenated over Zr-beta-supported nickel catalyst (Scheme 12). Consequently, four pairs of menthol enantiomers are formed, namely (±)-menthol **28a**, (±)-neo-menthol **28b**, (±)-iso-menthol **28c** and (±)-neo-iso-menthol **28d**.[46] A high selectivity towards (-)-isopulegol is preferred as compared to its counterparts. This compound is desirable in high yield for the synthesis of (-)-menthol. Additionally, (-)-menthol is the only isomer that is characterized with a perceptible cooling effect.[46,47]

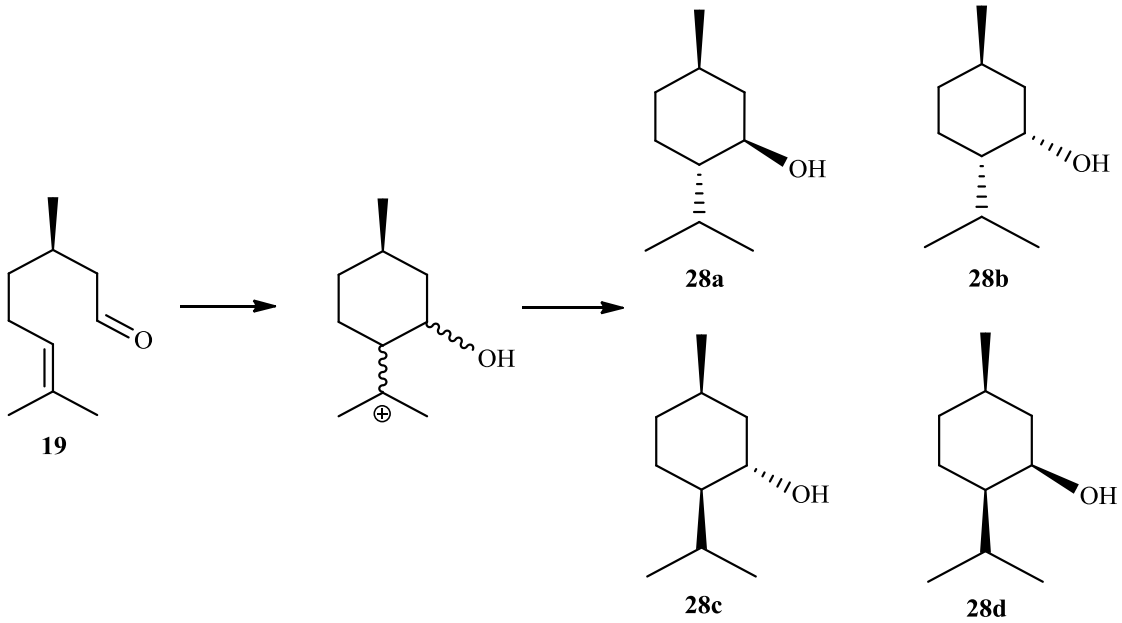

Scheme 12: Menthol isomers

1.2.4.4. Toxicity of citronellal

Citronellal is a natural existing essential oil extract that is obtained from the biodegradable material. Due to its biological properties such as analgesic, spasmolytic and anticonvulsant, it has

gained much attention as a potential chemotherapeutic agent in medical and pharmaceutical industries.[37,50] Essential oils (citronellal in particular), have been examined and certified by the Food and Drug Administration (FDA) and declared as non-toxic under the GRAS (Generally Regarded as Safe) category.[51] Therefore, it is approved to be used as a flavouring agent in food (≤ 5 mg/kg) and confectionery items (≤ 15 mg/kg) in Europe (Council of Europe, 1992).[29] Moreover, it is regarded as non-toxic on humans and is an environmental-friendly chemical. It is for this reason that we are interested in developing other value added products from this feedstock.

1.3. Overview of conventional batch-scale reactors

A chemical reactor is defined as a reaction vessel that is designed to contain and carry-out chemical reactions. Ideally, reactors should give highly efficient product output, high product yields with minimum effort required to operate the system. Understanding the chemical reaction kinetics is valuable, because it simplifies the selection of the optimum reaction conditions and the specifications required for the chemical reactor design.[52,53]

Most industrial processes for fine chemical manufacture are carried-out *via* batch-scale reactors, a well-developed procedure that works efficiently for most chemical reactions. However, its discontinuous form and the low surface-to-volume ratio of the reactor are its major disadvantages, especially when performing fast and highly exothermic reactions. These challenges are mostly encountered when scaling-up the reactions and they lead to severe limitations.[54,55]

On the other hand, continuous-flow reactors guarantee the necessary conditions for chemical reactions; these include large volume production through the replication of unit processes and also enable the direct transfer of laboratory optimized conditions into the production scale.[56] Moreover, continuous-flow reactors are characterized with higher heat and mass transfer rates, which enable fast and highly exothermic reactions to be performed under isothermal conditions. Thus, better product yields and selectivities are achieved more easily than in conventional reactors. Continuous flow reactors also enable better process control and well distributed production, especially when dealing with toxic or hazardous substances.[57]

A further advantage may be seen for countries like South Africa. In Europe many chemical manufacturing companies are available to assist in the large scale manufacture of commodity chemicals, however in South Africa that is not the case. Consequently the ability to use low cost, continuous flow reactors for the distributed manufacture of chemicals potentially makes more sense.

1.4. Overview of continuous flow fixed-bed reactors

Continuous flow reactors may be subdivided into liquid-liquid, gas-liquid, gas-liquid-solid phase reactors *etc*. When performing a gas or liquid phase reaction, process chemistry issues such as activation energy, substrate type, catalyst type and the desired product becomes the determining

factors for the substrate conversion, product yield and selectivity.[58,59] Iliuta *et al*. also specified that in multi-phase reactions such as gas-liquid, liquid-liquid or gas-liquid-solid, a substrate conversion or product selectivity of the reaction can be affected by several factors; these include the solid-liquid or gas-liquid mass transfer, axial mixing and catalyst wetting.[60] Furthermore, these factors have been found to be predominant over intrinsic kinetically fast reactions, especially in the stirred batch reactors. As a result, the reaction times become much longer than expected, due to the masking of mass transfer limitation on intrinsic kinetic rates of the reactions.

1.4.1. Mass and heat transfer in catalytic fixed-bed reactors

As a fluid flows through a packed-bed reactor containing catalyst particles, molecular diffusion occurs on the surface of the micro- and macro-pores of the catalyst. Subsequently, several processes take place on the catalyst particles concurrently (Figure 1.4). These include chemisorption of reactant(s), surface reaction, desorption of the product(s) and the back-diffusion of the product species. The mass and heat transfer of the reactor play a vital role in enhancing the performance of these processes, as to better a degree of reactant conversion and product selectivity.[58]

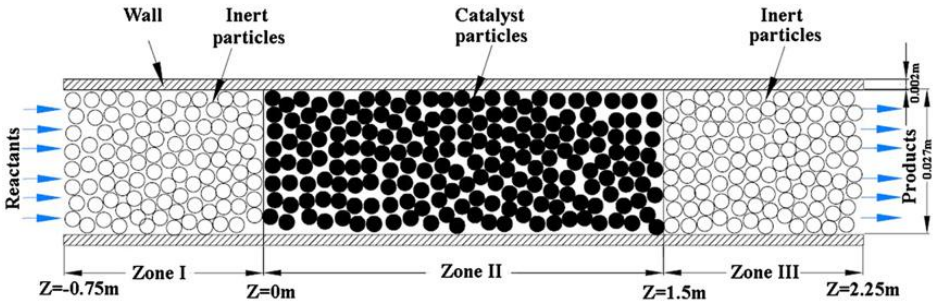

Figure 1. 4: Fixed-bed axial flow reactor[66]

Fixed-bed reactors are sensitive systems, as the reaction rates are temperature dependent and characterized with high system thermal capacity.[61] When designing a fixed-bed reactor, heat transfer parameters such as radial thermal conductivity of the bed and the wall-to-bed heat transfer coefficient are very important aspects that need to be properly calculated. Hence, an overlaying temperature profile can be simply generated numerically or by using design methods. In addition, by having a control over the temperature profile of a reaction also gives extra power to control the reaction selectivity, as well as to handle the exothermic reaction.[62]

In fixed-bed catalytic reactors, the temperature profile has a huge effect on the reactor stability, substrate conversion and product selectivity. In order to obtain the best substrate conversion and product selectivity, a reactor must be able to maintain the optimum reaction conditions. These include pressure, temperature profile, residence time and the concentration of reactant(s). A small deviation on the above mentioned variables, could result in a large variation between temperature and concentration or could lead to the reaction runaways.[61]

In the case of mass transfer, inconsistency of residence time distribution in the catalyst bed, directly affects the yield and selectivity of the product. Therefore, if the reaction rate is considerably lower than the mass velocity, the influence of mass-transport resistance in the catalyst particle can be omitted. As a result, good external mass transfer, short diffusion paths in catalyst particles with adequately large pores will be required. In general, the reaction rates must be controlled and limited by the packed-bed reactor temperature, in-particular in the case of exothermic reactions.[58,63]

1.4.2. Continuous flow catalytic fixed-bed reactors

1.4.2.1. Catalytic gas phase reactor

The catalytic gas-phase reactors are extensively used in commercial production of large scale basic chemical intermediates. The hydrodynamics, heat and mass transfer parameters of the reactor play a vital role during their selection and when designing a multi-phase reactor.[53,64,65] In the catalytic fixed-bed reactor, a catalyst is fixed in the reactor centre (see Figure1.4).[66] The reaction takes place on the interior or exterior surface of the catalyst, where the exchange of mass and heat transfer occurs. Highly exothermic gas phase reaction such as oxidative dehydrogenation and the synthesis of phthalate anhydride, maleic anhydride and acrolein are suitable reactions for this reactor design.[58,67]

Consider the synthesis of acrolein **30** as an example, which is an important chemical that is widely used in water treatment and in the petroleum industry as a biocide.[68] It is prepared from glycerol **29**, the by-product of the biodiesel synthesis process. The catalytic gas phase dehydration of glycerol is carried-out with various types of heterogeneous catalysts, namely $ZnSO_4$, AlO_3/PO_4, SiO_2/Al_2O_3, ZSM-11, WO_3/ZrO_2 *etc*. Ulgen *et al.* have performed this reaction in catalytic fixed-bed reactor over tungsten oxide supported on titanium oxide catalyst (WO_3/TiO_2) (Scheme 13).

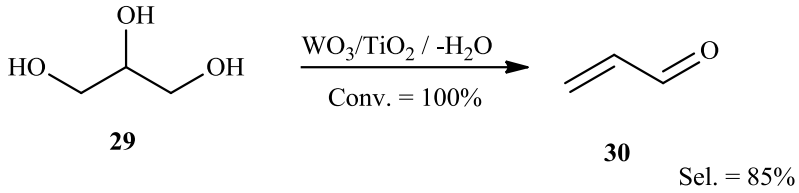

Scheme 13: Acrolein synthesis

In their work, a coiled stainless steel fixed-bed reactor (I.D = 0.6 cm. length = 100 cm) was used and fully packed with WO_3/TiO_2 catalyst. The catalyst mass used was approximately 5.0 grams and the reactor was heated to 280°C. An aqueous glycerol solution (20%) was pumped into the reactor at a rate of 23 g/h simultaneously with oxygen gas at 11.33 ml/min. As a result, a weight hourly space velocity (0.92 $mL.g^{-1}.h^{-1}$) and the residence time (0.324 s) were achieved. Their results showed that, in all unsupported titanium oxide catalysts, poor glycerol conversion and acrolein selectivity were observed. The glycerol conversion was ranging from 46 and 77 mol% and selectivity from 12 and 17 mol%. Whereas, when tungsten oxide support was loaded on titanium oxide, a significant improvement in acrolein selectivity was observed. Wherein, an increase in WO_3 loading has resulted in very high acrolein selectivity of 85% and almost 100% of glycerol conversion.[68] These results were found to be similar to those that were reported by Chai *et al.* whereby, a gas phase dehydration reaction of glycerol was performed in similar reaction conditions. The experimental observations revealed almost 100% of glycerol conversion and above 65% yield towards acrolein over WO_3/ZrO_2 catalyst.[69]

Another example of a catalytic gas phase oxidation reaction is the synthesis of phthalic anhydride **32** from *o*-xylene **31** or naphthalene **33** (Scheme 14).

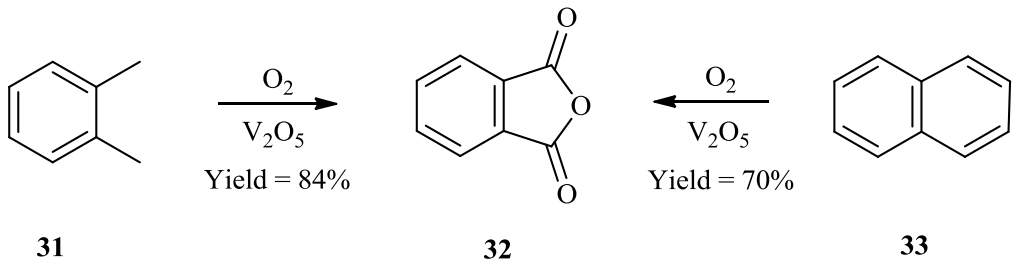

Scheme 14: Phthalic anhydride synthesis

The partial catalytic -oxidation of *o*-xylene **31** or naphthalene **33** is easily carried out in the fixed-bed reactor. A single tube pilot plant reactor (I.D: 25 mm, length: 325 cm) is normally used. The reactor is packed with catalyst pellets of vanadia-titania (1480 kg/m^3). The temperature measurement and the sampling of composition are done at 25 axial possible along

the reactor length. The following experimental conditions were used in the study (air flow-rate of 40 g/m^3, heating temperature range of 380–403°C and *o*-xylene composition range of 0.3–1.0 mol %). However, the hot-spot formation in the fixed-bed reactor was observed at the temperature range of 450–530°C. From this reaction, 99% *o*-xylene conversion was achieved with about 84% yield towards phthalic anhydride. It is also noted that the application of a dual catalyst bed, resulted to the significant yield improvement of the product and a sharp decrease of the undesired products was also observed at optimum temperature.[70,71]

1.4.2.2. Catalytic liquid phase reactor

The catalyst in these systems is arranged in the reactor similarly as in the gas phase reactor. However, liquid phase reactors are characterised with longer residence times when compared to the gas phase reactors.[64] In general, liquid-phase reactors favour the reactions that operates at high temperatures and those that are associated with higher boiling point compounds.[58] When performing a reaction in a liquid-phase reactor, a smaller ratio between a reactor column diameter and catalyst particle size is preferred. This ratio provides a better interaction between a liquid and solid material, thus becomes more effective than the gas-liquid phase reactors.[64,67] Typical reactions for this reactor set-up include the esterification, acetylation, etherification, isomerisation, cyclisation *etc*.[72,73]

As an example, consider a transesterification reaction of triglyceride **34** as a liquid-liquid-solid phase reaction. Transesterification of triglyceride is a synthesis route used to produce the fatty acid alkyl esters **35** (biodiesel). This process involve reaction of triglyceride and alcohol over an alkaline hydroxide (KOH) catalyst, which then results in the formation of biodiesel and glycerol **29** as by-product (Scheme 15).[74]

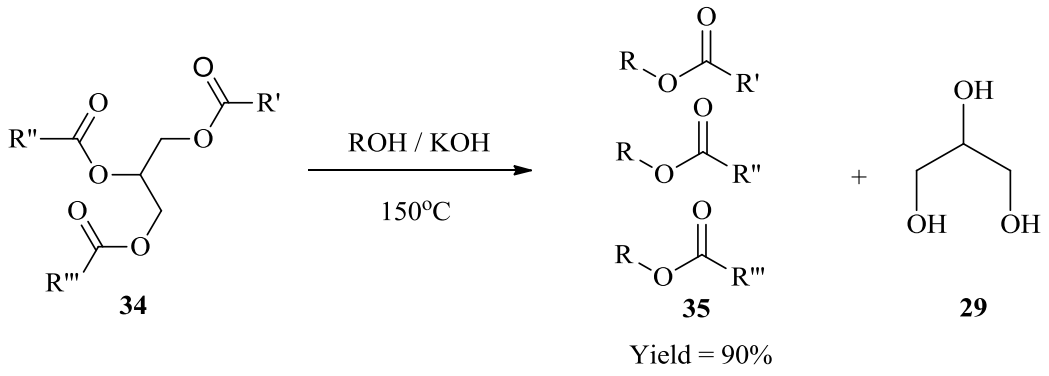

34 **35** **29**

Yield = 90%

Scheme 15: Transesterification of triglycerides

Buasri *et al*. reported an improved method for the synthesis of biodiesel in the continuous flow process. The reactor that was used comprised of water-jacket stainless steel column reactor (O.D: 60 mm, length: 345 mm). Heterogeneous potassium hydroxide supported on Jatropha curcas fruit shell (KOH/JS) was used as a solid-base catalyst. In the course of the reaction, a molar ratio of 3:1 towards the triglycerides and alcohol was used and pumped into the reactor at flow rate of 1-3 ml/min. The reaction temperatures were set below the boiling point of alcohol used to prevent the mixture from boiling within the reactor, as it was not pressurised. The condensed product was collected at the reactor exit and separated from the glycerol.

Their results revealed that the biodiesel yield was observed to increase from 61% to 87% as the reaction residence time was increase from 1 to 2h. It was also observed that the reaction temperature played a major role in improving the product yield; when the reaction was operated at the temperature range of 50 to 70^0C, the biodiesel yield increase ranged from 67 to 86%. Furthermore, the catalyst was shown to be reusable for five times without any signs of deactivation. Nevertheless, the saponification of the feedstock was a major challenge when high FFA were used.[75]

1.4.3. Disadvantages of heterogeneous catalytic fixed-bed reactors

Catalytic fixed-bed reactors suffer from several reaction limitations. Hot-spot formation is one of the major disadvantages, which is mostly encountered in industrial fixed-bed reactors. It is caused by limited heat transfer areas and poor radial heat transfer on the catalyst packing.[67] The other limitations include a substantial pressure drop, insufficient heat removal, maldistribution of flow, agglomeration and the clogging of reactor tubes *etc*.[67,76,77] Therefore, these challenges have the negative effect towards the reaction control and they result in poor product yields and selectivities.

On the other hand, industrial multi-tubular fixed-bed and slurry reactors also suffer from various catalysts challenges, when operated in highly exothermic reaction conditions. Some of these challenges include catalyst deactivation and the problem of scaling-up the process.[78] By taking a close consideration on the above mentioned challenges, a more sophisticated reactor design methods are required to better the operation and performance of continuous-flow reactor systems.

Recently, a new research approach on the design and operation of continuous flow reactors has been reported in the chemical engineering field. This research innovation has shown several positive aspects on reactor designs. It suggests that an ideal reactor should have small channel dimensions. This will provide a larger surface area-to-volume ratio and must be characterized by a short distance to the reactor wall. Moreover, they should have a significant improvement for heat and mass transfer properties. Thus, these specifications could lead to the better process intensification, broader reaction conditions, fast process development and distributed production.[76] Kiwi-Minsker *et al*. indicated that reactors must be able to perform fast and highly exothermic or strongly endothermic reactions.[79] Therefore, micro-structured reactors (MSRs) have been introduced to meet these requirements.

1.5. Overview of micro-structured reactors (MSR)

These reactors are characterized as micro-structured, because of their smaller inner dimension or carrying channel(s) with a size below 1mm, and often in the range of 10 and 300 µm.[80,54] The image of a MSR is presented below in Fig. 1.5 (a) and its cross section of the micro-channels in Fig. 1.5 (b). The smaller inner dimension of the MSR provides a high surface-area-to-volume ratio, which ranges between 10,000 and 50,000 m^2 m^{-3}.[54,81] Due to its higher surface area, enhanced mass and heat transfer are obtained in two order magnitude higher than the conventional reactors.[82] Process parameters such as temperature, residence time, pressure and flow-rate are easily controlled in reactions that occurs in these smaller reactor designs.[81]

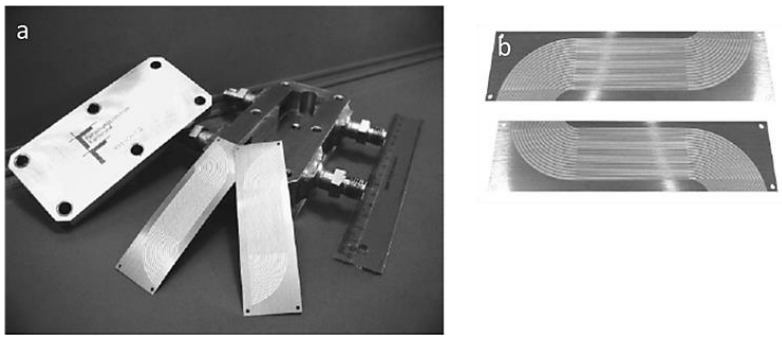

Figure 1. 5: Micro-structured reactor plate[79]

As mentioned above, the limited heat transfer area and poor radial heat transfer of catalyst packing results in hot-spot formation in continuous-flow fixed-bed reactors. Therefore, this results in the undesirable side reactions and also leads to the uncontrollable reactions. In micro-structured reactors, the presence of high heat transfer coefficients suppresses the formation of

hot-spots significantly. Hence, the occurrence of side reactions may be reduced.[58] In MSR heat transfer coefficient of the liquid is about 10 kW m^{-2} K^{-1}, which is one order magnitude higher than the conventional heat exchanger.[83] Besides, higher reaction temperatures are achieved to perform highly exothermic and strongly endothermic reactions.

Up-scaling of chemical reactions from the laboratory scale into the large industrial production scale, often becomes a challenge due to the lower levels of reaction control attained in large batch reaction vessels.[58] The large size of reaction vessels leads to a decrease in mixing quality, temperature gradient and poor heat transfer. As a result, this leads to higher safety risks.[54] The non-uniform temperature profile and hot-spots in the reactor vessel give rise to poor product yield and selectivity, and even cause catalyst deactivation.[65] In such cases, these limitations are overcome by the benefits of micro-structured reactors.

Considering the transport-kinetic interaction of chemical reactions, MSR offers several technical advantages because of the design of their parameters. They clearly explain the interaction between hydrodynamics, transport phenomena and reaction kinetics.[82] Furthermore, they describe the physical attributes of the specific device such as channel dimension, channel arrangement, number of channels, channel internals and layout, device wall thickness, fluid-flow paths and surface roughness *etc*.[84] The use of heat exchangers and micro-mixers offers added advantages. Wherein, heat transfer and mixing rates are easily controlled by adjusting the flow-rates, which in turn controls the reactions residence time.[85] Proper mixing of reactants leads to the desired process intensification and significantly eliminates the side reactions. The strict control of residence times and narrow residence time distribution, result to the fast reactions and thus leads to higher product yield and selectivity.[82]

1.5.1. Contact principles of micro-structured reactors

Micro-structured reactors are more advantageous over conventional reactors in chemical processing, because of their mixing characteristics. In MSR, reactant mixing is mainly due to molecular diffusion rather than the turbulent bulk mixing, occurring in a conventional batch reactors (Figure 1.6).[86] Better mixing characteristics are desirable in MSRs, because it enables the determination of the rate at which the reactants are converted into products. This phenomenon is observed mostly in fast reactions, whereby a reaction rate is faster than the mixing rate and in reactions where mass transfer across the boundary layer determines the reaction rate. During the course of the reaction, heat is consumed or released in the reactant

mixing process. Therefore, good heat transfer characteristics are also important for the device in use, whether it's a mixer or a reactor device.[58,85,86]

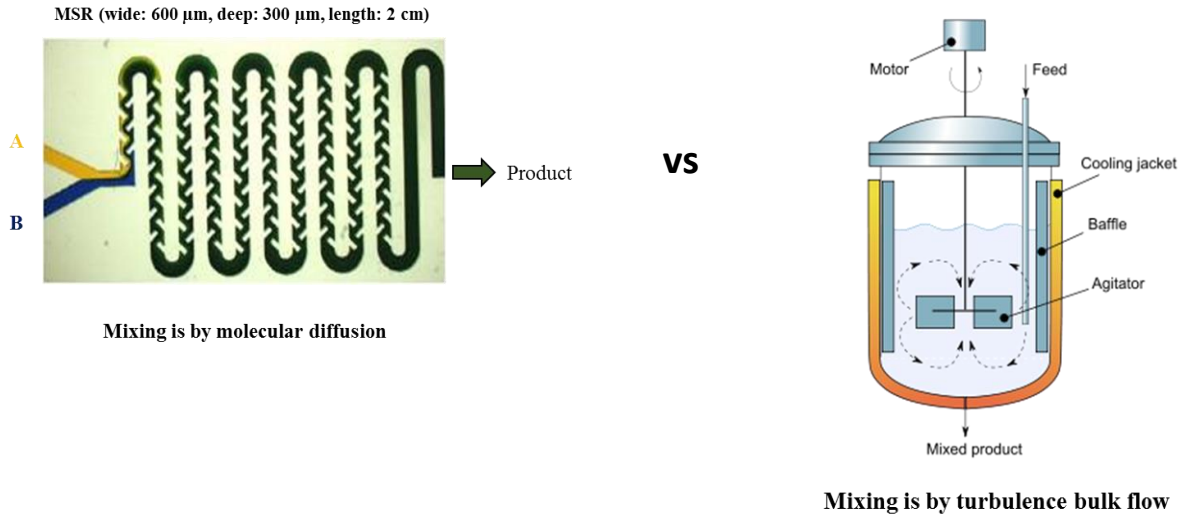

Figure 1. 6: Reactant mixing mode in different reactor systems

The reactant mixing method in the reactor can be classified into two categories, namely macro- and micro-scale mixing. *Macro-scale mixing* is achieved by the use of mechanical or magnetic stirrers, so as to generate a circular motion of large bodies. During this process, diffusion dominates at an even distribution of one reagent to the other. On the other hand, *micro-scale mixing* favours the formation of high viscous forces that eliminates the turbulent flow. It is the mixing method that is dominated by molecular diffusion, because it functions close to the molecular level. This type of mixing provides a better contact between the reacting compounds, thus producing the reactive collisions. The diffusive mixing occurs in the narrow, high aspect ratio reaction channels, that provides a high surface-to-volume ratio. Since molecular diffusion is a slow process, it can be accelerated by agitation within the channel as to create a turbulent-flow.[56,87]

By considering a single phase flow reaction, the reaction in a MSR is characterised with laminar flow (low Reynolds numbers).[88] The occurrence of laminar flow in the reactor is due to the design of the smaller inner dimensions of the reactor micro-channels.[54] These smaller micro-channels suppresses the back mixing and helps to avoid the occurrence of side reactions.[58] Whereas, when a micro-mixing device is used as a chemical reactor, the reaction is characterised with turbulent flow diffusion (high Reynolds number).[89] The turbulent flow is mainly due to the internal structuring of the mixing device and the flow-rate of the reacting substance in the micro-channels (Figure 1.7). MSRs are also characterised with large surface-to-volume ratio, which

leads to a good heat and mass transfer properties.[55] The design of micro reactors allow process parameters such as time, temperature and pressure to be easily controlled as compared to the conventional reactor systems.[54]

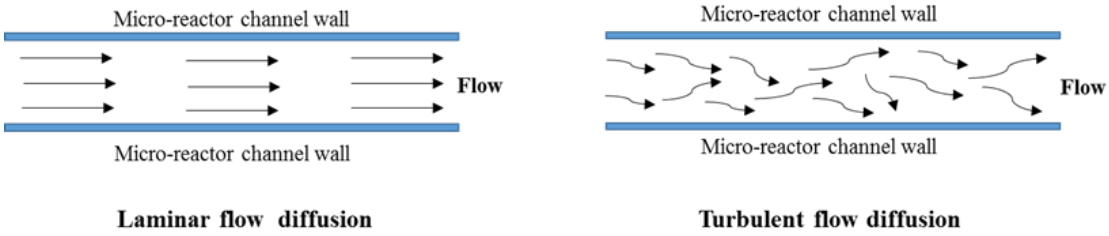

Figure 1. 7: Liquid flow in the micro-structure reactor channel

The effective reactant mixing in a MSR, often guarantees the reaction rates with better product space-time yield and improved selectivities. In general, space-time yield refers to the time necessary to process the substrate mixture in a reactor volume at given set of reaction conditions. This is true, because reactant mixing must be accomplished before the reaction is completed. Alternatively, the formation of reactive collisions that favours the by-product formation are reduced, mostly in case of multi-phase reaction or series reactions.[58,90]

There is another factor that also has an effect towards the space-time yields in MSR. This is the ability of the reactor to accommodate higher mass flow rates at tolerable pressure. To achieve the higher mass flow-rates, it's either by increasing a cross-sectional area of the reactor channels or by increasing the number of reactor channels.[58]

In multi-phase reactions, there are various reactor features that can affect the fluid flow and the interaction of reactants. Among these features, the flow of thin films can be affected by the surface characteristics of the reactor channels.[84] The surface quality of the coated micro-channels with catalyst material is also crucial for multi-phase reactions. Thus, the roughness of the inner micro-channel walls must be minimized. This will help to reduce the friction and breakage of the thin falling films.[57,85]

1.5.1.1. Multi-phase reaction in micro structured reactor

Multi-phase reactions have been employed extensively in various sectors of chemical processing and various types of micro reactors have been used for a number of reactions.[91] Some of these reactors include the micro-bubble column reactor, dual-micro-channel chip reactor, single or tri-channel thin-film micro-reactor and falling film micro-reactor.[92] In the following section, a brief

discussion will be given on the design of the falling film micro-structured reactor and its operation.

1.5.1.2. Falling film micro-structured reactor (FFMSR)

In multi-phase reactions, the falling film reactor is a commonly used system. It is classified as a continuous-phase contacting reactor, whereby a gas and liquid phase are flowing concurrent or counter-current from each other (Figure 1.8).[57] The operation principle of the FFMSR, is based on generating a thin liquid film from a liquid feed, which then fall down onto a micro-structured plate containing parallel micro-channels. The thin liquid film thickness is about 15 µm, of which the plate has a corresponding specific interfacial area of up to 20 000 m^2 m^3. The micro-channels on the reactor plate range from 100 µm to 1200 µm, depths of 100 µm to 600 µm and the length that varies depending on the residence time required for the reaction.[93]

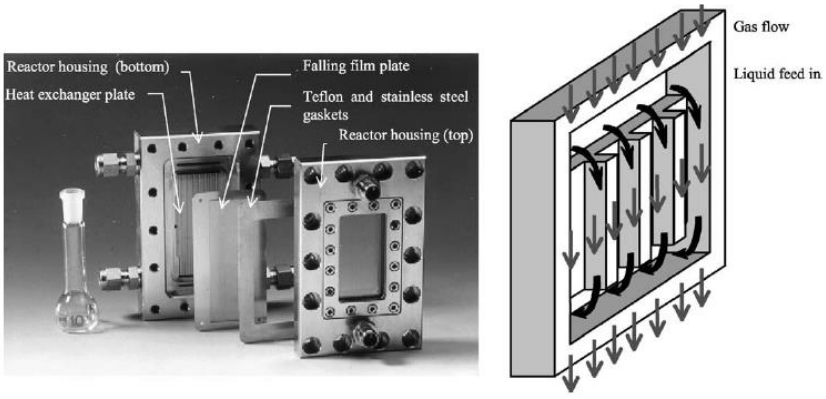

Figure 1. 8: Falling film micro-structured reactor[85]

The downward movement of the liquid results in parallel thin liquid films, which then stream down along the micro-channels.[57] Whilst the gas flows concurrently with the liquid through the open space that lies on the top cover of the reactor housing, the thin liquid films are then collected from the withdrawal zone, situated at the bottom of the reactor housing. The bottom housing section is equipped with the heat exchanger, which controls the fluid temperatures of the whole reactor.[93,94] The bottom housing section is followed by the micro-structured falling film plate, which is covered by Teflon and stainless steel gaskets. The top housing section comprises of the transparent glass that enables a clear view of the vertical micro-channels.[85,93]

The FFMSR is considered mostly for gas-liquid phase processes or catalysed gas-liquid phase reactions. In the gas-liquid phase reaction, the reaction takes place *via* a gaseous reactant diffusing into the liquid phase.[94] Whereas, in the catalysed gas-liquid phase reaction, a thin liquid

film is in contact with a solid catalyst layer coated on the vertical micro-channels of MSR plate. The large surface area in the micro-channels and the thin liquid falling film, ensure a rapid mass and heat transfer is achieved, while the reaction occurs *via* a laminar flow.[85] These reactor characteristics offer added advantage for highly exothermic reactions, whereby the generated heat at some stages in the reaction is removed continuously. Thus, resulting in a well-defined temperature profile over the reaction pathway.[54]

When conducting a liquid-liquid phase reaction, a number of reactor functions needs to be taken into consideration. Typically, the reactant components must be mixed efficiently, reaction space and time must be available, reaction heat must be dissipated and the phase interface must be available for multi-phase reactions.[95] The liquid-liquid mixing of reactants and the interfacial mass transfer are very important aspects when dealing with MSR. Unlike in conventional reactors where mixing of reactant components is carried-out by means of stirring, in order to increase an interfacial area between both phases. Mixing in MSR is realized through diffusion, whereby a longitudinal interface is created in between the flowing liquids. The large interfacial areas within MSR enable fast and efficient reactions as compared to conventional stirred reactions.[96] In addition, mixing of components in MSR is achieved in few seconds or even a few milliseconds.[95]

Similarly, as in a catalysed gas-liquid phase reaction, liquid-liquid phase reactions can be performed over a solid catalyst in FFMSR systems. In multi-phase reactions, a catalyst design and its integration within the reactor design are very crucial for product yield and selectivity. When designing a catalytic reactor, it is often important to take into consideration the factors that may influence the reaction. These include mass and heat transfer limitations, catalyst properties, fluid dynamics, flow regimes and pressure drops. Moreover, a catalyst design must be considered into three scale levels, namely nano-, micro- and macro-scale. However, these levels are not independent from one another, must be considered as an integrated approach in relation to the reactor design.[79]

1.5.1.3. Application of liquid-solid micro-structured reactors

In multi-phase reactions such as liquid-solid reactions, a benchmarked application of a FFMSR is in an array of reactions; typical examples of such reactions include nitration, oxidation, sulfonation, hydrogenation *etc*.[94] Some of these reactions are fast and highly exothermic. It is often important to control the temperature of such reactions.[96] In the case of reactions at higher

temperatures, it is recommended that the generated heat from the reaction must be removed continuously in order to obtain a product of high purity. In MSR, a well-defined flow profile is observed inside the reactor micro-channels. Thus, back mixing is suppressed and side reactions are avoided.[54] Consider the comparison between the continuous-flow fixed bed and micro-structured reactor as discussed below.

1.5.1.4. Intramolecular isomerisation reaction

The intramolecular isomerisation reaction of 1-hexene-3-ol **36** into 3-hexanone **37** has been reported (Scheme 16). The intramolecular isomerisation reaction was carried-out in a biphasic reaction. Wherein, *n*-heptane solvent, water and the substrate were co-fed simultaneously. The mixing of liquids was achieved by continuous pumping the substrate into an interdigital micro-mixer (IMM) and the product was analysed after flowing through a residence-time module (Figure 1.9).

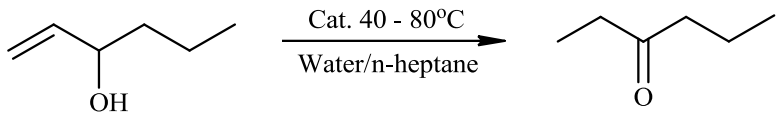

36 **37**

Conv. > 98%

Scheme 16: Intramolecular isomerisation reaction

The catalyst solution was injected in pulses *via* a commercial valve. The complete liquid mixing inside the micro-mixer was achieved within a residence time of 10^2 s, with only 1-2 µmol of catalyst being used. The results revealed 91-93% yield to 3-hexanone using an inorganic complex ($RhCl_3$-Tris(m-sulfonaphenyl)-phosphate) as catalyst. The effectiveness of the micro-system was observed through its ability to mix with the catalyst efficiency, although smaller catalyst amounts were used.[54,95,97]

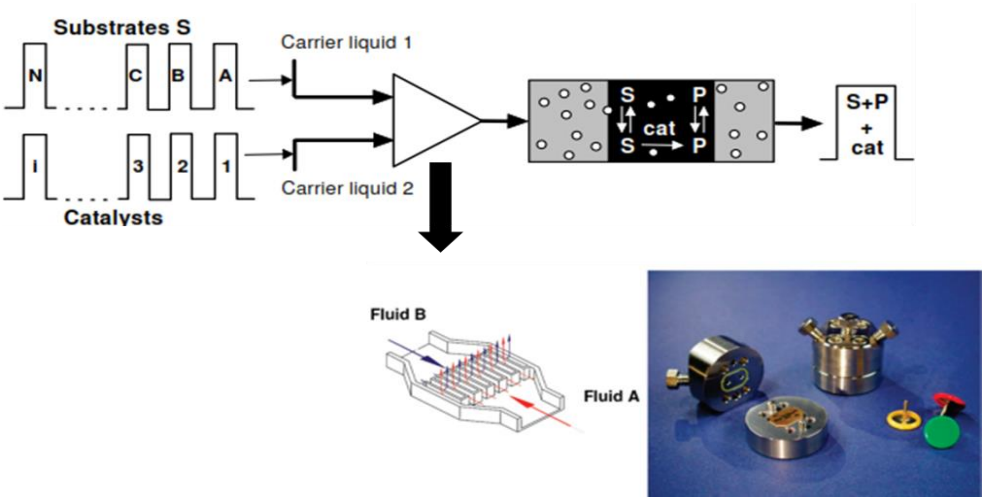

Figure 1. 9: High-throughput screening method

The extended scope of the above mentioned work was also performed by Bellefon *et al.* in the fixed-bed and MSR. The objective of their study was directed on the evaluation of the heterogeneous catalyst in both reactors. Their experimental results revealed that, the substrate conversion was equivalent in both reactors. They further explained that in the fixed-bed reactor flow singularities were observed and that resulted in greater residence time distribution (RTD). Nevertheless, good mass transfer was observed as compared to the MSR. In addition, an improved RTD was observed in the MSR, due to its micro-structuring of flow occurring in the micro-channels. However, poor mass transfer was observed when it was compared to the fixed-bed reactor performance.[76]

1.5.1.5. Esterification reaction

Esters **40** are prepared from the reaction of a carboxylic acid **38** or an acyl halide **39** and an alcohol (Scheme 17). Different types of acid or base catalysts are used during the synthesis. The reaction is carried-out in the presence of alcohol such as aliphatic (primary, secondary and tertiary), aromatic, polyol, cyclic allylic and acyclic allylic alcohols.[98-100] In the acylation reaction, high ester yields are achieved easily. In acylation reaction, the acid anhydride synthesis route is a better preference as compared to the acyl halide. Even though, the use of acyl halides results in high ester formation, however the synthesis route also leads to the large amount of toxic gas (hydrogen halide) being generated. As a result, it becomes a challenge to contain such corrosive substances, especially for the industrial production scale perspective. The carboxylic acid synthesis route has remained a method of choice in many in industrial processes and is regarded as environmentally friendly process.

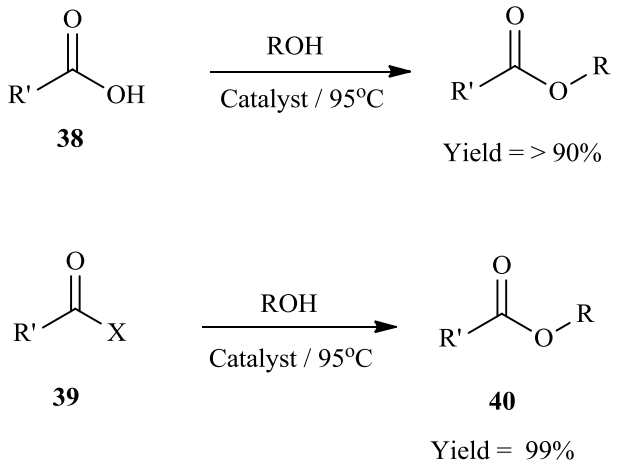

Scheme 17: Reaction paths for the esters synthesis

Short carbon chain esters are successfully prepared from the reaction of acetic acid and primary alcohols such as methanol, ethanol, *n*-propanol and *n*-butanol over acid catalysts. Although the esterification reaction is an equilibrium-limited reversible reaction high ester yields are achieved when one of the reactants is used in an excess amount. Alternatively, the Dean-Stark head is used to remove water (by-product) continuously as it formed.[101] In such cases a high boiling solvent, such as toluene, is generally used as a water entrainer.

The esterification reaction has been reported in the micro-structured reactors. Zhang *et al.* reported work in continuous-flow esterification process of acetic acid and short chain alcohols. In their studies, a quartz capillary micro-channel reactor (I.D: 0.25 and 0.53 mm and a length of 2.5 m) was used. *p*-Toluene sulphonic acid (PTSA) was employed as homogeneous catalyst. The catalyst was dissolved in acetic acid and mixed with the alcohol at a given molar ratio. The solution was transferred into a syringe pump and introduced into the micro-channel of the reactor. Their results revealed that, the micro-channel had a strong influence on the ester formation. The increase in catalyst dosage also found to alter the ester selectivity. Their conversions were ranging from 74, 70, 97, and 92% for the methyl-, ethyl-, *n*-propyl- and *n*-butyl acetates respectively.[102]

1.6. In-line analysis integrated to continuous flow reactors

Historically chemists would conduct a reaction and only analyse the product after reaction workup. Recent research has shown that sensor devices may be incorporated in the micro reactor systems. These devices allow one to monitor the chemical reaction occurring inside of the

reactor. Several types of sensor devices have been used for this purpose, namely thermal flow, impedimetric sensors *etc*.[103] The technology of microfluidics has advanced further to fluorescence-based methods. These sensor devices are meant for small-volume detection, due to their exceptional sensitivity and low mass detection limit.[104]. However, the fluorescence based methods are only limited to the reactions that produces coloured species and are not really that useful for organic chemistry applications.

On the other hand, other methods such as Raman (coherent anti-stoke and surface-enhanced), flow-NMR and Infrared spectroscopy were implemented for chemical analysis in these micro-fabricated devices. Among these methods, Fourier Transform Infrared (FT-IR) spectroscopy has remained a method of choice for chemical imaging.[105] The FT-IR imaging device uses a highly sensitive multi-pixel detector or focal plan array (FPA). Wherein, multiple reactant and product components are easily detected simultaneously. During the analysis of the chemical reaction, the IR detector detects the intrinsic molecular vibrations of chemical species and result in a measured spectrum. This detector consists of up to 16 384 pixels, that allow thousands of specially resolved infrared spectra to be collected. As a result, the collected spectra are used to generate various chemical maps to represent a special distribution of a particular component in the system. Nevertheless, the method is still unable to eliminate a photo-degradation and photo-bleaching issues, due to the low energy of infrared.[104,105]

A typical benchmark reaction has been reported, whereby the reactant species were detected by the FT-IR imaging device. The reaction involves the neutralization reaction of benzoic acid **41** with disodium hydrogen phosphate (Na_2HPO_4) **42** (Scheme 18). In this process, two liquid phase flow methods such as laminar and segmented flow have been used for the study. The FT-IR spectroscopic imaging device (IFS66s, Bruker Optics) was used to generate the chemical images, and was obtained from Germany.

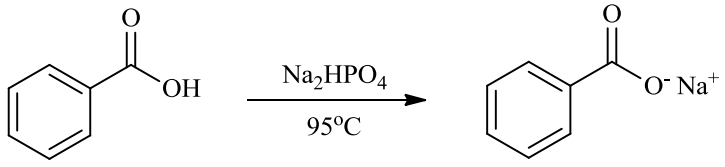

41 **42**

Scheme 18: Reaction of benzoic acid and disodium hydrogen phosphate

The Na_2HPO_4 solution was prepared by dissolving the Na_2HPO_4 powder into deionized water. A similar procedure was used for the preparation of benzoic acid solution, although decanol was used as a solvent. The laminar flow was realized by the use of T-junction to combine the two phase solution, whilst a nozzle was used to generate a segmented flow (Figure 1.10).

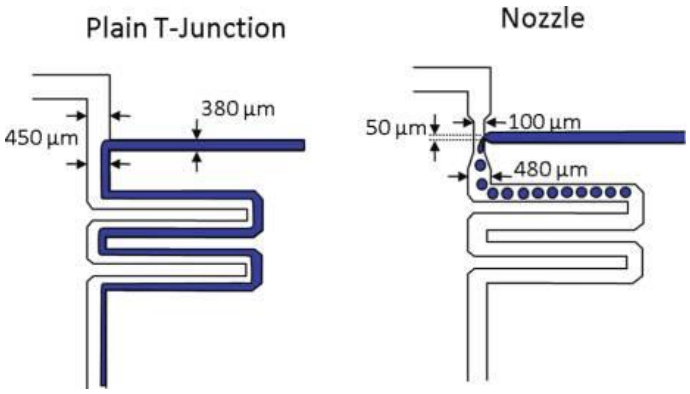

Figure 1. 10: Plain T-junction and Nozzle flow profiles[105]

The results showed that the FT-IR imaging device was able to capture the chemical images in both flows. Meaning, a clear view of the neutralization reaction was able to be monitored in both systems. The laminar flow was observed to be diffusion limited. Nevertheless a high reaction rate was achieved in the segmented flow. The determining factor between these systems, was a better mixing in the nozzle flow.[105]

Apart from the FT-IR imaging device, the ReactIR™ (Mettler Toledo) system are also widely used as advanced device to monitor the short-lived reactive intermediates.[106] The efficacy of this new device has been demonstrated by using a Paal-Knorr reaction of 2,5-hexadione **43** and ethanolamine **44** in dimethyl sulfoxide (DMSO) to perform a continuous monitoring the effluent from a silicon micro-reactor in pyrrole **45** synthesis (Scheme 19).

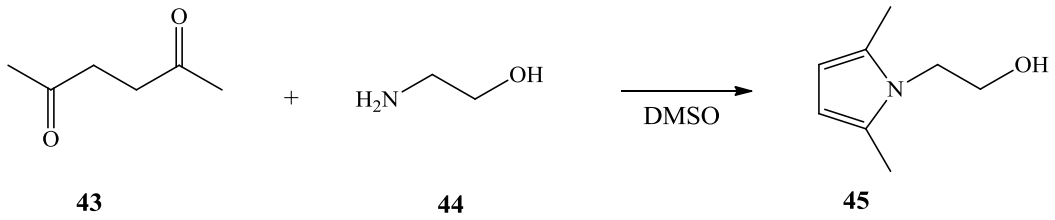

43 **44** **45**

Scheme 19: Paal-Knorr reaction

The Mettler Toledo ReactIR iC 10 fitted with DiComp ATR 10 µL flow cell is employed for continuous monitoring of reactions. This device functions by recording an average of 30 spectrum scans from an online reaction, wherein the recorded data is saved to an excel file once

every 15 seconds. The Labview software (version 8.5.1) is then used to establish a communication between a computer, syringe pumps and temperature controller. The Mettler Toledo ReactIR device further reads the excel report file and determine the reaction conversion of the substrate based upon calibrations of peak heights. On the other hand, the reaction temperature set points and pump flow-rates are controlled by the Matlab scripts (version 2010b) within Labview.[107] This newly developed technique is mostly used to monitor the reactions that occurs in the small fabricated devices and has proven to provide a better mechanistic understanding of the reacting species.

On the other hand, an integrated synthetic flow platform incorporating in-line NMR, as to characterise and monitor the reaction at the milli-fluidic scale has been introduced recently. The reactor design comprises of the NMR (Spinsolve from Magritek), which utilises the compact permanent magnet (43 MHz) based on the Hallbach design. The magnet is optimised to maximum sample volume, which makes it possible to work with standard 5 mm NMR tubes. Its cavity is perfect to accommodate the fluorinated polytetrafluoroethylene (PTFE) tubing, in order to permit the follow through of the reaction mixture to the core of the device. Besides the low field of the magnet, Spinsolve is characterised with an extraordinary sensitivity and stability, which allows acquiring spectra from several different nuclei such as ^{1}H, ^{13}C and ^{19}F (Figure 1.11).

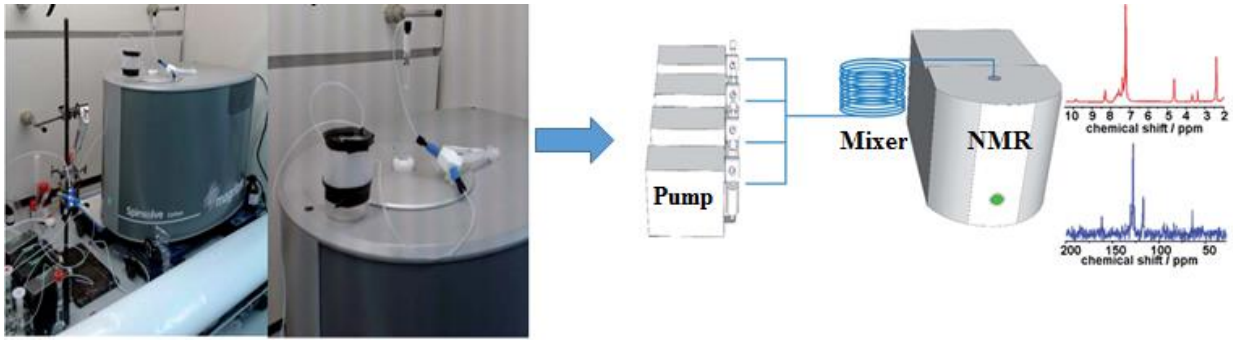

Figure 1.11: Flow-NMR platform[108]

The reactor design consists of a set of programmable syringe pumps (C3000, tricontinent) controlled though LabView software. The pumps are linked to the micromixer *via* a standard Omnifit 1/16″ O.D tubing and standard connectors. The tubular reactor made of (1/16″ OD, 0.8 mm I.D and 1/8″, 1.5 mm I.D) of different lengths depending on the reaction residence time was used. During the reaction, a 1:1 reagent mixture is ensured by controlling the flow-rate as to afford the controlled residence time before reaching the sensor. The condensation reaction

between benzylaldehyde **46** and benzylamine **47** to yield the corresponding imine, *N*-benzylidenbenzylamine **48**, was used as a proof of concept and as a configuration for the in-line NMR. (Scheme 20).[108]

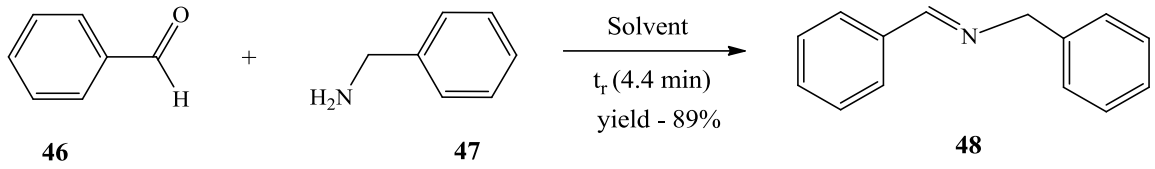

Scheme 20: Synthesis of *N*-benzylidenbenzylamine

In the course of the reaction, the flow rates of the reacting species were adjusted to ensure full magnetisation of the reaction mixture was observed before it reached the detector. Moreover, the correct residence time was achieved to afford a well-defined section of solution was reaching the detector from each acquisition pulse. The reacting species were dissolved in NaOH solution to produce 1M solution. Both solutions were pumped in a 1:1 molar ratio. It must be mentioned that the Spinsolve is able to function without the use of deuterated solvent. Therefore, this method results in a cost effective process, eliminates the isotopic effect and leads to the real working conditions. The reactor system has showed consistent results under flow employing 3D-printed milli-fluidic devices. The NMR demonstrated advantages as compared to other methods like FT-IR (discussed above), in a sense that the observed signals were found to be proportional to the analyte. Therefore, this ensures an easy way to calculate the conversion and yield, without the additional need for calibration or correction.[108]

1.7. Problem statement, research hypothesis and objective of the study

The first objective of the work described in this thesis, is to optimise the batch synthesis method of the isopulegyl ether-ester derivatives. The optimisation process will be carried-out in a continuous flow fixed-bed reactor. Below is a research hypothesis statement to be tested:

Ether-ester derivatives of isopulegol can be conveniently synthesised via a single continuous-flow process by using a fixed-bed reactor system.

To prove the above hypothesis statement is *true* or *false*, a baseline study will be conducted as to enable a direct comparison with conventional methods. The baseline studies will be based on the following objectives:

- To develop a continuous flow process for the synthesis of isopulegol from citronellal, identify the suitable catalyst for the reaction and deduce the optimum reaction conditions for the process.

- Investigate the continuous flow synthesis of isopulegyl-ethers from isopulegol, identify a suitable catalyst and deduce the optimum reaction for the process.

- To study the continuous flow synthesis of isopulegyl ether-ester, identify a suitable catalyst and deduce the optimum reaction conditions for the ether-ester formation.

- Combine all the above mentioned reaction steps into a single continuous-flow process.

- Investigate the batch-scale synthesis for the di-ester derivatives of *para*-menthane-3,8-diol and determine the optimum conditions for the process.

- Furthermore, optimise the developed batch-scale process using a continuous flow process *via* a use of microwave-assisted continuous flow reactor system.

CHAPTER 2

Experimental

2.1. Reagents and chemicals

All reagents used during the investigation are tabulated below (Table 2.1 and 2.2). This includes the suppliers and the respective grades. The reagents were used as received without further purification.

Table 2.1: Organic reagents

Chemical Name	Formula	Source	Grade	Purity (%)
Citronellal	$C_{10}H_{18}O$	Germany	-	-
Isopulegol	$C_{10}H_{18}O$	Lab prepared	-	95
para-Menthane-3,8-diol	$C_{10}H_{20}O_2$	Lab prepared	-	99
Dimethylformamide	C_3H_7NO	UniLAB	Ar	99.5
Tetrahydrofuran	C_4H_8O	Merc	Ar	99
Methanol	CH_4O	Merc	Ar	99.9
n-Propanol	C_3H_8O	Sigma-Aldrich	Ar	99
Ethyl acetate	$C_4H_8O_2$	Merc	Ar	98
Hexane	C_6H_{14}	Sigma-Aldrich	Ar	95
Acetone	C_3H_6O	Merc	C.P	-
Acetic anhydride	$C_4H_6O_3$	UniLAB	Ar	97
Propionic anhydride	$C_3H_6O_2$	Sigma-Aldrich	Ar	>99.5
Valeric anhydride	$C_5H_{10}O_2$	Sigma-Aldrich	Ar	99
Hexanoic anhydride	$C_6H_{12}O_2$	Sigma-Aldrich	Ar	99

Table 2.2: Inorganic reagents

Chemical Name	Formula	Source	Grade	Purity (%)
P-S Scandium triflate	PS-$Sc(OTf)_2$	Sigma-Aldrich	R&D	R&D
Sulphuric acid	H_2SO_4	Sigma-Aldrich	Ar	99
Amberlyst-15 dry	-	Sigma-Aldrich	R&D	-
H-beta Zeolite	-	Sued-Chemie	R&D	-
H-ZSM-5	-	Sued-Chemie	R&D	-
Aluminium oxide	Al_2O_3	Fluka chemical	Ar	-
Al-pillared clay	-	Fluka chemical	R&D	-
Nitric acid	HNO_3	Sigma-Aldrich	Ar	70
Hydrogen peroxide	H_2O_2	Sigma-Aldrich	Ar	35

2.2. Analytical procedures

The analyses of product mixtures were performed according to the procedures that are described below:

2.2.1. Gas chromatography

The GC samples were prepared by diluting one part of the product mixture with four parts of the appropriate reaction solvent. The prepared mixtures were then injected in the Agilent Gas chromatograph, equipped with a flame ionization detector. The Econocap-5 column (film thickness 0.25 µm; internal diameter 0.25 mm; length 30 m) was used for the separation of the components. Agilent ChemStation software was used for the recording and integrating of chromatograms. The instrument was programmed to the following conditions (Table 2.3).

Table 2.3: GC instrument conditions for the analysis

Instrument components	Conditions
FID temperature	300 °C
Carrier gas	N_2
Carrier gas flow	0.5 mL/min
Injector temperature	270 °C
Initial column temperature	70 °C
Initial hold-up time	5 min
Column ramp rate	10 °C/min
Final column temperature	270 °C/min
Final hold-up time	5 min
Run time	30 min

2.2.2. GC-MS analysis

The samples for GC-MS analysis were prepared in similar manner as stated above. The GC-Mass spectrometer was performed on a HP F5890 series LL plus gas chromatograph coupled to an HP 5972 series mass selective detector. The GC was equipped with a HP-5 MS capillary column (30 mm x 0.25 mm I.D). The mass spectra were recorded on a Trace Mass-Spectrometer. The GC-MS spectra were obtained by using a chemical ionisation (C.I.) (using helium as reagent gas) techniques. The Hewlett Packard personal computer was equipped with HP 61034 software and was used for data recording and analysis. The instrument column oven was programmed on the following conditions (Table 2.4).

Table 2.4: GC-MS instrument conditions for the analysis

Instrument components	Conditions
FID temperature	280 °C
Carrier gas	Helium
Carrier gas flow	0.1 mL/min
Injector temperature	250 °C
Initial column temperature	70 °C
Initial hold-up time	5 min
Column ramp rate	10 °C/min
Final column temperature	280 °C/min
Split flow	60 mL/min
Run time	30 min
MS-mass range	30 -550 amu

2.2.3. Nuclear magnetic resonance spectroscopy

Nuclear magnetic resonance (NMR) spectra were recorded as solutions in deuterochloroform. The spectra were recorded on a Bruker Ultrashield Plus spectrometer, which was operated at 400 MHz. The chemical shift values for all spectra are given in parts per million (ppm) with coupling constants in Hertz (Hz).

2.2.4. Fourier transform infrared spectroscopy (FTIR)

FT-IR characteristic peaks were recorded on a Bruker Platinum Tensor 27 spectrophotometer with an ATR fitting. The analysis of samples were recorded in the range 4000-600 cm^{-1} and the peaks are reported (υ_{max}) in wavenumber (cm^{-1}). The solid and liquid samples were analysed without modification.

2.2.5. Flash point, viscosity and density

Flash point is the lowest temperature at which a substance is ignited by the test flame. The flash points of the products were measured using a Miniflash FLPH (Grabner Instruments). Viscosity and density of the final products were recorded on a FLPH Viscometer and a pocket refractometer PAL-3 was used to measure the refractive indices of the products.

2.2.6. ICP-MS analysis method

The leaching of scandium metal from the polymer-supported scandium triflate (PS-Sc(OTf)$_3$) catalyst was determined by the use of an Element 2 ICP–SMS (Thermo Fisher Scientific ICP-MS, Bremen, Germany). The instrument is equipped with a guard electrode used to eliminate the second discharge in the plasma and to enhance the overall sensitivity. The quantification of the traces of scandium from the organic samples was determined by the use of micro volume auto-sampler (ASX 100, Cetac Technologies, Omaha, NE, USA). The sample introduction kit comprising a microflow PFA nebulizer connected either to a PEEK micro cyclone spray chamber arrangement and a sapphire injector tube were used. To reduce the risk of contamination by the peristaltic pump tutting, the low PFA nebulizer was operated in the self-aspirating mode. The further instrument details and the analysis specifications that were used in this method can be found elsewhere.

2.2.6.1. Sample preparation procedure for ICP-MS analysis

During the sample preparation, 1.0 gram of each sample was weighed into two separate 250 mL of volumetric flasks (reactors). Wherein, 9 mL of nitric acid was added in each of the reactors to facilitate the sample digestion. Furthermore, 2 mL of hydrogen peroxide was also added to the solution in order to enhance the oxidation properties of nitric acid. The reaction was allowed to reactor for a minute at room temperature with continuous stirring. The reaction temperature was further heated to 180^{0}C for 10 minutes and allowed to digest for an hour. The obtained solutions was cooled to room temperature and diluted with ultrapure water to an acid content below 5%. The solution was filtered and labelled samples were taken for the ICP-MS analysis.

2.2.7. Purification methods of the prepared compounds

The desired compounds were purified by vacuum distillation to remove the unreacted starting material and by-products. After the distillation process, the isolated compounds were further purified by using column chromatography if necessary. Wherein, Sigma-Aldrich silica gel 60

was used as a solid support. The mobile phase was made from a solvent mixture of hexane and ethyl acetate.

2.3. Continuous-flow synthesis of isopulegol

2.3.1. Experimental

2.3.1.1. Reactor system set-up

The continuous-flow synthesis of isopulegol was carried-out in a homemade tubular fixed-bed reactor made from ⅜th inch stainless steel tubing. The reactor (I.D: 9.53 mm and length: 120 mm), was packed with H-ZSM-5 catalyst (6.0 g) extrusions. At the terminal ends of the reactor column, 9.53 mm to 6.35 mm reducers (Swagelok) were used to connect the reactor to the ¼ inch tubing. The reactor was placed in the middle of the tubular furnace (Eurotherm). A semi-preparative HPLC pump was used to pump the substrate through the packed column. The tube-in-tube heat exchanger (detailed below) was used to condense the product mixture before exiting the reactor (Figure 2.1).

2.3.1.2. Tube-in-tube heat exchanger

The tubular fixed-bed reactor also has the option to cool down products before they exit the reactor system. The tube-in-tube heat exchanger consists of a 3.178 mm (OD) tube encased by a 6.35 mm (OD) (Swagelok) stainless steel tube and is approximately 0.5 m long.

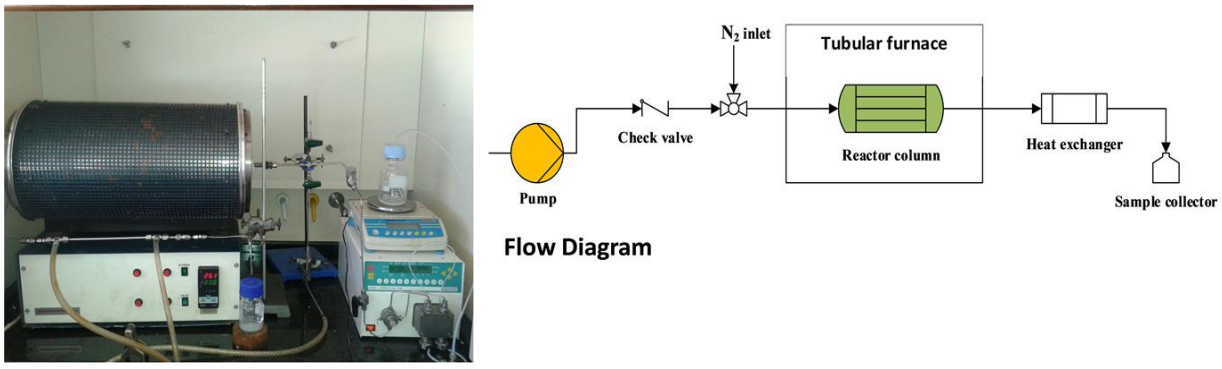

Figure 2.1: Conventional tubular fixed-bed reactor

The summary of the key reactor specifications are tabulated below (Table 2.5).

Table 2.5: Tubular fixed-bed specifications

Reactor specifications	Properties
Reactor type	Tube reactor
Dimensions	9.53 mm x 120 mm (stainless steel)
Reactor volume	8559.7 mm^3
Maximum operation temperature	1100^0C
Catalyst type	H-ZSM-5 extrudates

2.3.1.3. Synthesis of isopulegol

In the tubular fixed-bed reactor system (Figure 2.1), the solvent-free citronellal **19** feed was pumped through the packed bed reactor column containing 6 g of the activated H-ZSM-5 catalyst. Before the reaction was commenced, the catalyst was activated by drying at 110^0C for an hour and subsequently calcined at 350°C, while purging with nitrogen for 12 hours. During the cyclisation reaction, the reaction was carried-out at the following conditions; temperature range (80–100°C) and flow-rate range (0.1–0.5 mL/min), which afford the residence time range (1.4–0.29 hours). The sample mixtures were collected at the reactor exit for GC analysis (Scheme 21).

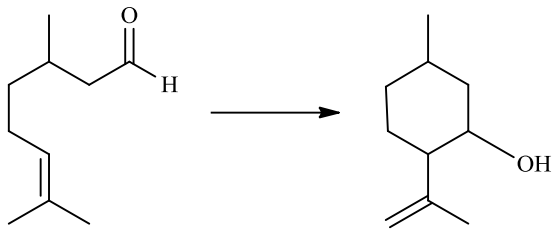

19 **22**

Scheme 21: Citronellal cyclisation process to afford isopulegol

The collected product samples were quantified by the gas chromatography. From the GC-trace, the isopulegol peak was observed to elute at a retention time of 11.7 minutes. Whereas, the citronellal starting material was observed at retention time of 10.3 minutes (see Figure 3.3). The isopulegol peak was further confirmed by the GC-MS (Figure 3.4). Other analytical techniques namely ^{1}H-NMR, ^{13}C-NMR and FT-IR were used to gather the conclusive characterisation data of the compound as shown below. **Isopulegol (22):** ^{1}H-NMR (400 MHz, $CDCl_3$, ppm) δ 0.85-0.93 (7H, m), 1.16-1.27 (6H, m), 1.28 (4H, s), 1.33-1.35 (4H, m), 1.57-1.65 (2H, m) and 5.06 (1H, s). ^{13}C-NMR (100 MHz, $CDCl_3$, ppm); δ = 17.6, 19.8, 25.3, 25.6, 27.7, 36.9, 50.9, 124.0 and 131.6. FT-IR (cm^{-1}): 3401, 2922, 1708, 1645, 1454, 965 and 933. *m/z* (C.I.) 154 (M^+, 1), 136

(100), 121 (80), 93 (60), 79 (60) and 59 (98). The raw data for the prepared isopulegol is shown in Appendix A1.

2.4. UniQsis FlowSyn design and isopulegyl-ether synthesis

2.4.1. Experimental

2.4.1.1. UniQsis continuous flow reactor system

UniQsis FlowSyn is a fully integrated and easy to use continuous-flow reactor system. The reactor system is used for the optimisation of synthesis reactions in continuous-flow processes. In addition, it is also used to scale-up reactions ranging from small volume, as in mg, to the larger volume as in grams (Figure 2.2).

Uniqsis continuous-flow reactor system

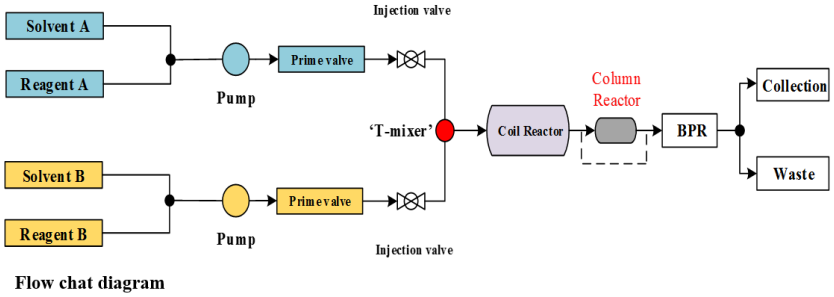

Flow chat diagram

1) prime valves and pressure transducers 2) High pressure pump 3) Back pressure regulator (PBR) 4) Waste collection bottle 5) Column reactor 6) User interface 7) Control pane 8) Coil reactor tensioning knob 9) Sample injection valve, 10) sample bottle

Figure 2.2: UniQsis FlowSyn reactor system

2.4.1.1.1. Prime valves and transducers

The system contains high pressure pumps that require priming with solvent before use. The reagent and solvent inlet line are primed independently from each other. The priming process is easily achieved by attaching a syringe to the prime valve situated on top of the instrument. This is followed by twisting the knob to open the valve and push the solvent through the valve. However, the valve must be closed before running the pumps to avoid air from entering the reagent lines. The reagent inlet line requires being primed up to the inlet valve and the solvent inlet should be used to prime the pump head. Only 2 mL of solvent can be pulled

through the pump head to ensure thorough priming. The priming can be done three times to ensure the gas bubbles are removed from the reagent line and on the pump head.

2.4.1.1.2. High pressure pump and back pressure regulator

The system is fitted with two high pressure pumps. The pumps are modified internally to offer high resistance to chemicals. The pumps can go down to a flow-rate of 0.02 mL/min to 10 mL/min and give a total flow-rate of 20 mL/min. The reactor system also contained a back pressure regulator (BPR). The capacity of the back pressure regulator can be varied by fitting different cartridges, ranging from 40–1000 psi. These cartridges are colour coded to denote a break pressure (i.e. green = 1, 000 psi (69 bar)).

2.4.1.1.3. Column and coiled reactors

The *column reactor unit* is designed to hold and heat a column 15 mm in diameter. The column heater has a heating element and pre-installed temperature probe, which are configured to be slightly hotter than the set temperature. This ensures that the temperature inside the column is in fact the set temperature. The reactor maximum temperature for the column is 150°C. Above these conditions, it is not recommended to use standard columns (with the white end pieces) above 110°C, however, the HT column with PEEK (brown) fitting can be used if needed (Figure 2.3).

Figure 2.3: Column reactor unit and reactor column

The *coil reactor* functions similarly as the column reactor. It also contains a heating element and temperature sensor. It is used to heat a coiled reactor and it consists of tubing wound in a helical groove on an aluminium former. The coiled reactor is available in different range of pre-wound sizes, which are easily fitted and removed from the heating module.

2.4.1.1.4. Sample injection valve and user interface

The reactor system is also fitted with high chemical resistance, electrically operated sample injection valves. The valves permit the introduction of reagent solution into the flow stream from the sample loops. They benefit from the enlarged internal flow paths that make the valves prone from blocking. PTFE (1mL) sample loops are fitted as standard. Moreover, any size of sample loop can also be fitted as desired. The system is easily controlled by the use of a user interface. The user interface panel made up four buttons: down and up arrows, escape and enter buttons. The up and down arrow buttons are used to scroll through the parameters on the screen. However, the escape button allows you to leave the page being viewed. By repeatedly pressing the escape button will stop the system. The enter button allow you to open a parameter setting, which can be changed by using an up and down arrow buttons.

2.4.1.2. Continuous-flow synthesis of isopulegyl-ether

In the UniQsis FlowSyn reactor system, homemade stainless steel reactor column (I.D: 9.53 mm and length: 120 mm) was packed with amberlyst-15 dry catalyst (1.0 g). The packed reactor tube was attached to the reactor system. A substrate solution of isopulegol (30.0 g, 0.195 mol) in *n*-propanol (23.4 g, 0.39 mol) (3.1M solution) was prepared in a 250 mL sample bottle. In this case, *n*-propanol was used as a reagent and the solvent in the reaction. The prepared solution was pumped into the packed-bed reactor, at the following reaction conditions; temperature range (50–90°C) and flow-rate range (0.1–0.3 mL/min), which afford the residence time range (1.4–0.29 hours). The reaction pathway for the synthesis of isopulegyl propyl-ether **49** is shown below (Scheme 22).

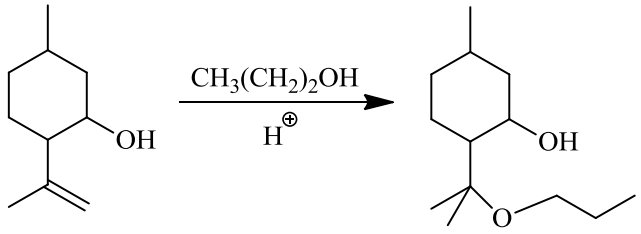

22 **49**

Scheme 22: Synthesis of isopulegyl propoxy-ether

The collected product mixtures were quantified by the GC and the peak was confirmed by the GC-MS. From the GC-trace, the peak that corresponded to the desired compound **49** was observed at the retention time of 17.3 minutes (see Figure 3.5). Other analytical techniques were

used for the further confirmation and results obtained are listed as follows: **Isopulegyl propoxy-ether (49):** ^{1}H NMR (400 MHz, $CDCl_3$, ppm); δ = 0.83-0.85 (6H, m), 3.24-3.38 (2H, m), 3.58 (1H, dt, *J* = 4.3). ^{13}C NMR (100 MHz, $CDCl_3$, ppm): δ = 10.6, 19.9, 24.1, 22.0, 23.5, 26.6, 30.9, 34.7, 43.9, 51.1, 62.5, 72.0 and 80.4. FT-IR (cm^{-1}): 3585, 2900, 1456 and 1053. *m/z* (C.I.) 256 (M^+, 1), 199 (2), 155 (15), 139 (10), 101 (100), 72 (85) and 59 (100).[26]

2.5. Batch-scale synthesis of *para*-menthane-3,8-diol (PMD)

2.5.1. Experimental

2.5.1.1. Batch-scale reaction

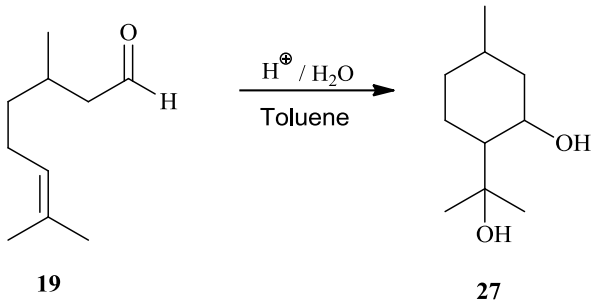

19 **27**

Scheme 23: Synthesis of *p*-Menthane-3,8-diol

The batch-scale synthesis of *para*-menthane-3,8-diol (PMD) was carried-out using a 500 mL three-neck glass reactor. The reactor flask was attached to the condenser, which was fitted with calcium chloride guard tube. A magnetic stirrer bar was inserted into the reactor flask for agitation. The oil bath temperature and stirring rate were controlled by means of magnetic stirring hot plate (Figure 2.4). Into the glass reactor flask, the dilute sulphuric acid (140 ml, 0.0076 mol of a 0.3% (v/v)) solution was transferred and allowed to equilibrate until the solution reached to the desired reaction temperature of 100°C. Citronellal (30.08 g, 0.193 mol) was added into the reactor as a single batch. The reaction was allowed to equilibrate at the reaction temperature, while agitated at the stirring rate of 5 rpm (Scheme 23). The reaction was followed by taking samples at hourly time intervals for GC analysis. The reaction was allowed to proceed for the pre-determined length of time (4 hours).[109]

Upon the completion of the reaction, the reactor contents were transferred into the separating funnel and the aqueous phase was separated from the organic phase. The organic phase was neutralised with 50.0 ml of a 2.5% (v/v) sodium hydrogen carbonate ($NaHCO_3$) solution to remove the remains of sulphuric acid catalyst. The organic layer distilled under vacuum (115°C

and 8 mBar) to recover the unreacted citronellal **19** and isopulegol **22** products. PMD was recovered as a thick viscous oil. The obtained product was further purified by crystallization in *n*-hexane at -18 °C for 24 hours. The white crystals of **27** formed were filtered under vacuum, washed with ice cold *n*-hexane (50 mL) and air dried at 25°C.

Figure 2.4: Batch-scale reactor set-up

The obtained white crystals were quantified by the gas chromatography and the **27** peak was observed at the retention time of 15.0 minutes (see Figure 3.13). The PMD peak was further confirmed by the GC-MS (Figure 3.14). ***p*-menthane-3,8-diol (27):** (96 %), ^{1}H NMR (400 MHz, $CDCl_3$, ppm); δ = 0.84-0.86 (6H, m), 0.89-0.90 (2H, m), 0.90 (2H, d, *J* = 24 Hz), 1.13 (6H, s), 1.30 (3H, s), 1.65-1.92 (11H, m), 3.8 (3H, m), 4.40 (1H, s). ^{13}C NMR (100 MHz, $CDCl_3$, ppm): 20.3, 22.2, 25.5, 28.9, 34.9, 42.5, 48.2, 67.9, and 73.2. FT-IR (cm^{-1}): 3220, 2941, 2911, 1158 and 931. *m/z* (C.I.) 172 (M^+, 1), 157 (9), 139 (20), 96 (50), 81 (100) and 59 (90); GC R_T = 15.0 min. The raw data of PMD analysis is shown below (Appendix A2).

2.6. Synthesis of *para*-menthane-3,8-diol ester derivatives

2.6.1. Experimental

2.6.1.1. General batch-scale procedure for the synthesis of di-ester derivatives

In the batch-scale reactor (Figure 2.3), the acylation reaction of PMD with acid anhydride was carried-out. The PMD (5.0 g, 0.029 mol) and appropriate acid anhydride (0.0871 mol, 2 equivalents) were transferred into the reactor concurrently. Both reagents were stirred and heated at 60°C at reflux for 10 minutes after which 0.3 g of polymer-bound scandium triflate (PS-

$Sc(OTf)_3$) catalyst was added into the reaction mixture (Scheme 24). The reaction was heated to reflux for 24 hours, while followed by sampling at an hourly time interval. Upon the completion of the reaction, the catalyst was separated from the product mixture by filtration and the acid by-product was removed by distillation. The obtained crude sample was concentrated *in vacuo* and the residue was purified by column chromatography Hexane/EtOAc (98:2).

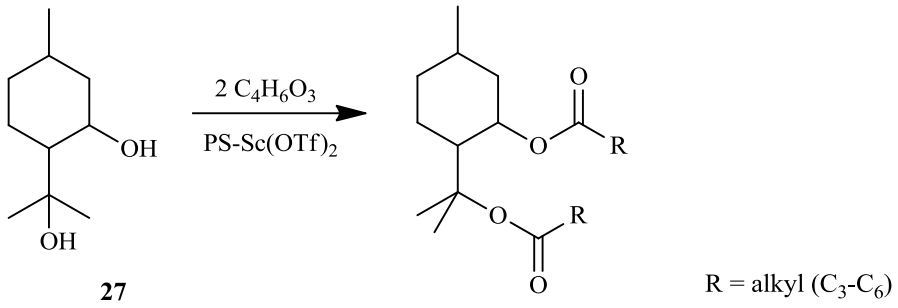

Scheme 24: Acetylation of *para*-menthane-3,8-diol

The samples were quantified by the gas chromatography and confirmed by the GC-MS, ^{1}H-NMR, ^{13}C-NMR and FT-IR. Other di-ester derivatives of **27** were prepared by the same method. The corresponding data of the prepared di-ester compounds is listed below and the raw data is shown in Appendix B.

Di-acetate (**50):** (6. 8 g, 91 %), ^{1}H NMR (400 MHz, $CDCl_3$, ppm); δ = 0.79 (3 H, d, *J* = 6 Hz), 0.89-1.05 (2H, m), 1.33-1.36 (6H, m), 1.53-1.60 (3H, m), 1.71-1.74 (1H, m), 1.81-1.85 (1H, m), 1.97 (3H, s), 1.89 (3H, s), 2.03-2.09 (1H, m). ^{13}C NMR (100 MHz, $CDCl_3$, ppm): 21.4, 21.9, 22.2, 22.3, 24.0, 25.1, 26.6, 34.6, 39.4, 47.3, 69.8, 84.2, 169.9 and 170.3. FT-IR (cm^{-1}): 2949, 1728, 1180 and 1144. *m/z* (C.I.) 256 (M^+, 1), 197 (78), 137 (71), 95 (62) and 81 (100); GC R_T = 17.8 min.

Di-propionate (51): (8.04 g, 97 %), ^{1}H NMR (400 MHz, $CDCl_3$, ppm); δ = 0.79 (3H, d, *J* = 6 Hz), 0.90-0.96 (1H, m), 0.99-1.09 (6H, m), 1.35 (5H, m), 1.50-1.61 (3H, m), 1.71-1.74 (1H, m), 1.82-1.86 (1H, m), 2.04-2.07 (1H, m), 2.14-2.28 (4H, m), 5.19 (1H, m). ^{13}C NMR (100 MHz, CDCl3, ppm): 9.2, 22.0, 22.1, 24.1, 25.2, 26.7, 28.1, 28.8, 34.7, 39.5, 47.6, 50.0, 69.7, 84.1, 173.4 and 173.9. FT-IR (cm^{-1}): 2946, 1728, 1169 and 1143. *m/z* (C.I.) 284 (M^+, 1), 211.4 (10), 136 (22), 81 (23) and 57 (100); GC R_T = 19.8 min.

Di-pentanoate (52): (10.2 g, 95%), ^{1}H-NMR (400 MHz, $CDCl_3$, ppm); δ = 0.79 (3H, d, *J* = 6 Hz), 0.84-0.85 (6H, m), 1.25-1.28 (5H, m), 1.35 (6H, m), 1.48-1.56 (7H, m), 1.71-1.74 (1H, m), 1.83-1.86 (1H, m), 2.03-2.06 (1H, m), 2.13-2.23 (4H, m), 5.10 (1H, m). ^{13}C NMR (100 MHz,

$CDCl_3$, ppm): 13.6, 13.7, 14.05, 22.2, 22.2, 22.3, 24.1, 24.6, 24.6, 25.1, 26.7, 27.0, 27.1, 47.4, 47.6, 69.7, 84.1, 84.3, 172.9 and 173.2,. FT-IR (cm^{-1}): 2954, 1727, 1169 and 1143. *m/z* (C.I.) 341 (M^+, 8), 281 (27), 207 (30), 93 (18), 85 (47) and 73 (100); GC R_T = 22.5 min.

Di-hexanoate (53): (10.4 g, 97%), 1H-NMR (400 MHz, CDCl3, ppm); δ = 5.20 (1H, m), 0.80-0.84 (9H, m), 0.92-1.07 (2H, m), 1.21-1.26 (8H, m), 1.37 (6H, d, *J* = 3 Hz), 1.51-1.62 (4H, m), 1.73-1.76 (1H, m), 1.84-1.88 (1H, m), 2.06-2.06 (1H, m), 2.18-2.26 (4H, m). ^{13}C NMR (100 MHz, $CDCl_3$, ppm): 13.8, 13.8, 21.9, 22.2, 22.3, 24.1, 24.6, 24.6, 25.1, 26.7, 31.2, 31.3, 34.7, 34.8, 35.5, 39.5, 47.5, 69.6, 77.4, 84.0, 172.6 and 173.1. FT-IR (cm-1): 2952, 1728, 1128 and 1107. *m/z* (C.I) 369 (M^+, 1), 253 (27), 136 (34) and 99 (100); GC R_T = 26.4 min.

2.6.1.2. General procedure for the batch-scale synthesis of mono-ester derivatives

In the batch-scale reactor (Figure 2.3), the acylation reaction of PMD with the relevant acid anhydride was carried-out. PMD (5.0 g, 0.029 mol) and acid anhydride (0.0436 mol, 1.5 equivalents) were transferred into the reactor concurrently. Both reagents were stirred and heated at 60^0C in refluxing for 10 minutes after which 0.3 g of polymer-bound scandium triflate (PS-$Sc(OTf)_3$) catalyst was added into the reaction mixture (Scheme 25). The reaction was allowed to reflux for 24 hours, while followed by sampling at an hourly interval. Upon the completion of reaction, the catalyst was separated from the product mixture by filtration and acid was removed by distillation. The obtained crude sample was concentrated *in vacuo* and the residue was purified by column chromatography Hexane/EtOAc (98:2).

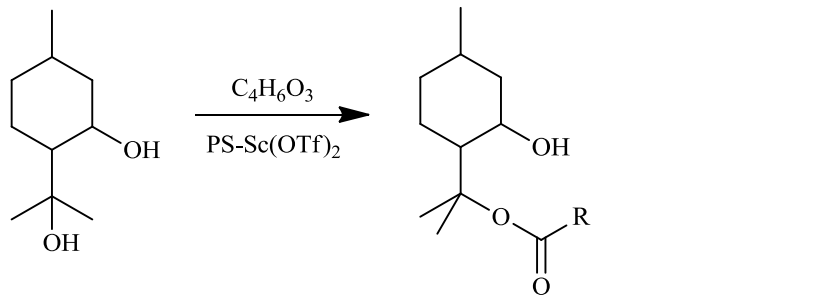

Scheme 25: Acetylation of para-menthane-3,8-diol

The collected samples were quantified by the gas chromatography and confirmed by the GC-MS, 1H-NMR, 13C-NMR and FT-IR. Other mono-ester derivatives of **27** were prepared by the same method. The corresponding data of the prepared mono-ester compounds is listed below and the raw data is shown in Appendix B.

Mono-acetate (**54):** (5.3 g, 85 %), ^{1}H NMR (400 MHz, $CDCl_3$, ppm); δ = 0.79 (3H, s), 0.80-0.95 (3H, m), 1.07-1.23 (3H, m), 1.5 (6H, d, *J* = 24), 1.11 (1H, s), 1.33 (1H, d, *J* = 12 Hz), 1.54-1.60 (3H, m), 1.66 (1H, d, *J* = 12 Hz), 1.75 (1H, d, *J* = 12 Hz), 1.98 (3H, s), 2.29 (1H, s), 5.29 (1H, s). ^{13}C NMR (100 MHz, $CDCl_3$, ppm): 21.5 21.9, 22.0, 26.5, 27.5, 28.5, 34.7, 39,4, 50.0, 71.1, 71.8 and 170.5. FT-IR (cm^{-1}): 3435, 2948, 1734, 1455, 1241 and 1080. *m/z* (C.I.) 214 (M^+, 1), 197 (100), 137 (70), 95 (65), 81 (100) and 59 (48); GC R_T = 16.2 min.

Mono-propionate (55): (5.8 g, 87.6 %), ^{1}H NMR (400 MHz, $CDCl_3$, ppm); δ = 0.78-0.81 (3H, m), 1.06-1.12 (9H, m), 1.34 (1H, d, *J* = 16 Hz), 1.55-1.61 (3H, m), 1.69 (1H, d, *J* = 36 Hz), 1.83 (1H, d, *J* = 12 Hz), 2.24-2.30 (2H, m), 3.78 (1H, br. s), 5.30 (1H, s). ^{13}C NMR (100 MHz, $CDCl_3$, ppm): 9.0, 21.9, 22.1, 26.6, 27.5, 28.2, 28.5, 34.7, 39.5 49.9, 71.0, 72.1, and 173.9. FT-IR (cm^{-1}): 3425, 2947, 2870, 2847, 1730, 1375, 1279 and 1191. *m/z* (C.I.) 228 (M^+, 1), 211 (10), 136 (20), 81 (25) and 57 (100); GC R_T = 17.3 min.

Mono-pentanoate (56): (6.7 g, 90.1 %), ^{1}H NMR (400 MHz, $CDCl_3$, ppm); δ = 0.78-0.85 (8H, m), 0.91-102 (8H, m), 1.04-1.11 (4H, m), 1.12-1.28 (6H, m), 1.31 (1H, d, *J* = 16 Hz), 1.59 (1H, d, *J* = 44 Hz), 1.86 (2H, s), 2.09 (2H, s), 5.29 (1H, s). ^{13}C NMR (100 MHz, $CDCl_3$, ppm): 13.6, 22.0, 22.1, 22.2, 22.6, 26.9, 27.6, 28.6, 34.6, 34.7, 39.5, 49.8, 71.0, 71.9 and 173.3. FT-IR (cm^{-1}): 3436, 2954, 2929, 2870, 1730, 1181, 1145 and 996. *m/z* (C.I.) 256 (M^+, 1), 136 (60), 86 (100), 57 (80), 29 (10); GC R_T = 18.1 min.

Mono-hexanoate (57): (6.9 g, 88.1 %), 1H-NMR (400 MHz, CDCl3, ppm); δ = 0.82-0.88 (7H, m), 0.89-0.98 (2H, m), 1.02-1.14 (6H, d, *J* = 16 Hz), 1.28-1.92 (8H, m), 2.24-2.31 (3H, m), 5.31 (1H, s). ^{13}C NMR (100 MHz, CDCl3, ppm): 13.6, 21.9, 22.1, 22.2, 26.6, 27.6, 28.6, 34.6, 34.7, 39.5, 49.9, 70.9, 71.9 and 173.3. FT-IR (cm^{-1}): 3436, 2952, 2931, 2870, 1729, 1181 and 1146. *m/z* (C.I) 270 (M^+, 1), 253 (10), 136 (20) and 99 (100); GC R_T = 19.2 min.

2.6.2. Microwave-assisted flow reactor set-up and optimisation process

During the optimisation process of the PMD acylation reaction, an ArrheniumOne microwave-assisted continuous-flow fixed-bed reactor system was used for the study (Figure 2.5). The microwave generator was used as a source of heat and was linked to the applicator *via* a coaxial waveguide cable. The substrate flow-rate was realised by means of an HPLC pump. Stainless steel tubing ($⅛^{th}$ inch) was used to connect the pump and the applicator containing a glass column reactor. The microwave generator was connected to tap water for auto-cooling.

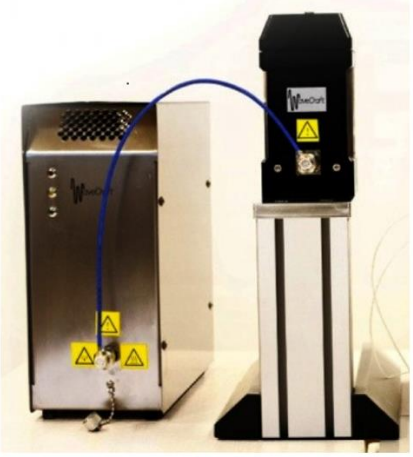

Microwave-assisted continuous-flow system

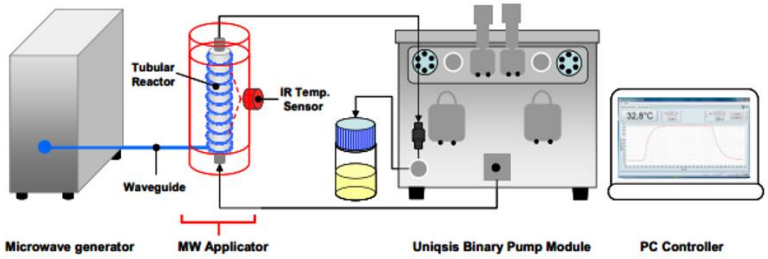

Flow diagram

Figure 2.5: microwave-assisted continuous-flow reactor system

The reactor system components are detailed and further discussed below as follows:

2.6.2.1. Microwave generator

In the microwave generator, a semi-conductor design is used to enable a dynamic optimization of the process conditions. The dynamic optimization is achieved by changing the power and frequency during heating. The heating process can range from 25 to 300°C with the typical temperature ramping range from 1 to 5 °C/Sec. The system pressure can be determined based on the reactor dimensions (*i.e.* 3 mm I.D: ambient to 50 bars and 6 mm I.D: ambient to 30 bars). The system is characterized with a microwave power range of 0 to 150 W and frequency range of 2.4 to 2.5 GHz.

2.6.2.2. Microwave applicator

The microwave applicator is a device where the generated microwaves meet and heat the reactor containing a material to be processed. It is linked to the microwave generator through a waveguide cable. The microwave applicator oven can tolerate temperature 300ºC at a frequency of 2.45 GHz. In addition, its household oven is associated with uniform heating pattern, which result in the final uniform temperature distribution. Moreover, a sensitive temperature infra-red detector probe is used for the online temperature monitoring.

2.6.2.3. Microwave glass reactors

The reactor system consists of 3 and 6 mm diameter glass column reactors (Figure 2.6). The flow reactor is assembled by opening a top lock of the applicator and carefully inserted on the Teflon

end sleeves. The top block is then mounted back on the applicator by locking and turning the nut firmly. The bottom part of the reactor is connected to the inlet ¼ inch tubing linking to the HPLC pump. The top reactor exit is linked to the back pressure regulator using ¼ inch tubing. The sample is collected from the terminal end of the back pressure regulator.

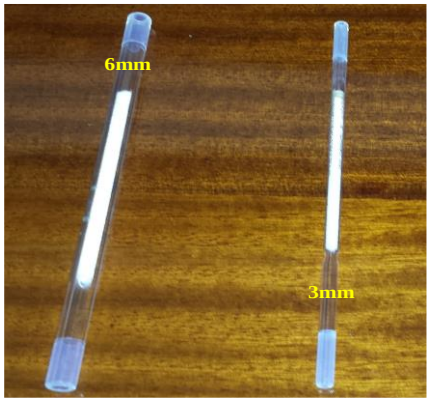

Figure 2.6: Microwave glass reactors

2.6.2.4. User interface

The microwave-assisted reactor system is controlled by pre-installed ArrheniusOne software. The software is installed on a personal computer running with Microsoft windows. The reactor system is linked to the PC *via* a universal serial bus (USB) connector. When running the reaction, the reagent is pumped into the reactor, while allowing a cooling water to circulate through the system. This is followed by turning on the power button of the microwave generator unit. When a microwave generator system is, the ArrheniumsOne software from a PC can be operated as desired.

2.6.3. Continuous-flow synthesis of mono- and di-ester derivatives

During the optimisation process of **27**, a microwave-assisted continuous-flow reactor set-up was used for the study. All the reactor parameters were allowed to equilibrate before each experiment within the central composite design (CCD). In a 250 mL sample bottle, a 1.6 M solution was prepared by dissolving **27** (65.0 g, 0.38 mol), and the appropriate acid anhydride (0.00113 mol, 2 equivalents) in tetrahydrofuran solvent (50 ml). The substrate mixture was pumped into the reactor column packed with 1.0 g of polymer-bound scandium triflate catalyst. The reactor temperatures were controlled by use of pre-installed Wavecraft software. The actual reactor temperatures were detected by the pre-installed IR-probe sensor device. The samples were collected at the reactor exit for the GC analysis. The reactor parameters were adjusted accordingly and allowed to equilibrate for three hours before taking another sample.

2.6.4. Quantification of the product mixture

The peak area of **27**, mono- and di-ester derivatives in the product mixtures were quantified by the GC as described above. The concentrations of the corresponding GC peak areas were determined in reference with multi-point external standard calibration curve method. The observed concentrations of these compounds were then used to determine the **27** conversion, mono- and di-ester selectivity by using the method discussed below.

2.6.4.1. Determination of *para*-menthane-3,8-diol conversion

The conversion of PMD was calculated by dividing the converted moles of PMD with its initial moles used (Equation 2.1).

$$PMD\,conversion\ (\%) = \frac{moles\,of\,PMD\,Converted}{Initial\,of\,PMD}\ x\ 100\,\% \qquad \textbf{(Eqn. 2.1)}$$

2.6.4.2. Determination of product selectivity

The di-ester selectivity was calculated by dividing the moles of di-ester formed with the moles of **27** converted. This is further illustrated below (Equation 2.2).

$$Di-ester\,sel.\ (\%) = \frac{Moles\,of\,di-ester\ formed}{Moles\,of\,PMD\,converted}\ x\ 100\ \% \qquad \textbf{(Eqn. 2.2)}$$

The moles of the di-ester formed were calculated by multiplying its final concentration with the sample volume collected. The final sample concentration used was determined by using a calibration curve approach as demonstrated above. The mono-ester selectivity was determined by using the same method.

2.6.5. Formula used to determine the unknown response values

2.6.5.1. Model derivation

The observed experimental data from the continuous-flow acylation of **27** was analysed by the use of multi-linear regression model (Equation 2.3). By using the general equation showed below, we able to analyse the effect of each reaction parameter towards the substrate conversion and the product selectivity statistically.

$$\hat{Y} = b_0 + b_1 T + b_2 F + b_3 T^2 + b_4 F^2 + b_5 TF \qquad \textbf{(Eqn. 2.3)}$$

Where: $\hat{Y}$ is the predicted response value, T = Temperature, F = Flow-rate and, i = 1, 2, 3, 4, 5 are the estimated regression coefficients.

2.6.5.2. Prediction intervals for the estimated responses

The predicted response value for the above response surface model is not conclusive enough without the estimated error uncertainty. Therefore, it is highly recommended to obtain the predicted interval, in which the predicted response value for the substrate conversion or product selectivity will lie within a given level of confidence. The error uncertainty of the predicted final response values were calculated by using the equation indicated below (Equation 2.4).

$$Y \pm t_{\alpha/2}^{n-k} \sqrt{S_e^2 + S_Y^2} \qquad \textbf{(Eqn. 2.4)}$$

Where: Y = predicted response value, t = t-distribution for degree of freedom = n-1, S_e^2 = standard error and S_Y^2 = standard error for the predicted value.

CHAPTER 3

Synthesis of isopulegol and isopulegyl-ethers

3.1. Continuous-flow citronellal cyclisation to afford isopulegol

3.1.1. Overview of isopulegol

Isopulegol **22** is a monoterpenic alcohol that can be synthesised from the cyclisation reaction of citronellal **19**.[47,110] Many authors have reported publications on isopulegol synthesis *via* the batch-scale process (scheme 26). The most competitive industrial scale process is the Takasago process.[47] The process involves the use of *(R)*-**19** to produce the **22a** isomer. The latter is used to produce menthol **28a**, which has broad industrial applications.[111] From the early reported batch-scale studies, high **19** conversions and excellent selectivities towards **22** are reported.[39,112] This reaction has been explored also in the continuous flow synthesis.

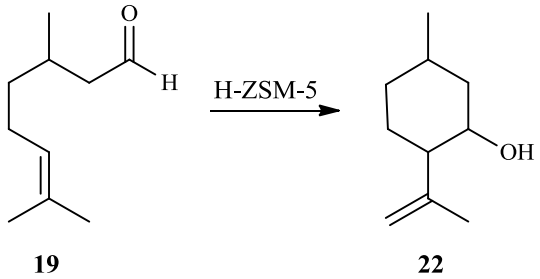

Scheme 26: Citronellal cyclisation reaction

As a typical example, Corma *et al.*, reported a cyclisation reaction of **19** in the fixed-bed reactor. The reactor was made from stainless steel and the column (I.D: 4mm, length: 130 mm) was loaded with tin-beta zeolite catalyst (0.5 g). During the cyclisation reaction, the reactor system was equilibrated to 80ºC, while **19** was pumped into the reactor at a weight hourly space velocity (WHSV) of 5 $ml.g^{-1}.h^{-1}$. Their results revealed 99% conversion of **19** with 98% selectivity towards **22**. The catalysts used revealed excellent catalytic performance in the reaction. However, the use of tin (Sn) containing catalyst is found to be a disadvantage. Moreover, the catalyst is characterised with complicated preparation procedure.[113]

Herein, we report a cyclisation reaction of **19** in a continuous flow fixed-bed reactor. The reaction is performed according to the basic method that was developed as part of collaboration with the University of Cape Town (UCT). Our fixed-bed reactor system was designed in similar

manner as their method and H-ZSM-5 was also employed as catalyst. Based on their results, 100% conversion of **19** was achieved with 95% selectivity towards **22**.

3.1.2. Results and discussion

3.1.2.1. Continuous-flow synthesis of isopulegol

As part of our effort, the reaction described above has been confirmed in our laboratory. The conformational studies were carried-out by using our tubular fixed-bed reactor system equipped with a reactor column (I.D: 9.53 mm and length: 120 mm). The reactor column was packed with H-ZSM-5 zeolite catalyst (6.0 g) extrusion. Prior to the reaction, the zeolite catalyst was activated under nitrogen before use as described in the experimental section. After the catalyst activation process, the reaction was carried-out by varying the reaction parameters as follows (temperature from 80 to 100°C and flow-rate from 0.1 to 0.5 ml/min).

From each set of parameters used, the samples were taken from the reactor exit for GC analysis. Below is a typical GC trace of **19** starting material and magnified GC peak is showed on the right hand side (Figure 3.1).

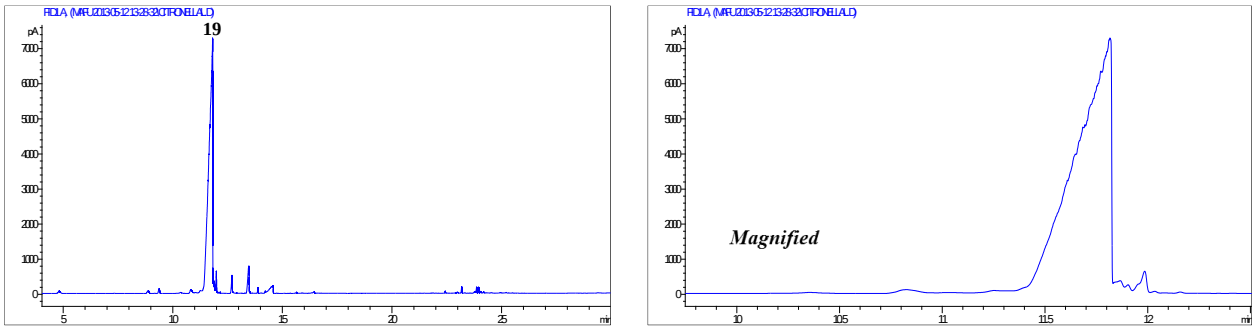

Figure 3.1: Citronellal GC trace

From the chromatogram shown above, a major peak of **19** can be seen at retention time 11.5 minutes. The major peak is accompanied by other minor peaks. These minor peaks denote the trace components that are present in citriodora oil. An almost pure starting material can be observed from the chromatogram. Our aim was to use the oil in its crude form without further purification. In doing so, we attempted to develop a cheap and easy to use process that produces isopulegol in high purity.

The major peak **19** has been confirmed by the GC-MS and its mass fragment pattern is shown below (Figure 3.2). The raw data for its characterisation can also be found below (appendix A1).

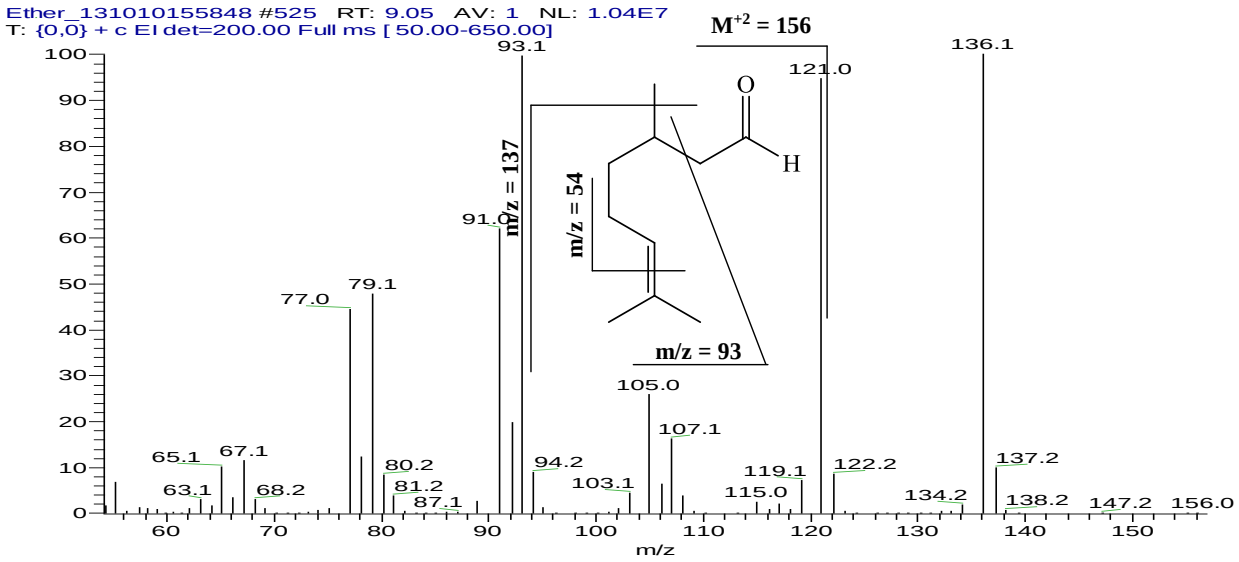

Figure 3.2: Citronellal mass fragment pattern

After the cyclisation reaction of **19**, a mixture of **22** isomers were obtained as indicated below (Figure 3.3). The four visible isomers of **22** were observed to vary in concentration. It must be mentioned that these isomers were not identified in this work, however were integrated as a single peak during the quantification of the product selectivity.

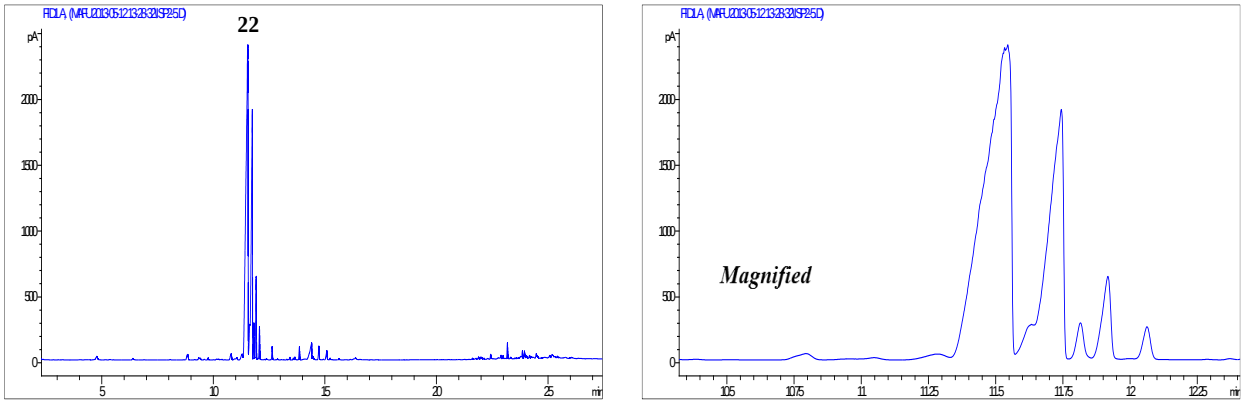

Figure 3.3: Isopulegol GC trace

Upon characterisation of **22**, the four peaks eluting at retention times 11.5, 11.7, 11.9 and 12.2 minutes show the same molecular mass fragment pattern, which is a characteristic of **22** (Figure 3.4). Additionally, the smaller peaks that can be observed from the chromatogram are denoting the carry-overs from the starting material **19**.

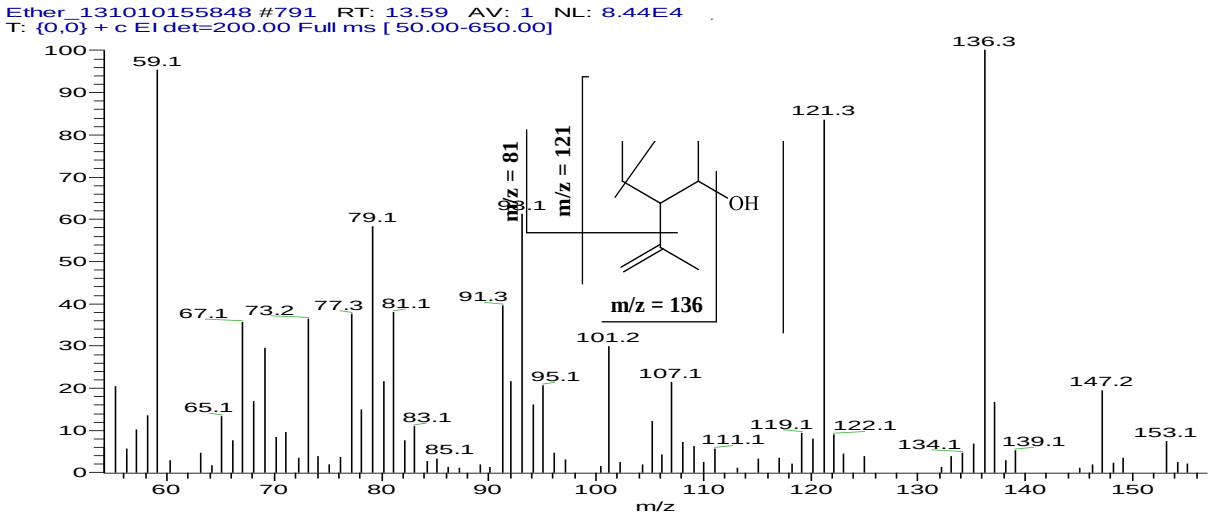

Figure 3.4: Isopulegol mass fragment pattern

After purification of **22** in the column chromatography, the FT-IR spectrum confirmed the disappearance of the carbonyl absorption band at 1725 cm^{-1} of the **19**. However, a broad hydroxyl absorption band at 3401 cm^{-1} was observed as evidence of **22** formation. The newly formed hydroxyl group was further confirmed by the ^{1}H-NMR and it was observed as a broad singlet at δ = 5.06. Moreover, the carbonyl carbon of **19** at δ = 202.86 was not observed from the ^{13}C-NMR spectrum (appendix A2).

It was also important to determine the effect reaction parameters such as temperature and flow-rate towards the **19** cyclisation reaction. It must be mentioned that, a complete conversion of the starting material was observed in every set of parameters used. Therefore, a close attention was given to the variation of **22** selectivity with change in temperature and flow-rate, respectively (Figure 3.5).

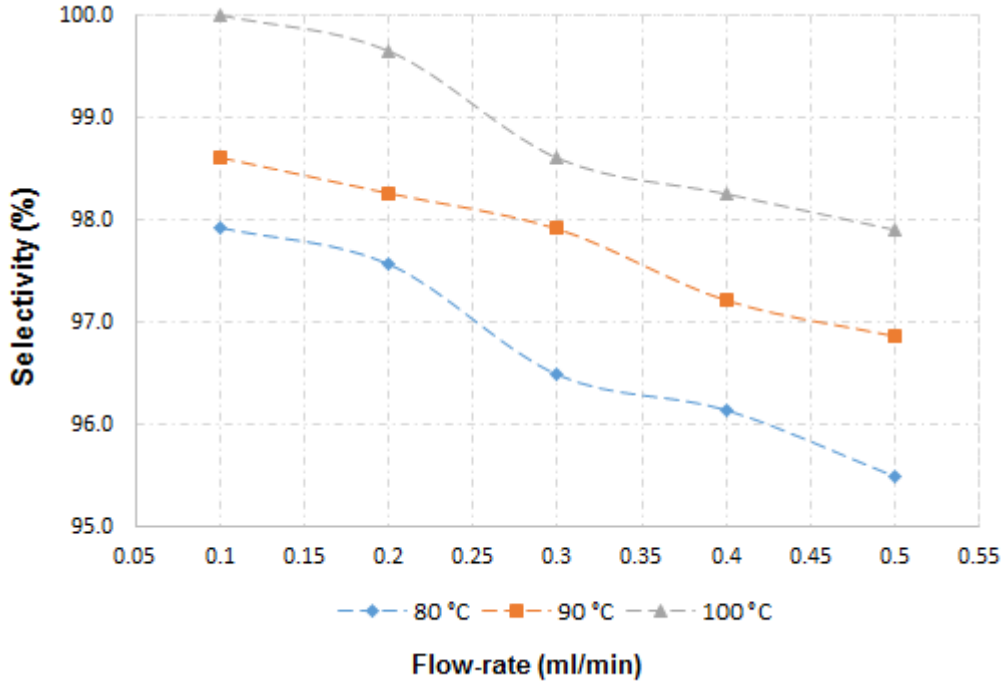

Figure 3.5: Effect of temperature and flow-rate in isopulegol selectivity

From the graph above, the cyclisation reaction of **19** shows that temperature and flow-rate has a small influence towards the **22** selectivity. Meaning, the increase in the reaction temperature with decrease in the flow-rate, result to the increase in **22** selectivity. It is also observed that when the reaction is performed at temperatures of 100°C and the flow-rate of 0.1 ml/min, 100% selectivity towards **22** is achieved. Thus, this clearly indicates that the above reactor parameters are the optimum conditions for the **19** cyclisation reaction. Furthermore, the flow-rate of 0.1 ml/min denotes an estimated residence time of 1.4 hours, when taking into account the reactor column specifications used as well as the catalyst loading.

3.1.3. Discussion

These results show the reaction process to be reproducible, when compared to the results that were obtained by the UCT group. Even though there is a smaller change in the reactor column designs, the reaction trend has remain unchanged. Furthermore, the activated H-ZSM-5 zeolite catalyst used in our work has revealed the results that are in agreement with those that were achieved over the Sn-beta zeolite and Zr-zeolite beta catalysts as reported in the literature.[114,113]

However, our results were found to contradict the work of Murzin *et al.*, wherein the low catalytic activity of H-ZSM-5 was reported in the batch-scale cyclisation reaction of **19**. The poor catalytic performance was explained as the resultant of poor diffusion. Moreover, there is no direct correlation made between the initial cyclisation rate, the specific surface area and the

concentration of the acid sites as compared to other catalysts like H-Beta, H-MCM-41, H-MORD, H-Y or H-MCM-22.[115]

Based on our experimental observations, the best catalytic performance has been achieved with the activated H-ZSM-5 catalyst in solvent-free continuous flow process. This catalyst has revealed excellent results in continuous flow process, and is characterised with less complicated preparation procedure as compared to other catalysts mentioned above. The reaction conditions such as temperature of 100°C and flow-rate of 0.1 ml/min, revealed the optimum **19** conversion (100%) and the **22** selectivity (100%). The reaction has showed to be stable for a prolong amount of time, more than 72 hours to be specific. Over this period, 1.5 kilograms of **19** was converted into the equivalent mass of **22**. Hence we believe this is a green, solvent-free method to produce multi-kilo quantities of product for further studies.

3.1.4. Concluding remarks

We can conclude that the continuous flow synthesis of **22** can be directly prepared from the treatment of the essential oil **19** over the activated H-ZSM-5 zeolite catalyst. A superior catalytic performance is observed under solvent-free and mild conditions. The developed environmentally friendly process involves low energy consumption, simple reactor operation, excellent citronellal conversion and high isopulegol selectivity. Other advantages include the elimination of toxic catalysts, the use of non-hazardous and less expensive natural existing reagent.

3.2. Continuous flow synthesis of isopulegyl propoxy-ether

3.2.1. Overview of ether synthesis

The acid-catalysed electrophilic addition of alcohols to an alkene is a well-established reaction and is of significant commercial importance. Typical reactions that lead to the ether formation include the olefin hydroalkoxylation, oxymercuration-demercuration, Williamson transformation *etc*.[116,117] Among these synthetic routes, the oxymercuration-demercuration offers high ether yields with good selectivities in short reaction times. Nevertheless, this process is less desirable, due to the presence of the highly toxic mercury salt.[118,119]

The other promising synthesis method for the preparation of ethers is an acid-catalysed alkoxylation of alkenes. The transformation of alkenes to the corresponding ethers is achieved by the use of acid-treated clays such as zeolites, mordenite, clinoptilolite and ferrierite as

heterogeneous catalysts. For example, two Chinese groups studied the alkoxylation of alpha-pinene **58** with methanol in a batch reactor under atmospheric pressure at a temperature of 50-100°C. The corresponding ether **59** yield of 35% was reported over the acid-treated mordenite catalyst in a 5 hour reaction time (Scheme 27).[119]

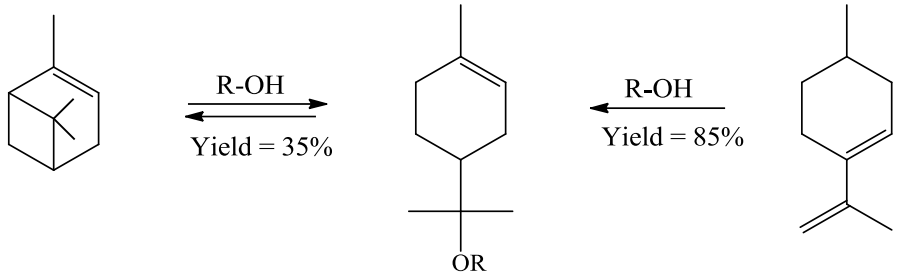

58 **59** **60**

Scheme 27: Alkoxylation of alpha-pinene and limonene

On the other hand, Hensen *et al.,* studied the alkoxylation reaction of **58** and limonene **60** with methanol carried out in the bath-scale and fixed-bed reactor (I.D: 9 mm O.D: 12 mm and length: 300 mm). In both reactors, methanol and **60** as feedstock gave 85% yield towards the corresponding ether **59** over the beta-zeolite catalyst. The catalyst appeared to be more active in the methylation reaction of **60**. However, the highest yield of around 50% towards the corresponding ether **59** was achieved with **58** in both reactors over the beta-zeolite catalyst.[119,120]

In our laboratory, the method for electrophilic addition of an alcohol to the alkene has been developed in a batch scale process. The developed method involves the addition of straight chain alcohols to the terminal alkene of **22**. In our previous study, several catalysts such as amberlyst-15 dry, sulphuric acid (H_2SO_4), boron trifluoride dietherate, aluminium, yttrium and bismuth triflate have been evaluated. Among these catalysts, a better performance was achieved over the amberlyst-15 dry catalyst. Nevertheless, the catalyst was associated with many side reactions, which obviously reduced the selectivity of the desired product.

As part of this investigation, our focus was directed on the optimisation process of the above mentioned reaction in a continuous flow fixed-bed reactor. Our aim was to utilise **22** as a feedstock material that is produced using the above mentioned method, to synthesise its corresponding ether derivative. In addition, to identify the optimum heterogeneous catalyst for the process, which could hopefully result in high **22** conversion and selectivity.

3.2.2. Results and discussion

3.2.2.1. Synthesis of isopulegol-ether derivative

The etherification of **22** with *n*-propanol was performed using a UniQsis FlowSyn reactor system. During the study, *n*-propanol was used as a model etherifying agent as well as a solvent. The working solution was prepared by dissolving **22** (30.0 g, 0.19 mol) in *n*-propanol (23.4 g, 0.39 mol) to produce a 3M solution. The prepared substrate mixture was pumped into the reactor column (I.D: 9.53 mm and length: 120 mm) packed with amberlyst-15 dry (1.0 g) catalyst. The reaction was performed by varying the substrate flow-rate from 0.1 to 0.5 ml/min and temperature from 50 to 90 °C (Scheme 28).

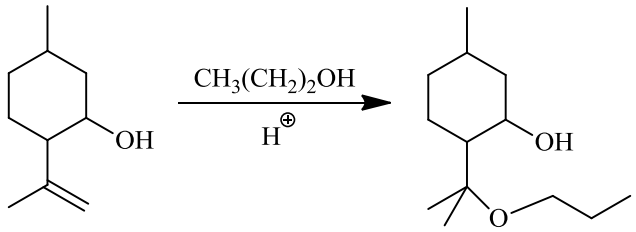

22 **49**

Scheme 28: Synthesis of isopulegyl propoxy-ether

The product samples were collected at the reactor exit for GC analysis. Below is a typical GC-trace of the product mixture observed (Figure 3.6).

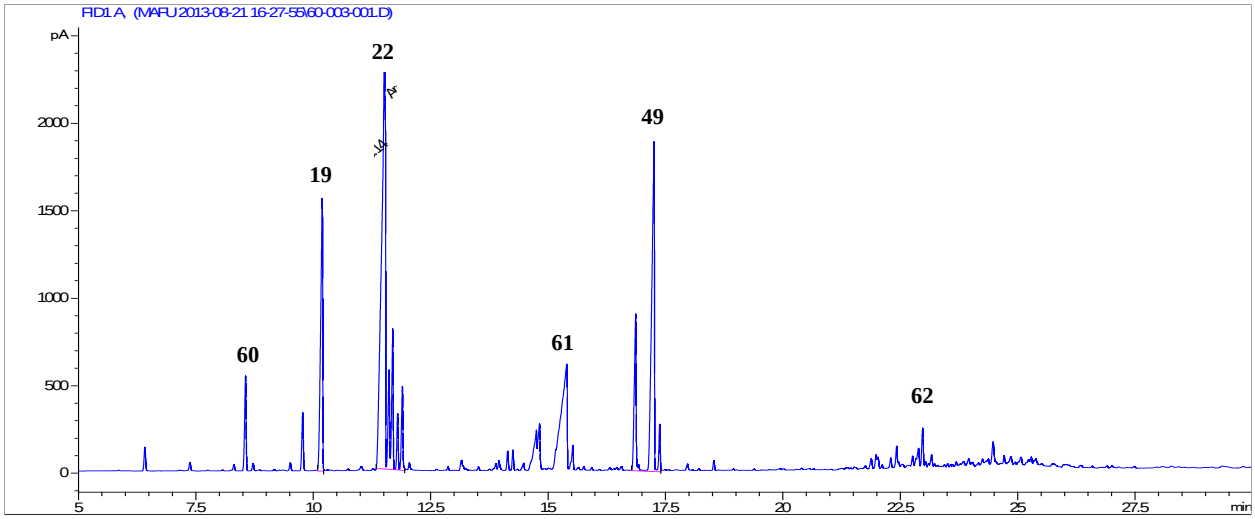

Figure 3.6: GC-trace of isopulegol etherification

From the GC-trace shown above, several additional peaks to the starting material are observed, including the peak of the desired isopulegyl-propoxy-ether **49** product. In our previous work, all

the peaks observed in the chromatogram have been isolated and characterised.[26] The observed peaks have been confirmed by the GC-MS as discussed below.

The peak eluting at 8.5 minutes showed the mass fragment pattern that denotes the dehydration of the starting material **22** to form **60** (Figure 3.7). The peaks eluting at 9.7 and 10.1 minutes also denotes the reverse reaction between **22** and **19** as discussed above (see Figure 3.1).

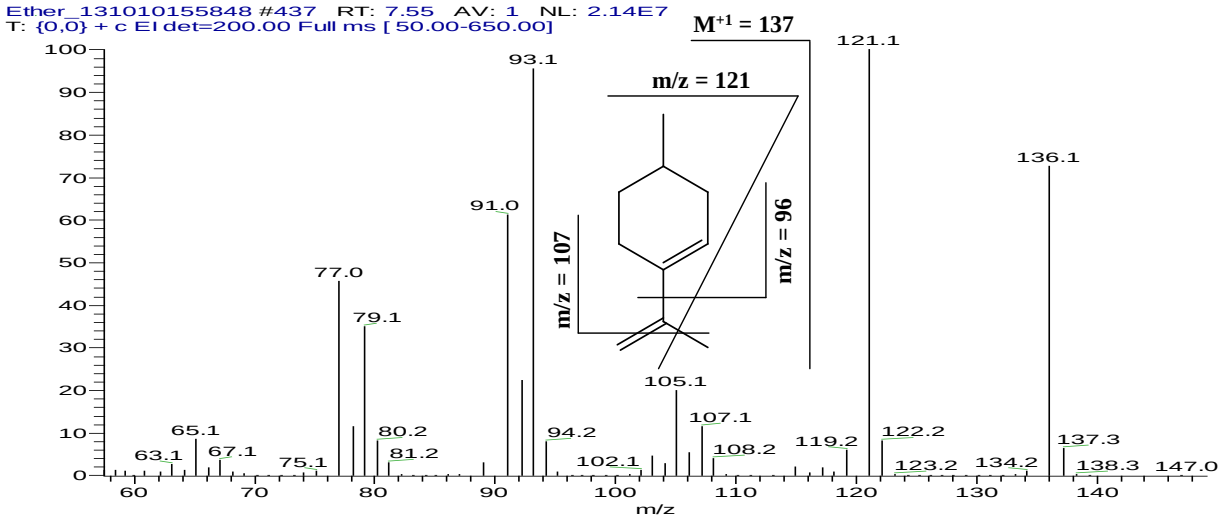

Figure 3.7: Limonene mass fragment pattern

The identity of the compound eluting at retention time 15.5 minutes denotes the dehydrated form of isopulegyl-propoxy-ether **61** derivative. Its molecular fragment pattern confirms the structure of the molecule as indicated below (Figure 3.8).

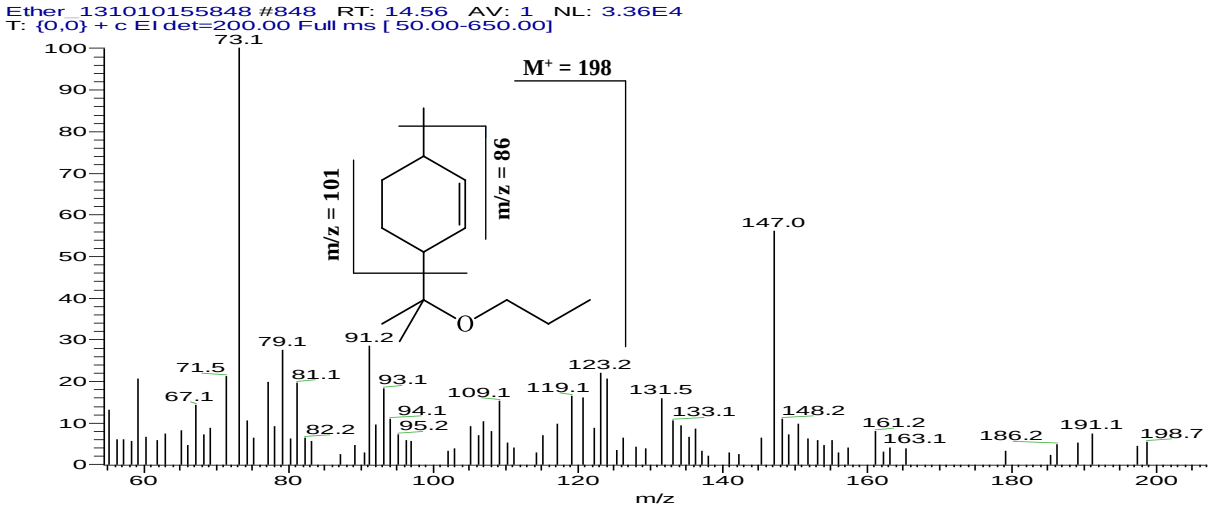

Figure 3.8: Dehydrated isopulegyl propoxy-ether mass fragment pattern

The desired isopulegyl propoxy-ether **49** is observed as a second major peak on the chromatogram at the retention time of 17.3 minutes. It molecular fragment pattern is denoted below (Figure 3.9).

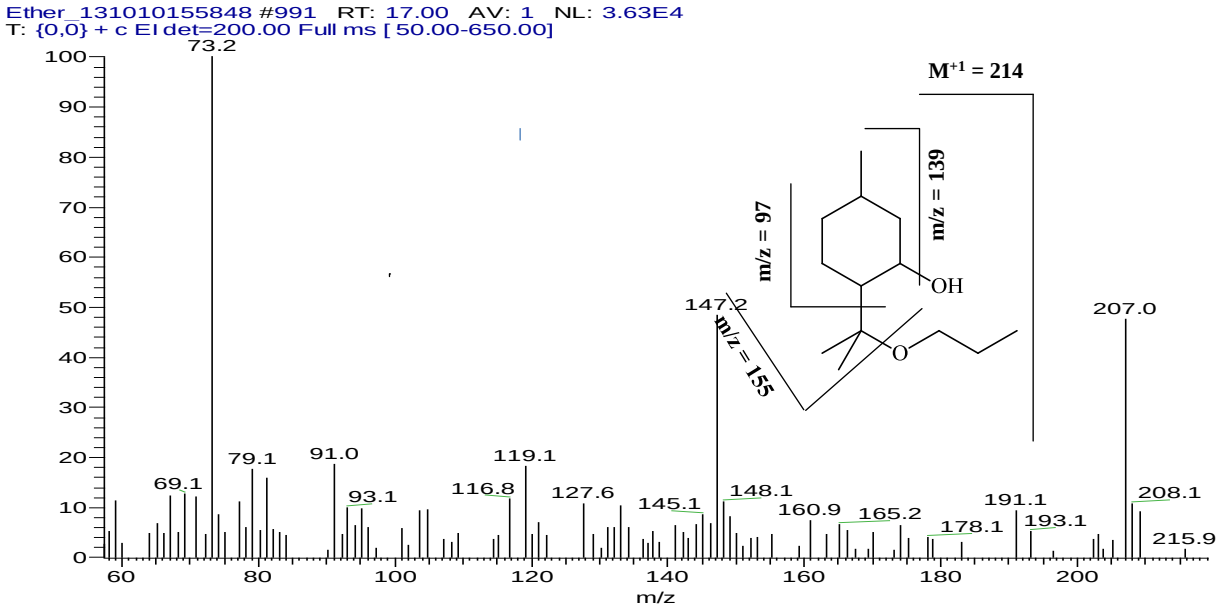

Figure 3.9: Isopulegyl propoxy-ether mass fragment pattern

The traces of **62** are also observed from the chromatogram (Figure 3.10). This compound is believed to be the trace component from the starting material; however it does not exist as the side product of the reaction.

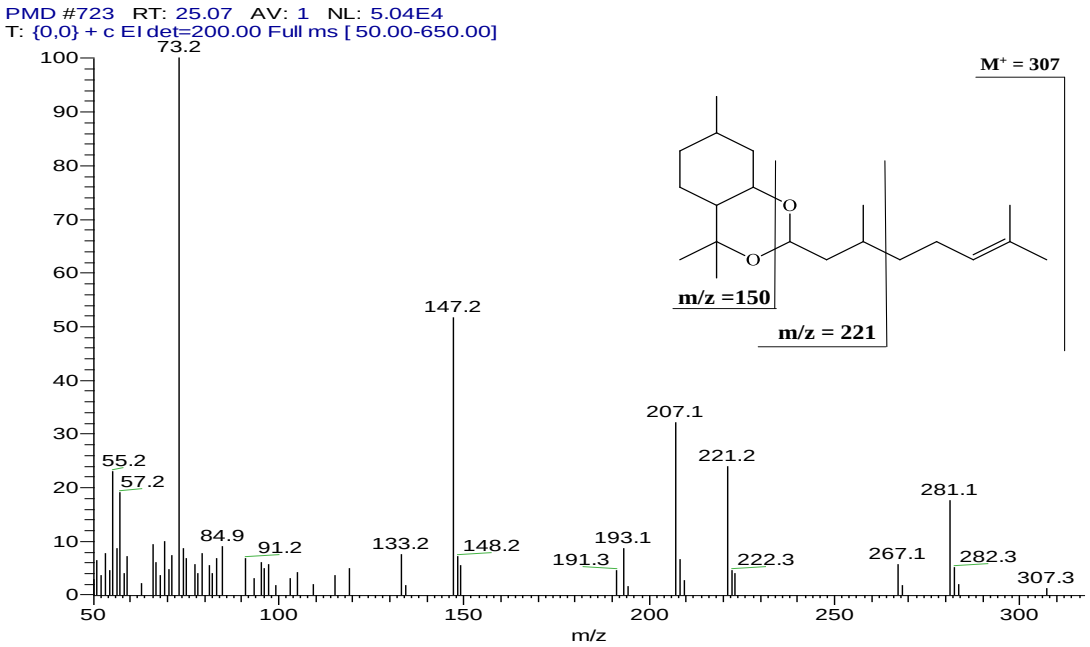

Figure 3.10: *para*-Menthane-3,8-diol-citronellal acetal mass fragment pattern

By considering the above assignments, the formation of isopulegyl propoxy-ether **49** and other by-products in **22** etherification reaction can be illustrated further as shown below (Scheme 29).

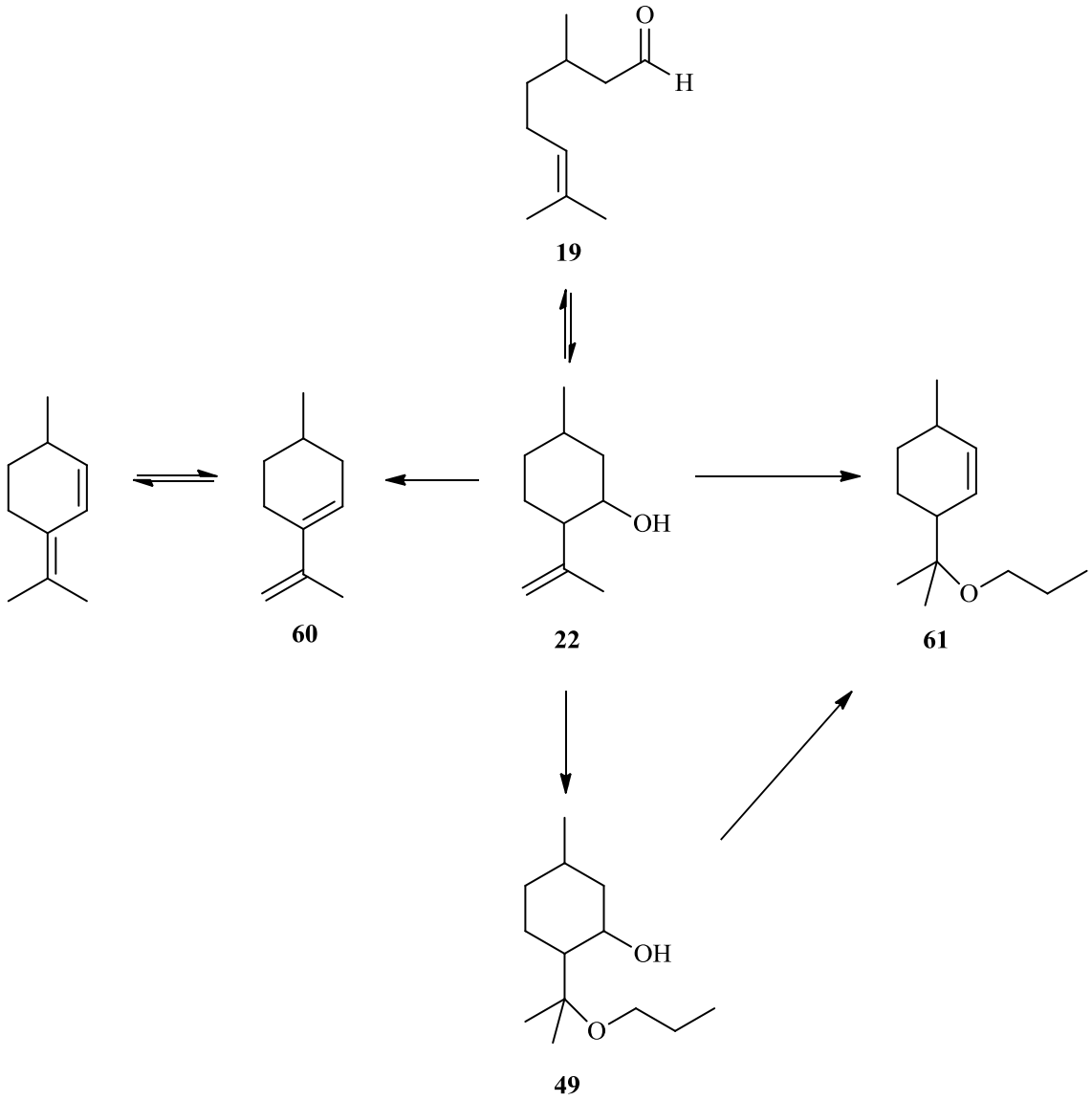

Scheme 29: Isopulegol etherification synthetic route

The effect of reaction variables such as temperature and flow-rate were investigated towards the isopulegol **22** conversion and isopulegyl propoxy-ether **49** selectivity. It must be mentioned that the quantification of the peak areas from the GC-trace was carried-out according to the method that is described in our previous work.[26] As stated in the previous work, this reaction gave very low ether selectivity in the batch-scale process. However, our aim was to see if the selectivity in flow could be enhanced through precise control of the reaction conditions.

3.2.2.2. Effect of temperature vs flow-rate

In order to investigate the optimum conditions for the isopulegyl propoxy-ether **49** synthesis, the effect of the reaction parameters such as temperature and flow-rate were investigated. During the study, the experiments were conducted at the temperature range of 50–90^{0}C and the flow-rate of 0.1–0.5 ml/min with estimated residence time range of 1.4–0.29 hours. After the substrate mixture has been pumped into the reactor as mentioned above, the samples were then collected from the reactor for GC analysis after an hourly equilibration time of the system.

The summary of the product distribution for the reaction that was performed at the flow-rate of 0.5 ml/min (shorter residence time) at varying reaction temperature is graphically presented below (Figure 3.11).

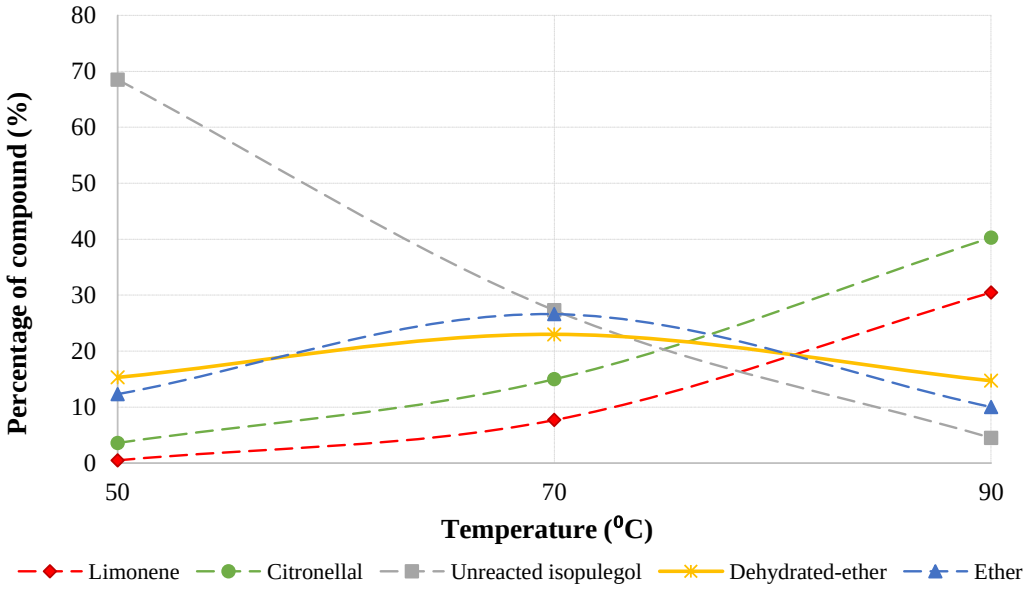

Figure 3.11: Isopulegol etherification using Amberlyst-15 catalyst at 0.5ml/min flow rate

What is observed from the data above is a significant increase in isopulegol **22** conversion with increase in temperature. The highest isopulegyl propoxy-ether **49** selectivity (29%) is observed at the temperature of 70°C. However, a rapid decrease in selectivity is observed with increase in temperature. The increase in the reaction temperature, result to the increase in **22** conversion. At elevated temperature conditions (greater than 90^{0}C), it can be observed that the side products dominate the reaction.

A similar trend was also observed at reduced substrate flow-rate (longer residence time). The reaction summary is graphically presented below (Figure 3.12).

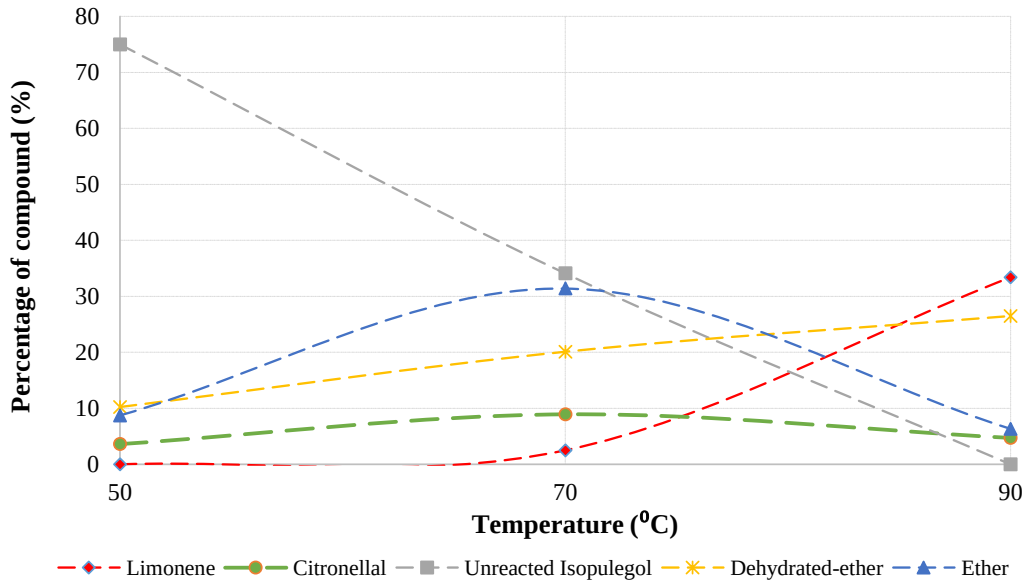

Figure 3.12: Isopulegol etherification using Amberlyst-15 catalyst at 0.1 ml/min flow rate

As indicated in Figure 3.12 above, a slight improvement in the isopulegyl propoxy-ether **49** selectivity (30%) is observed at lower flow-rate (long residence time). It also observed that, when the reaction is performed at high temperature levels, the reaction result to many side products. Consequently, the isopulegyl propoxy-ether selectivity is observed to decrease significantly.

It has been observed that the use of Brønsted acid catalyst (Amberlyst-15 dry) can afford the desired ether **49** product. Nevertheless, the desired product is achieved in low selectivity. This desired product is competing with the number of side reactions, which include the reverse reaction of **22** into **19**, dehydration of **22** to form **60** and the dehydration of the desired product to form compound **61**. The reaction is observed to be optimum when operated at the temperature of 70°C and flow-rate of 0.1 ml/min or residence time of 1.4 hours. At these conditions, the isopulegol **22** conversion (60%) and isopulegyl propoxy-ether **49** selectivity (30%) are achieved.

3.2.2.3. Evaluation of heterogeneous solid acid catalysts

In order to maximise or improve the isopulegyl propoxy-ether selectivity, other forms of heterogeneous acid catalysts like H-beta zeolite, Al-pillared clay, aluminium oxide (Al_2O_3) and H-ZSM-5 were evaluated in the reaction. The reactions were performed using the same conditions as indicated above. The reactor column (I.D: 9.53 mm and length: 120 mm) was packed with 6 grams of each catalyst with or without a catalyst packing material. The catalyst

extrusion such as H-ZSM-5, H-beta zeolite and aluminium oxide were packed in the reactor without a packing material. However, aluminum pillared-clay powder was packed using inert silicon carbide at a 2:1 molar ratio (mass/mass). This method used to overcome the issue of pressure drop limitation within the reactor.

All the catalysts packed in the reactor column were activated before use according to the method described above (subsection 2.3.1). The prepared substrate mixture was pumped into the reactor column at the flow-rate range (0.1–0.3 ml/min), while the reactor system temperatures were varied from 50 to 90°C. The product sample mixtures were collected from the reactor exit for GC analysis. Below is summary of the results that were obtained over the H-beta zeolite at the flow-rate of 0.1 ml/min at varying temperature (Figure 3.13).

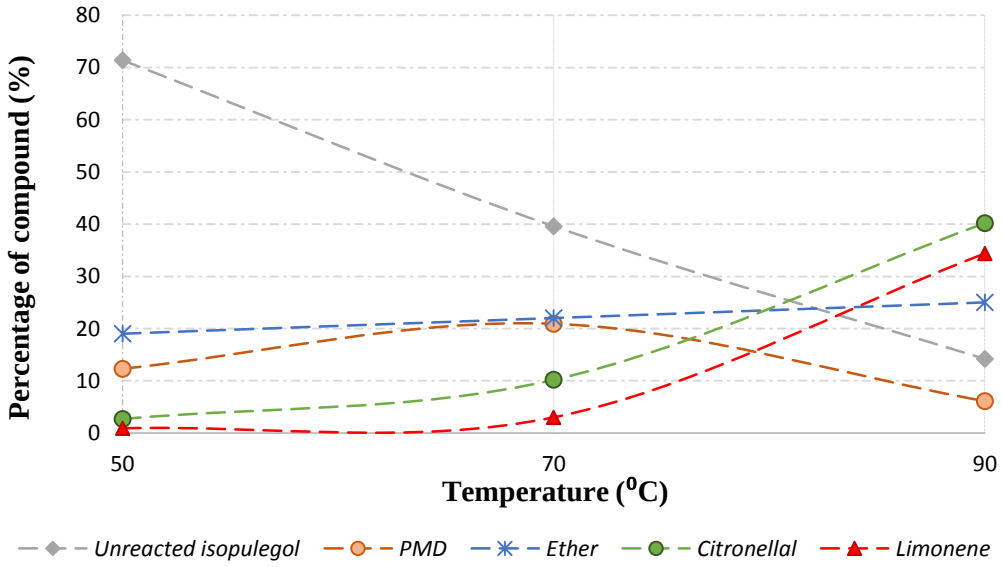

Figure 3.13: Isopulegol etherification using beta zeolite catalyst at 0.1ml/min flow rate

As shown in Figure 3.13 above, the **22** conversion is increasing with increase in temperature. Although, a slightly increase in **49** selectivity can be seen with increase in temperature. A number of side reactions are also visible from the graph. Among these side reactions, a reverse reaction of **22** into **19** is superior at elevated temperature. This is followed by the dehydration of **22** to form **60**. The resultant water molecule from the dehydration reaction of the starting material, reacts with the **22** and yield **27**.

On the other hand, when high substrate flow-rates (shorter residence time) are used, a significant decrease in substrate conversion is observed, which indicates poor catalyst interaction with the reagents. A lower catalytic activity can be observed towards the side reaction. The gradual

increase in **49** selectivity is evident with increase temperature. Nevertheless, the selectivity remains poor at all temperatures conditions studied (Figure 3.14).

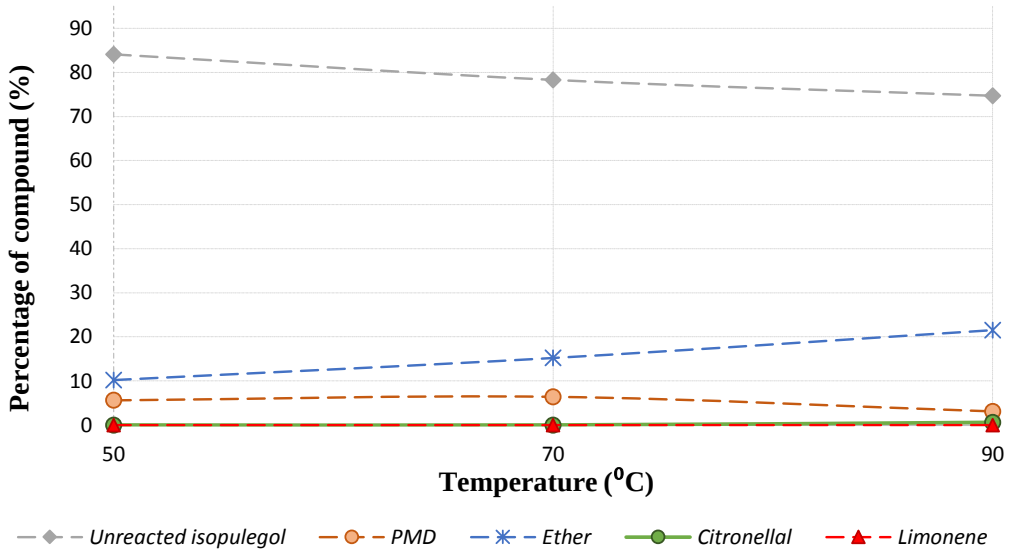

Figure 3.14: isopulegol etherification using beta zeolite catalyst at 0.5 ml/min flow rate

The aluminium-pillared clay has been screened in the reaction and the same reaction conditions were used for the study. A summary of the results that were obtained at the flow-rate of 0.1 ml/min and temperature from 50 to 90°C are graphically presented below (Figure 3.14).

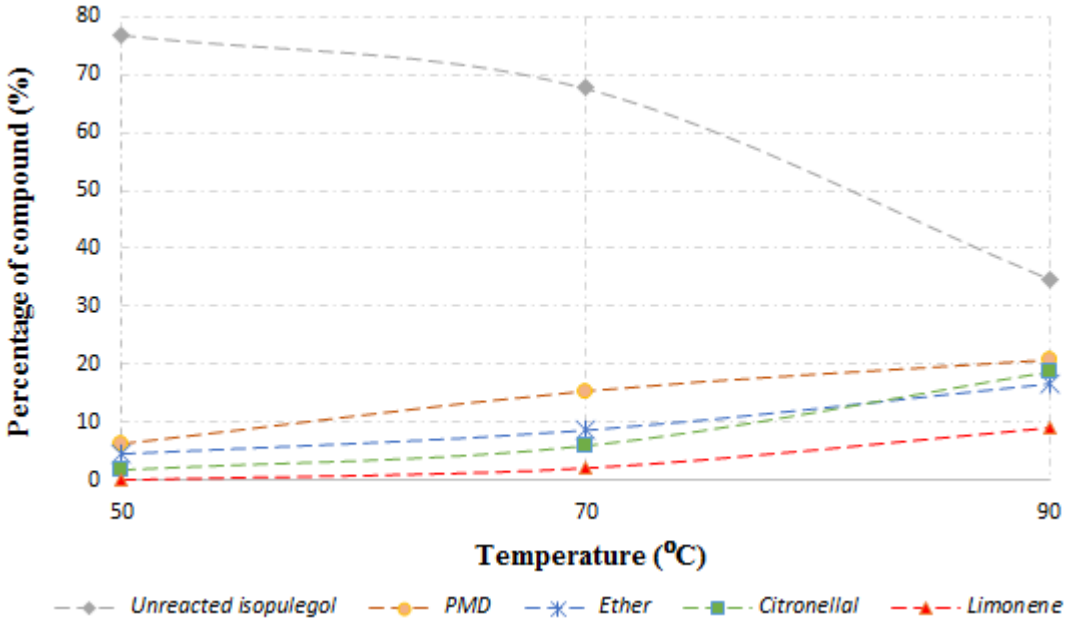

Figure 3.15: Isopulegol etherification using Al-pillared catalyst at 0.1ml/min flow rate

From Figure 3.15 above, a good substrate conversion is observed with a temperature increase at lower flow-rate. However, the selectivity towards **49** remains poor throughout the screening conditions. Again, the side reactions dominates with an increase in temperature.

A similar reaction trend has been observed when high substrate flow-rate was used in the reaction (Figure 3.15).

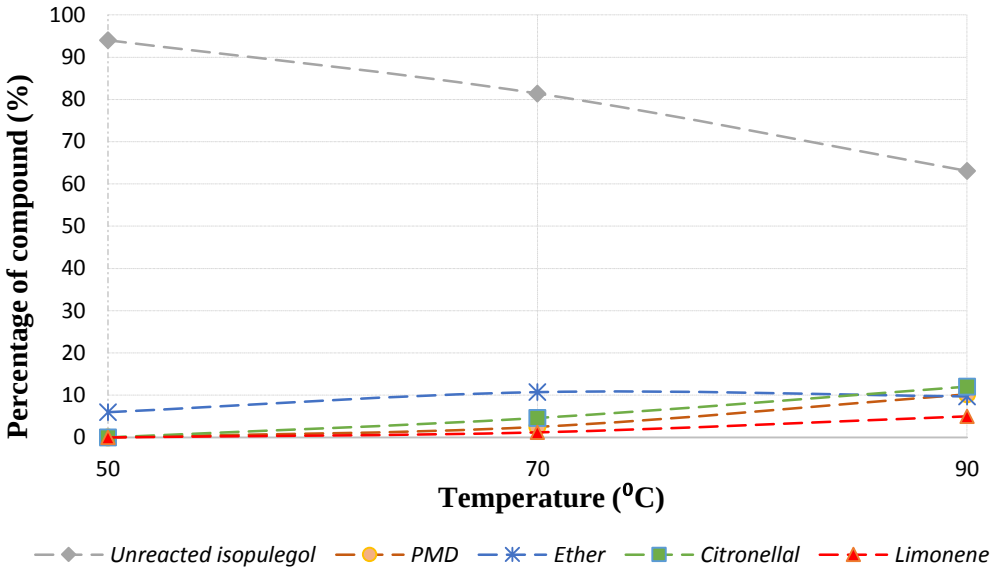

Figure 3.16: Isopulegol etherification using Al-pillared catalyst at 0.5 ml/min flow rate

Figure 3.16, clearly shows that the **22** conversion decreases with increase in the substrate flow-rate. Unfortunately, the same reaction trend can be seen with respect to the **22** etherification reaction.

3.2.3. Discussion

The Amberlyst-15 dry catalyst in the continuous flow reaction gave the **22** conversion (60%) and low **49** (31%) selectivity. The optimum **49** selectivity (31%) was achieved at a residence time of 1.4 hours. The effect of temperature and flow-rate were also found to play a significant role in determining the reaction outcome. The reaction suffered from a number of side reactions, which resulted to the decrease in the yield/selectivity of the desired product. It can be concluded that the Brønsted catalyst (amberlyst-15 dry) is less desirable in the reaction. Even though the catalyst showed a better activity between the reacting species. The presence of side products in the reaction are found to be the major disadvantages. These side reactions lead to the complicated and difficult to separate the desired product.

The H-beta zeolite catalyst has revealed the optimum **22** conversion (80%) and **49** selectivity (25%) when the reaction is operated at the temperature of 90°C and the flow-rate of 0.1 ml/min. However, when the substrate flow-rate is further increased to 0.5 ml/min, a significant decrease in the reaction efficiency is observed at all temperature levels. The same reaction trend has been observed from the reaction in every set of parameters. It is also believed that the presence of water from the dehydration of the starting material, resulted to the deactivation of the active Lewis acid sites in the catalyst.

When Al-pillared clay is used, a very low catalytic activity is observed in the reaction. At optimum conditions, the **22** conversion (65%) and the **49** selectivity (15%) has been observed. The catalyst also showed the same reaction trend as the H-beta zeolite. Other catalysts such as aluminium oxide (Al_2O_3) and H-ZSM-5 zeolite showed no catalytic activity in this reaction. In light of this, it does not appear that the process can be optimised any further in the continuous flow system.

3.2.4. Concluding remark

It can be concluded that the use of Brønsted acid (amberlyst-15 dry) catalyst showed a good conversion towards **22** and low selectivity towards **49**. The catalyst also showed a number of a number of side reactions. The use of Lewis acid catalysts showed good conversion towards **22** and very poor selectivity towards **49**. However, the number of side products were eliminated. None of the evaluated catalyst revealed a reasonable selectivity (greater than 70%). As a consequence, the **22** etherification reaction was terminated. Other citronellal alternative synthetic routes were explored to produce similar chemical derivatives.

CHAPTER 4

Batch-scale synthesis of para-menthane-3,8-diol and its esters derivatives

4.1. Synthesis of *para*-Menthane-3,8-diol

4.1.1. Introduction

para-Menthane-3,8-diol **27** was prepared according to our batch-scale synthesis method.[109] The reaction involve a one-pot acid catalysed hydration of citronellal **19** to produce **27** product. Mechanistically, the reaction is *via* the acid cyclisation of citronellal **19** to form isopulegol **22**, [121] which further reacts with water in the presence of the acid catalyst to afford **27** (Scheme 29).

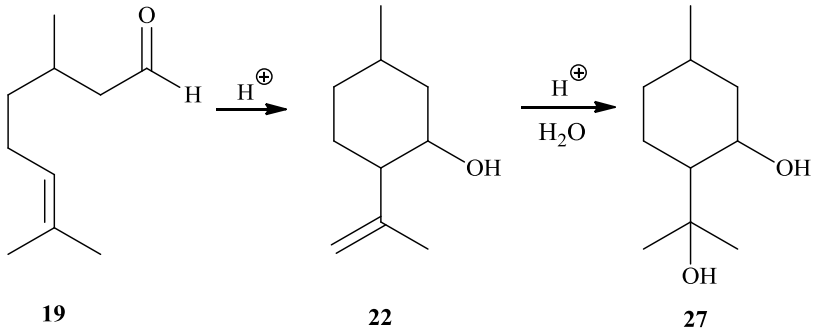

19 **22** **27**

Scheme 29: Synthesis route of *para*-methane-3,8-diol

A detailed batch-scale experimental procedure for the **27** synthesis is illustrated below. The product purification method is discussed in section 2.5 above.

4.1.2. Experimental synthesis method

During the method development, all the reactions were conducted using the batch-scale reactor as described earlier. A typical GC trace of the crude *para*-menthane-3-8-diol (starting material) is shown below (Figure 4.1).

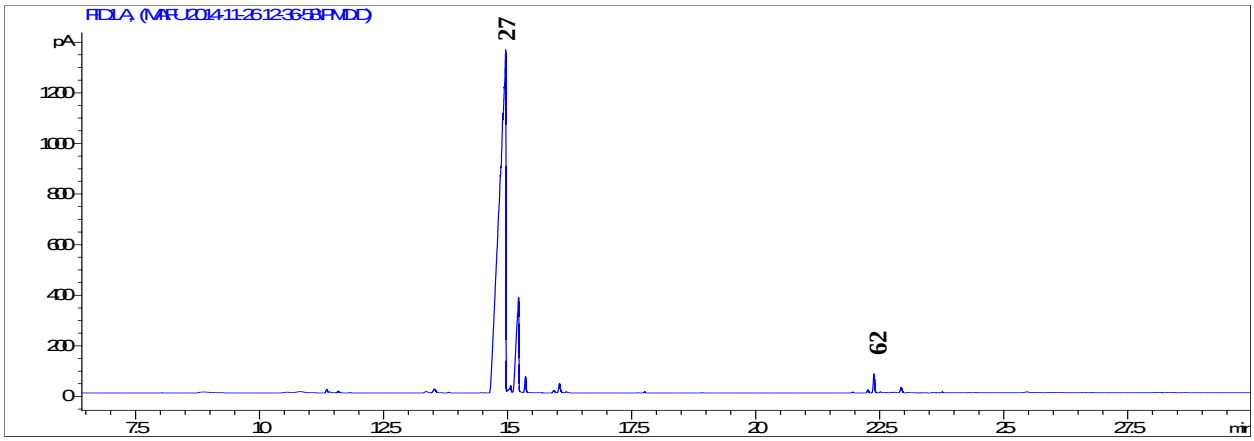

Figure 4.1: GC trace for the *para*-menthane-3,8-diol

From Figure 4.1, the *para*-menthane-3.8-diol **27** is observed as two peaks at retention time of 15.0 minutes. These peaks are accompanied by the smaller peak eluting at retention time 22.4 minutes. Upon confirmation from the GC-MS, the smaller peak eluting at retention time 22.4 minutes have been proven to be the trace of *para*-menthane-citronellal acetal **62**. This small peak is believed to be the carry-over from the starting material. The peak eluting at retention time 15.0 minutes was also confirmed by the GC-MS and its molecular fragment pattern is shown below (Figure 4.2).

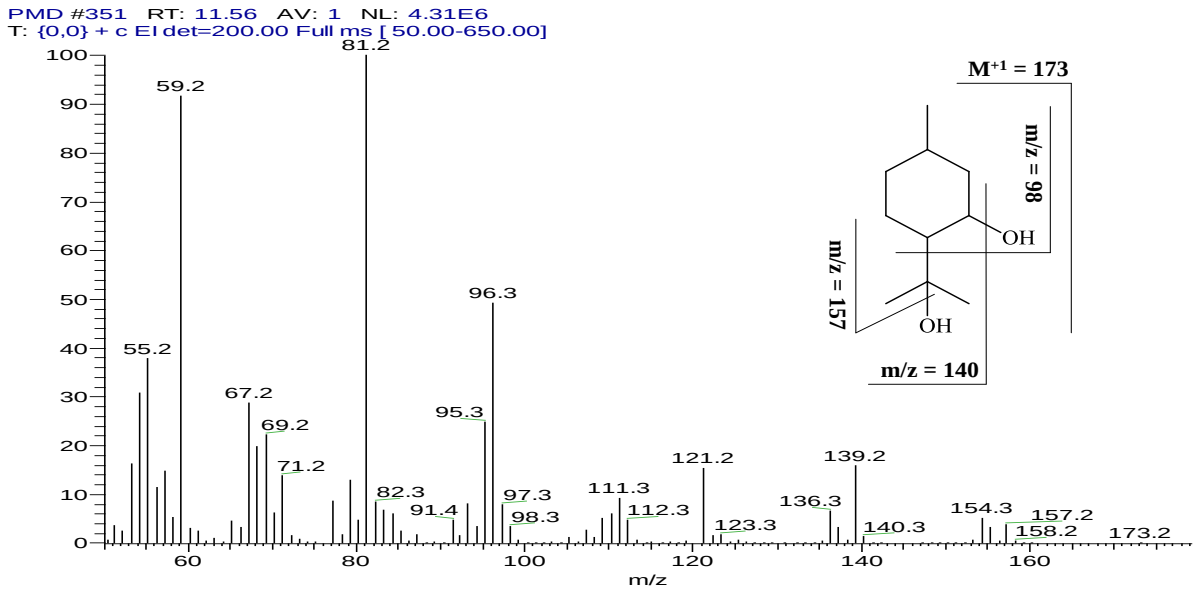

Figure 4.2: *para*-Menthane-3,8-diol mass fragment pattern

4.1.3. Results and discussion

The crude **27** was purified according to the methods described in section 2.5. The pure sample was characterised by the FT-IR, ^{1}H-NMR, ^{13}C-NMR to confirm the molecule structure. From the FT-IR spectrum, a broad tall peak at 3220 cm^{-1} was confirmed, which denotes the presence of

two hydroxyl groups in the molecular structure. The CH_3- groups were also evident by the appearance of three peaks around 2900 cm^{-1}. Other two peaks appeared at 1158 cm^{-1} and 931 cm^{-1} were found to correspond to two C-O groups, which denotes the two bonds of hydroxyl groups that link to the *para*-menthane backbone. The total number of carbons expected from the molecule were confirmed by the ^{13}C-NMR. Furthermore, the ^{1}H-NMR spectrum also confirmed the broad singlet at δ = 3.7, which denoted the protons of the two hydroxyl groups (Appendix A3).

Based on these observations, it can be concluded that the **27** has been obtained in high purity and this can be used as a feedstock material to prepare its di-ester derivatives.

4.2. Synthesis of para-Menthane-3,8-di-ester derivatives

4.2.1. Overview of acylation reaction

Acylation or esterification of alcohols is a fundamental reaction in organic chemistry. It is used mostly in the synthesis of esters or in protection of various functional groups like phenols, thiols, alcohol and amines *etc*.[110,122,123] Usually, activated carboxylic acids such as acid anhydrides, acyl halides, acyl imidazoles and acyl ureas are used as acylating agents.[122,124,125] The reaction is carried-out over a wide range of catalysts. In general, homogeneous Lewis acid catalysts ($AlCl_3$, BF_3, $TaCl_5$, $M(OTf)_3$), basic reagents (4-dimethylaminopyridine and tributylphosphine) or inorganic acids (H_2SO_4, PTSA, rare earth and alkali metals) are used in the reaction.[124,126-128] These catalysts have shown to effect the acylation reaction, although a superior performance has been observed over the metal triflates, scandium triflate ($Sc(OTf)_3$) in particular.[44,124,129] Because homogeneous catalysts are not easily recoverable, therefore are less desirable to be used in many reactions due to the environmental concerns. Moreover, they often lead to large amounts of toxic and corrosive waste being generated.[122,126,130-132]

On the other hand, the above mentioned challenges are well addressed with use of heterogeneous catalysts. In a number of publications, high ester yields are reported over these catalysts.[128,132,133] Some of these catalysts include zeolites, exchanged clays, KSF, Al-MCM-4, and other supported reagents.[126,127,132] However, when these catalysts are used, the reactions require the use of high temperatures and also require the use of non-environmentally friendly solvents.[126,132] In addition, these reactions requires longer reaction times in order to afford high product yields, especially when steric hindered alcohols are used.[124,132]

Herein, we report an acylation of *para*-menthane-3,8-diol (PMD) **27** with a variety of acid anhydrides in a batch-scale process. In this work, acid anhydrides with carbon chain length ranging from C_2-C_6 will be used for the study. Our aim was to prepare a variety of derivatives in order to evaluate their properties as plasticizers. The reaction is performed over the water resistant heterogeneous Lewis acid catalyst, namely the polymer-bound scandium triflate (PS-$Sc(OTf)_3$). The effect of reaction parameters such as temperature, residence time and reactant concentration will be investigated in the process towards the di-ester selectivity. Whereas, the **27** conversion and di-ester selectivity will be the response factors. The acylation synthesis route for **27** is shown below (Scheme 30).

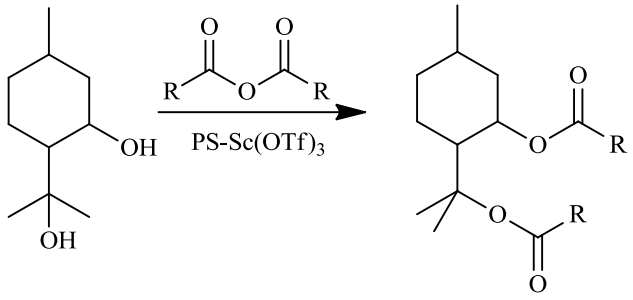

27

Scheme 30: Acylation of *para*-menthane-3,8-diol

4.2.2. Experimental synthesis method

In the first instance, the acetylation reaction of **27** was investigated *via* the batch-scale process. Wherein, acetic anhydride was used as the model acetylating agent over the polymer-bound scandium triflate catalyst. The batch-scale reactions were carried-out by using the reactor set-up as shown in section 2.5 above. During the study, the equimolar ratio of 1:2 (mol/mol) towards **27** and acetic anhydride was used, given that the aim was to react both alcohol functional groups during the reaction. The reaction was allowed to proceed at 60^0C for a period of 24 hours, while 0.3 g of catalyst was used. The reaction was followed by taking samples from the reactor at hourly interval for GC analysis. A typical GC trace of the crude product mixture from the acetylating reaction is showed below (Figure 4.3).

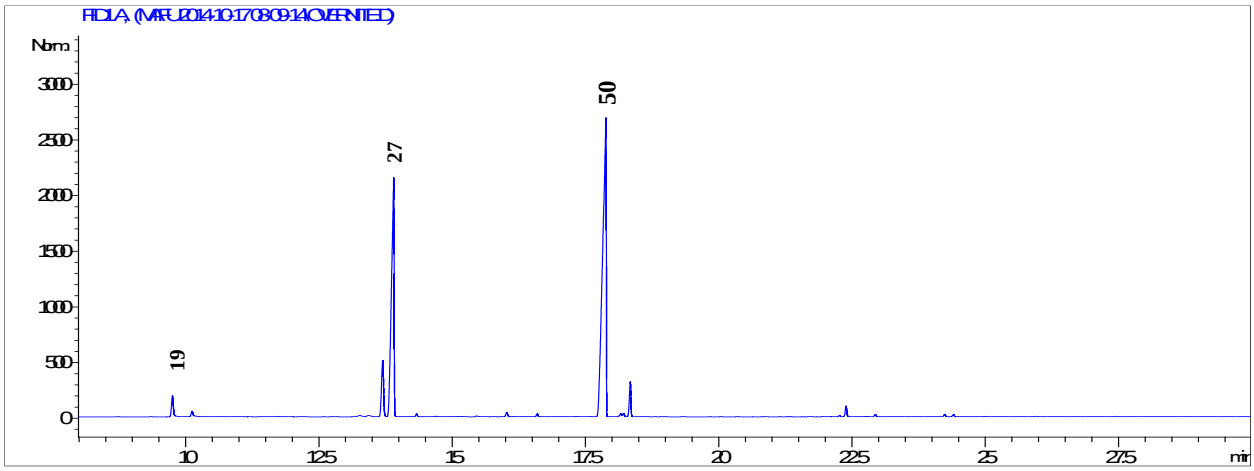

Figure 4.3: GC trace of the di-ester product mixture

4.2.3. Results and discussion

As shown in Figure 4.3 above, the peak eluting at retention time 13.8 minutes is observed to be the least reactive isomer remained unreacted from the starting material. This peak has been confirmed by the GC-MS and its molecular fragment patterns have been observed to be the same as that of the starting material (Figure 4.2). The peak at retention time 17.8 minutes was evident to be the corresponding di-acetate **50** product. Its molecular fragment pattern is showed below (Figure 4.4).

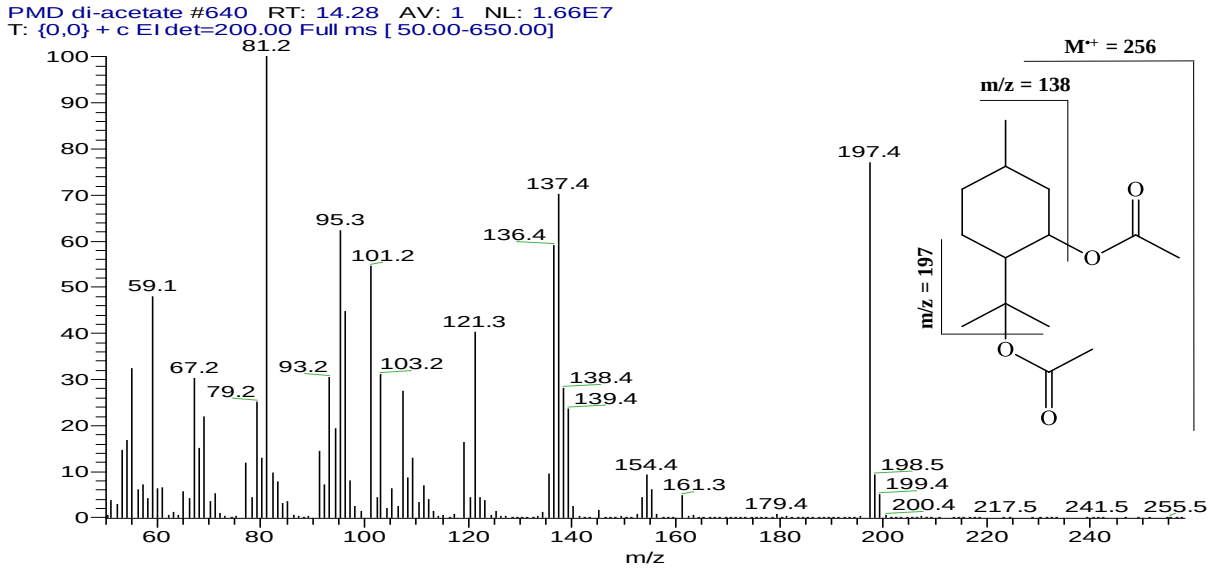

Figure 4.4: Di-acetate mass fragment pattern

As demonstrate in Figure 4.4 above, a weak molecular ion (M^+ = 256) of **50** molecule is observed. This molecular ion corresponds to the compound with a molecular formula of $C_{14}H_{24}O_4^+$. Upon fragmentation of this molecular ion, it can be observed that the first ester

fragment (m/z = 59) is observed between m/z = 256 to 197. After this ester fragment, the second ester fragment (m/z = 59) is observed between m/z = 197 and 138. Finally, the molecule undergo the loss of methyl (-CH_3) and the terminal propyl (-$(CH_2)_2CH_3$) fragments as they are observed between (m/z = 137 to 81). The remainder of the molecule leads to the base peak (m/z = 81), which correspond to $C_6H_9^+$ molecular fragment.

From the FT-IR spectrum of the compound, a very sharp peak is observed at 1728 cm^{-1}. This carbonyl peak denotes the presence of the ester group(s). The disappearance of the broad hydroxyl group peak at 3220 cm^{-1} also confirms that the prepared molecule is definitely the di-ester **50** derivative. Furthermore, two peaks at 1180 cm^{-1} and 1144 cm^{-1} also show the presence of two C-O-C vibration bands on the molecule. These vibration bands denote the bonds of the two ester groups that are linked to the *para*-menthyl backbone. From ^{13}CNMR spectrum, both carbonyl carbon peaks at δ = 170.3 and 169.9 are evident from the molecule. In addition, all the expected number of hydrogen atoms from the molecule were assigned in ^{1}H-NMR spectrum (Appendix B2).

During the course of reaction, the maximum selectivity towards a mono-acetate **54** derivative was observed within an hour of batch reaction time. From the GC trace, the peak that correspond to the mono-acetate **54** derivative was observed at retention time 16.2 minutes. This peak has been confirmed by the GC-MS and its molecular fragment pattern is showed below (Figure 4.5).

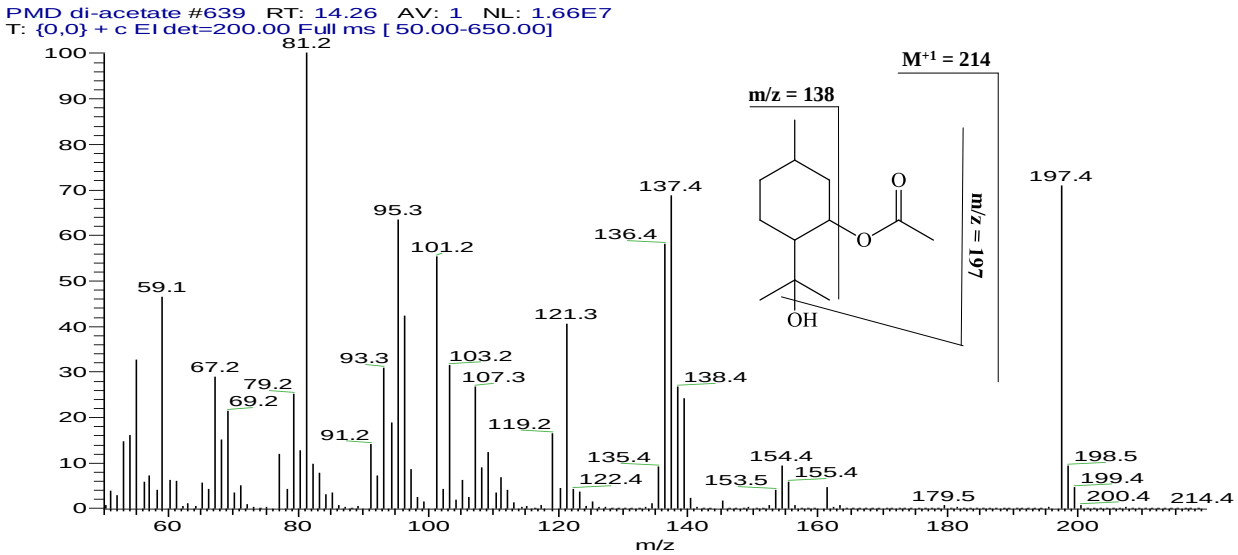

Figure 4.5: Mono-acetate mass fragment pattern

From the above spectrum, a weak molecular ion (M^{+1} = 214) of **54** derivative can be observed. This molecular ion correspond to $C_{12}H_{22}O_3$ and its base peak can be seen at m/z = 81 with the

corresponding empirical formula $C_6H_9^+$. The loss of the hydroxyl group (-OH) fragment (m/z = 17) is evident between m/z = 214 and 197. This is followed by the loss of the ester fragment between m/z = 197 and 138. The dislocation of the terminal propyl (-$(CH_2)_2CH_3$) and methyl (CH_3-) fragments are both observed between m/z: 138 to 81, thus result to the base peak.

The FT-IR spectrum of molecule **54**, has revealed the expected functional groups of the molecule. The hydroxyl group vibration band has been evident at 3435 $cm^{-1.}$ Whereas, the carbonyl carbon (1734 cm^{-1}) and carbon-oxygen (1241 cm^{-1}) vibration bands were also present. These functional groups also provide the conclusive evidence to prove that the obtained compound is a mono-ester derivative.

A further confirmation was done on ^{13}C-NMR, which revealed all the expected number of carbon atoms of the molecule. Additionally, among the observed carbon atoms, a single carbonyl carbon at δ = 170.3 which correspond to the ester group was present. From the ^{1}H-NMR spectrum all the expected number of hydrogen atoms were confirmed from the molecule, including even that of hydroxyl group at δ = 3.70.

Based on the above assignments, the formation of **50** and **54** from the acetylation of **27** can be illustrated as follows (Scheme 31).

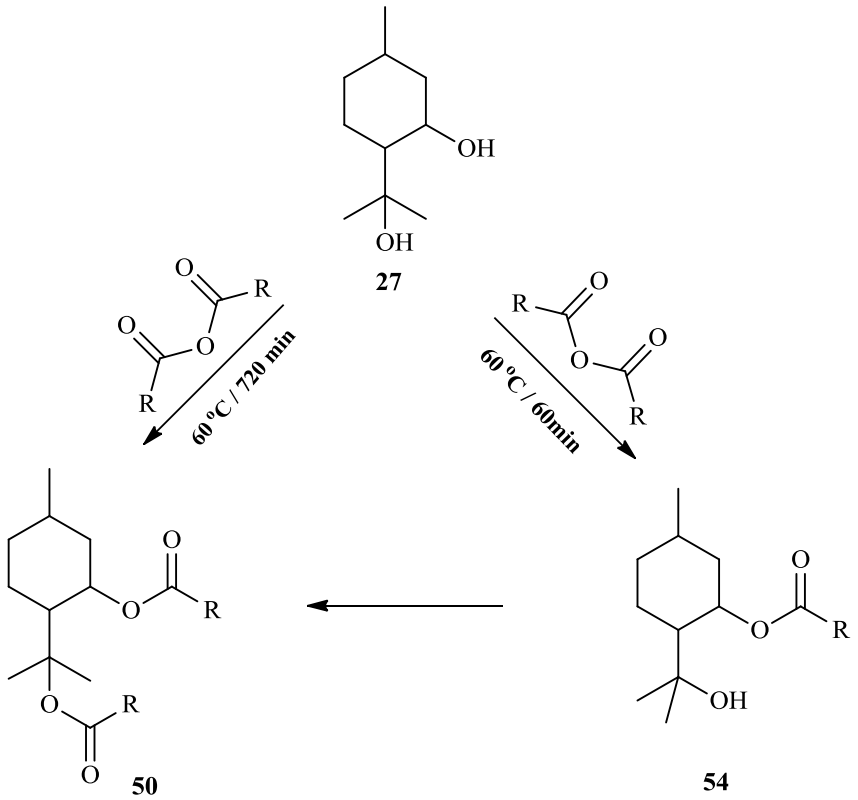

Scheme 31: Acetylation reaction of *para*-Menthane-3,8-diol

The effect of reaction parameters such as temperature, time and reactant concentration were investigated towards the substrate conversion and the product selectivity.

4.2.3.1.1. Effect of temperature and reaction time on substrate conversion

The effect of reaction temperature and reaction time towards **27** conversion were investigated simultaneously. During the study, the reaction was carried-out by varying temperature from 50, 60, 70 to 80°C. Whilst, the equimolar reactant concentration of 1:2 (mol/mol) was maintained. The reaction was allowed to proceed for predetermined length of time (24 hours). The catalyst mass was kept at constant mass of 0.3 g. The samples were taken from the reactor at hourly time interval for GC analysis. The distribution of the reaction product species with respect to the substrate conversion is shown below (Figure 4.6).

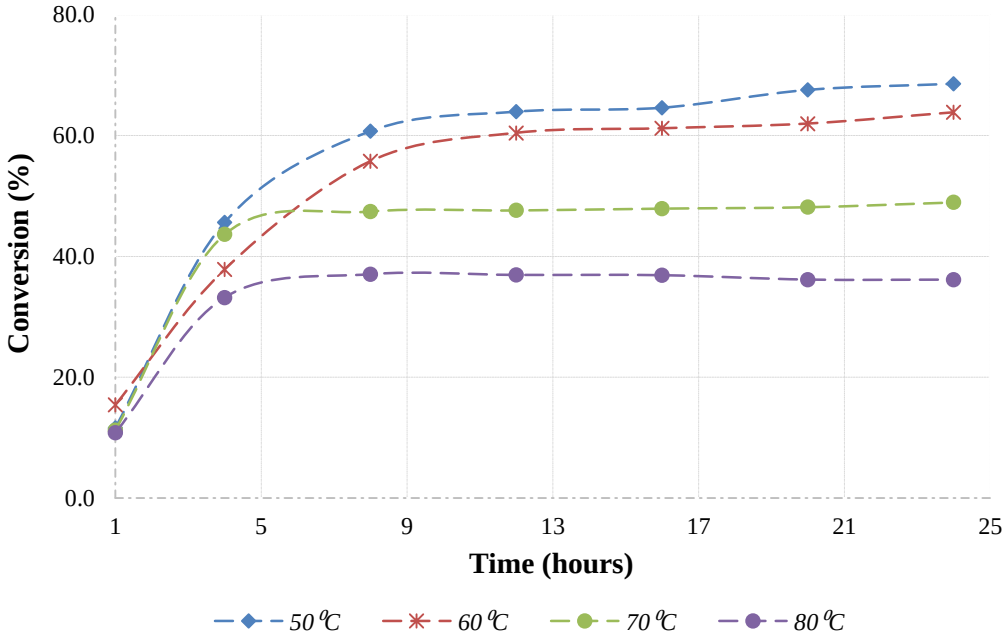

Figure 4.6: Product distribution as a function of time

As it can been seen from the figure above, the substrate conversion to desired product is favoured by operating the reaction at low temperatures such as 50 and 60°C. A further increase in the reaction temperature result to the unreacted isomer of the starting material. Furthermore, the substrate conversion increases with increase in the reaction time, especially when operating the reaction at lower temperature.

4.2.3.1.2. Effect of temperature and reaction time on product selectivity

The reaction was conducted as detailed in the experimental section. The samples were taken from 1 to 24 hours in order to monitor the reaction profile. The reaction is observed to be selectivity enough towards the mono-acetate **54** formation at shorter reaction time (Figure 4.7). This is true, because secondary alcohols are known to be more reactive than tertiary alcohols.[134]

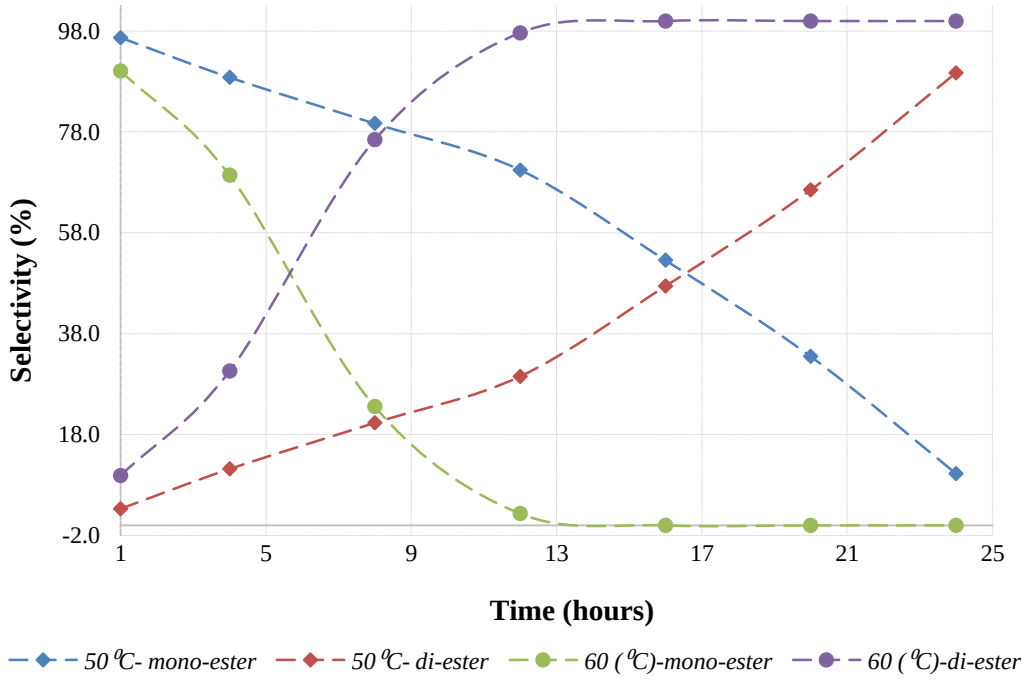

Figure 4.7: Product distribution as a function of time

However, when a reaction is allowed to proceed for longer reaction time, a slow improving selectivity towards the di-acetate **50** formation is observed. The improving selectivity towards **50**, signify the acylation of the tertiary alcohol. It can also be observed that there is a slowly decrease in the mono-ester **54** selectivity with increase in the **50** formation.

On the other hand, the rate of the reaction showed to improve with increase in the reaction temperature to 60^0C. When operating the reaction at these conditions, two substrate isomers are have showed to be less reactive. Therefore, this means that the increase in temperature result the decrease in the substrate conversion. This scenario is also observed when temperature is further increase to 70 and 80^0C (Figure 4.8). Even though the enhanced reaction rates are observed at 70^0C with respect to the di-ester formation.

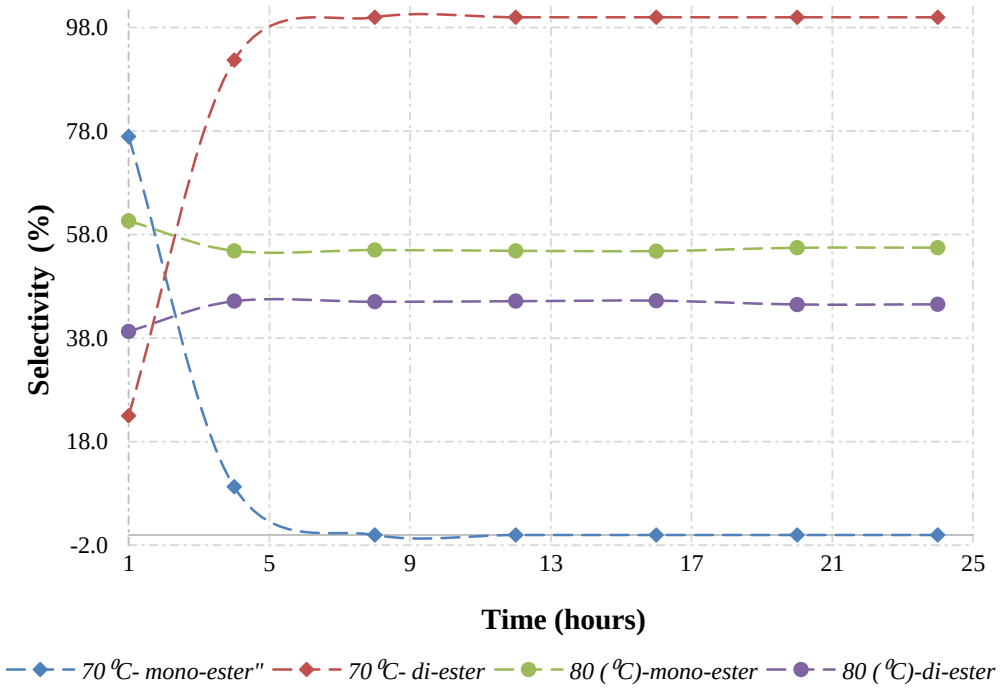

Figure 4.8: Product distribution as a function of time

At the temperature of 80^0C, the poor substrate conversion and poor selective towards **50** are observed. Based on these reaction conditions, it can be concluded that the synthesis of di-ester derivative does not require the use of high reaction temperatures and shorter reaction time. For the optimum substrate conversion and good di-ester selectivity, lower reaction temperatures and longer reaction times are required to be used.

4.2.3.1.3. Effect of molar ratio

We further investigated the effect of molar ratio towards the substrate conversion and di-ester selectivity. Bearing in mind that the reaction temperature of 60^0C is the optimum temperature conditions for the reaction, from previous data, the experimental reactions were performed by keeping other reaction parameters constant such as temperature (60^0C), stirring rate (500 rpm), reaction time (12 hours) and catalyst (0.3 g). Whereas, the molar ratio of the reacting anhydride was varied from 2, 3, 4, 5 and 6, respectively. The observed results are summarised by the product distribution graph as indicated below (Figure 4.9).

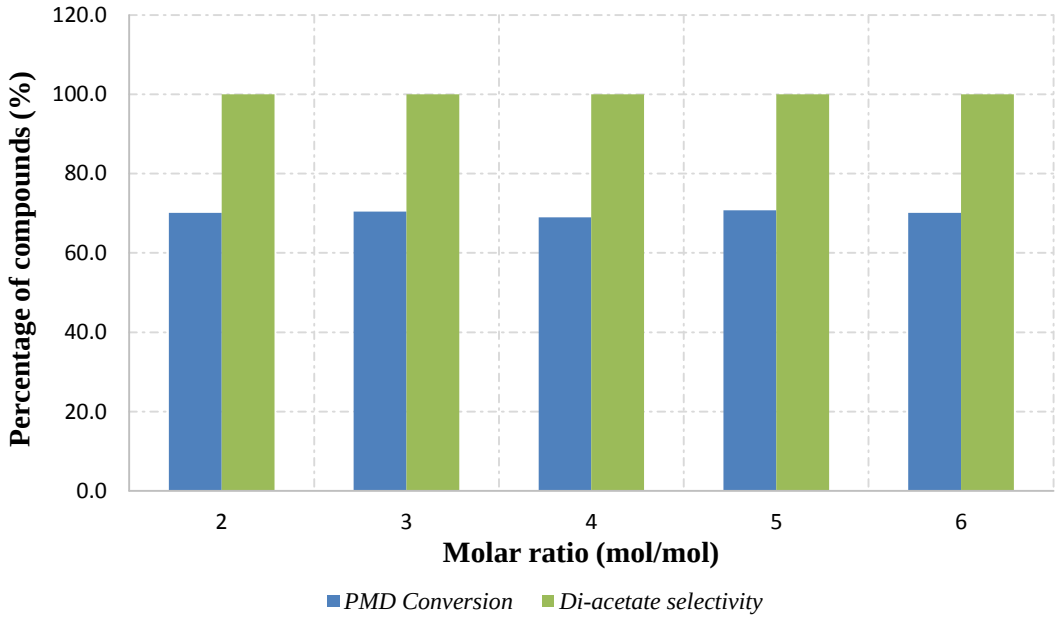

Figure 4.9: Effect of molar ratio in product distribution

From the graph above, it can be seen that the use of excess acid anhydride does not enhance the conversion of the starting material or the selectivity of the desired product. The equimolar ratio of 1:2 (mol/mol) proved to be sufficient in the reaction. Moreover, this reduces the use of excess amount of acid anhydride and also reduces the carboxylic acid by-product, thus leads to the more environmentally-friendly process.

4.2.3.1.4. Kinetic studies of the batch acetylation reaction

It was also important to deduce the order of the reaction that leads to the formation of the desired product. In this section, our focus is to investigating the overall kinetic studies that favours the conversion of the starting material.

The overall rate equation of the reaction was determined with respect to the consumption rate of **27** and can be expressed as follows: *Where A represent compound **27** (PMD)*

$$-\frac{d[A]}{dt} = k[A] \qquad \textbf{(Eqn. 4.1)}$$

By integrating the above equation in terms of *d[A]* and *dt*, this leads to the following equation:

$$\int_{[A]_0}^{[A]} -\frac{d[A]}{dt} = -k_1 \int_0^t dt \qquad \textbf{(Eqn. 4.2)}$$

Where [A] = [A]$_o$ at time (t = 0) and [A] = [A] at time (t = t)

Therefore, the above formula can be expressed as follows with respect to the first order dependence equation:

$$\int_{[A]_0}^{[A]} \frac{d[A]}{dt} = -k_1 \int_0^t dt \quad \rightarrow \quad \ln\left(\frac{[A]}{[A]_0}\right) = -kt \qquad \textbf{(Eqn. 4.3)}$$

The final first-order dependence reaction equation can be expressed as follows:

$$\frac{[A]}{[A]_0} = e^{-k_1 t} \quad \text{or} \quad [A] = [A]_0 \, e^{-k_1 t} \qquad \textbf{(Eqn. 4.4)}$$

Integrating equation 3.1 in terms of d[A] and dt for second-order dependence, this leads to the following equation:

$$\frac{[A]}{[A]_0} = \frac{1}{1 + k_2 [A]_0 t} \quad \text{or} \quad \frac{1}{[A]} = k_2 t + \frac{1}{[A]_0} \qquad \textbf{(Eqn. 5.5)}$$

As the conversion of **27** has been measured as a function of time (Table 3.2), therefore a rate law of the reaction can be determined from the plots of [A] vs time (zeroth-order kinetics), ln[A] vs time (first-order kinetics) and $[A]^{-1}$ vs time (second-order kinetics). Based on the plots that are presented below (Figure 4.10, 11 and 12), the observed data can be explained by the zeroth-order (plot of [A] vs time) which revealed a better correlation square (R^2 =0.9331).

Table 4.1: *para*-Menthane-3,8-diol conversion data

Time (hours)	PMD Conv. (%)	In [A]	$[A]^{-1}$
1	15.4	2.734	0.065
4	31.8	3.460	0.031
8	55.7	4.021	0.018
12	60.4	4.101	0.017

- Zeroth-order kinetics plot is presented below as follows (Figure 4.10):

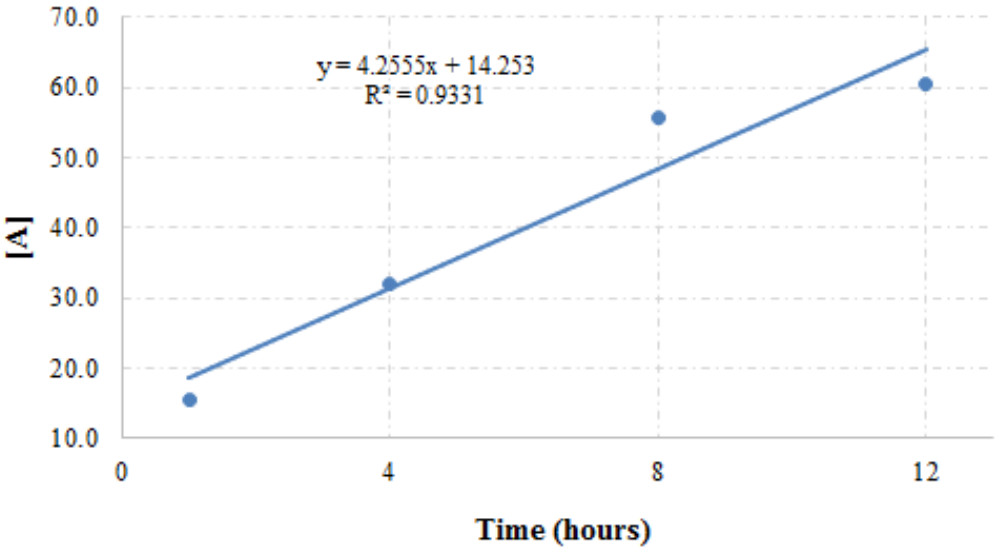

Figure 4.10: Zeroth-order kinetics plot

- First-order kinetics plot is presented below as follows (Figure 4.11):

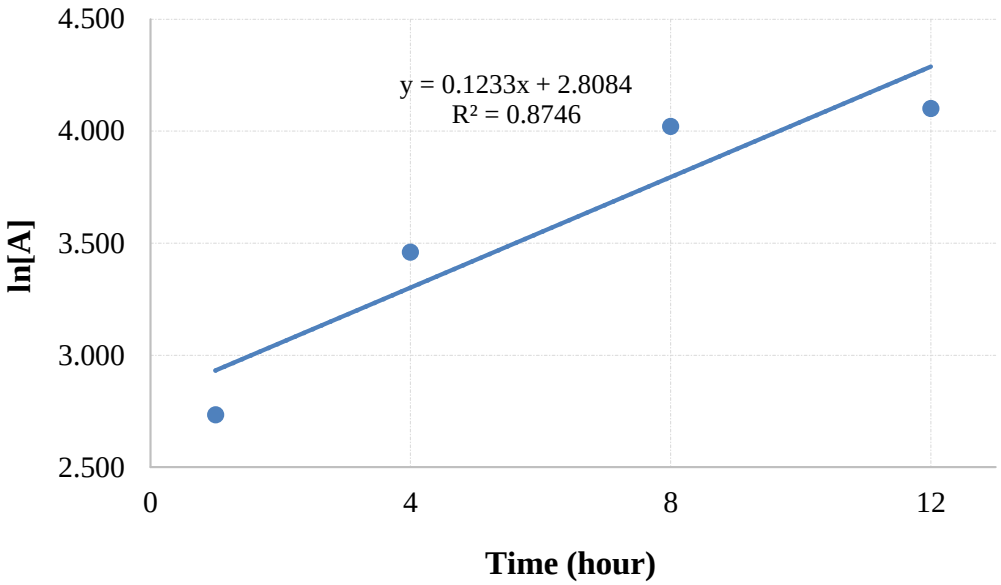

Figure 4.11: First-order kinetics plot

- Second-order kinetics plot is presented below as follows (Figure 4.12).

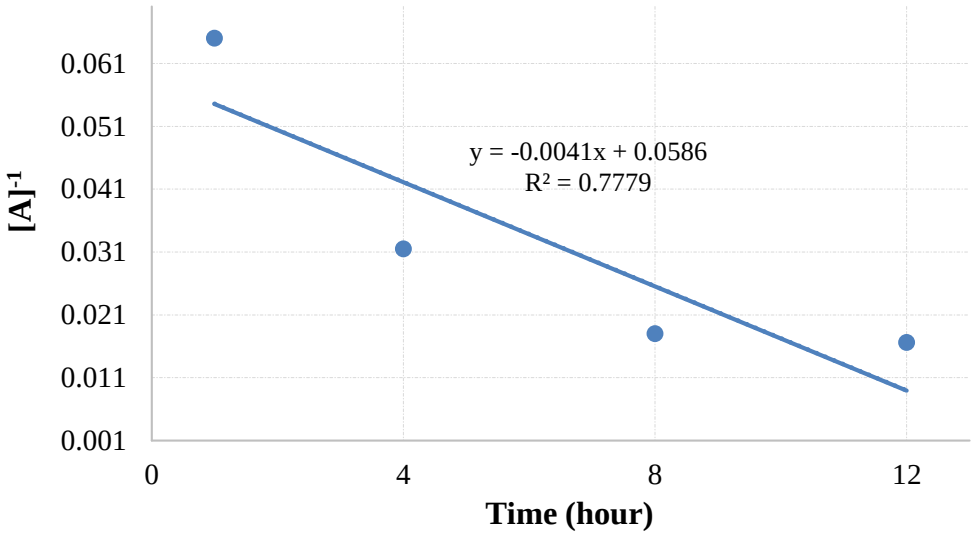

Figure 4.12: Second-order kinetics plot

Therefore, it is concluded that the zeroth-order kinetics can at least describe the observed acetylation data over the polymer-bound scandium triflate catalyst. Furthermore, the slope of the straight line (Figure 4.13) of the zeroth-order rate constant (k_1) was found to be 3.75 hr^{-1}.

It was also important to use a substrate conversion at constant reaction time to determine whether the reaction obeys an Arrhenius law. The variation of the rate constant (k_1) with temperature was then estimated from the substrate conversion data at three temperature levels (50, 60 and 70°C). Wherein, a constant reaction time of 12 hours being selected as the optimum reaction time. The obtained results are presented below (Table 4.2).

Table 4.2: Variation in the zeroth-order rate constant (k_1) with temperature

Entry 1	K	ln (K)	Tempe (K)	Temp (K^{-1})
1	1.90000	0.6	323	0.0031
2	3.75241	1.3	333	0.0030
3	5.60000	1.7	343	0.0029

In the graph presented below (Figure 4.13), a straight line was observed, which confirms that the **27** acetylation reaction does obey an Arrhenius law (Eqn. 4.6).

$$k_1 = Ae^{-EA/RT} \qquad \textbf{(Eqn. 4.6)}$$

Where: k_1 is first order rate constant (min^{-1}); A is pre-exponential factor (min^{-1}); E_A = activation energy ($J\ mol^{-1}$); R is gas constant; and T is the temperature (K).

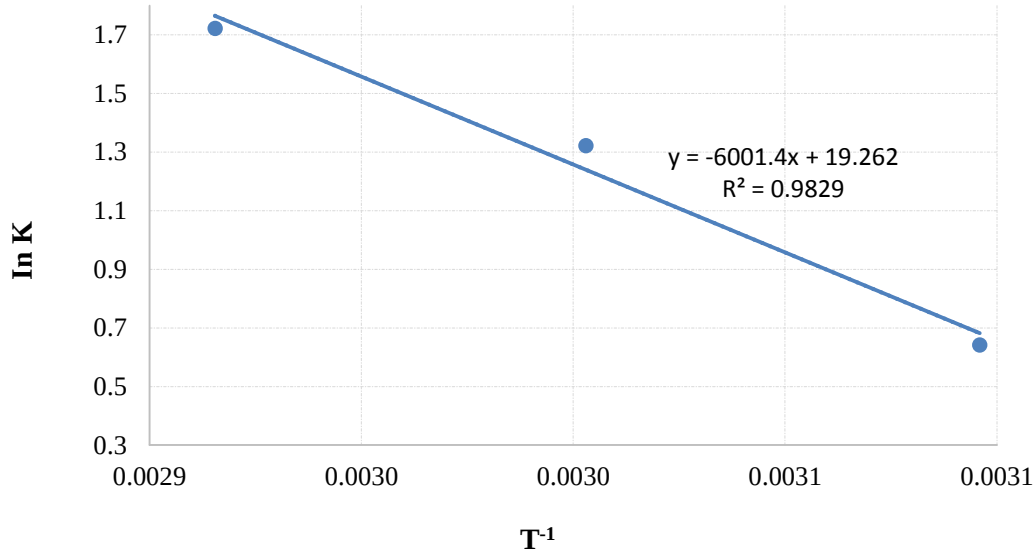

Figure 4.13: Graphical presentation of ln(K) vs T^{-1}

The activation energy (E_A) of the reaction was deduced from the slope ($-E_A/R$) and the pre-exponential factor was estimated from the intercept. The activation energy was found to be 49.89 $KJ.mol^{-1}$ and the pre-exponential factor was $2.31x10^9$ min^{-1}.

4.2.3.1.5. Isolation and purification of di-acetate

The unreacted **27** and acetic acid (by-product) were removed from the product mixture by the vacuum distillation. The obtained **50** product was further purified by the use of column chromatogram over a silica gel 60 (70-230 mesh) stationary phase. Wherein, a mixture of hexane-ethyl acetate 98:2 (v/v) was used as mobile phase. The pure **50** was isolated in almost 100% purity (Figure 4.14). It was characterised by ^{1}H-NMR, ^{13}C-NMR, FT-IR and GC-MS. The observed characterisation data is listed above (subsection 2.6.1) and the raw data can be found below (Appendix B4).

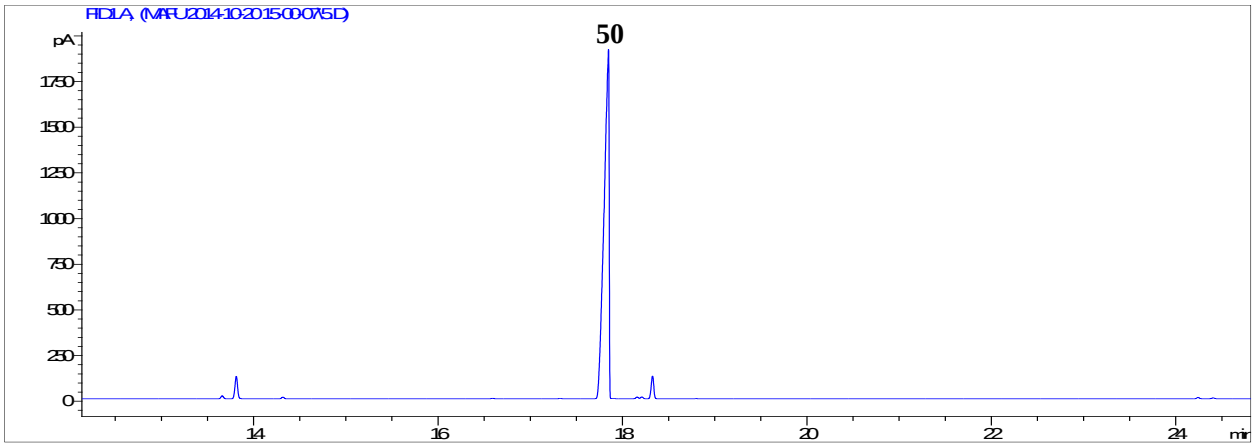

Figure 4.14: GC-trace of pure di-acetate

From the GC-trace shown above, the **50** peak can be observed at retention time 17.8 minutes together with the trace component of the starting material at retention time 13.9 minutes and the raw data can be found below (Appendix B4).

4.2.3.1.6. Synthesis of propyl-, pentyl- and hexyl di-ester derivatives

Another three types of di-ester derivatives (di-propionate **51,** di-pentanoate **52** and di-hexanoate **53)** including their mono-ester derivatives **(**mono-propionate **55,** mono-pentanoate **56** and mono-hexanoate **57** were also prepared according to the method described above. During the synthesis of these compounds, different types of acetylating agents were used, namely propionic, pentanoic and hexanoic anhydride. The prepared compounds were quantified by the gas chromatography and the obtained results are summarised below (Table 4.3).

Table 4.3: PMD acetylation with different types of acid anhydride

Reagent	PMD(conv.) %	Mono-ester (sel.) %	Di-ester (sel.) %
Propionic anhydride	70.5	0	65.8
Pentanoic anhydride	69.6	10	63.2
Hexanoic anhydride	70.1	16	60.4

The product mixtures of the prepared compounds were purified by vacuum distillation and the desired mono- and di-ester compounds were further isolated by the column chromatography. The GC-traces of the vacuum distilled di-ester compounds are shown below (Figure 4.15).

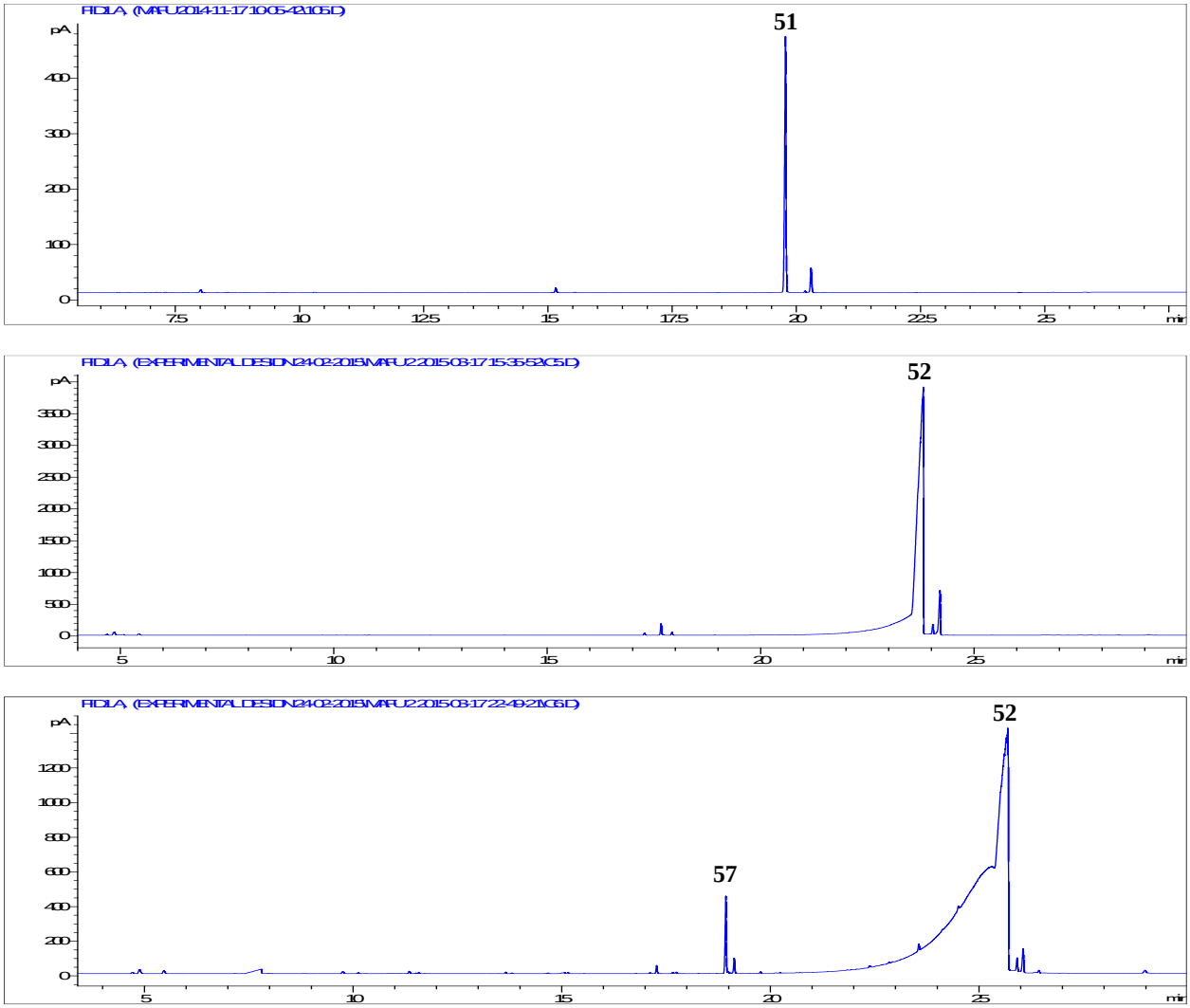

Figure 4.15: *para*-Menthane-3,8-diesters

The acylation reaction trend of the prepared di-ester compounds, which are demonstrated above (Table 4.3) are also graphically presented below (Figure 4.16).

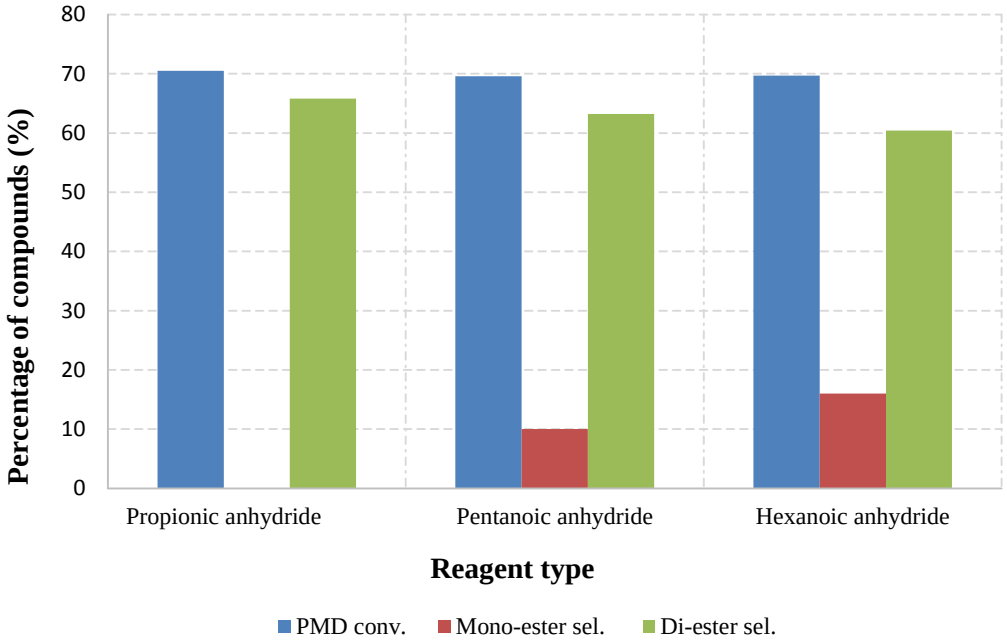

Figure 4.16: PMD acylation with different acid anhydride

What can be seen in Figure 4.16, is a decrease in di-ester selectivity with increase in the carbon chain length of the acylating agent. This indicates that an increase in the carbon chain length of the acylating agent result in slower reaction rate as compared to that of the shorter carbon chain length. As a consequence, the reaction times become longer than expected in order to achieve the higher degree of di-ester formation.

4.2.3.1.7. Physical properties of *para*-menthane-3,8-di-ester derivatives

Given that the aim was to use the di-esters as potential plasticisers, we wanted to check that the physical properties of these derivatives were similar to those of commercial plasticisers. When considering the physical properties of the di-ester derivatives, the observed data show no significant difference as compared to the conventional plasticisers. All the prepared di-ester compounds are of higher molecular weight, oily liquids and having higher boiling points (greater than 200ºC). However, the minor differences can be observed in other properties such as density, flash point and viscosity. In table 4.4 below the comparison between the conventional plasticisers (DEHP, and DPP) and the di-ester derivatives (Di-acetate and Di-propionate) are indicated. The properties of other di-ester derivatives are further showed under Appendix C.

Table 4.4: Comparison between the conventional plasticiser and di-ester derivatives

Properties	DEP	DPP	Di-acetate	Di-propionate
physical state	oily liquid	oily liquid	oily liquid	oily liquid
M. W (g/mol)	222.224	250.229	256.17	284.4
Formula	$C_{12}H_{14}O_4$	$C_{14}H_{18}O_4$	$C_{14}H_{24}O_4$	$C_{16}H_{28}O_4$
colour	Colourless	Colourless	colourless	colourless
boiling point (°C)	298	317	288	319
Flash point (°C)	117	166	122.1	129.1
Density @20 °C g/cm3	1.178	1.08	1.0018	1.0034
Odour	Odourless	odourless	odourless	odourless

Therefore, it can be concluded that these natural based di-ester derivatives of **27** can be used as potential replacement for the conventional phthalate plasticisers. Furthermore, they are expected to be less toxic for human use and environmentally-friendly since are derived from natural compound.

4.2.4. Discussion

In this work, the synthesis of *para*-menthane-3,8-diesters has been successfully demonstrated in the batch-scale process. The following reaction aspects have been observed from the study:

PMD conversion: The substrate conversion has been found to decrease with increase in temperature above 70^0C. Moreover, two isomers of the starting material are found to be less reactive in these conditions. The reaction showed to be optimum at the temperature of 60^0C and below. Furthermore, the use of an excess amount of acylating agent does not play any significant role in enhancing the substrate conversion.

Mono-ester selectivity: the reaction has been found to be selective to the mono-ester derivative if short reaction times are used. This confirms a rapid reaction between the highly reactive secondary substituted hydroxyl group and the acylating agent. When longer carbon chain length of the acylating agent is used, there is an observed decrease in rate of mono-ester consumption.

Di-ester selectivity: On the other hand, the di-ester selectivity was found increase with increase in reaction time when operating the reaction at lower temperature conditions. This was due to the slow reaction of the tertiary hydroxyl group of the substrate with acylating agent. The reaction rate was also observed to drop significantly with increase in the carbon chain length of the acylating agent. As a result, more reaction time was required to better the degree of the di-ester formation.

4.2.5. Concluding remarks

Herein, we have demonstrated a green synthesis method for the di-ester derivative of *para*-menthane-3,8-diol in the batch-scale process. The reaction is readily carried-out in solvent-free system at mild reaction conditions. The use of polymer-supported scandium triflate catalyst as heterogeneous Lewis acid catalyst showed to be stable in the reaction. The catalyst showed to be re-usable with no observed change on the substrate conversion or product selectivity. Our further work is optimise this method in continuous flow chemistry to see if even high selectivity can be observed.

CHAPTER 5

Continuous-flow synthesis of para-menthane-3,8-esters

5.1. Optimisation process for the mono- and di-ester synthesis

5.1.1. Overview

Reactions performed with traditional heating equipment such as oil bath, sand bath and heating material result in slow reactions. Moreover, they create a hot surface on the reactor, which can lead to the decomposition of the product, reagents and substrate species over time.[138] As early as the mid-1980s, microwave irradiation has been used as an alternative energy source to perform various organic reactions.[139-143] This method has revealed excellent performance as a heating source. Wherein, enhanced reaction rates and improved product yield have been achieved in shorter reaction times.[144] Most reactions were carried-out using the domestic microwave oven, thus this method has suffered from many challenges. Such challenges that include the issue of scale-up capability, poor control over reaction temperature together with the reagent mixing and the use of open vessels, *etc*.[145] Therefore, these challenges tend to hinder the implementation of this technology in large production scale.

Recently, a new research approach has been reported that combine the milli-reactor operation and the microwave-assisted heating as an advanced organic synthesis method.[54,145,106] The advantage of this method, allows one to have good control over temperature and residence time. Additionally, it is compatible with many organic solvents, able to transfer the laboratory reactions into industrial process, safer process and easy to use *etc*.[146]

As part of our investigation, herein we report an optimisation process of *para*-menthane-3,8-diol **27** acylation reaction with acid anhydride (Scheme 32). This study involves the utilisation of the combined technology of milli-reactor operation and microwave-assisted irradiation. In addition, the process employs polymer-bound scandium triflate (PS-Sc(OTf)$_3$) as the catalyst. This new technology will allow us to accurately measure the reaction temperatures and residence times of the substrate mixture. The design of reactor set-up allows an easy separation of the product mixture from the catalyst. As a result, the product mixture will be collected from the reactor exit as it forms without a need for catalyst work-up.

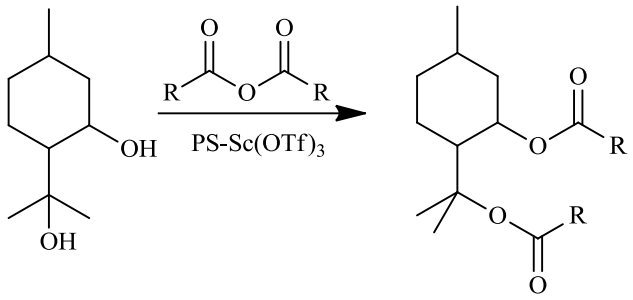

27

Scheme 32: Acylation of *para*-menthane-3,8-diol

5.1.2. Experimental design and model validation

During the acylation of **27**, acetic anhydride has been used as the initial acetylating agent and the reaction was optimised in the microwave-assisted continuous-flow-reactor system. After several reactions have been carried-out in the reactor system at various temperature conditions, the experimental domain was established as shown below (Table 5.1).

Table 5.1: Experimental domain

	Temperature (°C)	Flow-Rate (mL/min)	Residence time (hours)
Minimum	60	0.01	2.40
Maximum	80	0.05	0.47

As demonstrate in the previous chapter, the reaction was found suitable at reaction temperature of 60^0C. Having that in mind, we were still keen to determine the effect of higher temperature conditions towards the substrate conversion and product selectivity in continuous-flow process to see if very accurate control of the conditions could fine-tune the process. Hence, the maximum reaction temperature of 80°C is used as the extreme reaction conditions. We have seen in the batch-scale process the reaction really required long reaction time of 12 hours.

The experimental domain indicated above was further used to create the central composite design (CCD) to execute the experiments in a well-developed fashion. In this case, a total of 12 experiments were developed from the central composite design. However, before these experiments were executed, the microwave-assisted reactor system was evaluated for the repeatability.

5.1.2.1. Method uncertainty

To establish the repeatability of the experimental method, the reactor system was allowed to equilibrate at the temperature of 70^{o}C and the substrate mixture was pumped at the flow-rate of 0.01 mL/min. After two hours of equilibration time, three replicate samples were taken from the reactor system for GC analysis. The results that were obtained from GC quantification were used to determine the relative standard deviation to confirm the repeatability of the reactor system (Table 5.2).

Table 5.2: Method uncertainty

Replicates	PMD (%)	Mono-ester (%)	Di-ester (%)
Run-1	72.3	12.1	67.5
Run-2	71.9	12.6	66.8
Run-3	72.1	12.4	67.4
Average	72.1	12.4	67.2
S	0.2	0.3	0.4
T	4.303	4.303	4.303
Uncertainty (95%)	0.5	0.6	0.9
% RSD	0.28	2.03	0.56

The average amount of di-ester selectivity over three replicate runs was found to be 67.2 ± 0.9 (95% confidence) and the average amount of *para*-menthane-3,8-diol **27** conversion over three replicate run was found to be 72.1 ± 0.5 (95% confidence). From the table indicated above, the results observations were found to be consistent as evident by the small relative standard deviation (RSD). Therefore, this clearly indicates that the reactor is repeatable and can be used to optimise the **27** acylation reaction.

5.1.2.2. Gas chromatography uncertainty

To determine the instrumental error, the sample labelled as run-2 as indicated above was further analysed three times in the instrument to achieve three replicate runs. The relative standard deviation (RSD) was determined from the observed data in order to confirm the repeatability of the GC instrument (Table 5.3).

Table 5.3: Gas chromatogram uncertainty

Replicates	PMD (%)	Mono-ester (%)	Di-ester (%)
Run-2 (i)	72.9	12.6	66.8
Run-2 (ii)	72.4	12.3	66.5
Run-2 (iii)	71.4	12.9	66.9
Average	72.9	12.3	66.4
S	0.5	0.4	0.5
T	4.303	4.303	4.303
Uncertainty (95%)	0.2	0.9	1.1
% RSD	0.7	2.86	0.69

The GC analysis results also showed the repeatable data with a small relative standard deviations, which indicates that the instrument can be used to quantify the product mixtures.

5.1.2.3. Central composite design and observations

The central composite design (CCD) was established from the experimental domain (Table 5.1) to optimise the di-ester synthesis. The optimisation process was performed by varying temperature and flow-rate. The central composite design of experiments and the reaction observations are detailed below (Table 5.4). The substrate conversion, mono- and di-ester selectivities were used as the response factors to investigation the response surface modelling.

Table 5.4: Central composite design for PMD acetylation reaction

Run	Temp (^{0}C)	FR (mL/min)	PMD conv. (%)	Mono-ester sel. (%)	Di-ester sel. (%)
1	60	0.03	60.1	32.9	50.8
2	77	0.02	65.2	21.5	58.9
3	63	0.02	66.5	22.3	61.3
4	80	0.03	61.4	33.8	34.2
5	70	0.03	72.1	31.9	44.8
6	63	0.04	61.6	38.7	40.2
7	70	0.03	73.4	32.4	45.2
8	70	0.01	71.3	16.7	67.4
9	70	0.05	68.5	41.8	26.8
10	70	0.03	72.6	31.9	44.6
11	77	0.04	66.9	41.5	22.9
12	70	0.03	71.8	32.0	43.9

5.1.3. Result and discussion

5.1.3.1. Response surface modelling for the PMD conversion

The reaction variables such as temperature and flow-rate were investigated for their statistic significant influence on the observed **27** conversion data (Table 5.4). The variation of the observed data was investigated by using a multi-linear regression model.

5.1.3.1.1. Model derivation

The observed experimental data of **27** conversion was fitted on the general proposed multi-linear regression model as showed above (Equation 2.3). The estimated regression coefficients from the analysed experimental data are summarized below (Table 5.5). In this work, all estimated coefficients whose p-value is below 5%, will be assumed to be statistically significant. Therefore, those corresponding variables will be known to have a significant effect towards **27** conversion.

Table 5.5: Estimated regression coefficients & associated statistics

Coefficient	Term	b	Std. err.	t(6)	p-value
$\mathbf{b_0}$	Intercept	-459.995	18.103	-25.409	<0.0001
$\mathbf{b_1}$	T	15.456	0.501	30.822	<0.0001
$\mathbf{b_2}$	F	-750.588	166.131	-4.518	0.004
$\mathbf{b_3}$	T^2	-0.113	0.004	-31.83	<0.0001
$\mathbf{b_4}$	F^2	-5343.75	886.49	-6.027	0.001
$\mathbf{b_5}$	TF	-5343.75	2.242	6.465	0.001

In order to obtain the final response surface model, all the insignificant terms (p-value > 0.05) must be eliminated from the predicted model. In this instance, all the observed estimated coefficients are found to be significant enough to define the model. Therefore, the final regression model with respect to the substrate conversion are has remain the same as the general model (Equation 5.1).

$$\textbf{PMD conv.(\%)} = b_0 + b_1T + b_2F + b_3T^2 + b_4F^2 + b_5TF \qquad \textbf{(Eqn. 5.1)}$$

From data presented in table 5.5 above, the final model shows that temperature plays a significant role towards the substrate conversion. However, the flow-rate does not really have an effect on the reaction. Therefore, the increase in the flow-rate with decrease in the residence

time results to the significant decrease in the conversion of the starting material. Alternatively, the increase in temperature result to the increase of the substrate conversion.

5.1.3.1.2. Model validation

Before the final response surface model is accepting the model as a good description of data, it is recommended to determine the variation on the observed conversion data and indicate the possible outliers.

5.1.3.1.2.1. Analysis of variance

The variation of substrate conversion data points are explained by the quadratic response surface model as showed above. The smaller p-values of the estimated coefficients reveal that the observed conversion data points actual fits the chosen quadratic model well. The high correlation square ($R^2 = 0.990$) also confirmed a good correlation on the data points.

5.1.3.1.2.2. Analysis of residuals

The validity of the model described above can be confirmed by performing the residual analysis on the experimental data. The residual analysis can be expressed in form of scatter diagram together with the normal probability plot. The scatter diagram indicates the variation of residuals around the regression line (predicted values). Whereas, a normal probability plot measures the degree of deviation between the observed and expected normal values. The distribution of residual for the substrate conversion is summarised below in a form of scatter (Figure 5.1).

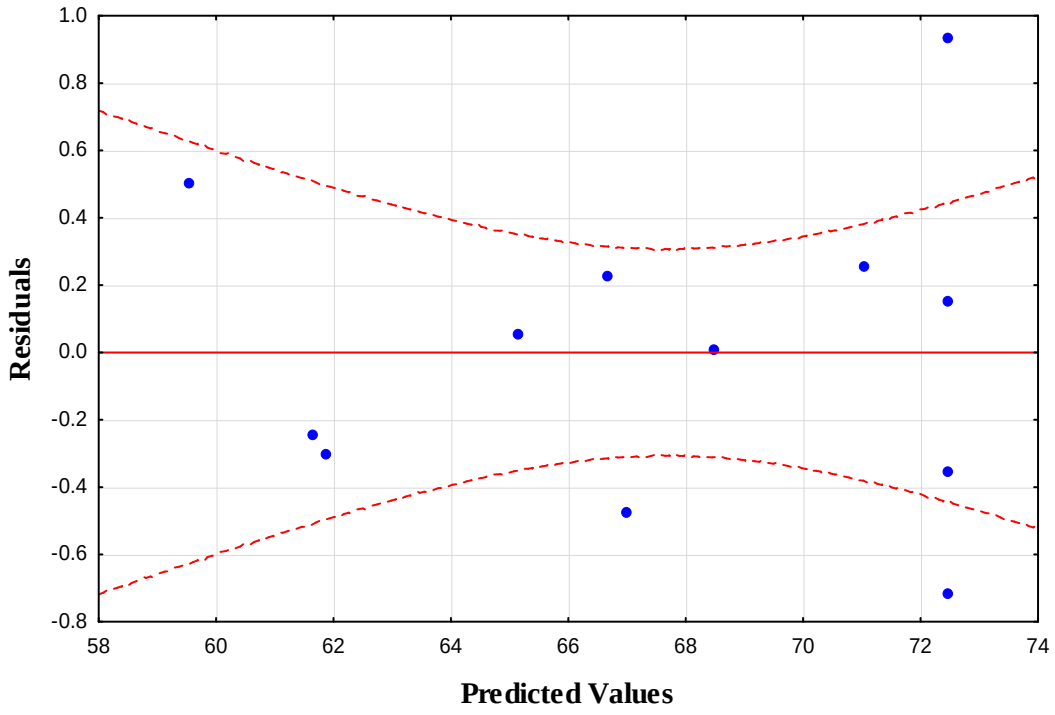

Figure 5.1: Outlier scattered plot of residuals for PMD conversion

From the graph denoted above, the residuals are observed to be randomly distributed around the regression line (non-heteroscedasticity). Therefore, there are no outliers observed from the substrate conversion data (none of the residuals is below -2 or above 2). Additionally, the observed data set is normally distributed as showed above (Figure 5.2).

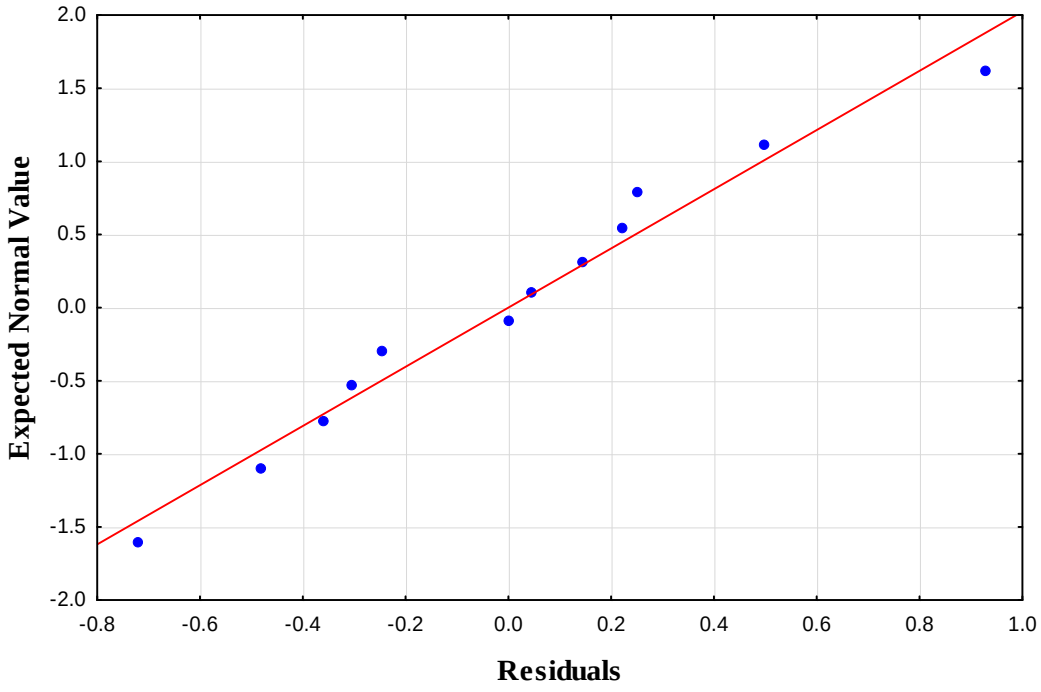

Figure 5.2: Normal probability plot for PMD conversion

The data presented above appear to be normal distributed around the straight line of the expected normal values. There is no observed defined pattern from the graph and the model is reasonable good to define the conversion data. As a result, the model is accepted as a good description of data with respect to the substrate conversion. Furthermore, it can be used to predict the reaction outcome with regards to the substrate conversion from any set of reaction conditions.

The effect of reaction parameters such as temperature and flow-rate towards the substrate conversion can be presented by means of profile plots. Below is a summary on the variation of these parameters towards the substrate conversion.

5.1.3.1.3. Effect of temperature and flow-rate in PMD conversion

The effect of temperature on the substrate conversion has been investigated and the data observed is graphically presented as follows (Figure 5.3).

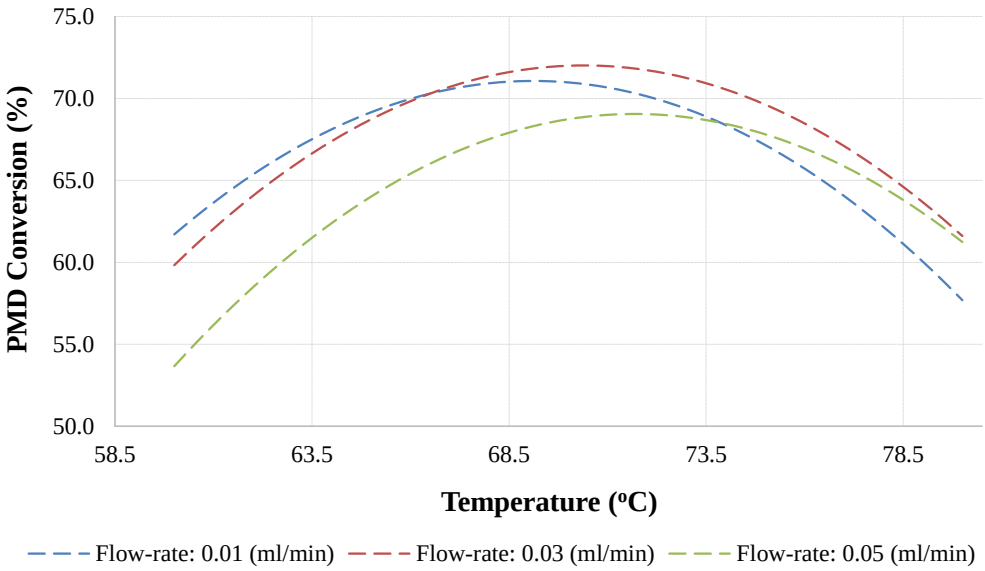

Figure 5.3: Effect of temperature on the conversion

What is observed from Figure 5.3, the substrate conversion is increasing with increase in the reaction temperature. The substrate conversion signifies the acylation of hydroxyl groups of the molecule. The conversion is showing to be stable at the temperature range of 69–73°C.

On the other hand, the effect of flow-rate on the substrate conversion was also investigated at three temperature levels. The observed experimental data is graphically presented below (Figure 5.4).

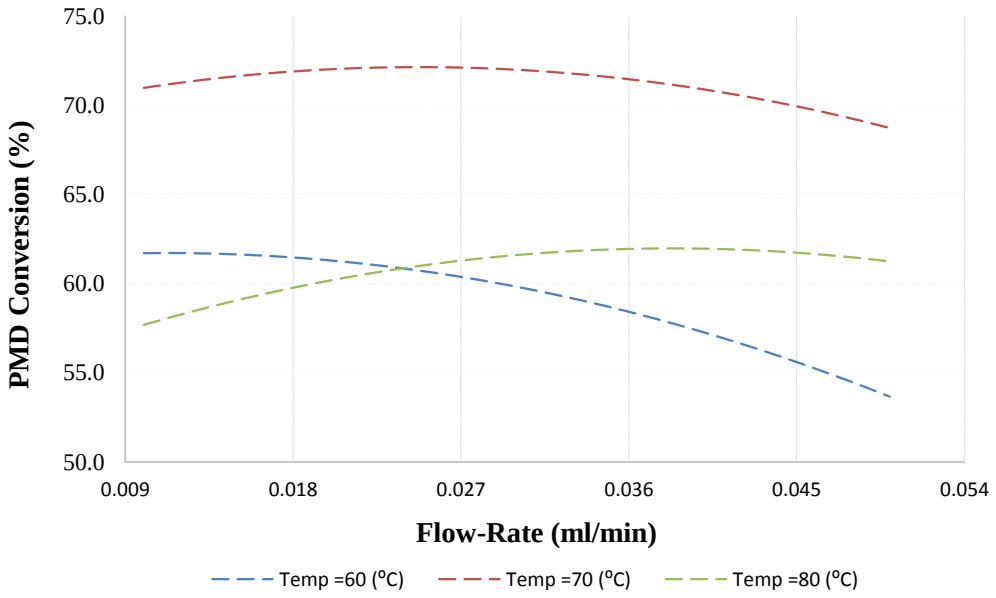

Figure 5.4: Effect of flow-rate on PMD conversion

From the graph shown above, it is clearly observed that flow-rate has a significant effect in the reaction. When a reaction is operated at lower temperature of 60°C and flow-rate of 0.01 mL/min, more of substrate was converted in the reaction. The further increase in flow-rate to 0.05 ml/min (shorter residence time), a significant decrease in the substrate conversion is observed. This signifies a poor catalytic interaction with the reacting species. An improved reaction rate has been observed when a reaction is operated at the temperature of 70°C. The substrate conversion is found to be optimum at the temperature of 70°C and flow-rate of 0.01 ml/min.

5.1.3.1.4. Prediction intervals for estimated responses

The above final response surface model can be used to predict the substrate conversion from any set of parameters. Nevertheless, the predicted conversion value is not conclusive enough without the estimated error uncertainty. Therefore, it is highly recommended to obtain the predicted interval in which the predicted substrate conversion will lie within a given level of confidence. The error uncertainty was calculated by using the equation indicated above (Equation 2.4).

In this work, the error uncertainty was calculated based on the optimum conditions (run-8) as shown in the central composite design (Table 5.4). This set of data was used to calculate the error uncertainty at 95% confidence interval. Based on the calculations, the observed substrate conversion and its error uncertainty are expressed as follows; *PMD conversion* = 71.05 ± 1.92. It can be seen that the data is characterised with smaller error uncertainty value that is less than 5%, which confirms that the observed final response model fits data well.

5.1.3.1.5. Model interpretation

The final quadratic response surface model of the observed data points is can be presented graphically as showed below (Figure 5.5).

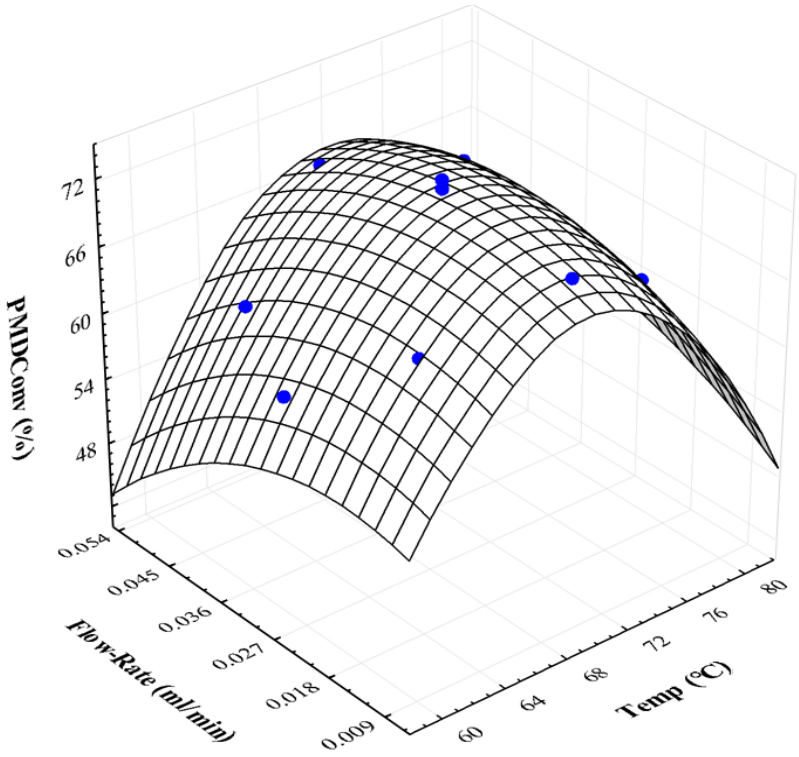

Figure 5.5: 3-D surface plot for the PMD conversion

From Figure 5.5 above, a 3-D surface plot shows that the substrate conversion increases with decrease in the residence time (flow-rate of 0.01 mL/min) at lower reaction temperature. When shorter residence time (flow-rate of 0.05) is used, there is a significant decrease in the substrate conversion. This clearly indicates that the increase in the flow-rate does not provide a sufficient interaction between the reacting species and the catalyst.

5.1.3.2. Response surface modelling for the di-ester selectivity

After the acetylation reaction took place, the di-acetate **50** was observed as a major product. The acetylation reaction pathway is demonstrated below (equation 5.2).

$$\underset{\text{PMD}}{C_{10}H_{20}O_2\ (l)} + 2\,\underset{\text{Acetic anhdride}}{C_4H_6O_3\ (l)} \rightarrow \underset{\text{Di - acetate}}{C_{14}H_{24}O_4\ (l)} + 2\,\underset{\text{Acetic acid}}{C_2H_4O_2\ (l)} \qquad \textbf{(Eqn. 5.2)}$$

From the experimental observation in Table 5.4 above, the di-ester selectivity data has been validated statistically as demonstrated above.

5.1.3.2.1. Model derivation

The proposed general response surface model (Equation 2.3) was fitted on the di-ester selectivity data. The regression results of the estimated coefficients and their associated statistics are tabulated as follows (Table 5.6).

Table 5.6: Estimated regression coefficients & associated statistics

Coefficient	Term	b	Std. err.	t(6)	p-value
$\mathbf{b_0}$	Intercept	-22.9	35.99	-0.64	0.549
$\mathbf{b_1}$	T	2.6	1	2.64	0.038
$\mathbf{b_2}$	F	1139.1	330.25	3.45	0.014
$\mathbf{b_3}$	T^2	0	0.01	-2.31	0.05
$\mathbf{b_4}$	F^2	7488	1762.26	4.25	0.005
$\mathbf{b_5}$	TF	-37.2	4.46	-8.34	0

The response surface model for the di-ester selectivity revealed the same reaction trend as the proposed general model. The estimated coefficients are found to be significant enough to describe the proposed model by showing the smaller p-values (<0.05). Furthermore, it is also noted that temperature^2 (T^2) is characterised with high p-value as compared to other estimated coefficients. Its p-value is found to be equivalent to the maximum accepted p-value level of 0.05. Therefore, it is not conclusive enough to remove this coefficient from the final model. The proposed final response surface model for the di-ester selectivity has remain unchanged as the general proposed model (Equation. 5.3).

$$\textbf{Di - ester sel.(\%)} = b_0 + b_1T + b_2F + b_3T^2 + b_4F^2 + b_5TF \qquad \textbf{(Eqn. 5.3)}$$

In the final response surface model, all the estimated coefficients are showing to play a significant role towards the di-ester formation. The interaction between temperature and flow-rate directly affect the di-ester formation negatively. Meaning, a smaller increase in temperature or flow-rate result to the significant decrease in the di-ester formation.

5.1.3.2.2. Model validation

The obtained final response surface model was further validated by determining the variation of the observed di-ester selectivity data and the possible outliers.

5.1.3.2.2.1. Analysis of variance

The final response surface model was analysed of the variance. The results revealed that the observed di-ester selectivity data can be explained by the final response surface model. The smaller p-values also proved that the estimated coefficients have the significant effect towards the di-ester formation. This is further confirmed by the high correlation square (R^2 = 0.997), which indicates that the final model fits the observed di-ester selectivity data very well.

5.1.3.2.2.2. Analysis of residuals

The scatter diagram of the di-ester selectivity data also reveal a very good correlation square. This suggest that all the residuals are randomly distributed around the regression line (predicted values). None of the residuals is below -2 or above 2, thus are within the expected range. The observed scatter plot for the di-ester selectivity is shown below (Figure 5.6).

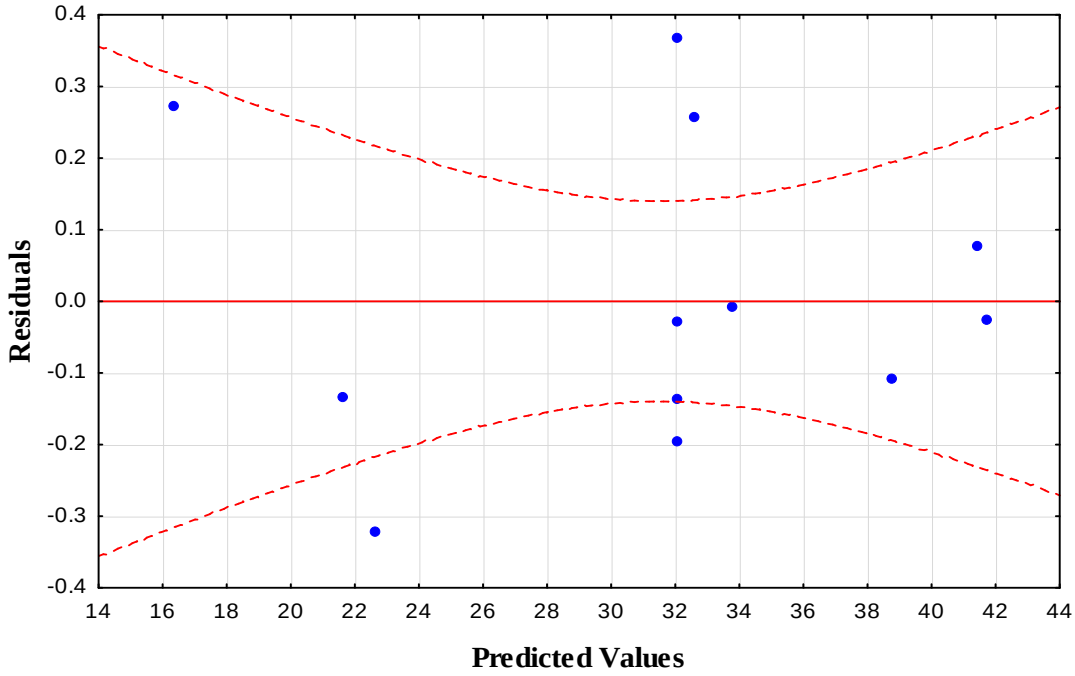

Figure 5.4: Scatter diagram for the di-ester selectivity

The normal probability plot of the di-ester selectivity (Figure 5.7), also showed a non-heteroscedasticity pattern. Meaning, the distribution of residuals is normal and it does not form a defined pattern. This indicates that the final model can be accepted as a good description of data.

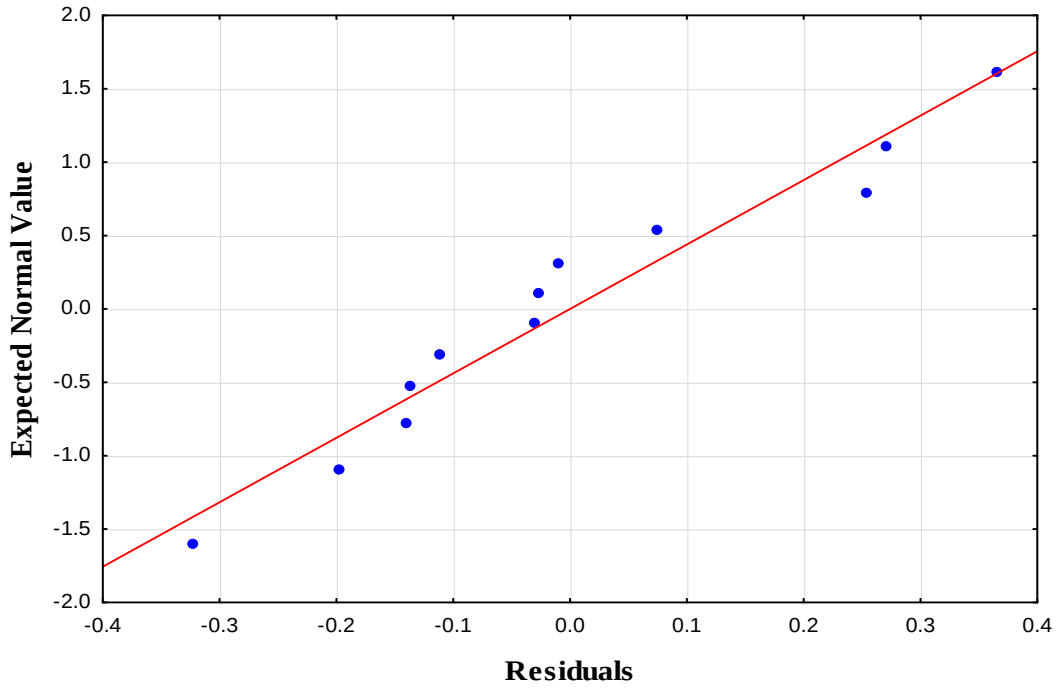

Figure 5.7: Normal probability plot for the di-ester selectivity

The effect of temperature and flow-rate towards the di-ester selectivity was also investigated. The observed results are discussed as follow.

5.1.3.2.3. Effect of temperature and flow-rate di-ester selectivity

As demonstrated in Figure 5.8 below, it can be seen that the di-ester selectivity is optimum when a reaction is operated at the temperature of 60^0C and longer substrate residence time (flow-rate of 0.01 mL/min) is used. This signifies that temperature has lesser effect towards the di-ester formation. Moreover, both reacting species can interact effectively on the catalyst to produce the di-ester product. It can also be seen that the use of shorter residence time (higher flow-rate > 0.01 mL/min) result to the significant decrease in the di-ester formation. Thus, the reaction leads to the mono-ester formation. In these conditions, it has been observed that the acylation reaction favours the mono-acetate **54** formation.

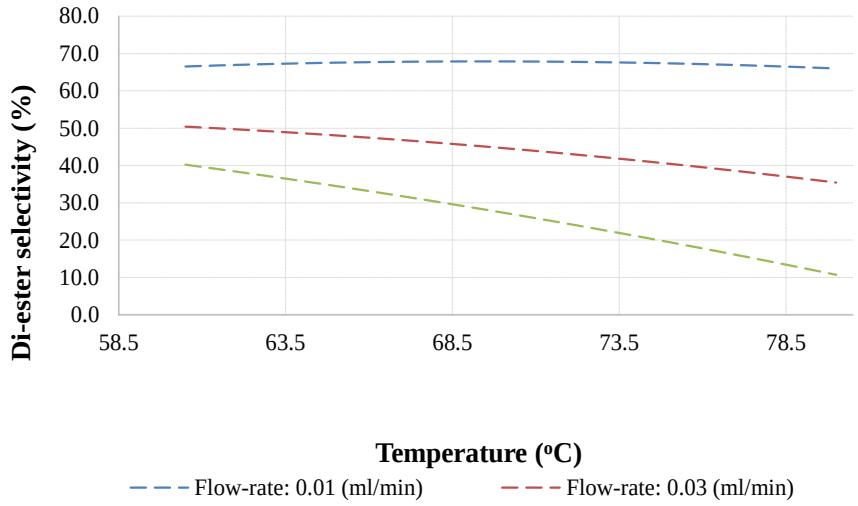

Figure 5.8: Effect of temperature in di-ester selectivity

When this reaction is operated at longer residence time (flow-rate of 0.01 mL/min), the di-ester selectivity remains optimum with slightly temperature increase (Figure 5.9). This scenario is good for the industrial process, because a small change in temperature has little to cause the negative change in the reaction outcome. However, when shorter residence time (flow-rate of 0.03 mL/min) is used, di-ester selectivity is affect significantly. This scenario shows that the shorter residence time provide less interaction between the reacting species on the catalyst. As discussed in the previous chapter, tertiary hydroxyl group are characterised with poor reactivity. Hence, it was expected in this work that longer residence time should be used to

enhance the rate acylation reaction. Indeed, upon the optimisation process in continuous flow reactor is found to behave in the same manner.

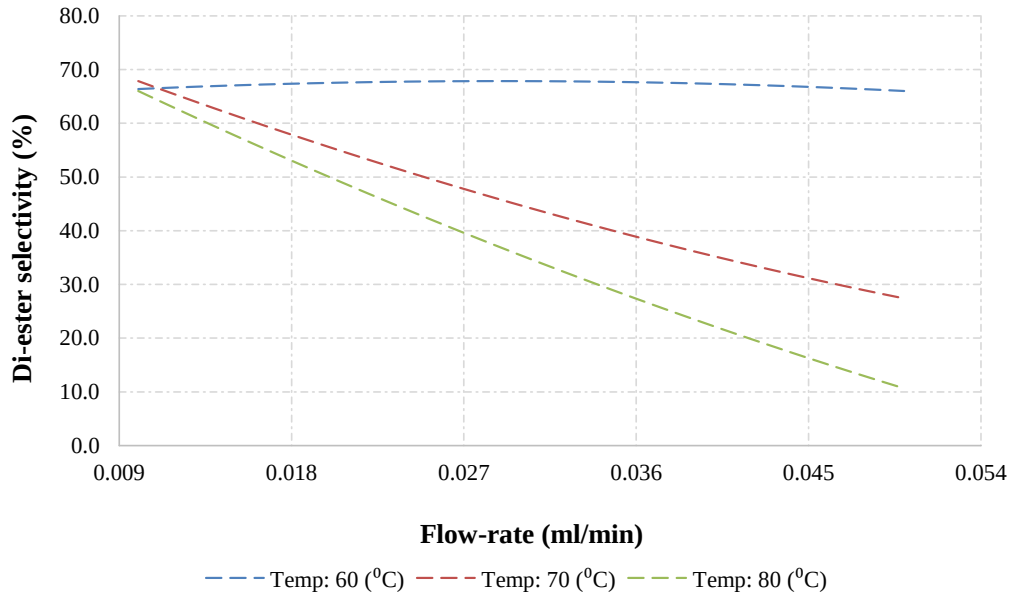

Figure 5.9: Effect of flow-rate on di-ester selectivity

As it can be observed on the graph above, the mono-ester formation is favoured by higher temperatures and longer residence time. This clearly show the poor reactivity of the tertiary hydroxyl group at these conditions.

5.1.3.2.4. Prediction intervals for estimated responses

We further used the data set (run-8 in Table 5.4) as the optimum conditions to determine the error uncertainty for the di-ester selectivity at 95% confident interval. The error uncertainty formula described above (equation 2.4) was used to calculate the error uncertainty for the observed di-ester value. The observed di-ester selectivity value and its error uncertainty at 95% confidence can be expressed as follows; *Di-ester selectivity* = 67.88 ± 2.8. The error uncertainty was found to be very small (<5%), which signifies that the observed di-ester value is closer to the predicted (accepted) value by the final response surface model. As a result, the final response surface model has been accepted as good description of the observed data.

5.1.3.2.5. Model interpretation

From the final response surface model, it can be seen that the di-ester selectivity data fits the proposed quadratic model very well. Nevertheless, a slightly larger error uncertainty is

observed from the data. Below is a 3-D surface plot for the observed di-ester selectivity data points versus temperature and flow-rate (Figure 5.10).

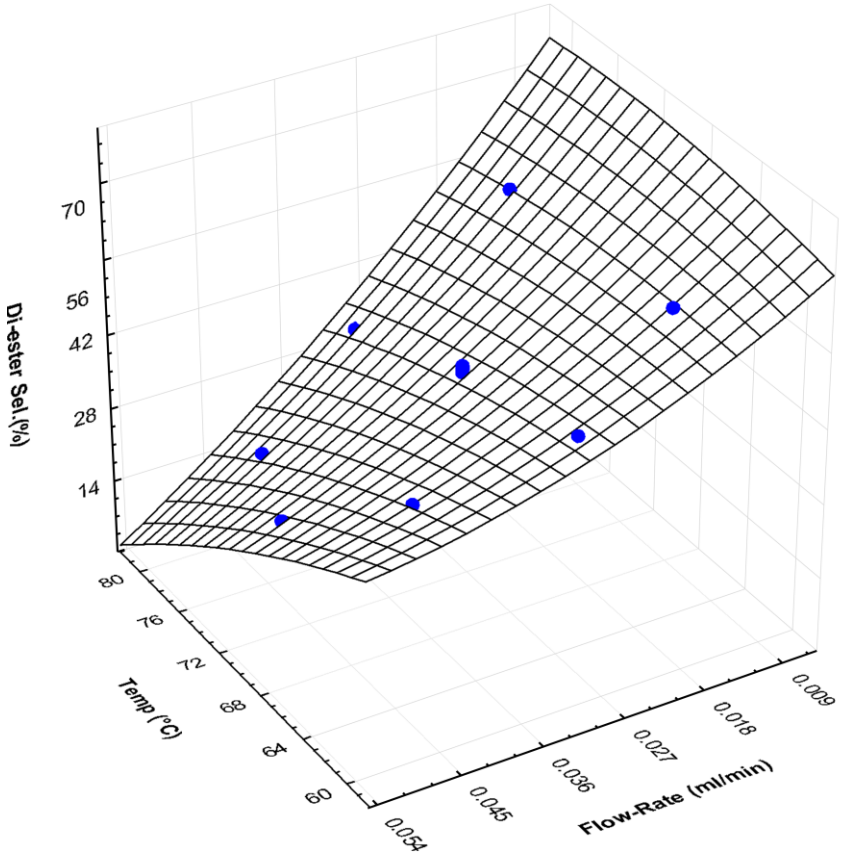

Figure 5.10: 3-D surface plot for the di-ester selectivity

What can be seen in Figure 5.10 above, there is an increase in the di-ester selectivity with decrease in residence time (lower flow-rate) and increase in temperature. Alternatively, at shorter residence time (higher flow-rate) a significant decrease in the di-ester formation is observed with increase in temperature. This clearly shows that the substrate residence time plays a significant role in determining the reaction outcomes.

5.1.3.3. Response surface modelling for the mono-ester selectivity

The mono-acetate **54** has been observed a minor product from the acetylation reaction. The reaction equation that denotes its synthesis route is showed below (Equation 5.4).

$$\underset{\text{PMD}}{C_{10}H_{20}O_2\ (l)} + \underset{\text{Acetic anhdride}}{C_4H_6O_3\ (l)} \rightarrow \underset{\text{Mono - acetate}}{C_{12}H_{22}O_3\ (l)} + \underset{\text{Acetic acid}}{C_2H_4O_2\ (l)} \qquad \textbf{(Eqn. 5.4)}$$

It was also important to determine the reaction conditions that favours the mono-ester formation. In doing so, we will be able to control the reaction parameter that favour its selectivity in process.

5.1.3.3.1. Model derivation

Again, a general proposed response surface model (Equation 2.3) was fitted to the observed mono-ester selectivity data points. Below is a tabulated summary of the estimated coefficients and their associated statistics (Table 5.7).

Table 5.7: Estimated regression coefficients & associated statistics

Coefficient	Term	B	Std. Err.	t(6)	p-value
b_0	Intercept	76.7	11.33	6.76	0.00051
b_1	T	-1.8	0.31	-5.73	0.00123
b_2	F	44.4	104.01	4.27	0.00525
b_3	T^2	0.0	0.00	5.10	0.00223
b_4	F^2	-7482.4	555.00	-13.48	<0.00001
b_5	TF	9.1	1.40	6.51	0.00063

In the case mono-ester selectivity, the final response surface model is observed to be the same as the general proposed model. All the estimated coefficients showed to be significant enough in describing the final response surface model, by showing small p-values. The proposed final response surface model for the mono-ester selectivity is presented below (Equation 5.5).

$$\textbf{Mono-ester sel.(\%)} = b_0 + b_1T + b_2F + b_3T^2 + b_4F^2 + b_5TF \qquad \textbf{(Eqn. 5.5)}$$

The final response surface model suggest that the flow-rate has a significant effect towards the mono-ester formation. Meaning, when a reaction is operated at higher temperature conditions with shorter residence time (higher flow-rate), this result in higher mono-ester formation. As we mentioned earlier, when shorter residence time is used in this reaction the synthesis route favour the acylation secondary hydroxyl group. Reason being, there is less reaction for the tertiary hydroxyl group to react. Therefore, the reaction result to the formation mono-ester derivative rather than the di-ester derivative.

5.1.3.3.2. Model validation

We then validated the obtained final response surface model by determining the variance and the residual analysis. The method validation results are further discussed below.

5.1.3.3.2.1. Analysis of variables

The analysis of variance also showed that the observed experimental data can be explained by the final response surface model (Eqn.5.5). The smaller p-values of the estimated coefficients and high correlation square (R^2 = 0.998) indicates that the final model fits the observed experimental data. Furthermore, the residual analysis was performed before the final model was accepted as a good description of the observed data.

5.1.3.3.2.2. Analysis of residuals

The scatter diagram show that the residuals are randomly distributed around the regression line (predicted values). Furthermore, none of the residuals is below -2 or above 2, hence are within the expected range. The observed scatter plot of the observed mono-ester selectivity data is showed below (Figure 5.11)

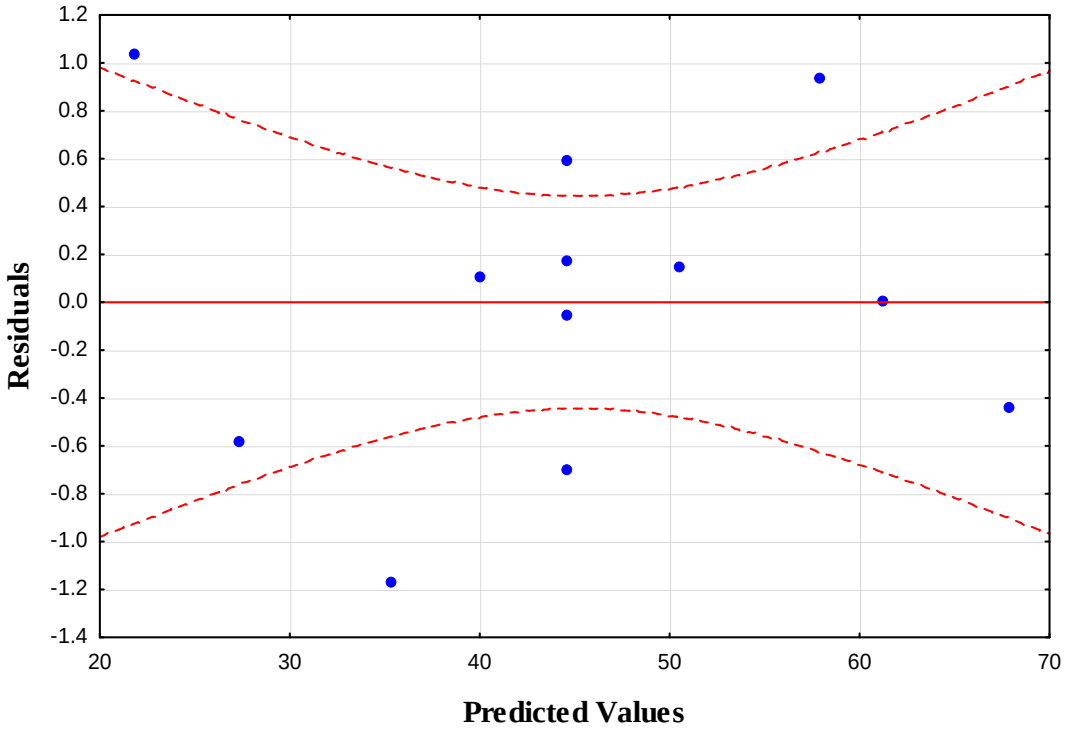

Figure 5.11: Scatter diagram for the mono-ester selectivity

The normal probability plot for the mono-ester residuals (Figure 5.12), also show a non-heteroscedasticity pattern. Meaning, the distribution of residuals is normal and they do not form a distinctive pattern. Therefore, this indicates that the final model can be accepted as a good description of data.

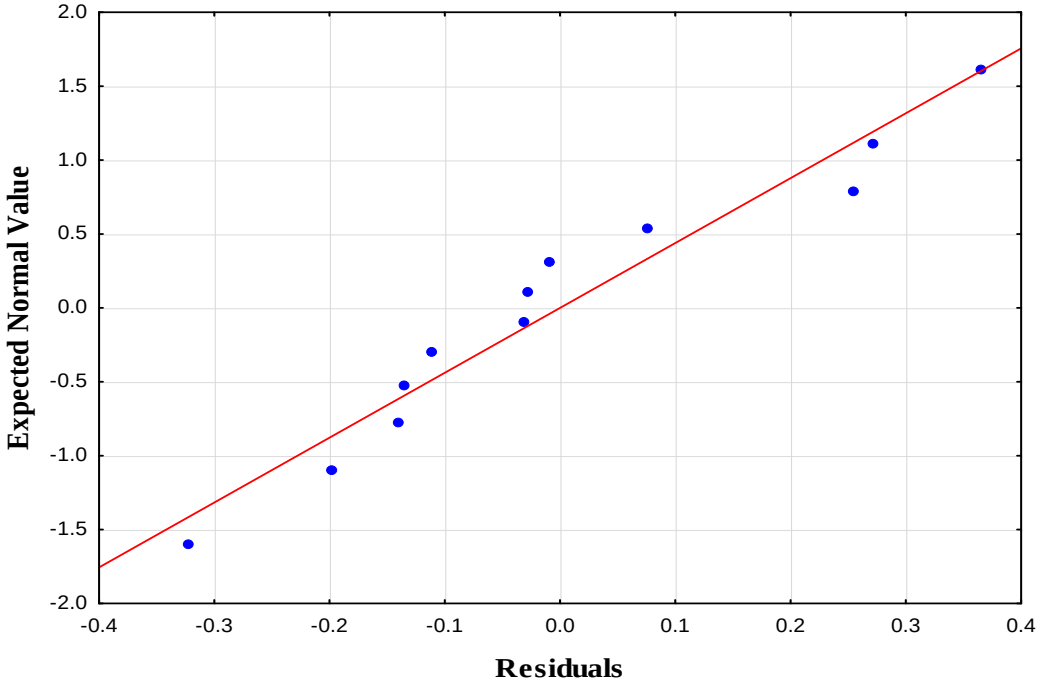

Figure 5.12: Normal probability pot for the mono-ester selectivity

5.1.3.3.3. Effect of temperature and flow-rate in mono-ester selectivity

The effect of temperature in mono-ester selectivity was studied. The observed results are graphically summarised below (Figure 5.13).

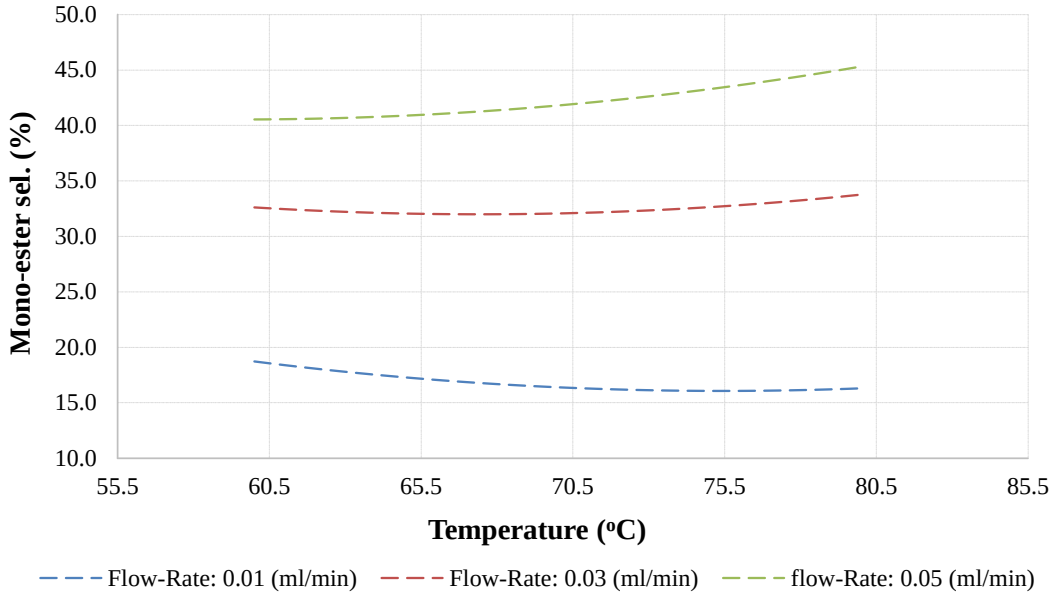

Figure 5.13: Effect of temperature in mono-ester selectivity

From the graphs showed above, it can be seen that the temperature does not have effect towards the mono-ester formation. The reaction temperature has a slightly effect only when a reaction is operated at shorter residence time (high flow-rate). Therefore, the mono-ester selectivity can be minimise by operating the reaction at lower temperatures and longer residence time. In doing so, a better interaction between the tertiary hydroxyl group and acylating agent on the catalyst can be achieved.

This scenario can still be observed in the case of residence time. The mono-ester selectivity is minimum at longer residence time (lower flow-rate) irrespective of the reaction temperature. The increase in the residence time result to the improving selectivity towards the mono-ester derivative (Figure 5.14).

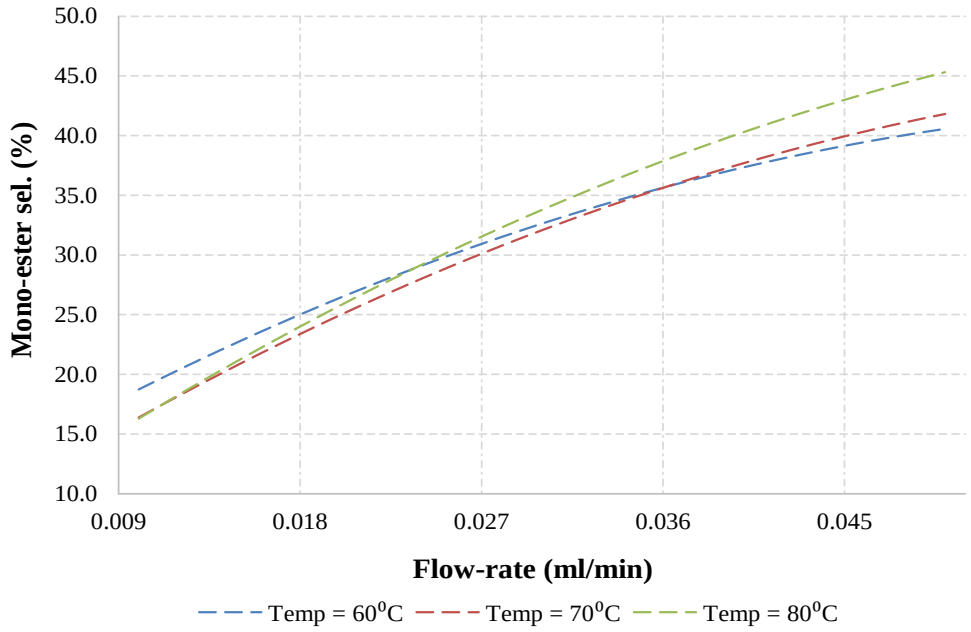

Figure 5.14: Effect of flow-rate on mono-ester selectivity

It is therefore observed that the mono-acetylation reaction is favoured by concurrent increase in flow-rate and temperature. This clearly shows that the secondary hydroxyl group of the substrate reacts much faster with acid anhydride at higher temperature and flow-rate conditions. Whereas, a slow reaction towards tertiary hydroxyl group is observed at these conditions.

5.1.3.3.4. Prediction intervals for estimated responses

The error uncertainty for the mono-ester selectivity was determined at 95% confidence by using a formula described above (equation 2.4). Similarly as indicated above, the reaction set of data (run-8, Table 5.4) was used to determine the error uncertainty for the mono-ester selectivity. The mono-ester selectivity and its error uncertainty at 95% confidence can be expressed as follows; *Mono-ester selectivity* = 16.38 ± 0.04. It can be seen that there is very small error uncertainty towards the mono-ester formation. This signifies that the observed mono-ester selectivity value is very close to the accepted value as predicted by the final response surface model.

5.1.3.3.5. Model interpretation

The final response surface model can be graphically presented inform of 3-D surface plot to show the interaction between the mono-ester selectivity, flow-rate and temperature (Figure 4.15).

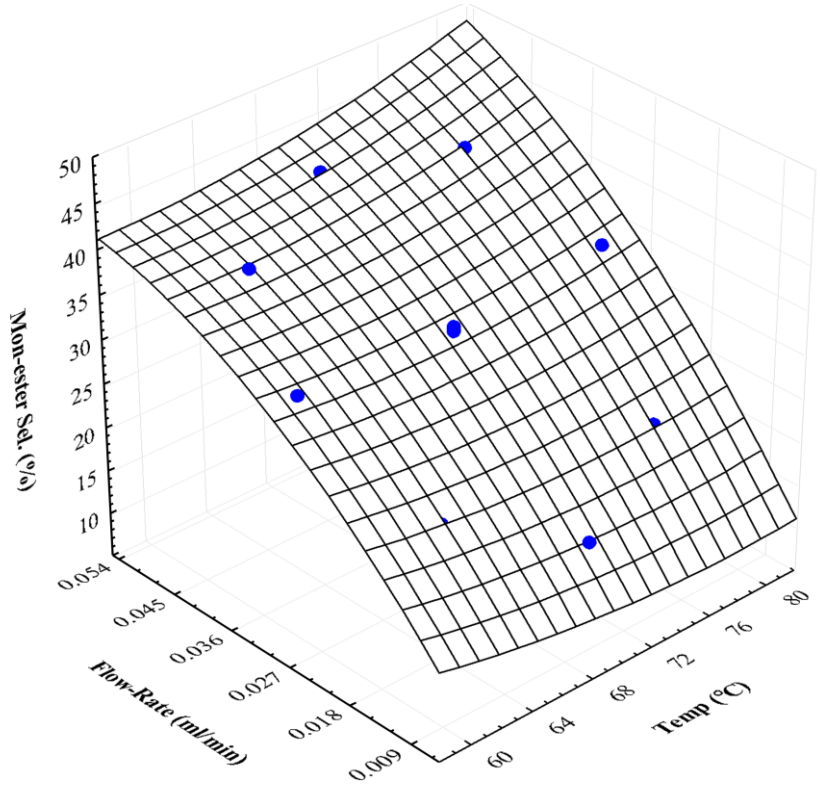

Figure 4.15: 3-D response surface plot for the Mono-ester selectivity

From the above 3-D response surface plot, it can be observed that the mono-ester selectivity is favoured by the concurrent increase of the flow-rate and temperature. Therefore, the mono-ester selectivity can be reduced by operating the reaction at longer residence time (lower flow-rate) and slightly higher temperature.

5.1.3.4. Leaching test of the scandium metal from PS-Sc(OTf)$_3$ catalyst

The leaching test of scandium metal from the polymer-supported scandium triflate (PS-Sc(OTf)$_3$) catalyst into the product mixture was performed by using the ICP-MS method mentioned above in section 2.2.6. The samples were taken from the batch-scale process (labelled as Sample A) and from microwave-assisted continuous flow process (labelled as Sample B). The aim of the study was to determine the process that is characterised with catalyst leaching. The samples were prepared according to the method described in section 2.2.6.1 above. The observed results from the ICP-MS analysis are tabulated below (Table 5.8).

Table 5.8: ICP results for the Scandium metal content (ppb)

	Mass (g)	Replicate-1	Replicate-2	Replicate-3
Sample A	1	161.9	154.2	165
Sample B	1	< 0.001	< 0.001	< 0.001

It can be observed on the table above that the batch-scale process is characterised with too much catalyst leaching. This is due to the crushing of the catalyst particles by the magnetic stirrer bar during the agitation process in the reactor. In some instances, the catalyst paste was observed during the catalyst separation stage. On the other hand, there were no traces of scandium metal observed from the continuous flow process. This data provide a sufficient evidence to prove that the continuous flow process is the cost effective and environmentally-friendly process in the case of catalyst re-usability when compared to the batch-scale process.

5.1.4. Summary

The optimisation process of the acylation reaction of *para*-menthane-3,8-diol in flow system has been demonstrated to be successful in the microwave-assisted flow process. The following reaction aspects have been established towards the substrate conversion, mono- and di-ester selectivity.

***Substrate conversion*:** it is demonstrated from the study that the substrate conversion is affected by temperature significantly. The substrate conversion is found to increase with slight increase in temperature, while the reaction is operated at longer residence time (lower flow-rate). The further increase in the reaction temperature results in two substrate isomers that are less reactive in the reaction. Whereas, the shorter residence time (higher flow-rate) result in completely poor substrate conversion. The optimum conditions for the substrate conversion are found to be the temperature of 70°C and flow-rate of 0.01 mL/min, which then afford the conversion of 71% ± 1.92, respectively.

***Di-ester selectivity*:** In the case of di-ester formation, the substrate residence time is observed to be the determining factor. The increase in the reaction temperature has been found to improve the rate of reaction as compared to what has been observed from the batch-scale process. At the optimum reaction conditions, the di-ester formation is found to be 68% ± 2.8 at total residence time of 226 minutes. However, in the batch-scale process the substrate conversion of 60% and di-ester selectivity of 67% were achieved after a total residence time of 12 hours.

***Mono-ester selectivity*:** The mono-ester selectivity has shown to increase with concurrent increase in the flow-rate and temperature. The secondary hydroxyl group was the only functional group that was able to be acylated in the reaction under these conditions. Therefore, to ensure both functional groups are acylated, the reaction was allowed to proceed for prolong residence time or lower flow-rate. At optimum reaction conditions, the mono-ester derivative was able to be minimised to the selectivity of 16% ± 0.44. It can be seen from these results that the reaction still requires more residence time to convert the mono-ester derivative to its corresponding di-ester derivative. This can be confirmed by the results that were obtained in the batch-scale studies, wherein the substrate material was completely converted into the di-ester product without any observed traces of the mono-ester derivative.

5.1.5. Concluding remarks

Herein, we have demonstrated the synthesis of *para*-menthane-3,8-di-ester derivative in a continuous flow process. The combined strategy of milli-reactor operation and the microwave-assisted heating has provided an excellent control over temperature and residence time. As a result, improved conversions were observed with slow increase in reaction temperature (below 70°C). However, the substrate conversion was observed drop significantly with the temperature increase (greater than 70°C). Moreover, the issue of residence time has remained a major challenge towards the di-ester formation. In addition, the reaction pathway has clearly showed that more of the reaction time is required to acylate the hydroxyl groups of the PMD in both processes. In conclusion, it is recommend to carry out the acylation reaction of *para*-menthane-3,8-diol in the batch scale process for smaller production scale. As demonstrate above, the continuous flow process requires very long residence times in order to form reasonable selectivities towards the di-ester derivatives.

CHAPTER 6

Conclusion and recommendations

This research project was directed on optimising the synthesis of ether-ester derivatives of isopulegol **22** by using a single continuous flow fixed-bed reactor system. The research work was initiated by designing a continuous flow fixed-bed reactor for the synthesis of isopulegol **22** from citronellal **19**. It must be mentioned that the isopulegol **22** synthesis reaction was done in collaboration with the University of Cape Town (UCT). Wherein, H-ZSM-5 zeolite was identified as a suitable catalyst for the reaction. Moreover, a tubular fixed-bed reactor used in the reaction was made from ¾th inch stainless steel tubing (I.D: 16 mm and length: 550 mm). At optimum reaction parameters such as temperature of 90°C and Flow-rate of 0.2 mL/min, 100% of citronellal **19** conversion and almost 100% selectivity towards isopulegol **22** were observed.

As part of our investigation, the reproducibility of this work was investigated by using our laboratory designed tubular fixed-bed reactor. Our reactor column (I.D: 9.53 mm and length: 120 mm) was made from ⅜th inch stainless steel tubing. Wherein, H-ZSM-5 zeolite extrusions (6.0 g) were packed neatly in the reactor column. The solvent-free citronellal **19** was pumped into the reactor column at the flow-rate of 0.2 ml/min at the reaction temperature of 90°C. The optimum citronellal **19** conversion achieved was 100% and the isopulegol **22** selectivity was almost 100%. It was therefore concluded that our laboratory results were comparable to the results that were achieved by the UCT group. The H-ZSM-5 catalyst showed a good catalytic performance in the reaction and was also found to be stable in the process.

The second reaction step of the process was to optimise the synthesis of isopulegyl propoxy-ether **49** in continuous flow fixed-bed reactor. The synthesis of ether derivative of isopulegol was developed *via* the batch-scale process as reported in our early developed method. From the batch-scale studies, an amberlyst-15 dry was identified as a suitable catalyst for the reaction. However, the side reactions that include the dehydration of desired isopulegyl propoxy-ether **49** and isopulegol **22** were observed from the catalyst. Additionally, the reverse reaction between the isopulegol **22** and citronellal **19** were found to be the additional disadvantage. At optimum conditions such as temperature of 65°C and reaction time of 24 hours, the best selectivity towards isopulegyl propoxy-ether **49** (67%) was achieved in excess alcohol.

In this work, the etherification of isopulegol was optimised using the UniQsis FlowSyn fixed-bed reactor system. The reactor column (I.D: 9.53 mm and length: 120 mm) was used for the study

and packed with amberlyst-15 dry catalyst (1.0 g). Wherein, *n*-propanol was used as a model etherifying agent as well as the solvent. The *n*-propanol-isopulegol ratio of 3:1 (mol/mol) was used to prepare the reagent mixture. The prepared substrate mixture was pumped into the reactor from a flow-rate of 0.1 to 0.3 ml/min and the temperature of 50 to 90°C. From this experimental domain, the reaction was found to be highly temperature and flow-rate dependent. The increase in the reaction temperature and the substrate flow-rate resulted in high isopulegol conversion and low ether selectivity. The dehydration of isopulegol **22** and isopulegyl propoxy-ether **49** were favoured by high reaction temperature and flow-rate. From the optimisation process, the reaction has revealed 30% selectivity towards the isopulegyl propoxy-ether **49** at the temperature of 70°C and flow-rate of 0.1 ml/min. The increase in temperature and flow-rate have also showed the dehydration of isopulegol **22** and the desired product to prevail.

Other heterogeneous catalysts such as H-Beta zeolite, H-ZSM-5, aluminium pillared clay and aluminium oxide were also screened in the above reaction. The reactions were carried out using the method described above. The catalytic activity with respect to the isopulegyl propoxy-ether **49** selectivity was ranging as follows; H-Beta zeolite (19%) and aluminium pillared clay (5%). However, from the use of H-ZSM-5 zeolite and aluminium oxide there was no catalytic activity observed. These catalysts were found to be moisture sensitive, meaning the use of undried regents can easily deactivate the active acid sites of the catalyst. The catalyst deactivation mainly occurs when water molecule hydrate the metal oxide (Lewis acid sites) to form the less active metal hydroxide. Therefore, the metal hydroxide so-formed act as the Brønsted acid sites in the reaction and result to the dehydration of the hydroxyl group to form the alkene.

Based on the above mentioned results, the etherification process was regarded as unsuccessful. The third step of the process was unable to be investigated as to synthesize the isopulegyl ether-ester derivatives from isopulegyl-ether. At least 70% selectivity towards the isopulegyl propoxy-ether **49** was required from the previous reaction step. From the evaluated catalysts, none provided the desired selectivity. In light of this, the isopulegol **22** etherification synthetic route was terminated. Consequently, another analogue of citronella **19** was used as the alternative intermediate to replace the isopulegol **22**, namely *para*-menthane-3,8-diol (PMD) **27**. Unlike the isopulegol **22** synthetic route, the di-ester derivatives were expected as the target compound from para-menthane-3,8-diol **27** reaction.

The ground work studies for the synthesis of the novel di-ester derivatives of para-menthane-3,8-diol **27** was performed in the batch-scale reactor. The solvent-free reaction conditions were used in the study, wherein the acetic anhydride was used as a model acetylating reagent as well as the solvent. The reaction was performed over the polymer-bound scandium triflate (PS-Sc(OTf)$_3$)

catalyst. The effect of reaction parameters such as temperature, molar ratio, and reaction time were studied towards the para-menthane-3,8-diol **27** conversion, and di-acetate **50** selectivity. The optimum para-menthane-3,8-diol **27** conversion (70%), and di-acetate **50** selectivity (67%) were achieved at the temperature of 60°C and reaction time of 12 hours. The acylation reaction was found to follow the zeroth order kinetics with respect to para-menthane-3,8-diol **27** conversion and also obeyed the Arrhenius equation. Other form of di-ester derivatives were synthesized from para-menthane-3,8-diol **27** by using the method described above. Wherein, the carbon chain length of the acetylating agents was varied from C_3–C_6, respectively.

The developed method was further optimised by using an ArrheniumOne microwave-assisted continuous-flow fixed-bed reactor system. A detailed experimental design was used to carry out the reactions. The reaction parameters such as temperature and flow-rate were studied towards the para-menthane-3,8-diol **27** conversion and di-acetate **50** selectivity. From the experimental design analysis, the di-acetate **50** selectivity was found to depend highly on the flow-rate and significantly on temperature. The para-menthane-3,8-diol **27** conversion and di-acetate **50** selectivity were found to increase with decrease in the flow-rate.

The para-menthane-3,8-diol **27** conversion and di-acetate **50** selectivity results achieved in the continuous-flow process were found to be similar to those of the batch-scale process. However, longer residence times were required in the microwave-assisted continuous-flow process. In addition, the continuous-flow process found to be characterised with less catalyst leaching when compared to the batch-scale process. Furthermore, all the prepared di-ester derivatives were found to possess similar physical properties as the conventional phthalate plasticisers.

Further work

The outcome of this research work has revealed that the para-menthane-3,8-diol di-ester derivatives can be synthesised in the batch-scale and in the microwave-assisted continuous flow process. In light of this, the future work should be to consider the recycling of the generated carboxylic acid (by-product) into acid anhydride. Moreover, a broader study should be to evaluate different types of heterogeneous catalysts in the reaction in order to minimise the process cost from the use of expensive polymer-bound scandium triflate catalyst.

REFERENCES

1. N. Gil, I. Negulescu, M. Saska, *Evaluation of the effects of bio-based plasticizers on thermal and mechanical properties of poly (vinyl- chloride)*., 2006, **102**, 366–73.
2. A. M. Reid, C. Brougham, A. M. Fogarty, J.J. Roche., *Accelerated solvent-based extraction and enrichment of selected plasticisers and 4-nonylphenol, and extraction of tin from organotin sources in sediments, sludges and leachate soils*., *Anal Chim Acta*., 2009, **634**, 197–204.
3. H.C. Erythropel, M. Maric, D. G. Cooper., *Designing green plasticizers: Influence of molecular geometry on biodegradation and plasticization properties*., *Elsevier Ltd*., 2012, **86**, 759–66.
4. M. Rahman and C. Brazel., T*he plasticizer market: an assessment of traditional plasticizers and research trends to meet new challenges.*, *Prog Polym Sci*., 2004, **29**, 1223–48.
5. Y. Guo and K. Kannan., *Challenges encountered in the analysis of phthalate esters in foodstuffs and other biological matrices.*, *Anal Bioanal Chem*., 2012, **404**, 2539–54.
6. M. Bonini, E. Errani, G. Zerbinati, E. Ferri, S. Girotti., *Extraction and gas chromatographic evaluation of plasticizers content in food packaging films.*, *Microchem J.*, 2008, **90**, 31–6.
7. M. Rahman and C. S. Brazel., *Ionic liquids: New generation stable plasticizers for poly(vinyl chloride).*, *Polym Degrad Stab*., 2006, **91**, 371–82.
8. M. G. A. Vieira, M. A. da Silva, L. O. dos Santos, M. M. Beppu., *Natural-based plasticizers and biopolymer films: A review.*, *Eur Polym J.*, 2011, **47**, 254–63.
9. S. Nalli, D. G. Cooper, J. A. Nicell., *Biodegradation of plasticizers by Rhodococcus rhodochrous.*, 2003, 343–52.
10. R. Mayelı, L. Marı, A. Sa, A. Jime., *Effect of pressure, temperature and time on supercritical fluid extraction of citrate and benzoate plasticisers from polyvinyl chloride.*, *Supercrit Fluids.*, 2002, **22**, 111–8.
11. I. V. O. Mersiowsky and M. Weller., *Fate of plasticiser pvc product under landfill conditions.*, *A laborator-scale landfill.*, 2001, **35**, 3063–70.
12. A. O. Earls, I. P. Axford, J. H. Braybrook., *G as chromatography – mass spectrometry determination of the migration of phthalate plasticisers from polyvinyl chloride toys and*

childcare articles., J Chromatogr., 2003, **983**, 237–46.

13. O. Lau., *Mathematical model for the migration of plasticisers from food contact materials into solid food., Analytica Chimica Acta.,* 1997, **347**, 249-56 .

14. S. S. Hill, B. R. Shaw, A. H. B. Wu., *The clinical effects of plasticizers , antioxidants , and other contaminants in medical polyvinylchloride tubing during respiratory and non-respiratory exposure., Clin Chim Acta.,* 2001, 3**04**, 1–8.

15. U. Heudorf, V. Mersch-sundermann., *Phthalates : Toxicology and exposure*., *Elsevier*., 2007, **210**, 623–34.

16. R. Sankar, M. Jain, V. K. Ramkumar, J. Joshi, Y. M. *Rheological characterization of styrene-butadiene based medium and its finishing performance using rotational abrasive flow finishing process*., *International Journal of Machine Tools & Manufacture.,* 2011, **51**, 947-957.

17. M. Altenhofen da Silva, M. G. Adeodato Vieira, A. C. Gomes Maçumoto, M. M. Beppu., *Polyvinylchloride (PVC) and natural rubber films plasticized with a natural polymeric plasticizer obtained through polyesterification of rice fatty acid., Polym Test Elsevier* Ltd., 2011, **30**, 478–84.

18. N. Tanaka, Y. Nomura, R. Nishikiori, S. Shibata, K. Shirai, M. Fujitani., *Temporary restorative resins using non-phthalate ester plasticizers*., *Journal of Dentistry*., 2005, **33**, 577–83.

19. T. Maharana, B. Mohanty, Y. S. Negi., *Progress in Polymer Science Melt – solid polycondensation of lactic acid and its biodegradability*., Progress in Polymer Science., 2009, **34**, 99–124.

20. M. Tarvainen, R. Sutinen, S. Peltonen, H. Mikkonen, J. Maunus, K. Vähä-Heikkilä., *Enhanced film-forming properties for ethyl cellulose and starch acetate using n-alkenyl succinic anhydrides as novel plasticizers*., Eur J Pharm Sci., 2003, **19**, 363–71.

21. Q. Wang and B. K. Storm., *Separation and analysis of low molecular weight plasticizers in poly(vinyl chloride) tubes*., Polym. Test., 2005, **24**, 290–300.

22. L. Shen, J. Haufe, M. K. Patel., *Product overview and market projection of emerging bio-based plastics.,* Gr. Sci. Technol. Soc., 2009, **41**, 1-243.

23. M. N. Abdorreza, L. H. Cheng, A. A. Karim., *Effects of plasticizers on thermal properties and heat sealability of sago starch films*., *Food Hydrocoll.,* 2011, **25**, 56–60.

24. M. Rahman and C. S. Brazel. *The plasticizer market : an assessment of traditional*

plasticizers and research trends to meet new challenges., *Prog. Polym. Sci.*, 2004, **29**, 1223–48.

25. C. Palm, O. I. L. As, A. B. In, B. Films., *Crude palm oil as a bioadditive in polypropylene blown films.*, *Chem. Environ. Eng.*, 2012, **7**, 859–67.

26. G. Upenyu, Ph.D. Thesis, Nelson Mandela Metropolitan University, 2012.

27. D. R. Batish, H. P. Singh, N. Setia, S. Kaur, R. K. Kohli., *Chemical composition and phytotoxicity of volatile essential oil from intact and fallen leaves of Eucalyptus citriodora.*, *Z. Naturforsch,* 2006, **61**, 465–71.

28. Manika N, Mishra P, Kumar N, Chanotiya CS, Bagchi GD. Effect of season on yield and composition of the essential oil of Eucalyptus citriodora Hook . leaf grown in sub-tropical conditions of North India. 2012;6(14):2875–9.

29. H. Pal, S. Kaur, K. Negi, S. Kumari, V. Saini, D. R. Batish., *LWT - Food Science and Technology Assessment of in vitro antioxidant activity of essential oil of Eucalyptus citriodora (lemon-scented Eucalypt ; Myrtaceae) and its major constituents.*, *LWT - Food Sci. Technol.*, 2012, **48**, 237–41.

30. E. J. Lenardão, G. V. Botteselle, F. de Azambuja, G. Perin, R. G. Jacob., *Citronellal as key compound in organic synthesis.*, *Tetrahedron*, 2007, **63**, 6671–712.

31. D. R. Batish, H. P. Singh, N. Setia, S. Kaur, R. K. Kohli., *Chemical composition and inhibitory activity of essential oil from decaying leaves of Eucalyptus citriodora.*, *Z. Naturforsch*, 2006, ***61***, 52–6.

32. M. Moudachirou, J. D. Gbhou, J. C. Chalchat, *Chemical Composition of Essential Oils of Eucalyptus from Bénin : Eucalyptus citriodora and E . camaldulensis . Influence of Location , Harvest Time , Storage of Plants and Time of Steam Distillation.*, *J. Essent. Oil Res.*, 2011, **11**, 109–18.

33. Z. Yongzhong, N. Yuntong, S. Jaenicke, G. K. Chuah., *Cyclisation of citronellal over zirconium zeolite beta— a highly diastereoselective catalyst to (±)-isopulegol.*, *J. Catal.*, 2005, **229**, 404–13.

34. J. Drapeau, M. Rossano, D. Touraud, U. Obermayr, M. Geier, A. Rose., *Green synthesis of para-Menthane-3,8-diol from Eucalyptus citriodora: Application for repellent products. Comptes Rendus Chim.*, 2011, **14**, 629–35.

35. C. B. Cortés, V. T. Galván, S. S. Pedro, T. V. García., *One pot synthesis of menthol from (±)-citronellal on nickel sulfated zirconia catalysts.*, Catal. Today, 2011, **172**, 21–6.

36. M. R. Gomes-carneiro, I. Felzenszwalb, F. J. R. Paumgartten., *citronellal , ž y / -menthol and terpineol with the Salmonellarmicrosome assay., Genet. Toxicol. Environ. Mutagen.*, 1998, **416**, 129–36.

37. M. I. G. Silva, M. A. G. Silva, M. R. de Aquino Neto, B. A. Moura, H. L. de Sousa, de E. P. H. Lavor., *Effects of isopulegol on pentylenetetrazol-induced convulsions in mice: possible involvement of GABAergic system and antioxidant activity., Fitoterapia,* 2009, **80**, 506–13.

38. B. Solomon, F. F. Sahle, T. Gebre-Mariam, K. Asres, R. H. H. Neubert., *Microencapsulation of citronella oil for mosquito-repellent application: formulation and in vitro permeation studies., Eur. J. Pharm. Biopharm.*, 2012, **80**, 61–6.

39. R. G. Jacob, G. Perin, L. N. Loi, C. S. Pinno, E. J. Lenardão., *Green synthesis of (−)-isopulegol from (+)-citronellal: application to essential oil of citronella., Tetrahedron Lett.*, 2003, **44**, 3605–8.

40. J. E. R. Nascimento, A. M. Barcellos, M. Sachini, G. Perin, E. J. Lenardão, D. Alves., *Catalyst-free synthesis of octahydroacridines using glycerol as recyclable solvent., Tetrahedron Lett.*, 2011, **52**, 2571–4.

41. N. N. Doan, T. N. Le, P. E. Hansen, F. Duus. *Fast preparation of dihydrocyclocitral from citronellal under solventless microwave irradiation., Tetrahedron Lett.*, 2005, **46**, 6749–51.

42. V. P. Kamat, H. Hagiwara, T. Katsumi, T. Hoshi., *Ring Closing Metathesis Directed Synthesis of (R) - (±) -Muscone from (+) -Citronellal., Tetrahedron.*, 2000, **56**, 4397–403.

43. G. D. Yadav and S. V. Lande., *Novelties of kinetics of chemoselective reduction of citronellal to citronellol by sodium borohydride under liquid–liquid phase transfer catalysis., J. Mol. Catal. A. Chem.*, 2006, **247**, 253–9.

44. B. Hill, *Scandium Trifluoromethanesuffonate, an Efficient Catalyst for the lntermolecular Carbonyl-Ene Reaction and the Intramolecular Cydisation of Citronellal., Tetrahedron Lett.*, 2000, **39**, 1997–2000.

45. P. R. S. Braga, A. Costa, E. F. de Freitas, R. O. Rocha, J. L. de Macedo, A. S. Araujo, *Intramolecular cyclization of (+)-citronellal using supported 12-tungstophosphoric acid on MCM-41., J. Mol. Catal. A Chem.*, 2012, **358**, 99–105.

46. Y. Nie, W. Niah, S. Jaenicke, G. Chuah., *A tandem cyclization and hydrogenation of (±)-citronellal to menthol over bifunctional Ni/Zr-beta and mixed Zr-beta and Ni/MCM-41., J. Catal.*, 2007, **248**, 1–10.

47. K. Dasilva, *Cyclization of (+)-citronellal to (?)-isopulegol catalyzed by H3PW12O40/SiO2., Catal. Commun.,* 2004, **5**, 425–9.

48. M. L. Clarke and M. B. France. *The carbonyl ene reaction., Tetrahedron,* 2008, **64**, 9003–31.

49. K. da Silva Rocha, P. Robles-Dutenhefner, E. M. B. Sousa, E. F. Kozhevnikova, I. V. Kozhevnikov, E. V. Gusevskaya, *Pd–heteropoly acid as a bifunctional heterogeneous catalyst for one-pot conversion of citronellal to menthol., Appl. Catal. A Gen.,* 2007, **317**, 171–4.

50. H. P. Singh, S. Kaur, K. Negi, S. Kumari, V. Saini, D. R. Batish, *Assessment of in vitro antioxidant activity of essential oil of Eucalyptus citriodora (lemon-scented Eucalypt; Myrtaceae) and its major constituents., LWT - Food Sci. Technol.,* 2012, **48**, 237–41.

51. S. P. Bhatia, D. McGinty, C. S. Letizia, M. Api., *Fragrance Material Review on isopulegol., Food Chem. Toxicol.,* 2008, **46**, 185–9.

52. J. Harmand and D. Dochain., *The optimal design of two interconnected (bio)chemical reactors revisited., Comput. Chem. Eng.*, 2005, **30**, 70–82.

53. M. Cassanello, O. Martı, R. S. Ana, L. Cukierman., Liquid hold-up and backmixing in cocurrent upflow three-phase fixed-bed reactors. Chem. Eng. Sci., 1998, **53**, 1015-1025.

54. T. Illg, P. Löb, V. Hessel., *Flow chemistry using milli- and microstructured reactors-from conventional to novel process windows., Bioorg. Med. Chem.,* 2010, **18**, 3707–19.

55. C. Wiles and P. Watts. *The scale-up of organic synthesis using micro reactors. chimica. oggi/Chemistry Today,* 2010, **28**, 3–5.

56. P. Watts and C. Wiles, *Recent advances in synthetic micro reaction technology., R. Soc. Chem.,* 2007, **28**, 443–67.

57. G. Yue and J. Yuan., *Gas-Liquid Microreaction Technology: Recent Developments and Future Challenges.,* Chinese Journal of Chemical Engineering, 2008,**16**, 663-9.

58. B. Mpuhlu, Ph.D. Thesis, Nelson Mandela Metropolitan University, 2012.

59. P. L. Mills, R.V. Chaudhari, *Multiphase catalytic reactor engineering and design for pharmaceuticals and fine chemicals.,* 1997, **37**, 367-404.

60. I. Iliuta, F. C. Thyrion, O. Muntean., *Axial dispersion of liquid in gas-liquid., Trans. IChemE.,* 1998, **76**, 65-72.

61. Z. M. Cheng and W. K. *Yuan., Simultaneous estimation of kinetic and heat transfer parameters of a wall-cooled fixed-bed reactor., Chem. Eng. Sci.,* 1996, **51**, 4791–800.

62. B. Babu and K. K. Sastry., *Estimation of heat transfer parameters in a trickle-bed reactor using differential evolution and orthogonal collocation., Comput. Chem. Eng.,* 1999, **23**, 327-39.

63. G. Eigenberger, C. Verfahrenstechnik, U. Stuttgart., *Fixed-Bed Reactors. Ullmann's Encyc1opedla of Industnal Chemistry*, 1992, **B4**, 200-238.

64. I. Iliuta, F. C. Thyrion., *Residence time distrribution of the liquid in gas-liquid concurrent upflow fixed-bed reactors., Chemi. Engin. Sci.,* 1996, **51**, 4579-4593 .

65. T. Wang, J. Wang, Y. Jin. *Slurry Reactors for Gas-to-Liquid Processes: A Review., Ind Eng. Chem. Res*., 2007, **46**, 5824–47.

66. X. Gao, Y. P. Zhu, Z. Luo, *CFD modeling of gas flow in porous medium and catalytic coupling reaction from carbon monoxide to diethyl oxalate in fixed-bed reactors. Chem. Eng. Sci*., 2011, **66**, 6028-38.

67. R. Guettel and T. Turek, *Assessment of micro-structured fixed-bed reactors for highly exothermic gas-phase reactions. Chem. Eng. Sci.,* 2010, **65**, 1644–54.

68. A. Ulgen and W. F. Hoelderich, *Conversion of glycerol to acrolein in the presence of WO3/TiO2 catalysts., Appl. Catal. A Gen.,* 2011, **400**, 34–8.

69. S. H. Chai, L. Z. Tao, B. Yan, J. C. Vedrine, B. Q. Xu., *Sustainable production of acrolein: effects of reaction variables, modifiers doping and ZrO_2 origin on the performance of WO3/ZrO2 catalyst for the gas-phase dehydration of glycerol. RSC*. Adv., **4**, 4619.

70. T. Mongkhonsi and L. Kershenbaum., *Sustainable production of acrolein: effects of reaction variables, modifiers doping and ZrO_2 origin on the performance of WO_3/ZrO_2 catalyst for the gas-phase dehydration of glycerol. Appl. Catal. A.*, 1998, **170**, 33-48.

71. A. I. Anastasov, V. A. Nikolov., *Optimal Policies of Operation of a Fixed-Bed Reactor for Oxidation of o-Xylene into Phthalic Anhydride*. Ind. Eng. Chem., 1998, **5885**, 3424-33.

72. P. Gallezot and D. Richard., *Selective hydrogenation of α, β-unsaturated aldehydes., Catal. Rev.: Sci. and Eng.,* 2006, **40**, 37-41.

73. D. Shieh, C. Tsai, A. Ko., *Liquid-phase synthesis of isopulegol from citronellal using mesoporous molecular sieves MCM-41 and zeolites., React. Kinet. Catal. Lett*., 2003, **79**, 381-9.

74. U. Schuchardt, R. Sercheli, R. Matheus., *Transesterification of vegetable oils : a review general aspects of transesterification of vegetable oils acid-catalyzed processes base-catalyzed processes. Chem. Soc.,* 1998, **9**, 199-210.

75. A. Buasri, N. Chaiyut, V. Loryuenyong, C. Rodklum, T. Chaikwan, N. Kumphan, *Continuous process for biodiesel production in packed bed reactor from waste frying oil using potassium hydroxide supported on jatropha curcas fruit shell as solid catalyst., Appl. Sci.,* 2012, **2**, 641-53.

76. H. Bakhtiary-Davijany, F. Hayer, X. Kim Phan, R. Myrstad, P. Pfeifer, H. J. Venvik, *Performance of a multi-slit packed bed microstructured reactor in the synthesis of methanol: Comparison with a laboratory fixed-bed reactor., Chem. Eng. Sci.,* 2011, **66**, 6350–7.

77. L. Martínez-Latorre, S. Armenise, E. Garcia-Bordejé, *Temperature-mediated control of the growth of an entangled carbon nanofiber layer on stainless steel micro-structured reactors., Carbon,* **48**, 2047-56.

78. S. Chambrey, P. Fongarland, H. Karaca, S. Piché, Griboval-Constant, D. Schweich, *Fischer–Tropsch synthesis in milli-fixed bed reactor: Comparison with centimetric fixed bed and slurry stirred tank reactors., Catal. Today,* 2011, **171**, 201–6.

79. L. Kiwi-Minsker and A. Renken., *Microstructured reactors for catalytic reactions. Catal. Today,* **110**, 2–14.

80. G. Kolb and V. Hessel. *Micro-structured reactors for gas phase reactions., Chem. Eng. J.,* 2004, 98, 1–38.

81. A. Kundu, J. E. Ahn, S. S. Park, Y. G. Shul, H. S. Han., *Process intensification by micro-channel reactor for steam reforming of methanol. Chem. Eng.*, 2008, **135**, 113-9.

82. M. N. Kashid, A. Renken, L. Kiwi-Minsker., *Microstructured reactors and supports for ionic liquids. Chem. Eng. Sci.*, 2011, **66**, 1480–9.

83. A. Renken., V. Hessel, P. Löb, R. Miszczuk, M. Uerdingen, L. Kiwi-Minsker., *Ionic liquid synthesis in a microstructured reactor for process intensification. Chem. Eng. Process.* 2007, **46**, 840–5.

84. P. L. Mills, D. J. Quiram, J. F. Ryley, *Microreactor technology and process miniaturization for catalytic reactions-A perspective on recent developments and emerging technologies. Chem. Eng. Sci.*, 2007, **62**, 6992–7010.

85. P. R. Makgwane, Ph.D. Thesis, Nelson Mandela, Metropolitan University, 2009.

86. B. Moghtaderi, *Effect of enhanced mixing on partial oxidation of methane in a novel micro-reactor., Fuel.*, 2007, **86**, 469–76.

87. P. D. I. Fletcher, S. J. Haswell, E. Pombo-villar, B. H. Warrington, P. Watts, Y. F. Wong,

Micro reactors : principles and applications in organic synthesis., *Tetrahedron*., 2002, **58**, 4735–57.

88. V. Hessel, H. Löwe, F. Schönfeld, *Micromixers-a review on passive and active mixing principles., Chem. Eng. Sci.*, 2005, **60**, 2479–501.

89. N. Dupont, G. Germani, A. Vanveen, Y. Schuurman, G. Schafer, C. Mirodatos, *Specificities of micro-structured reactors for hydrogen production and purification. Int. J. Hydrogen Energy*, 2007, **32**, 1443–9.

90. G. H. Seong, R. M. Crooks, *Efficient Mixing and Reactions within Microfluidic Channels Using Microbead-Supported Catalysts. J. Am. Chem. Soc.*, 2002, **124**, 3360–1.

91. W. Liu and S. Roy, *Effect of channel shape on gas/liquid catalytic reaction performance in structured catalyst/reactor., Chem. Eng. Sci.*, 2004, **59**, 4927–39.

92. P. Löb, H. Löwe, V. Hessel, *Fluorinations, chlorinations and brominations of organic compounds in micro reactors., J. Fluor. Chem.*, 2004, **125**, 1677-94.

93. J. Commenge, T. Obein, G. Genin, X. Framboisier, S. Rode, V. Schanen., *Gas-phase residence time distribution in a falling-film microreactor., Chem. Eng. Sci.*, 2006, **61**, 597–604.

94. M.N. Kashid and L. Kiwi-Minsker, *Microstructured Reactors for Multiphase Reactions: State of the Art., Ind. Eng. Chem. Res.*, 2009, **48**, 6465-85.

95. K. Jähnisch, V. Hessel, H. Löwe, M. Baerns, *Chemistry in Microreactors Chemistry in Microstructured Reactors Angewandte., Chem. Microprocess Eng.*, 2004, **43**, 406–46.

96. S. Hu, A. Wang, H. Löwe, X. Li, Y. Wang, C. Li, Kinetic study of ionic liquid synthesis in a microchannel reactor. Chem. Eng. J., 2010, **162**, 350-4.

97. C. De. Bellefon, S. Caravieilhes, *Efficient catalytic isomerization of allylic alcohols to carbonyl compounds with water soluble. Surf. chemi. and catal.*, 2000, **3**, 607–14.

98. N. Bhatt and A. Patel. *Esterification of 1° and 2° alcohol using an ecofriendly solid acid catalyst comprising 12-tungstosilicic acid and hydrous zirconia. J. Mol. Catal. A. Chem.*, 2005, **238**, 223-8.

99. B. Zhao, C. H. Lu, M. Liang, *Solvent-free esterification of poly(vinyl alcohol) and maleic anhydride through mechanochemical reaction. Chinese Chem. Lett.*, 2007, **18**, 1353-6.

100. P. Taylor, *A new simplified method for esterification of secondary and tertiary alcohols. Synth. Commun.*, 1997, **27**, 2777-81.

101. T. A. Nijhuis, A. E. W. Beers, F. Kapteijn, J. A. Moulijn, *Water removal by reactive*

stripping for a solid-acid catalyzed esteriÿcation in a monolithic reactor. Chemi. Engin. Sci., 2002, **57**, 1627–32.

102. X. Yao, Æ. J. Yao, Æ. L. Zhang, *Fast esterification of acetic acid with short chain alcohols in microchannel reactor. springer Link J.,* 2009, **132**, 147–52.

103. T. Jacobs, C. Kutzner, M. Kropp, G. Brokmann, W. Lang, A. Steinke, *Combination of a novel perforated thermoelectric flow and impedimetric sensor for monitoring chemical conversion in micro fluidic channels. Procedia Chem.,* 2009, **1**, 1127–30.

104. K. L. A. Chan, S. Gulati, J. B. Edel, A. J. de Mello, S. G. Kazarian. *Chemical imaging of microfluidic flows using ATR-FTIR spectroscopy. J. Royal Society of Chemi.,* 2009, **9**, 2909-13.

105. K. L. A. Chan and S. G. Kazarian, *FT-IR Spectroscopic imaging of reactions in multiphase flow in microfluidic channels., pubs.acs.org/ac.,* 2012, **84**, 4052–6.

106. C. Wiles, P. Watts, *Continuous flow reactors: a perspective. Green Chem.* 2012, **14**, 38.

107. J. S. Moore and K. F. Jensen. *Batch kinetics in Flow : Online IR Analysis and Continuous Control., Chemi. Eng. and Proc.* 2015, **53**, 470–473;

108. V. Sans, L. Porwol, V. Dragone, L. Cronin, Chemical Science using real-time in-line NMR spectroscopy., Chem. Sci., 2015, **6**, 1258-64.

109. B. Mpuhlu. Ph.D. Thesis, Nelson Mandela Metropolitan University, 2007.

110. R. Qiu, Y. Zhu, X. Xu, Y. Li, L. Shao, X. Ren, *Zirconocene bis (perfluorooctanesulfonate) s-catalyzed acylation of alcohols, phenols, thiols, and amines under solvent-free conditions. Catal. Commun.,* 2009, **10**, 1889-92.

111. S. Imachi, K. Owada, M. Onaka, *Intramolecular carbonyl-ene reaction of citronellal to isopulegol over $ZnBr_2$-loading mesoporous silica catalysts. J. Mol. Catal. A Chem.,* 2007, **272**, 174-81.

112. S. Serra, E. Brenna, C. Fuganti, F. Maggioni, *Lipase-catalyzed resolution of p -menthan-3-ols monoterpenes :preparation of the enantiomer-enriched forms of menthol, isopulegol, trans- and cis-piperitol, and cis-isopiperitenol. Tetrah.,* 2003, **14**, 3313–9.

113. A. Corma, M. Renz, I. D. T. Química, A. D. L. Naranjos, *Sn-Beta zeolite as diastereoselective water-resistant heterogeneous Lewis-acid catalyst for carbon-carbon bond formation in the intramolecular carbonyl-ene reaction., rsc.org/chemcomm.* 2004, 550–1.

114. Z. Yongzhong, N. Yuntong, S. Jaenicke, G. Chuah, *Cyclisation of citronellal over*

zirconium zeolite-beta a highly diastereoselective catalyst to (±)-isopulegol. J. Catal., 2005, **229**, 404–13.

115. P. Makiarvela, *Cyclization of citronellal over zeolites and mesoporous materials for production of isopulegol., J. Catal.*, 2004, **225**, 155–69.

116. D. B. G. Williams, M. S. Sibiya, P. S. van Heerden. *Efficient hydroalkoxylation of alkenes to generate octane-boosting ethers using recyclable metal triflates and highly active metal triflate/Brønsted acid-assisted catalysts. Fuel Process. Techn.*, 2012, **94**, 75-9.

117. R. D. Crouch, J. F. Mehlmann, B. R. Herb, J. V. Mitten, H. G. Dai., *Selective conversion of nol ethers into alcohols in the presence of alkenes using $Hg(OAc)_2$-$NaBH_4$. synthesis (Stuttg).*, 1999, **4**, 559–61.

118. D. Paul, The solvomercuration-demercuration of representative olefins in the presence of alcohols. J. Am. Chem. Soc., 1969, **1522**, 5646–7.

119. K. Hensen, C. Mahaim, W. F. Hislderich, *A : Alkoxylation of limonene and alpha-pinene over beta zeolite as heterogeneous catalyst., Appl. Catal. A Gen.*, 1997, **149**, 311–29.

120. Ã. KADS, *Catalytic transformations of the major terpene feedstocks. Trop. Catal.*, 2004, **27**, 1–4.

121. G. K. Chuah, S. H. Liu, S. Jaenicke, L. J. Harrison, cyclisation of citronellal to isopulegol catalysed by hydrous zirconia and other solid acids., 2001, **359**, 352–9.

122. A. K. Chakraborti and R. Gulhane, *Indium (III) chloride as a new , highly efficient, and versatile catalyst for acylation of phenols, thiols, alcohols, and amines., Tetrahedron Lett.*, 2003, **44**, 6749-53.

123. R. Gulhane and A. K. Chakraborti., *Zinc perchlorate hexahydrate $[Zn(ClO_4)_2 .6H_2O]$ as acylation catalyst for poor nucleophilic phenols, alcohols and amines: Scope and limitations, J. Mol. Catal. A Chem.*, 2007, **264**, 208–13.

124. K. L. Chandra, P. Saravanan, R. K. Singh, V. K. *Singh. Lewis acid catalyzed acylation reactions: scope and limitations., Tetrahedron*, 2002, **58**, 2–7.

125. M. Harmer and Q. Sun, *Solid acid catalysis using ion-exchange resins. Appl. Catal. A Gen.*, 2001, **221**, 45–62.

126. B. C. Gagea, G. Poncelet, V. I. Pa., *Acylation of alcohols and activated aromatic compounds on silica embedded-triflate catalysts.*, 2006, **301**, 133–7.

127. H. Firouzabadi, N. Iranpoor, S. Farahi., *J. Mol. Catal. A Chem.*, 2008 **289**, 61–8.

128. M. Akçay, The catalytic acylation of alcohols with acetic acid by using Lewis acid

character pillared clays. Appl. Catal. A: Gen., 2004, **269**, 157–160.

129. J. L. Babu, A. Khare, D. Y. Vankar., *$Bi(OTf)_3$ and SiO_2-$Bi(OTf)_3$ as Effective catalysts for the ferrier rearrangement, Molecules*, 2005, **10**, 884–92.

130. S. R. Kirumakki, N. Nagaraju, S. A. Narayanan, *Comparative esterification of benzyl alcohol with acetic acid over zeolites Hβ, HY and HZSM5., Appl. Catal. A Gen.,* 2004 **273**, 1–9.

131. K. P. Boroujeni, *Silica gel supported $AlCl_3$ catalyzed Friedel-Crafts acylation of aromatic compounds., Chinese Chem. Lett.*, 2010, **21**, 1395–8.

132. P. Kumar, R. K. Pandey, M. S. Bodas, S. P. Dagade, M. K. Dongare, A. V. Ramaswamy, *Acylation of alcohols, thiols and amines with carboxylic acids catalyzed by yttria-zirconia-based Lewis acid., J. Memb. Sci.*, 2002, **181**, 207–13.

133. S. L. Barbosa, G. R. Hurtado, S. I. Klein, V. L. Junior, M. J. Dabdoub, C. F. *Guimarães, Niobium to alcohol mol ratio control of the concurring esterification and etherification reactions promoted by $NbCl_5$ and Al_2O_3 catalysts under microwave irradiation. Appl. Catal. A Gen.*, 2008, **338**, 9-13.

134. M. Nahmany, A. Melman, *Chemoselectivity in reactions of esterification, R. Soc. Chem.*, 2004, **2**, 1563–72.

135. A. K. Chakraborti and R.Gulhane, *Indium (III) chloride as a new, highly efficient, and versatile catalyst for acylation of phenols, thiols, alcohols, and amines., Tetrahedron Lett.*, 2003, **44**, 6749–53.

36. E. Vedejs, O. Daugulis, *Dual activation in the esterification of $MgBr_2$ and a tertiary Amine. Org. Chem.*, 1996, **3263**, 5702–3.

137. B. R. Jermy, A. *Pandurangan, Catalytic application of Al-MCM-41 in the esterification of acetic acid with various alcohols. Appl. Catal. A Gen.*, 2005, **288**, 25-33.

138. F. Mavandadi, Å. Pilotti, *The impact of microwave-assisted organic synthesis in drug discovery., Elsevier*, 2006, **11**, 165-74.

139. J. Tierney, J. *Westman, Microwave assisted organic synthesis-a review, Tetrahedron*, 2001, **57**, 9226-83

140. A. M. Balu, J. M. Campelo, R. Luque, A. A. Romero., *One-step microwave-assisted asymmetric cyclisation/hydrogenation of citronellal to menthols using supported nanoparticles on mesoporous materials., Org. Biomol. Chem.*, 2010, **8**, 2845–9.

141. D. H. More, D. G. Hundiwale, U. R. Kapadi, P. P. *Mahulikar, Microwave assisted solvent-*

free o-alkylation and acylation of thymol and geraniol using fly ash as solid support., J. Sci. Ind. Res., 2006, **65**, 817-20.

142. I. Plazl, S. LeskovSek, T. Koloini, *Hydrolysis of sucrose by conventional and microwave heating in stirred tank reactor., Chemi. Engin. J.*, 1995, **59**, 253-257

143. A. Madhvi, Surati, S. Jauhari, K. R. Desai., *A brief review : Microwave assisted organic reaction., Archives of Applied Science Research*., 2012, **4**, 645-61.

144. B. Roberts and C. R. Strauss, *Toward rapid, "green", predictable microwave-assisted synthesis., Acc. Chem. Res.*, 2005, **38**, 653-61.

145. W. Shieh, S. Dell, O. Repic., *Large scale microwave-accelerated esterification of carboxylic acids with dimethyl carbonate., Tetrahedron Letters*, 2002, **43**, 5607–09

146. F. Benaskar, N. G. Patil, V. Engels, E. V. Rebrov, J. Meuldijk, L. Hulshof, *Microwave-assisted Cu-catalyzed Ullmann ether synthesis in a continuous-flow milli-plant., Chem Eng. J.*, 2012, **207-208**, 426-39.

147. M. Nahmany and A. Melman., *Chemoselectivity in reactions of esterification., R. Soc. Chem.*, 2004, **2**, 1563–72.

148. N. U. Kumar, B. S. Reddy, V. P. Reddy, R. Bandichhor, *Zinc triflate catalyzed acylation of alcohols, phenols, and thiophenols. Tetrahedron Lett.*, 2014, **55**, 910-2.

149. T. Miyazawa, M. Yamamoto, Y. Maeda, *Microwave-accelerated selective acylation of (Hydroxyalkyl)phenols using acid chlorides., Synth. Commun.*, 2009, **39**, 1092–9.

Appendix

Raw data of the prepared compounds

Appendix A:

1. Citronellal

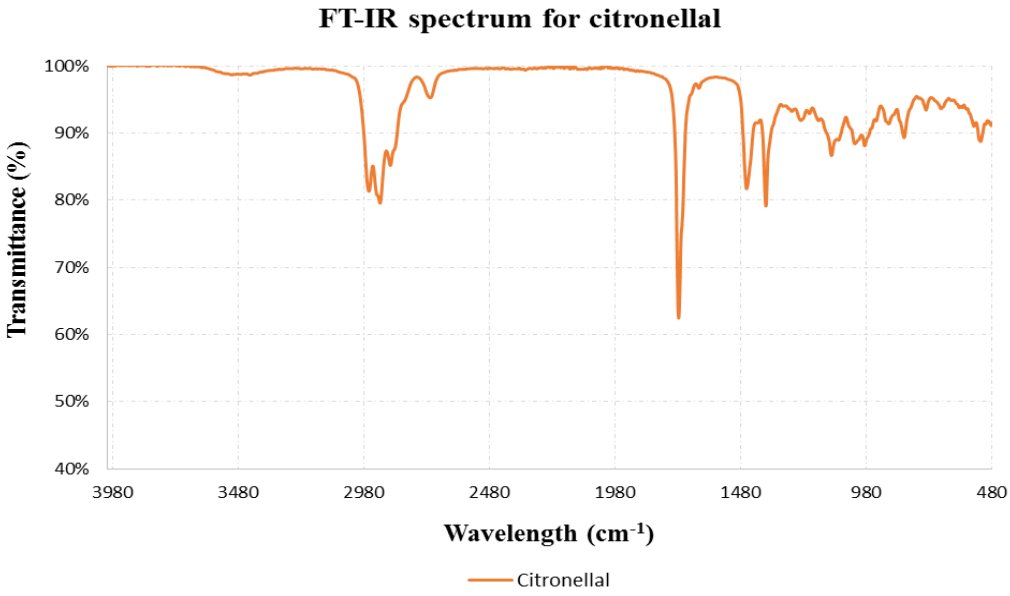

FT-IR- spectrum for citronellal

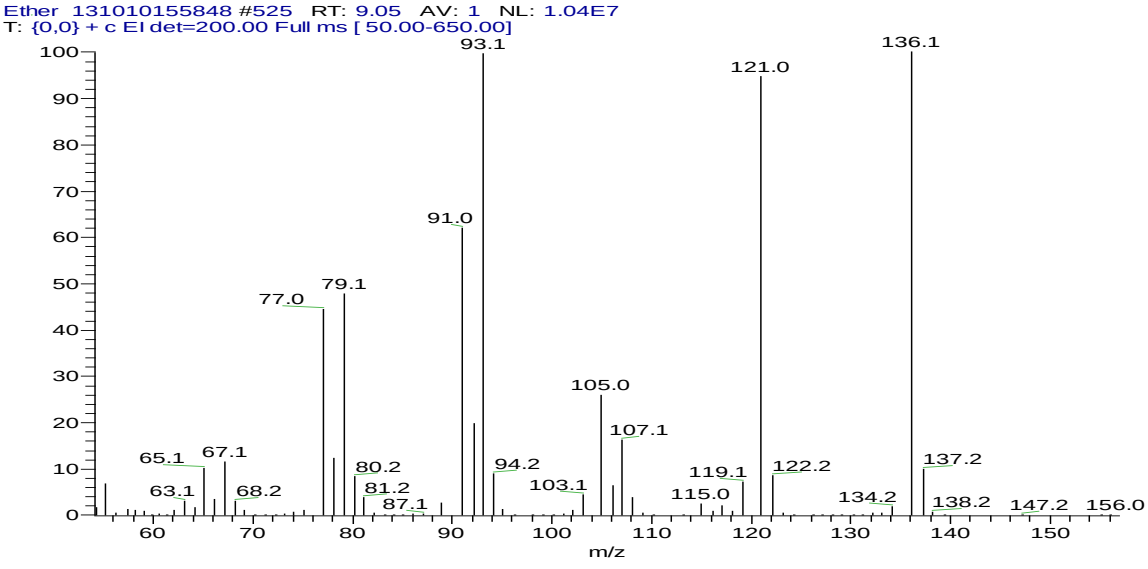

GC-MS spectrum for citronellal

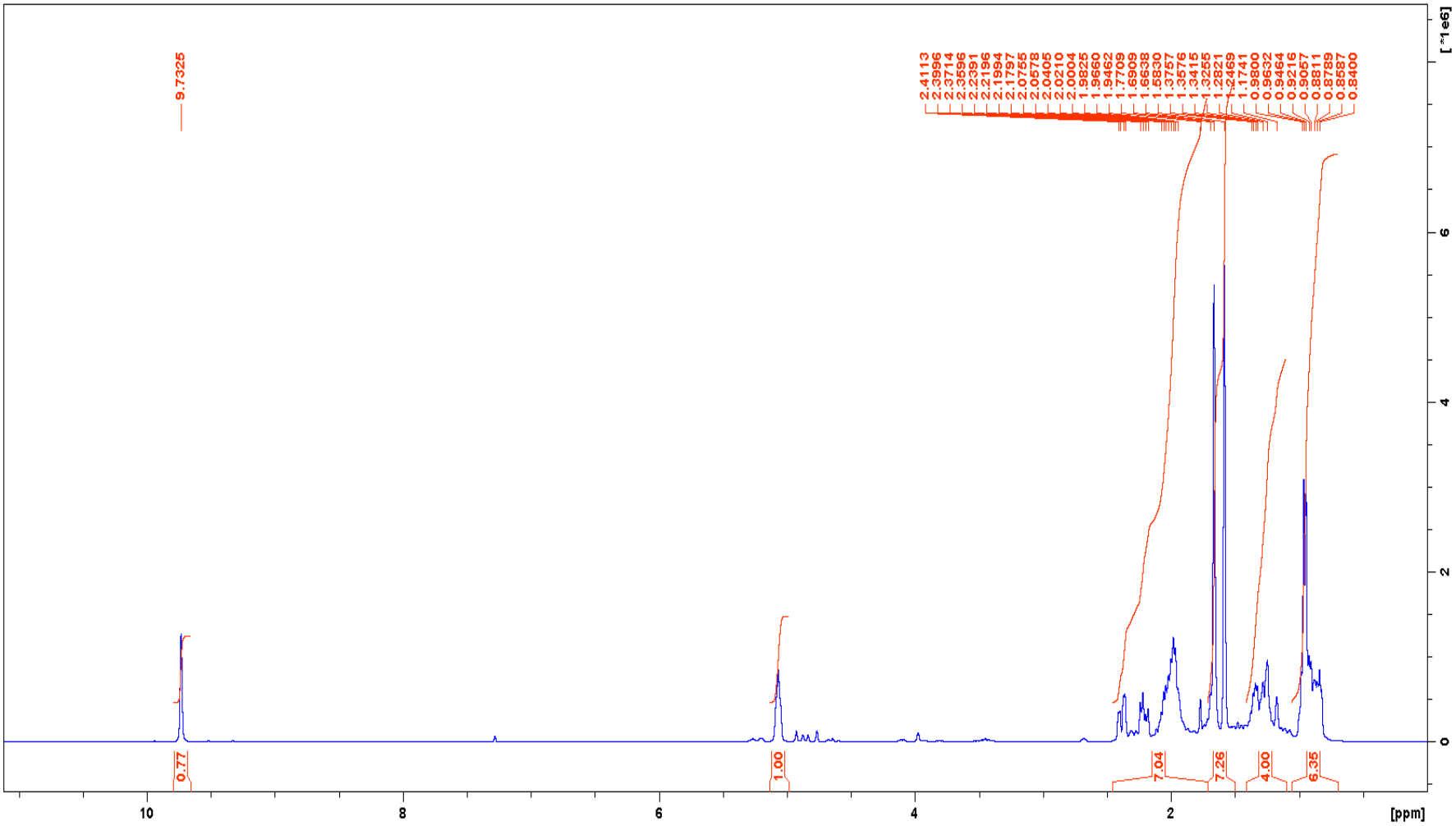

^{1}H-NMR spectrum for citronellal

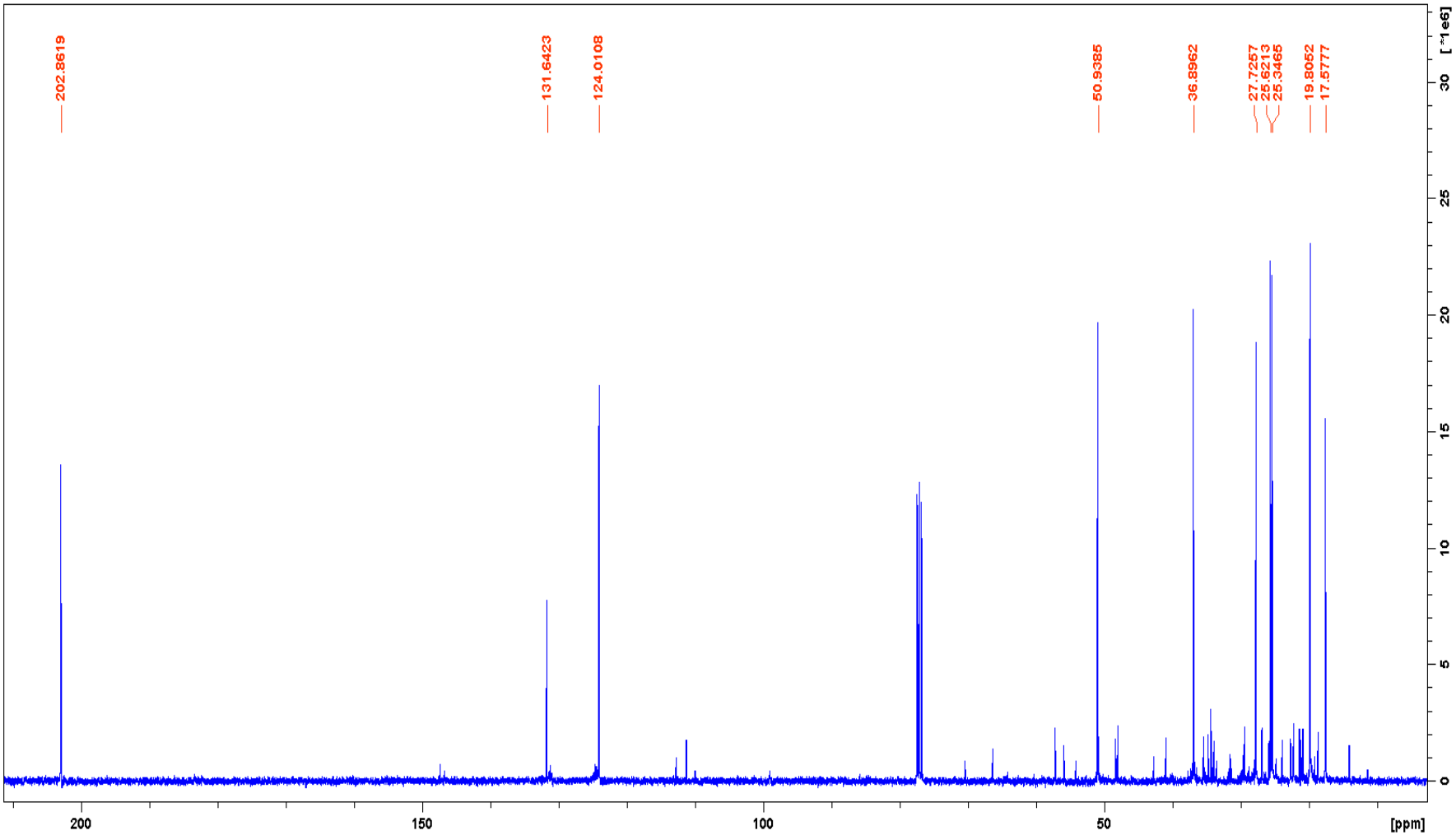

^{13}C-NMR spectrum for citronellal

2. Isopulegol

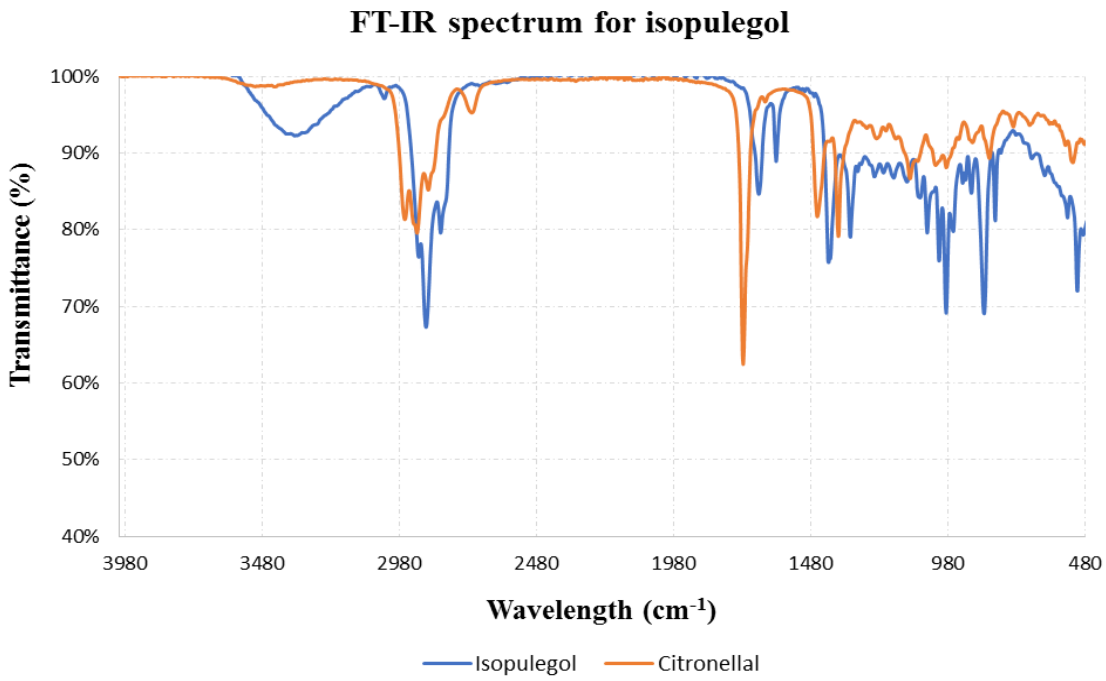

FT-IR spectrum for isopulegol

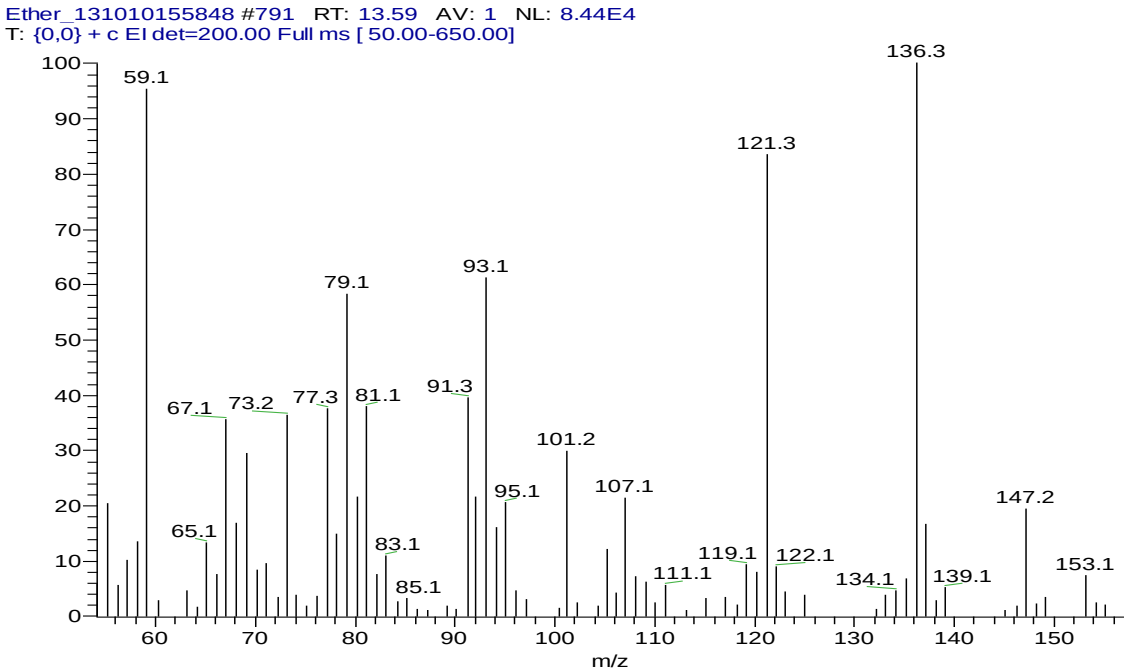

GC-MS spectrum for isopulegol

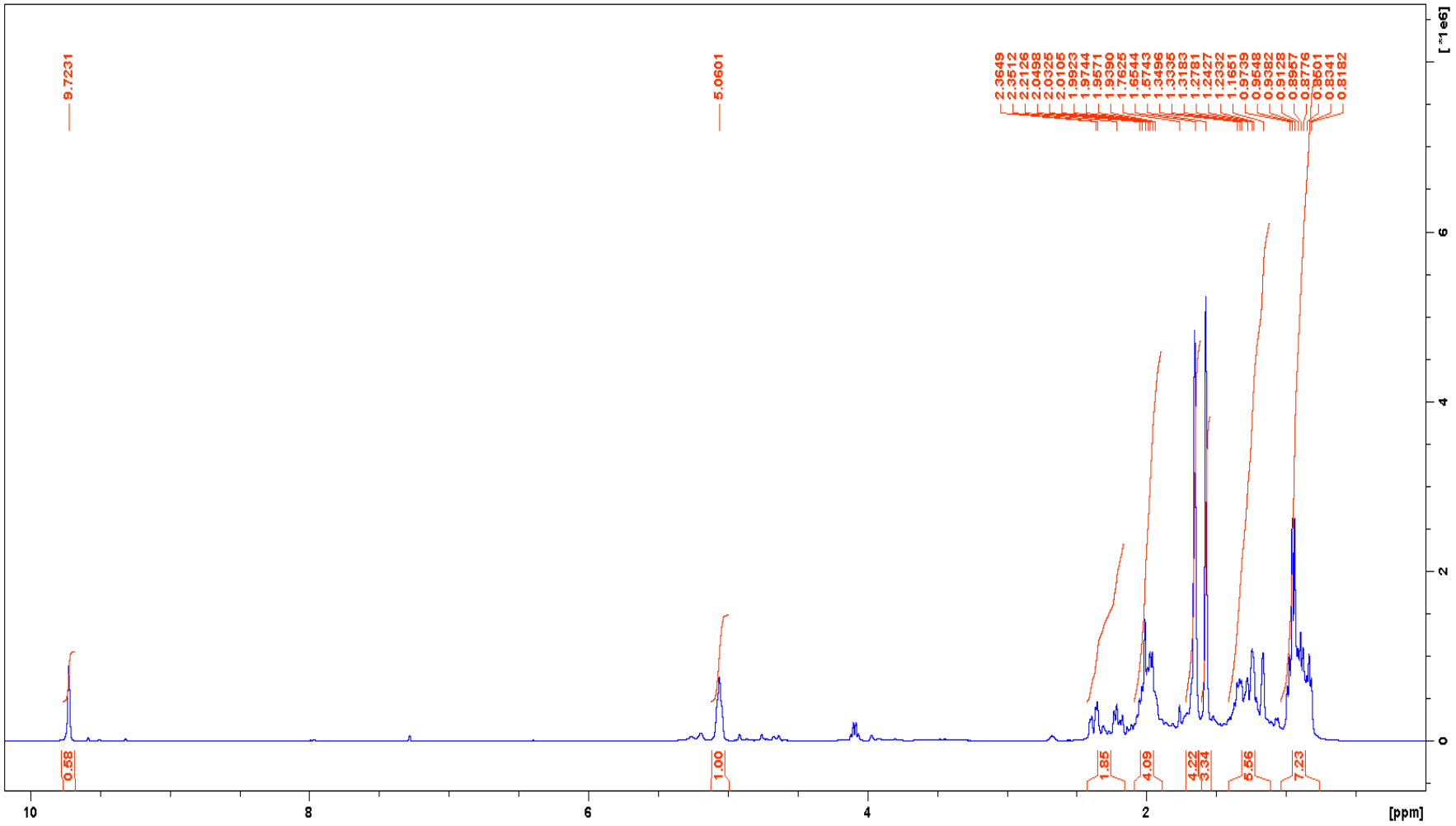

^{1}H-NMR spectrum

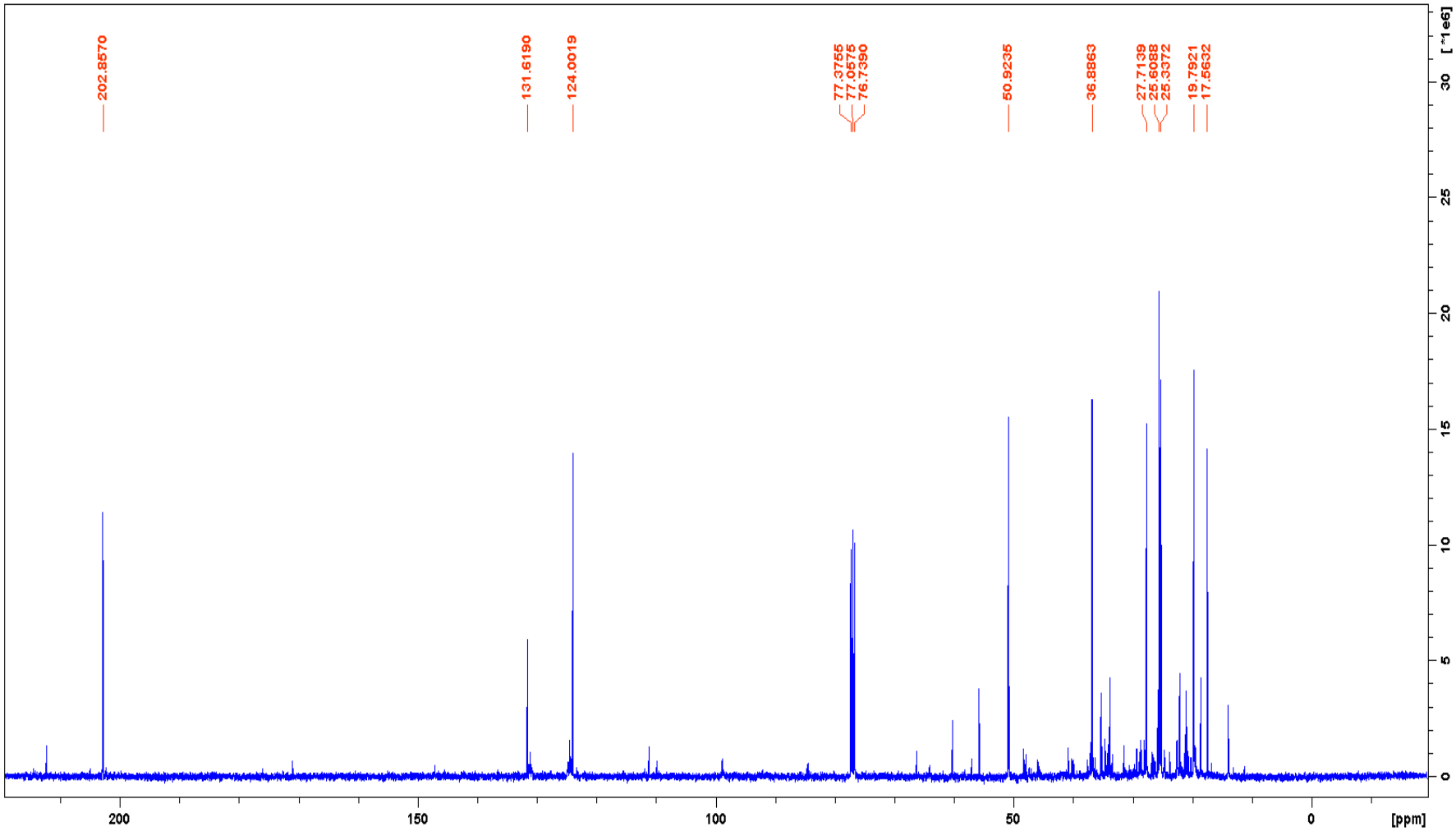

^{13}C-NMR spectrum

3. *para*-menthane-3,8-diol

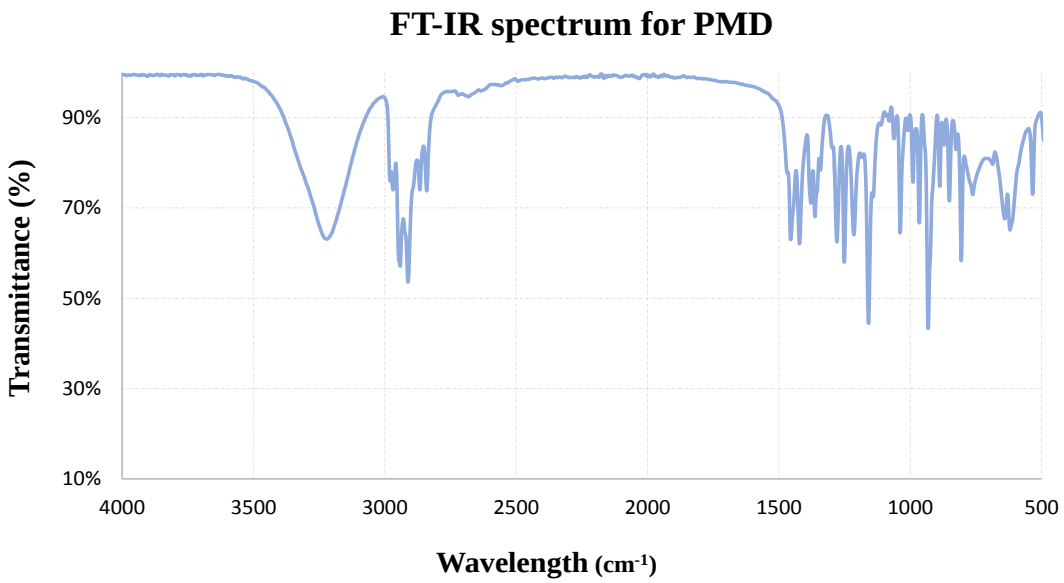

FT-IR spectrum for *para*-menthane-3,8-diol

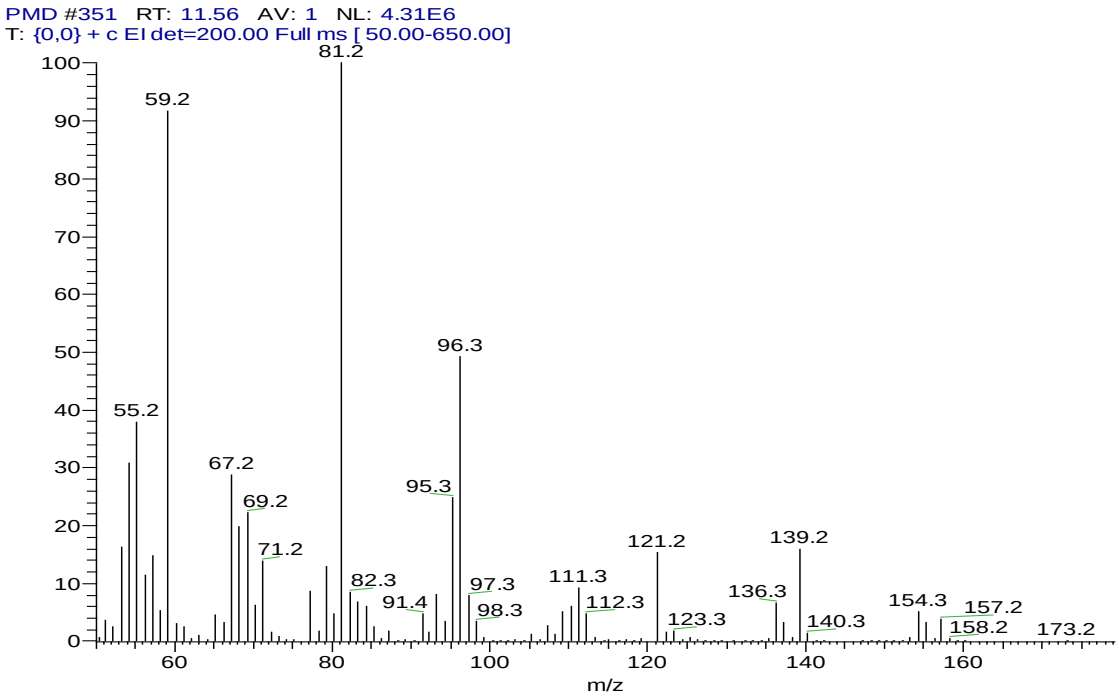

GC-MS spectrum for *para*-menthane-3,8-diol

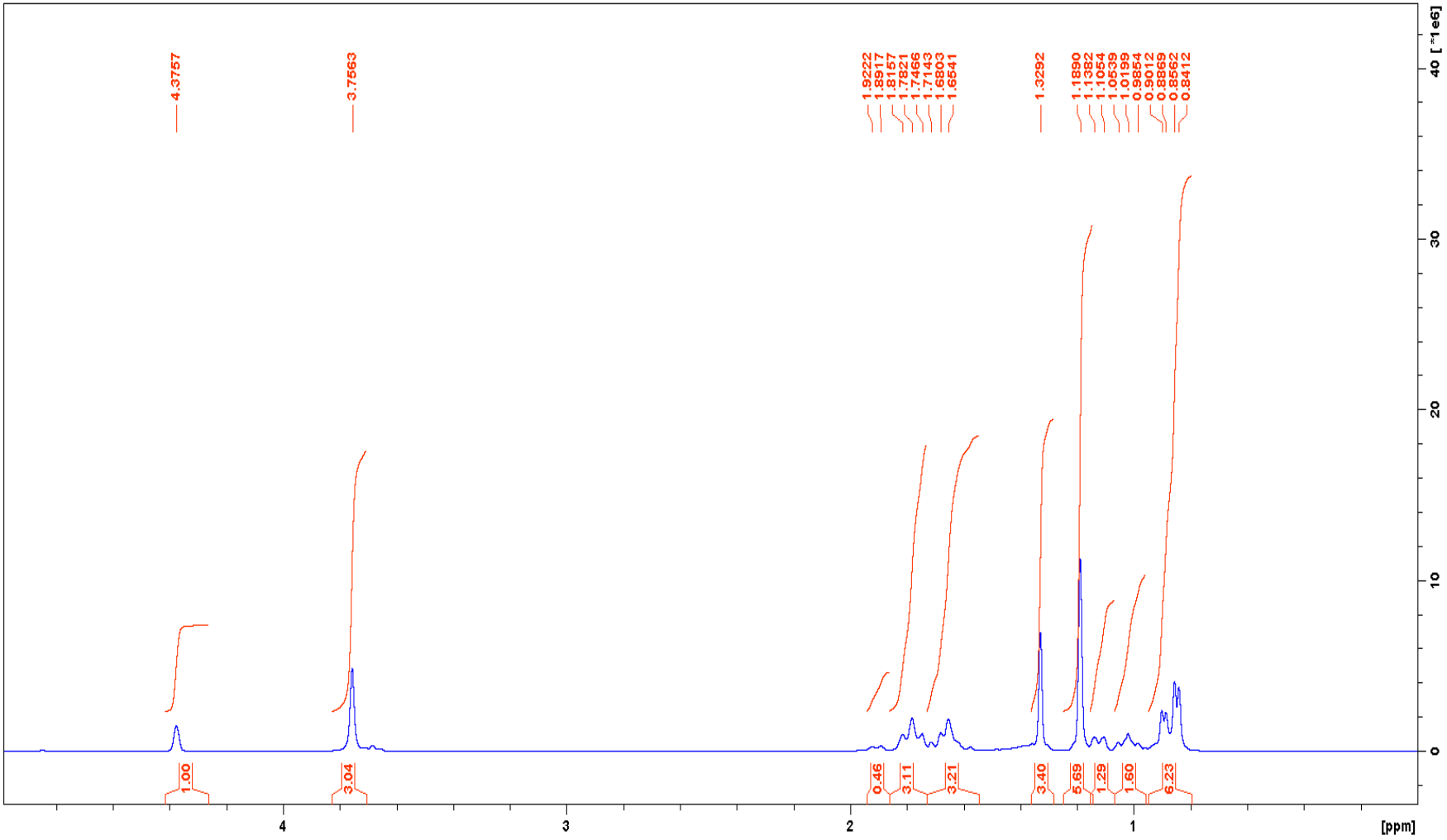

[1]H-NMR spectrum for *para*-menthane-3,8-diol

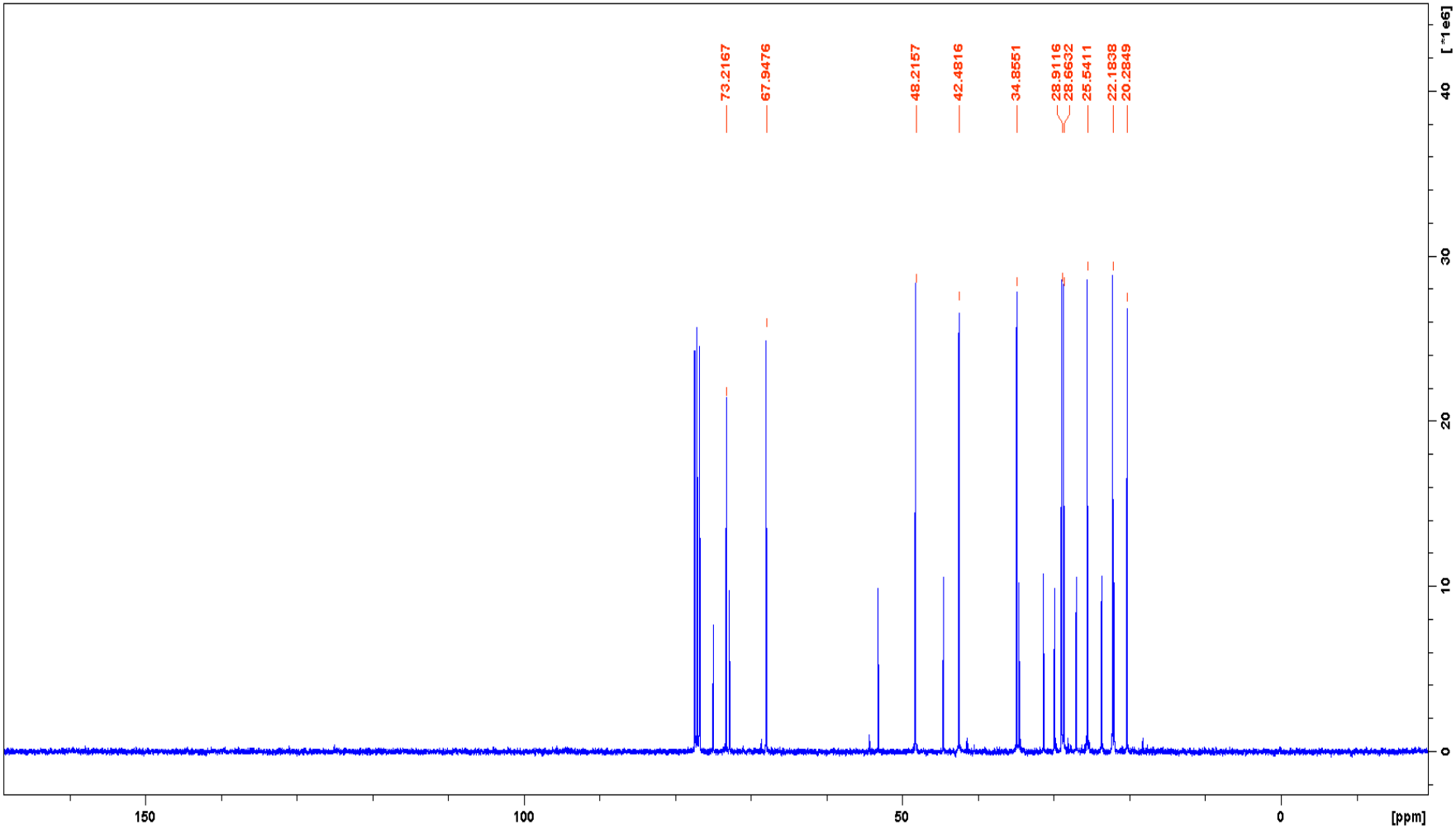

^{13}C-NMR spectrum for *para*-menthane-3,8-diol

Appendix B:

4. *para*-menthane-3,8-diester derivatives

4.1. Mono-acetate

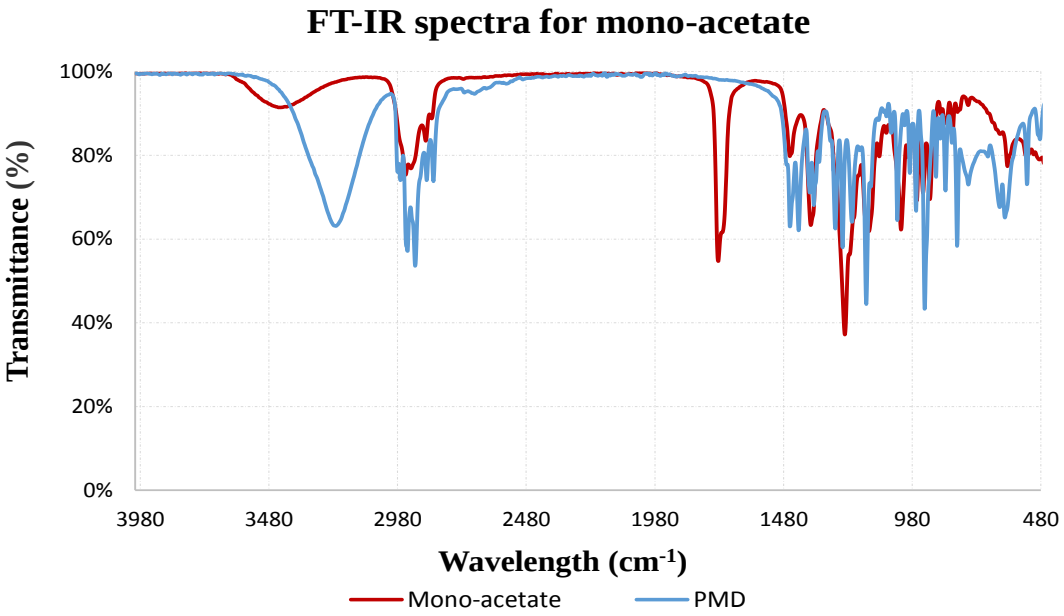

FT-IR spectrum for Mono-acetate

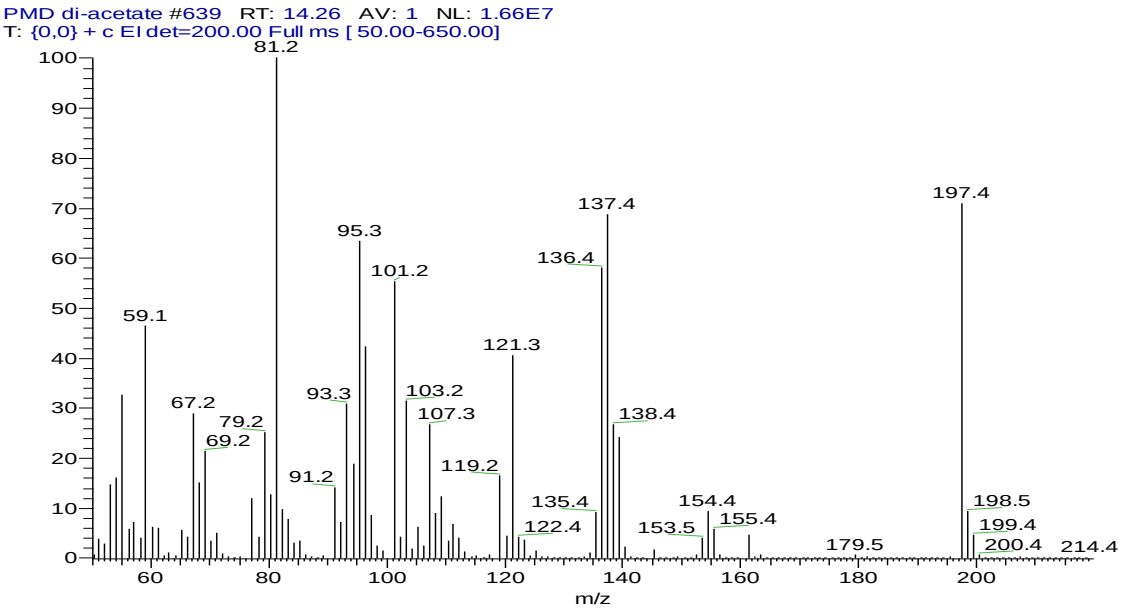

GC-MS spectrum for Mono-acetate

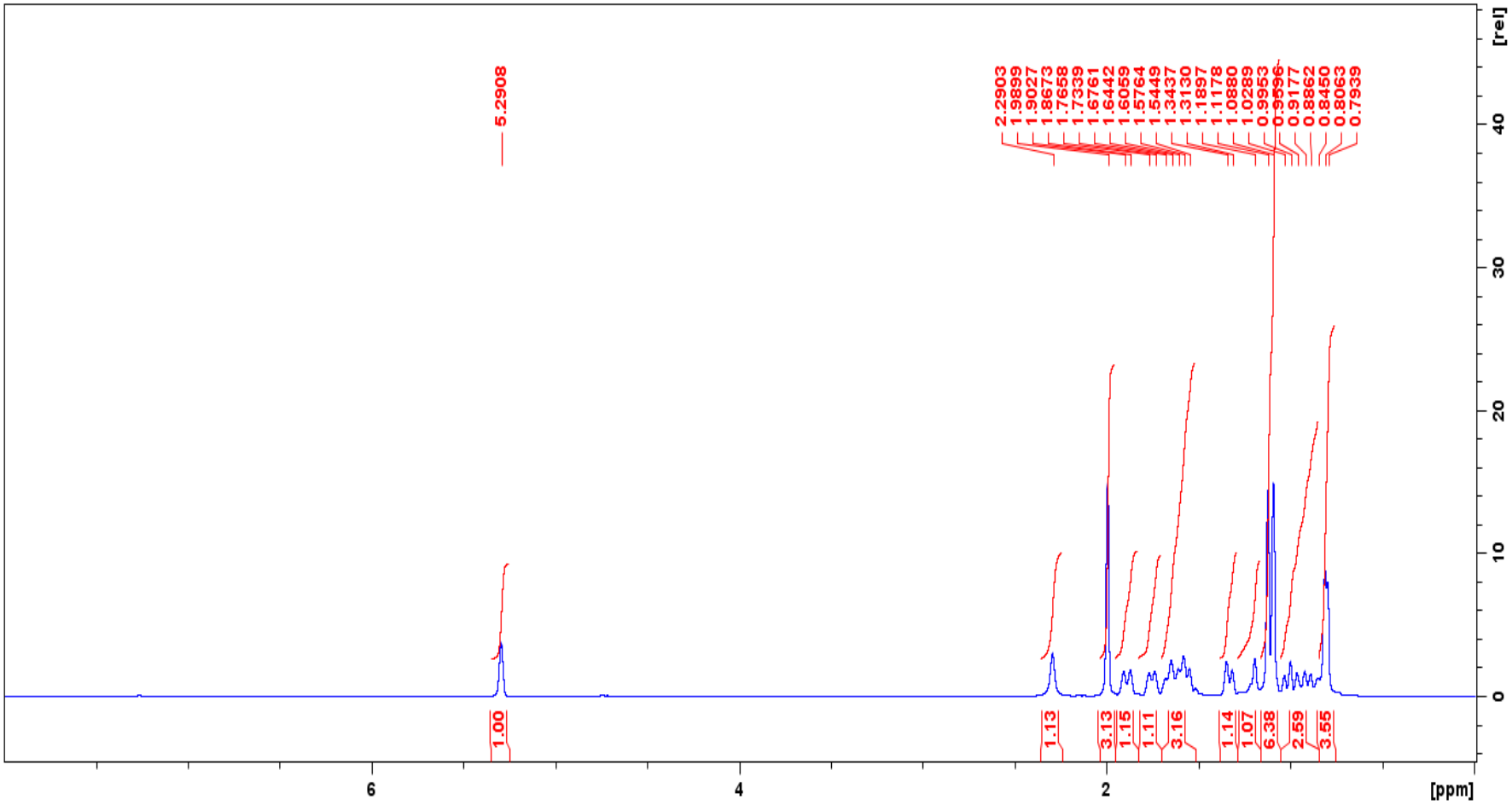

[1]H-NMR spectrum for Mono-acetate

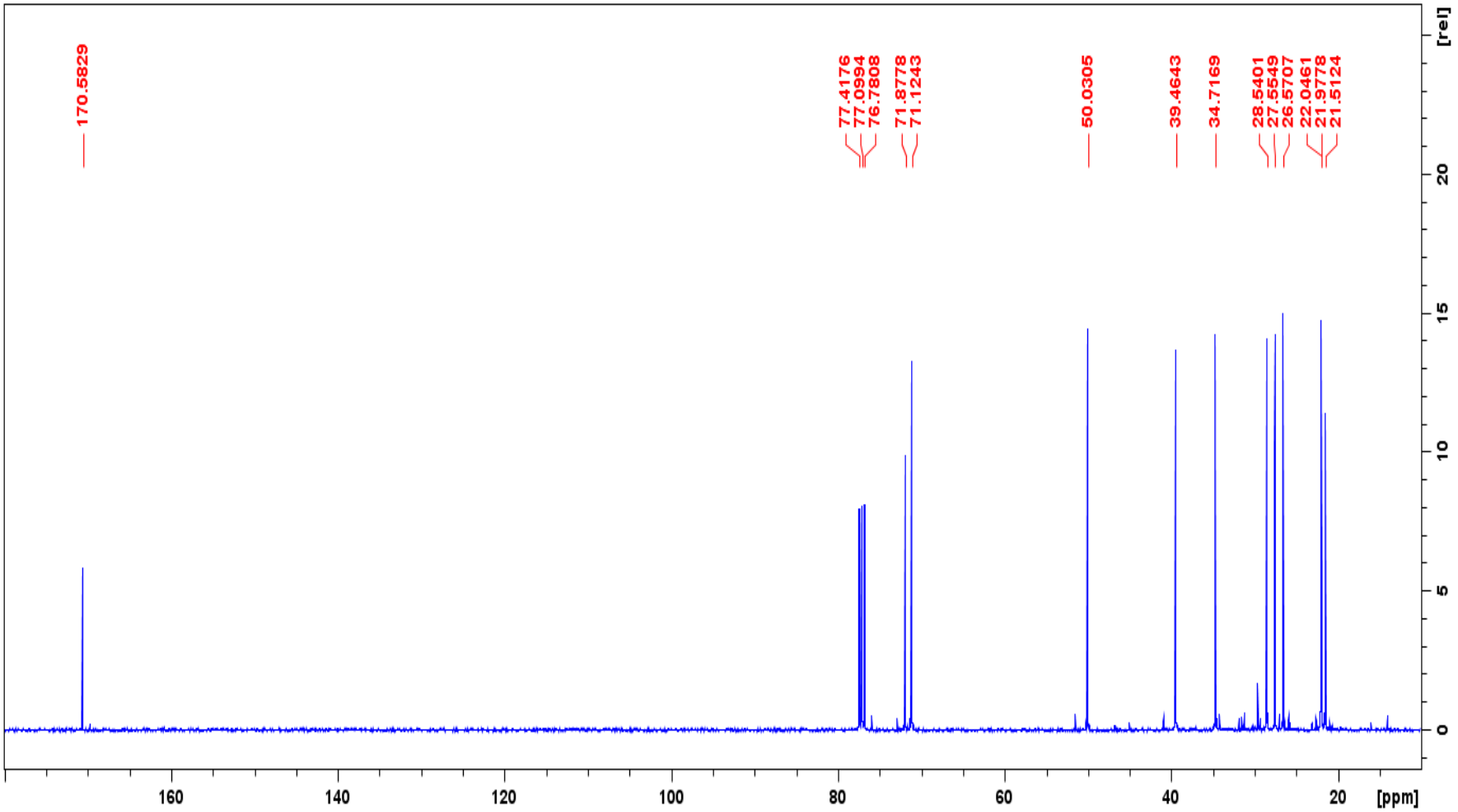

^{13}C-NMR spectrum for Mono-acetate

4.2. Di-acetate

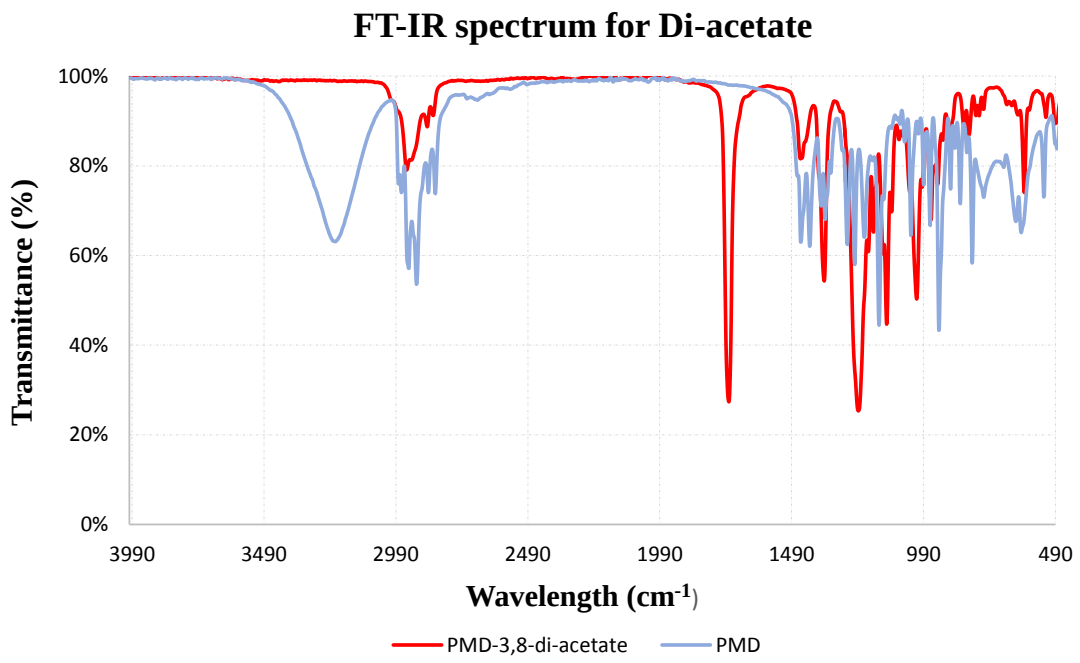

FT-IR spectrum for Di-acetate

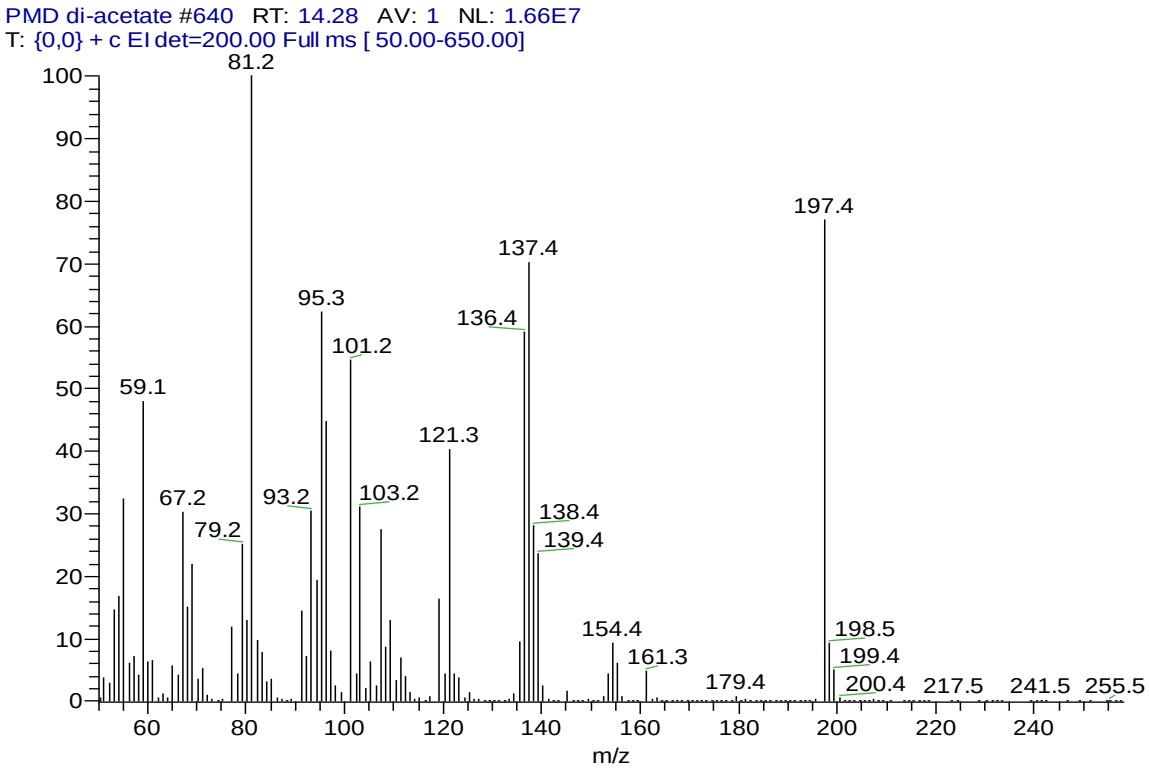

FT-IR spectrum for Di-acetate

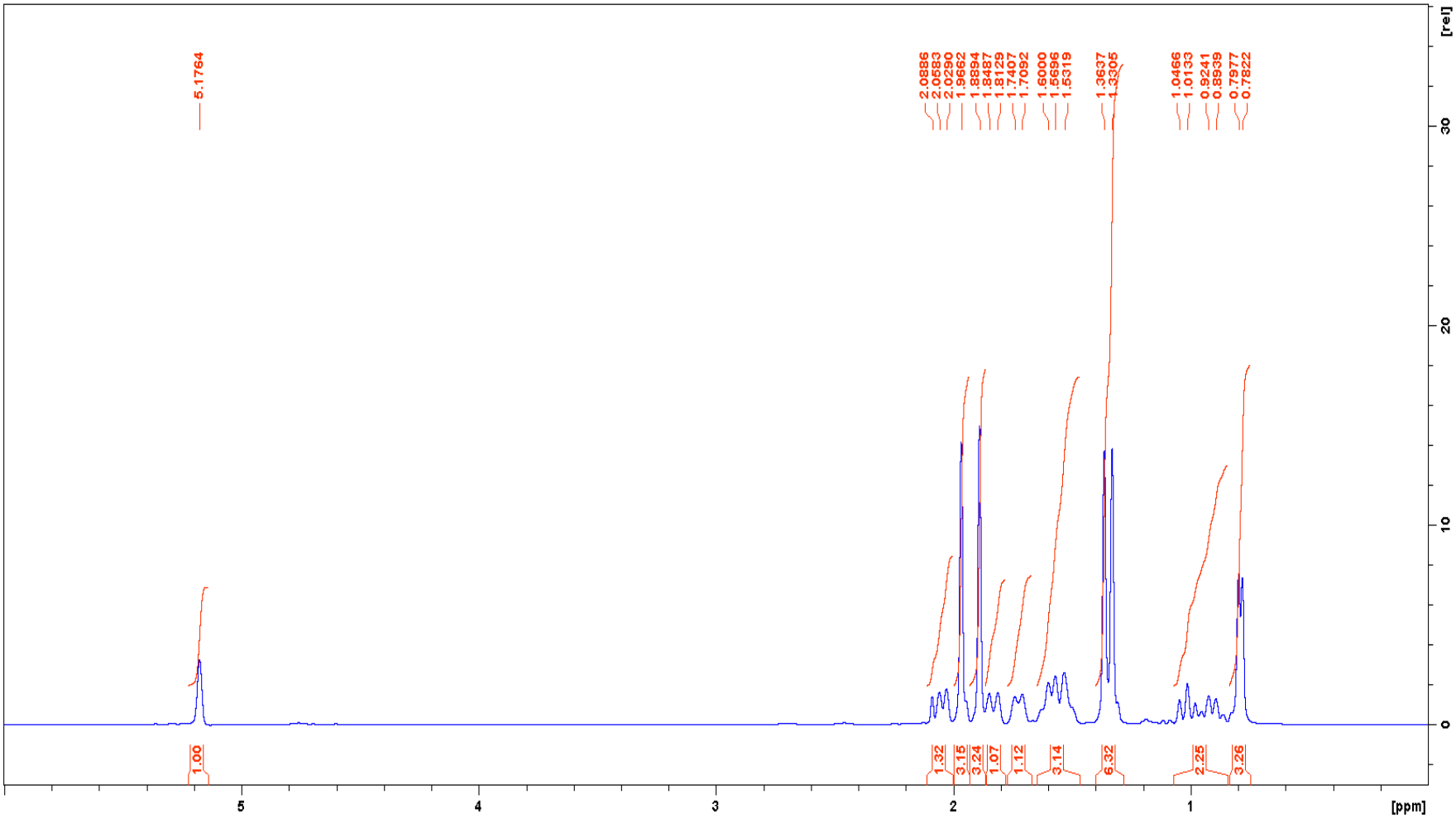

^{1}H-NMR spectrum for Di-acetate

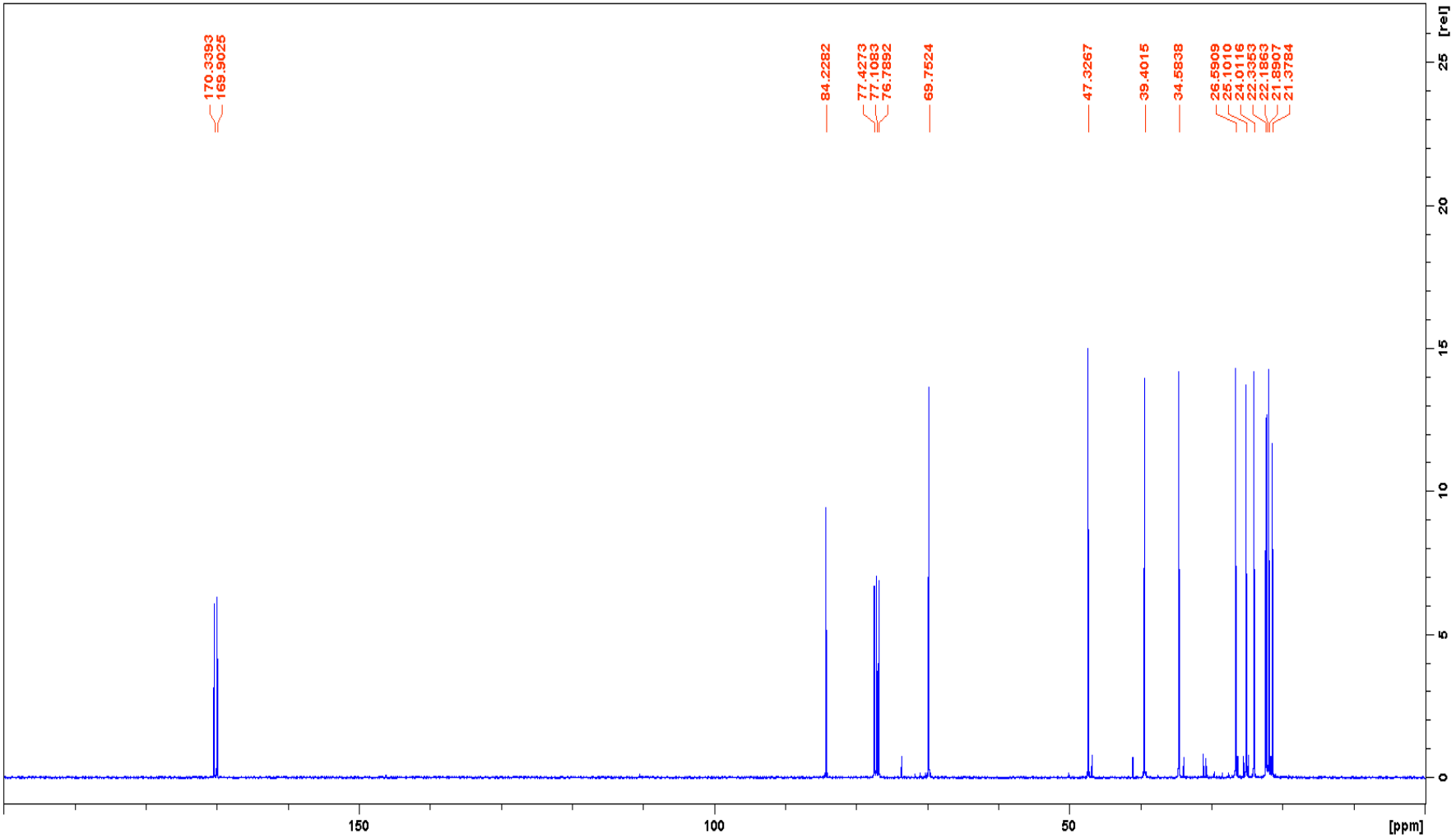

^{13}C-NMR spectrum for Di-acetate

4.3. Mono-propionate

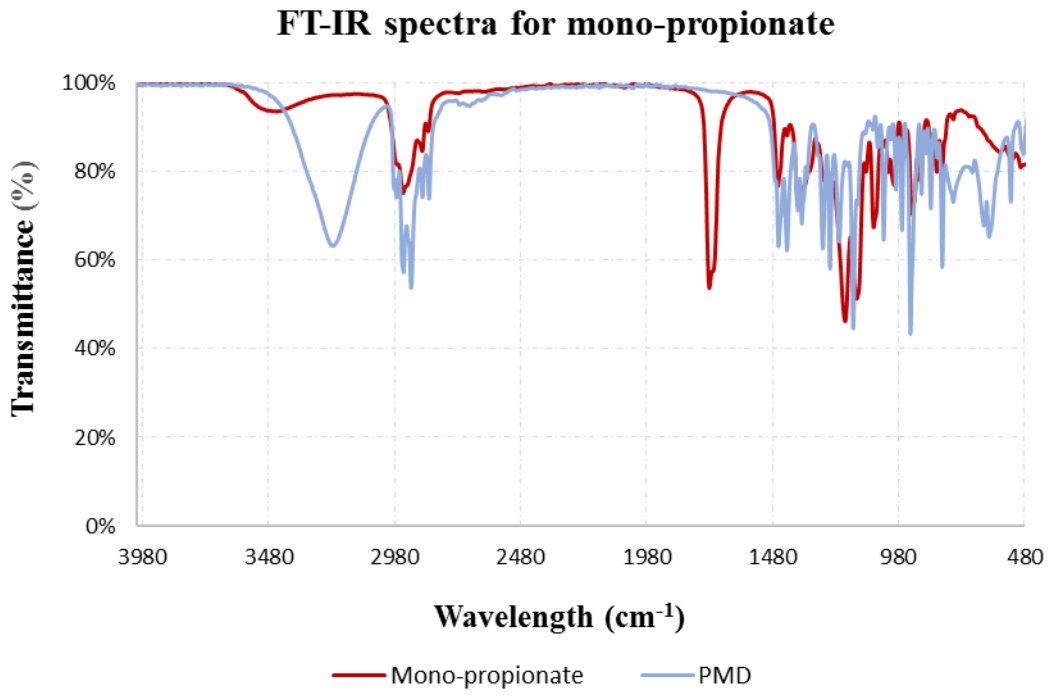

FT-IR spectrum for Mono-propionate

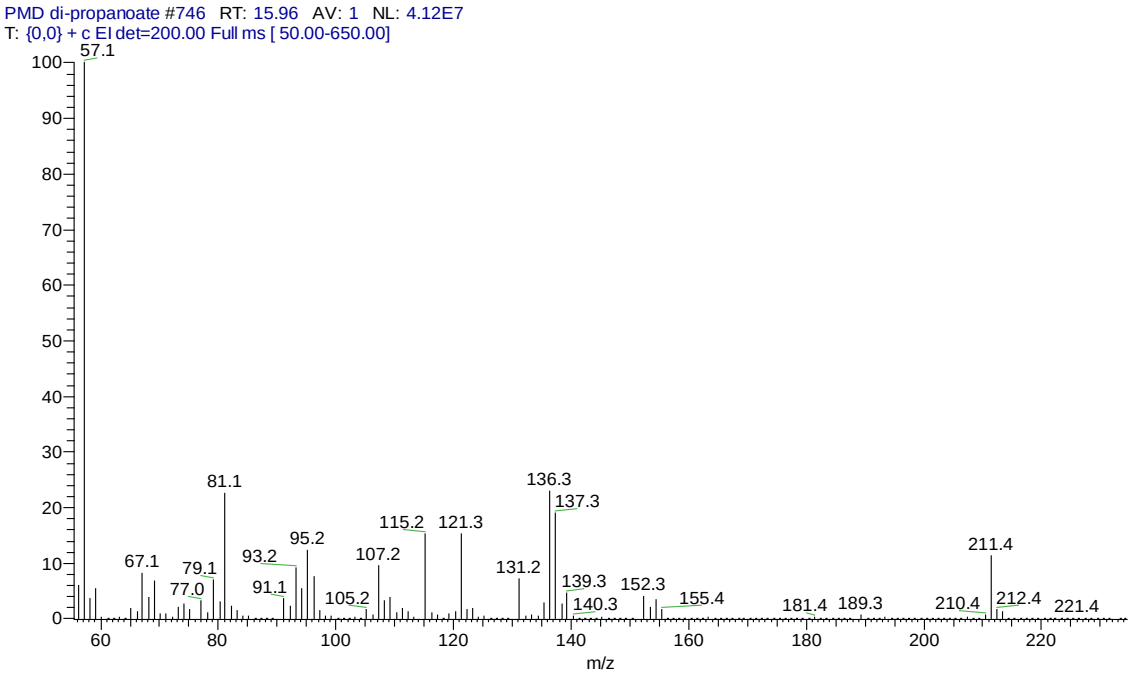

GC-MS spectrum Mono-propionate

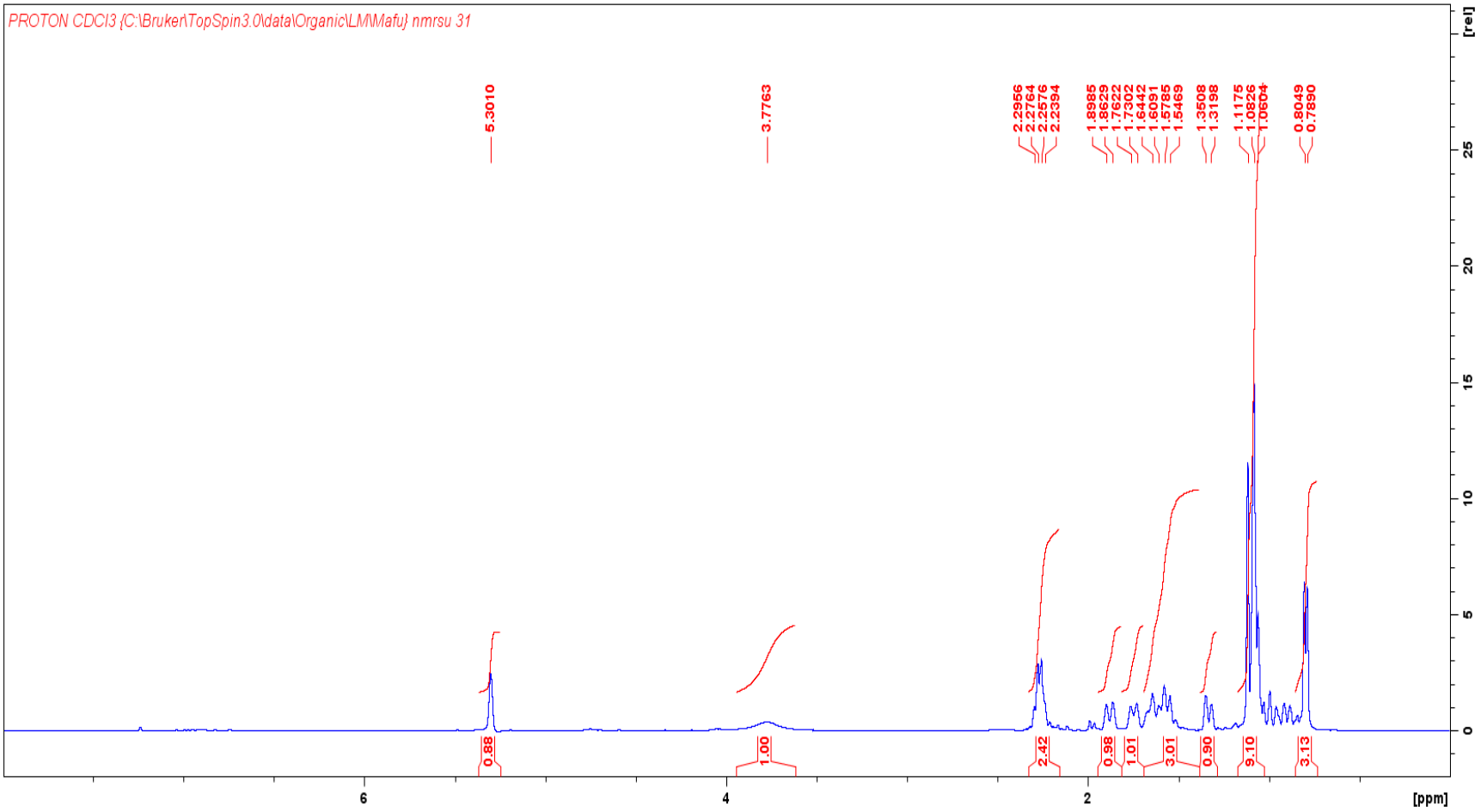

^{1}H-NMR spectrum Mono-propionate

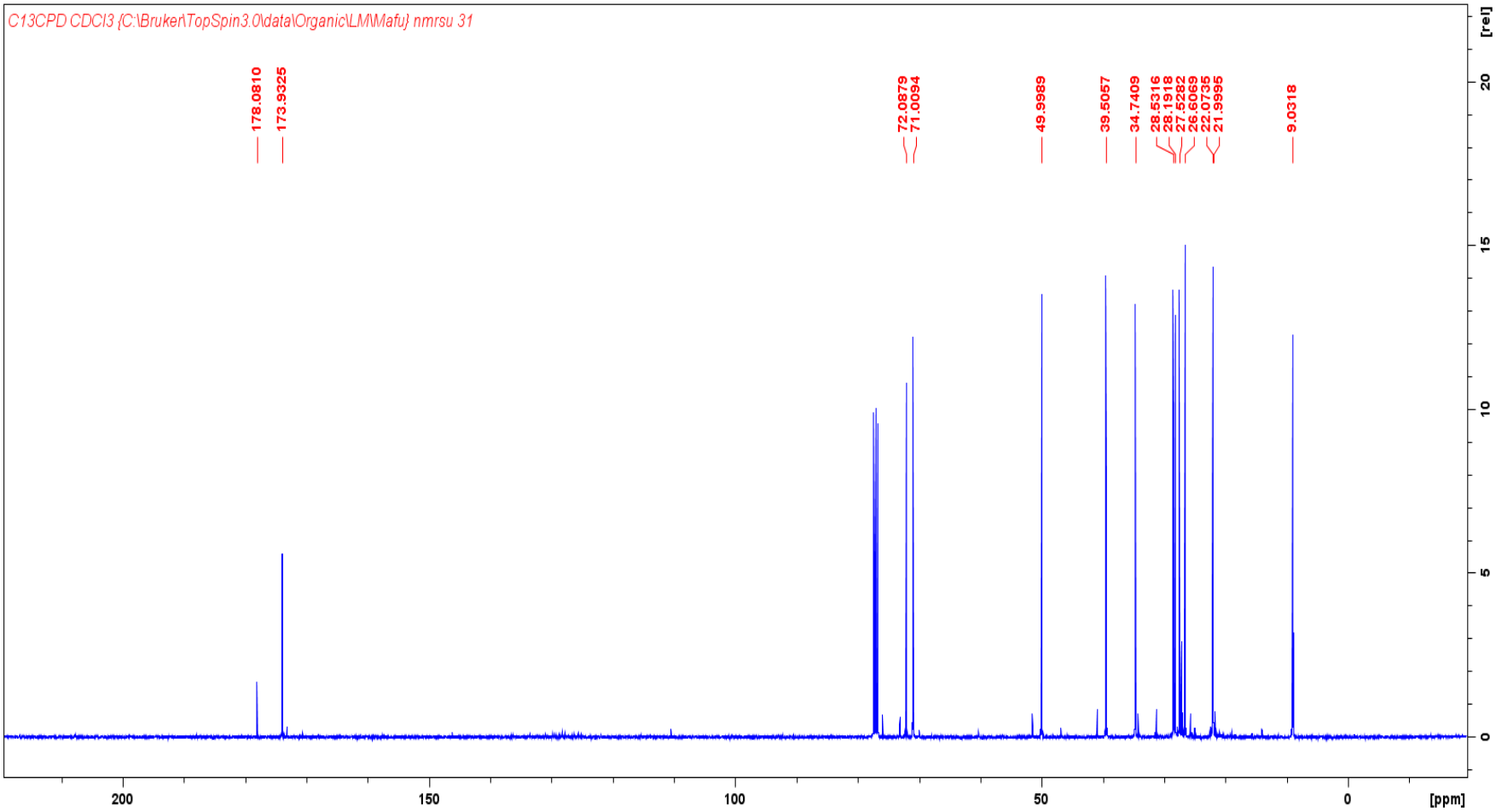

^{13}C-NMR spectrum Mono-propionate

4.4. Di-propionate

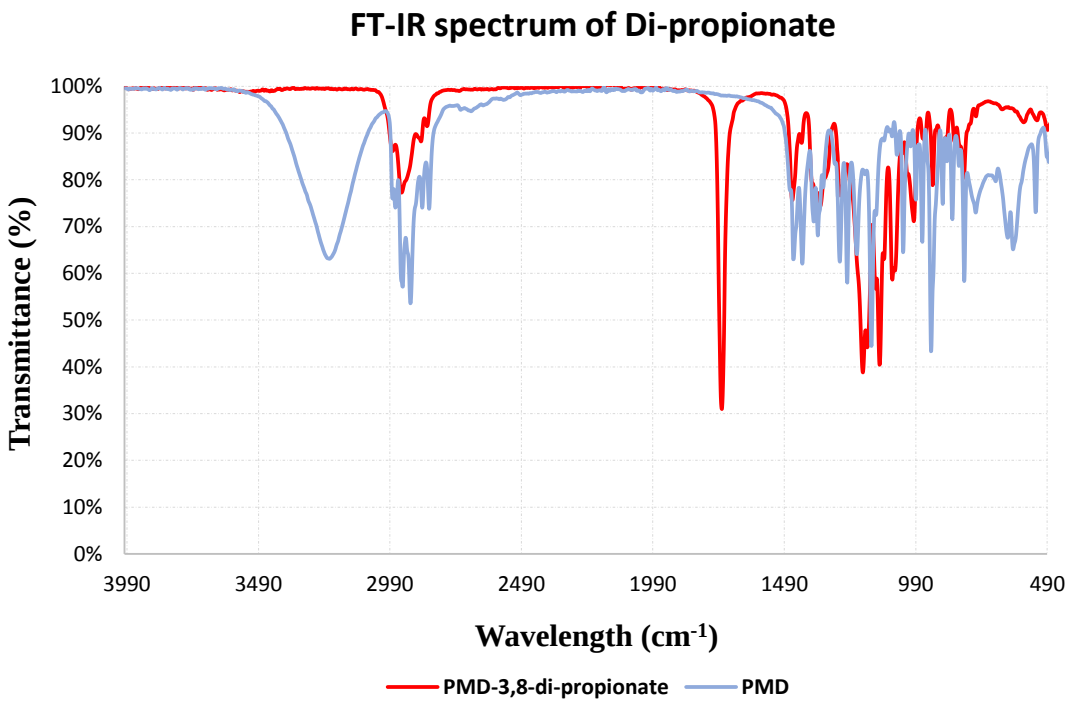

FT-IR spectrum for Di-propionate

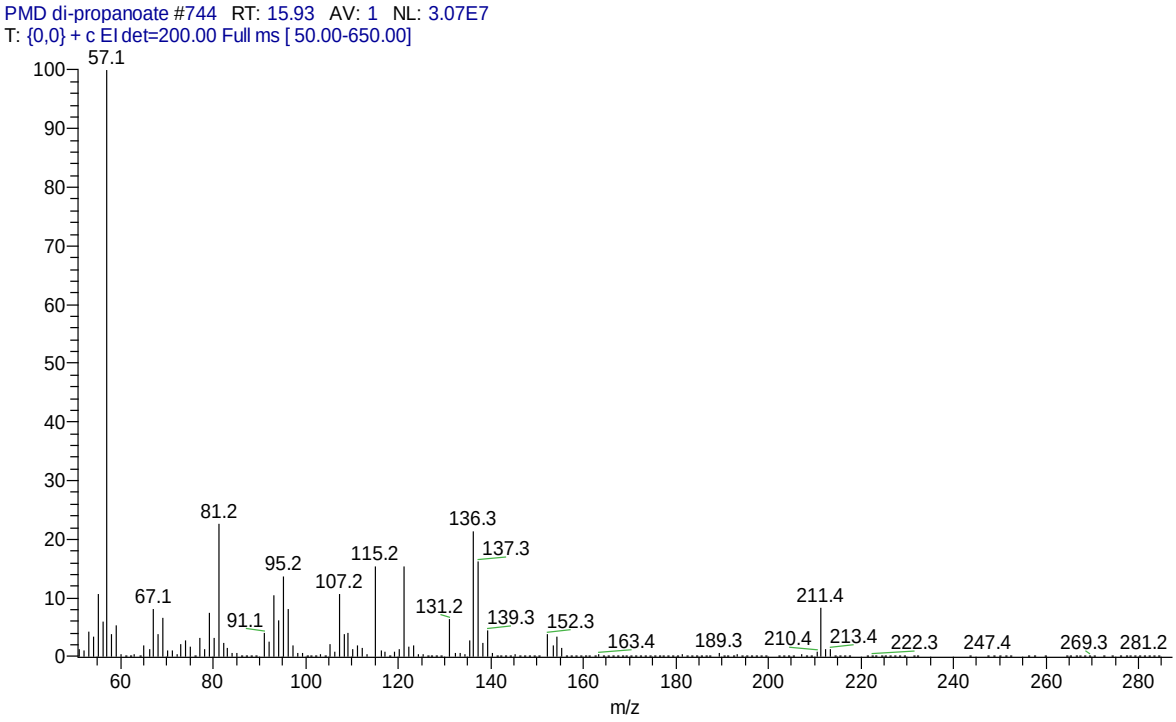

FT-IR spectrum for Di-propionate

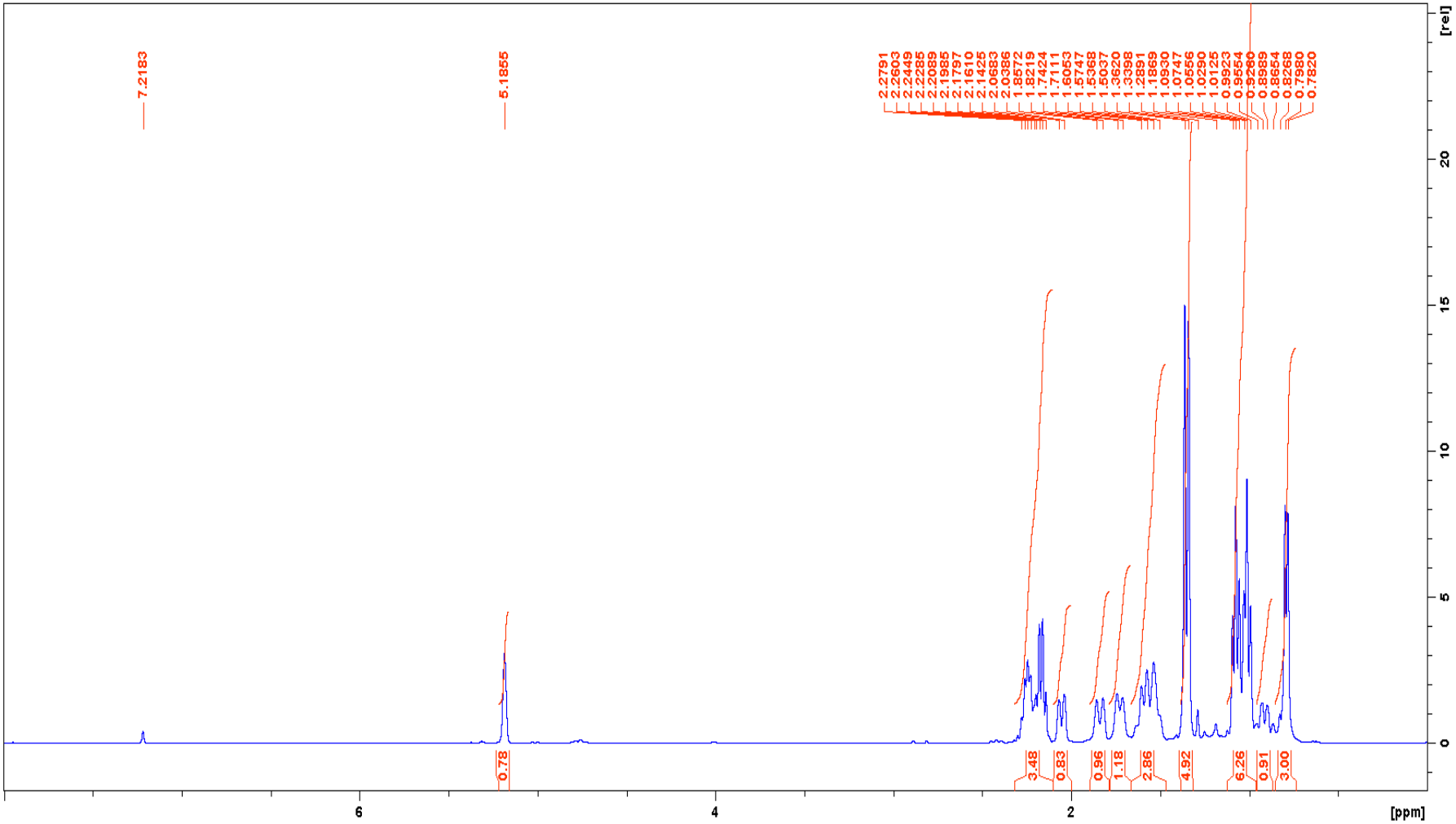

[1]H-NMR spectrum for Di-propionate

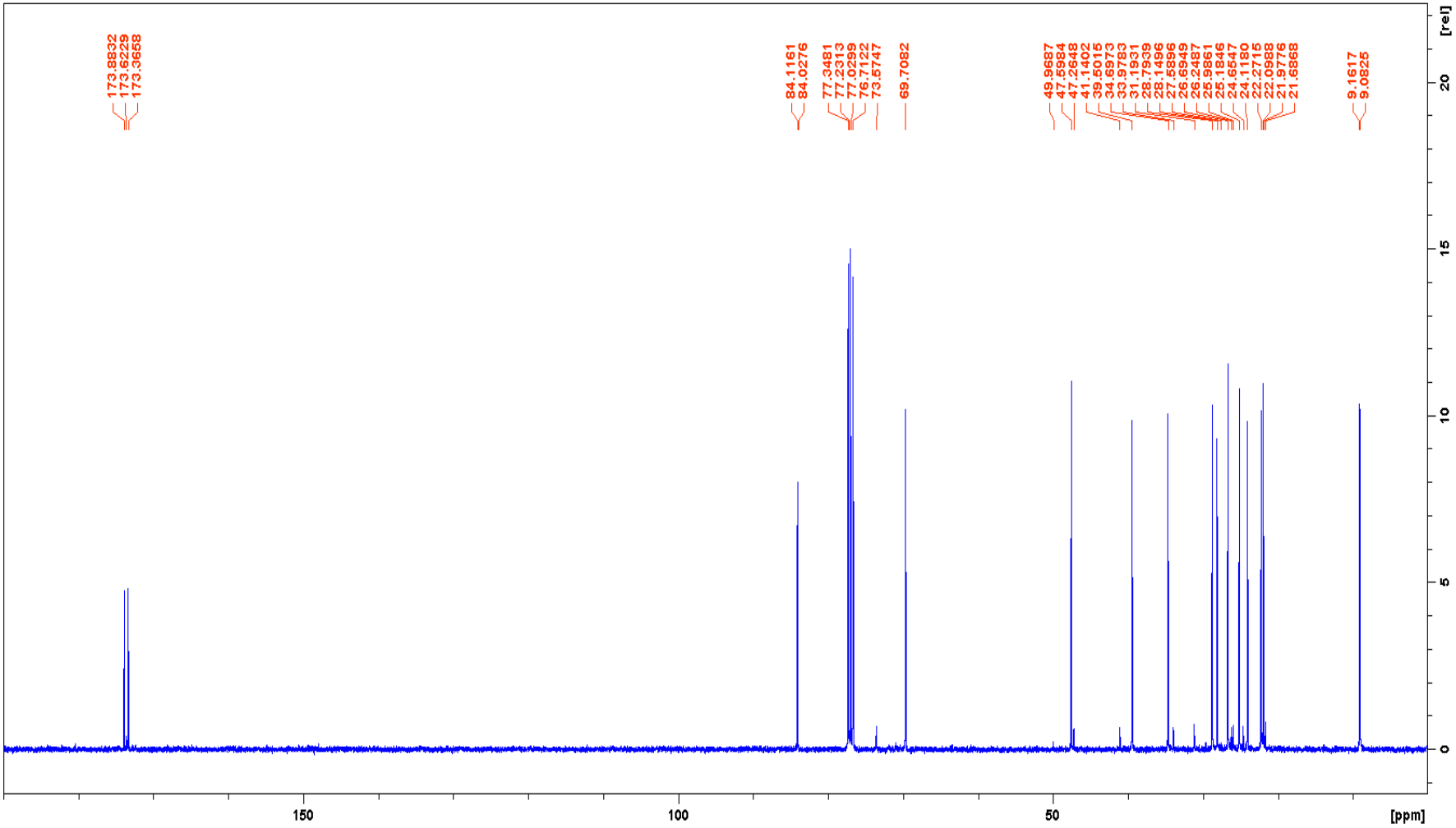

^{13}C-NMR spectrum for Di-propionate

4.5. Mono-pentanoate

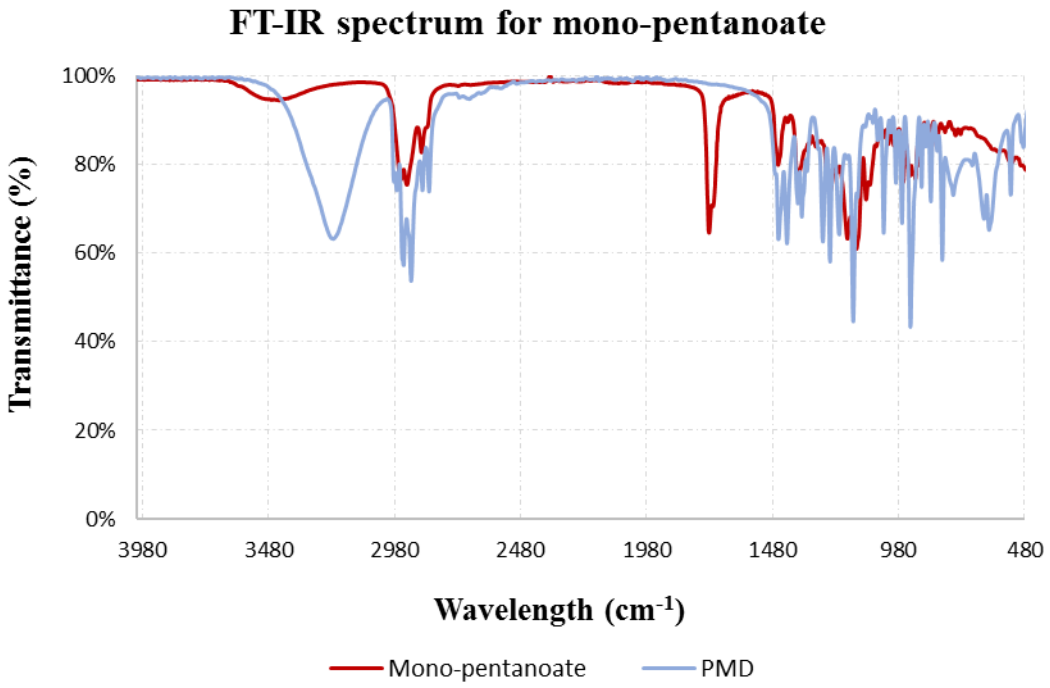

FT-IR spectrum of Mono-pentanoate

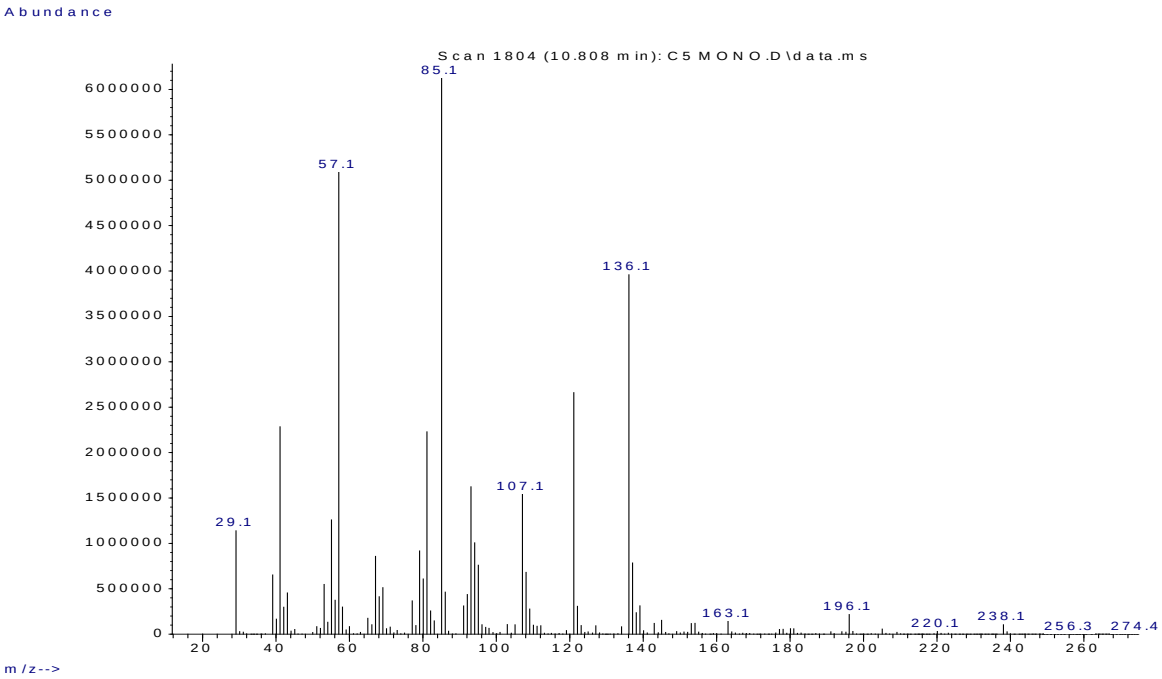

GC-MS spectrum of Mono-pentanoate

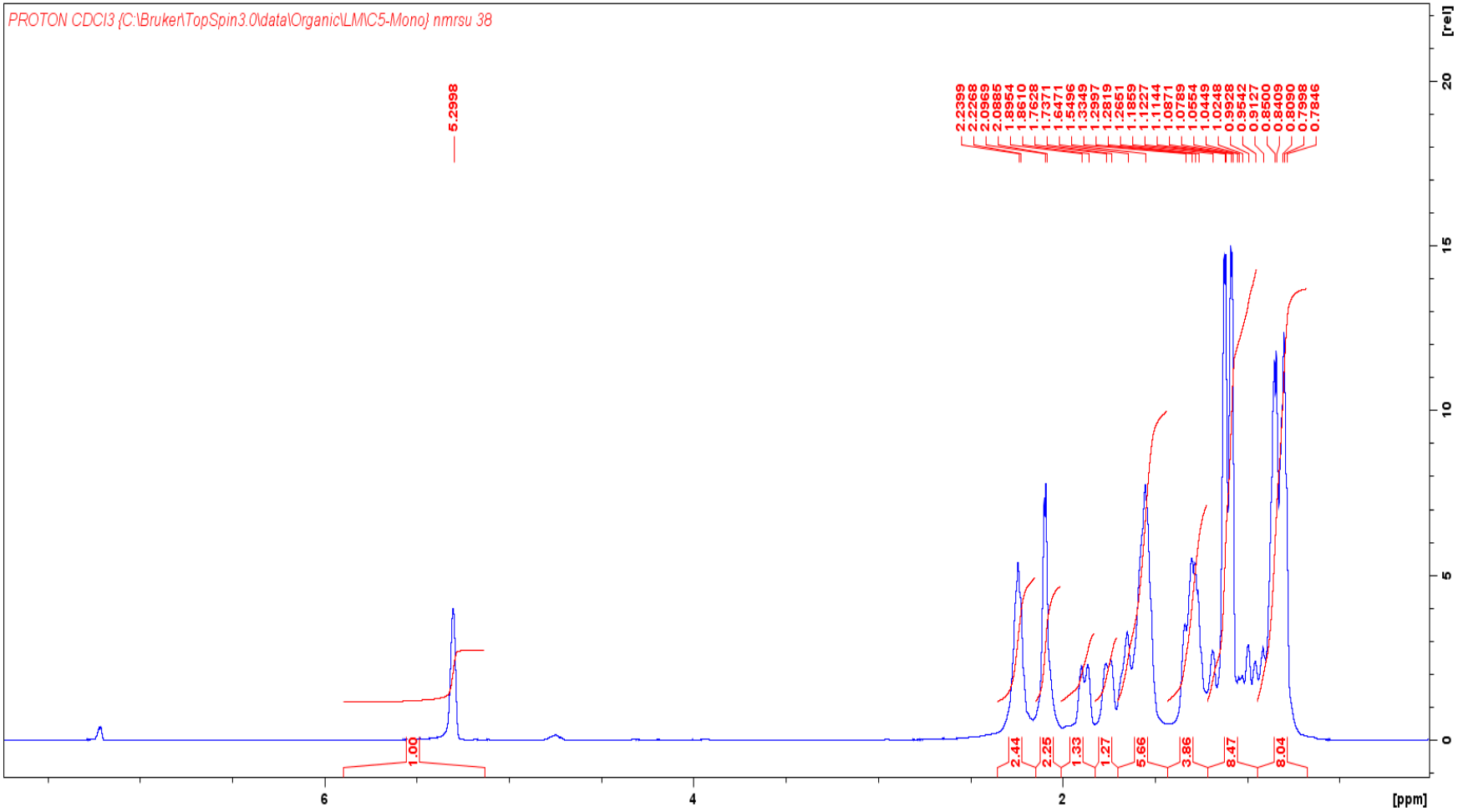

^{1}H-NMR spectrum of Mono-pentanoate

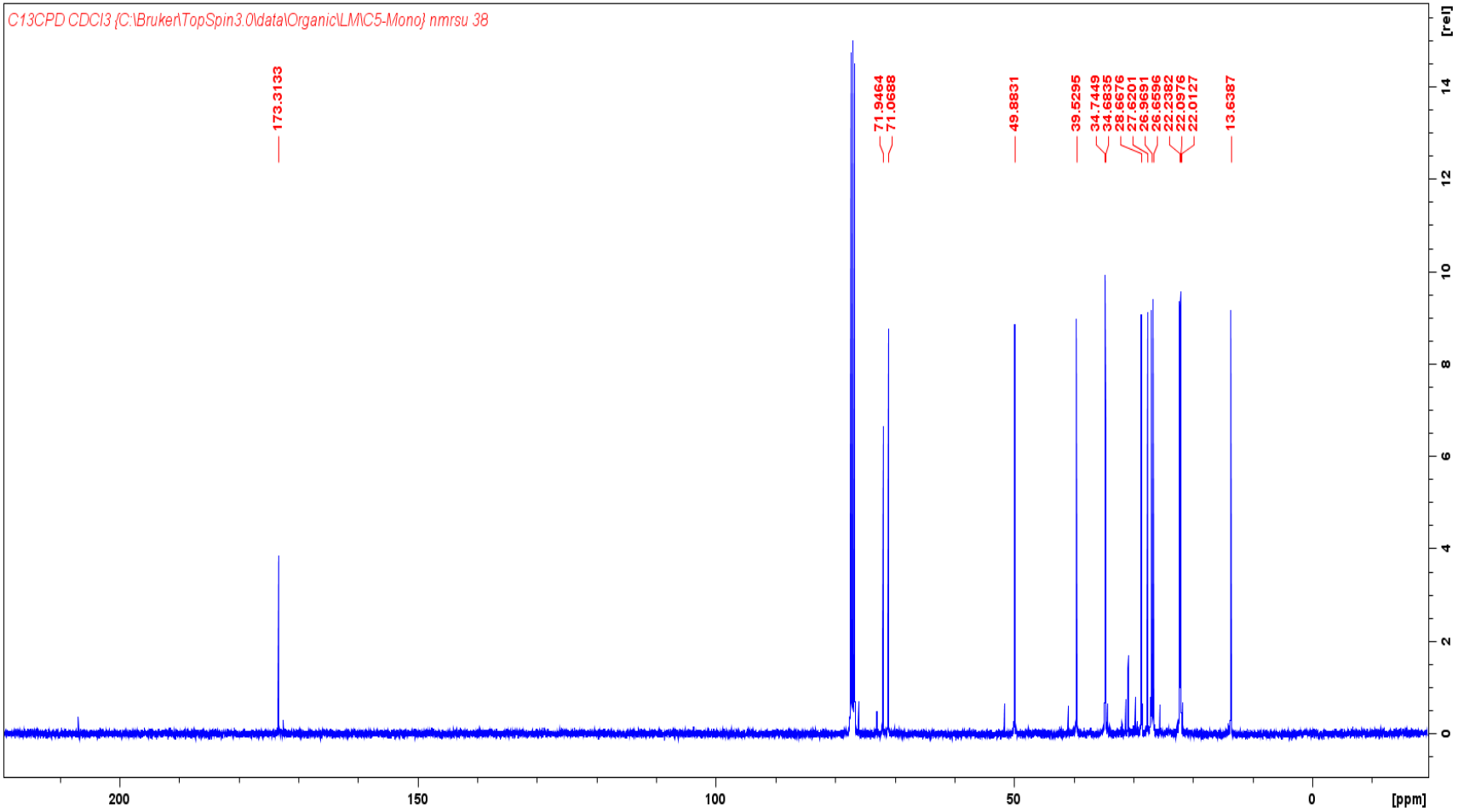

^{13}C-NMR spectrum of Mono-pentanoate

4.6. Di-pentanoate

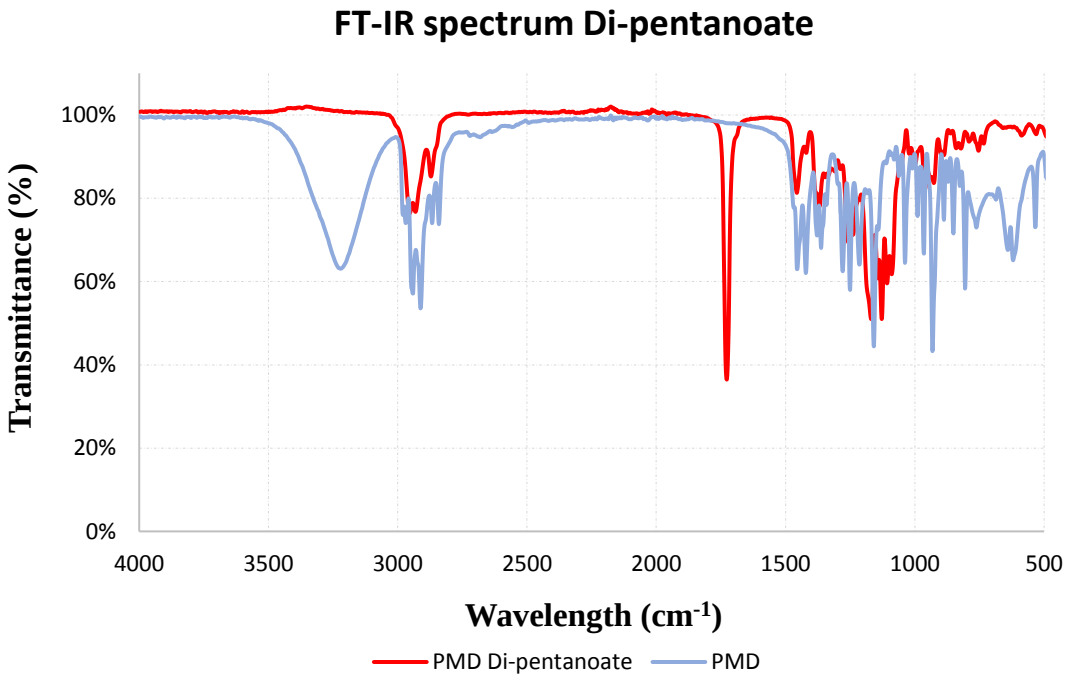

FT-IR spectrum of Di-pentanoate

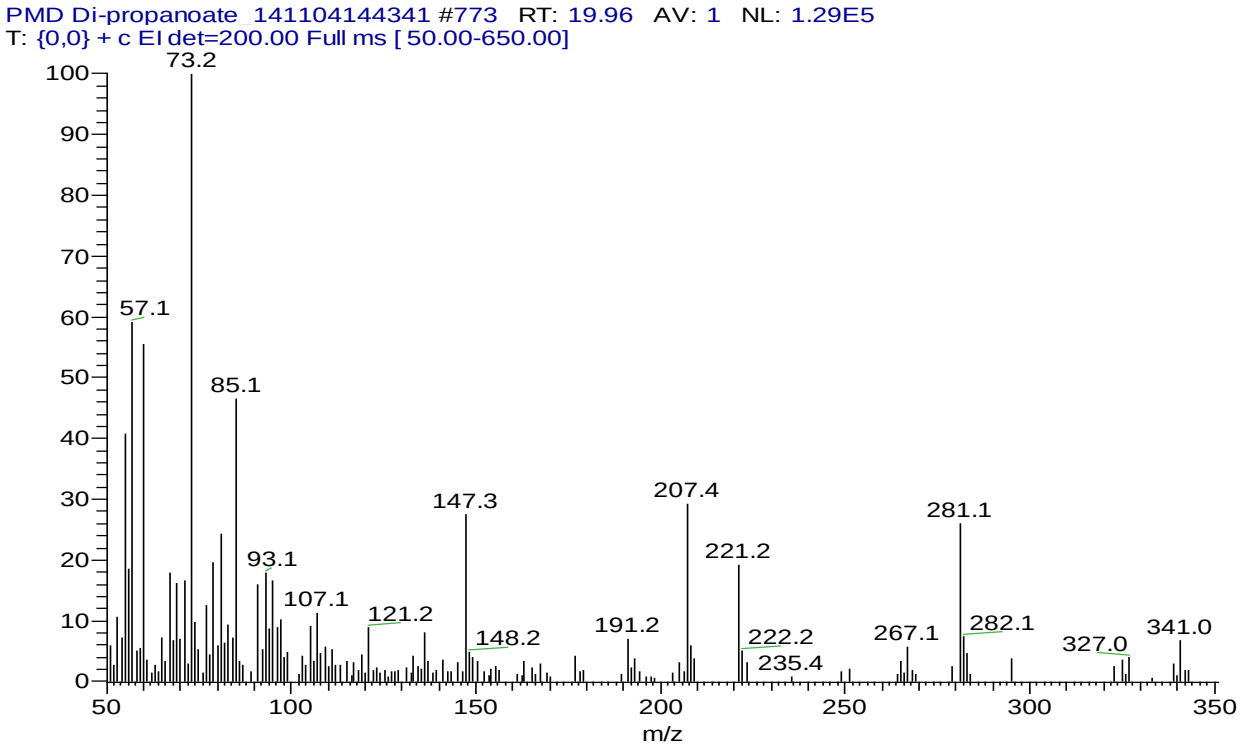

FT-IR spectrum of Di-pentanoate

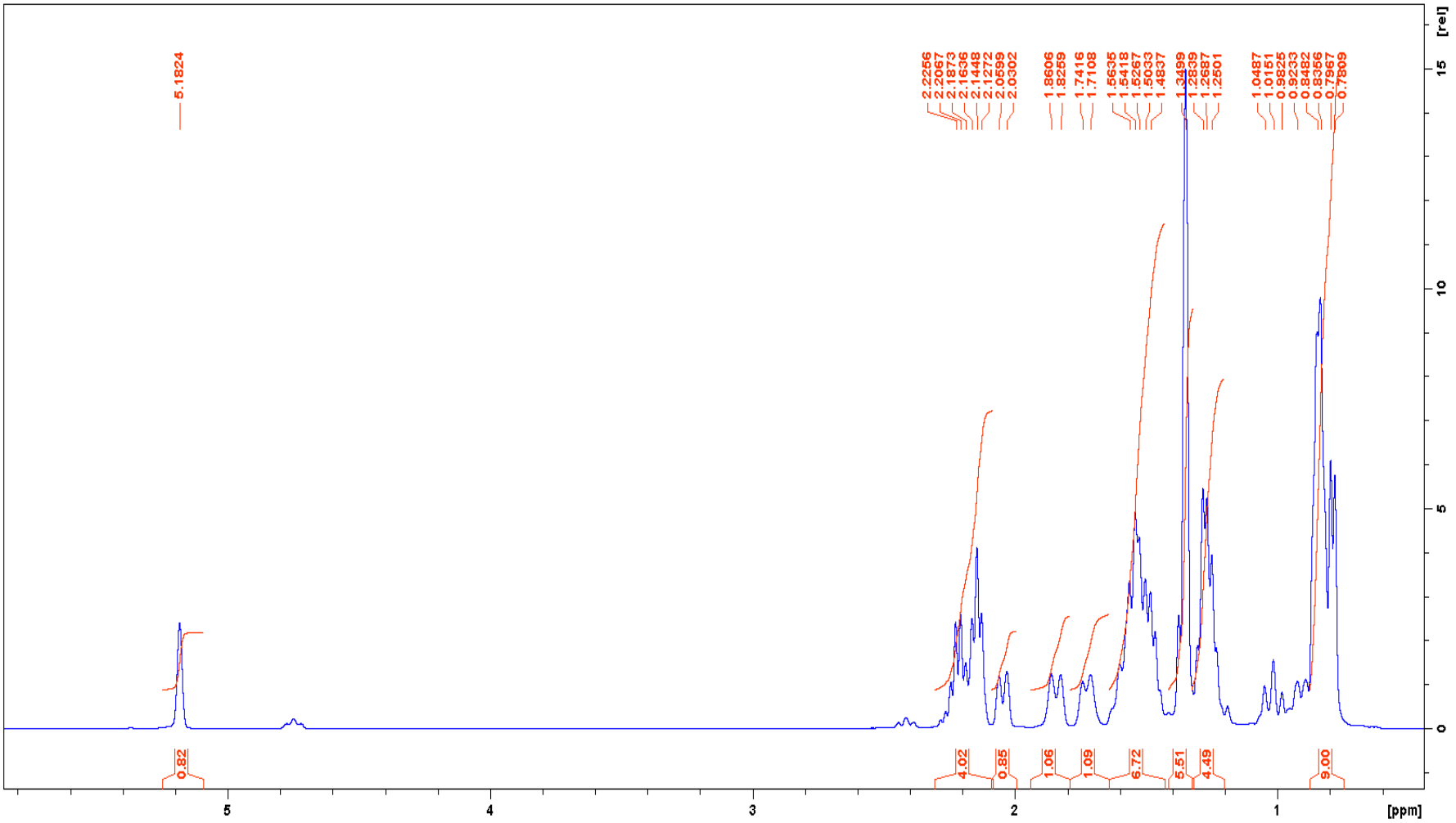

^{1}H-NMR spectrum of Di-pentanoate

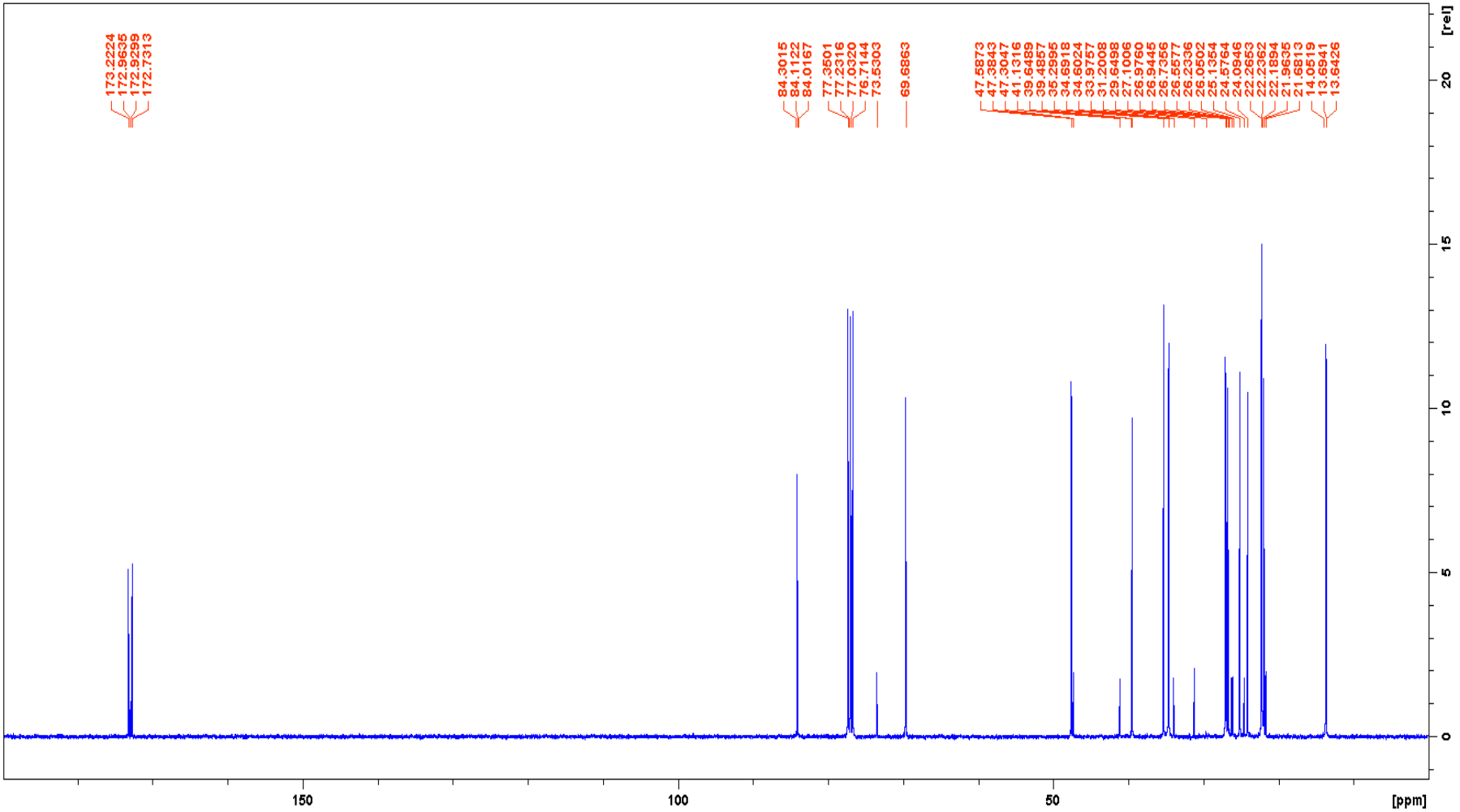

^{13}C-NMR spectrum of Di-pentanoate

4.7. Mono-hexanoate

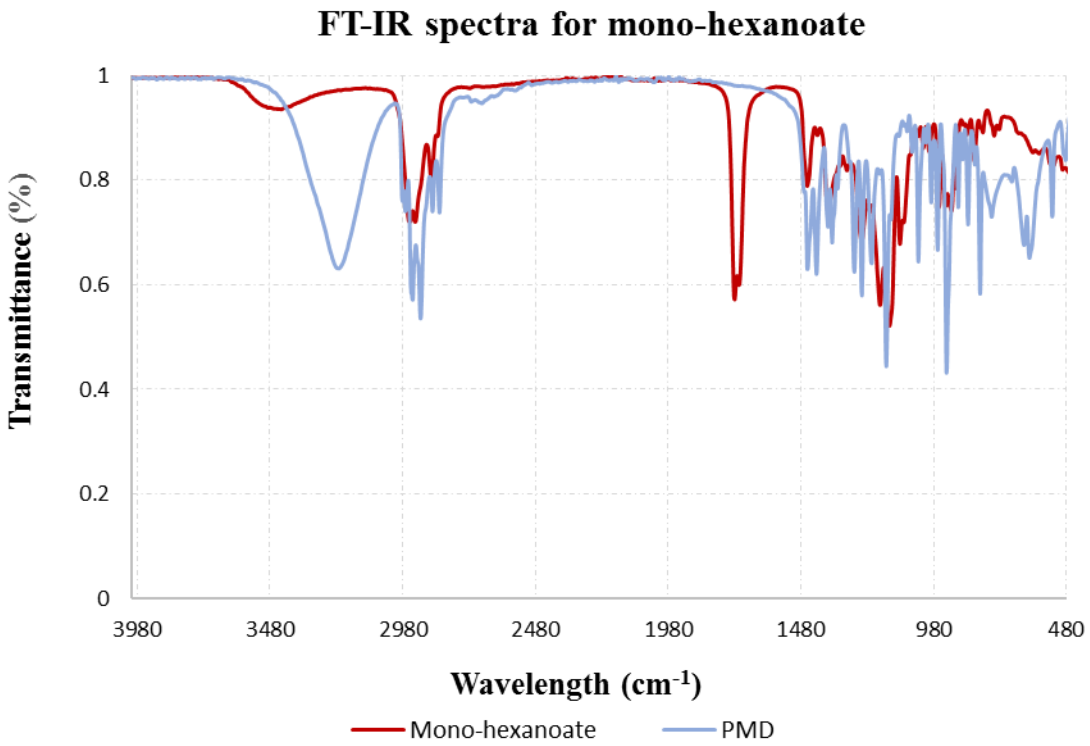

FT-IR spectrum for Mono-hexanoate

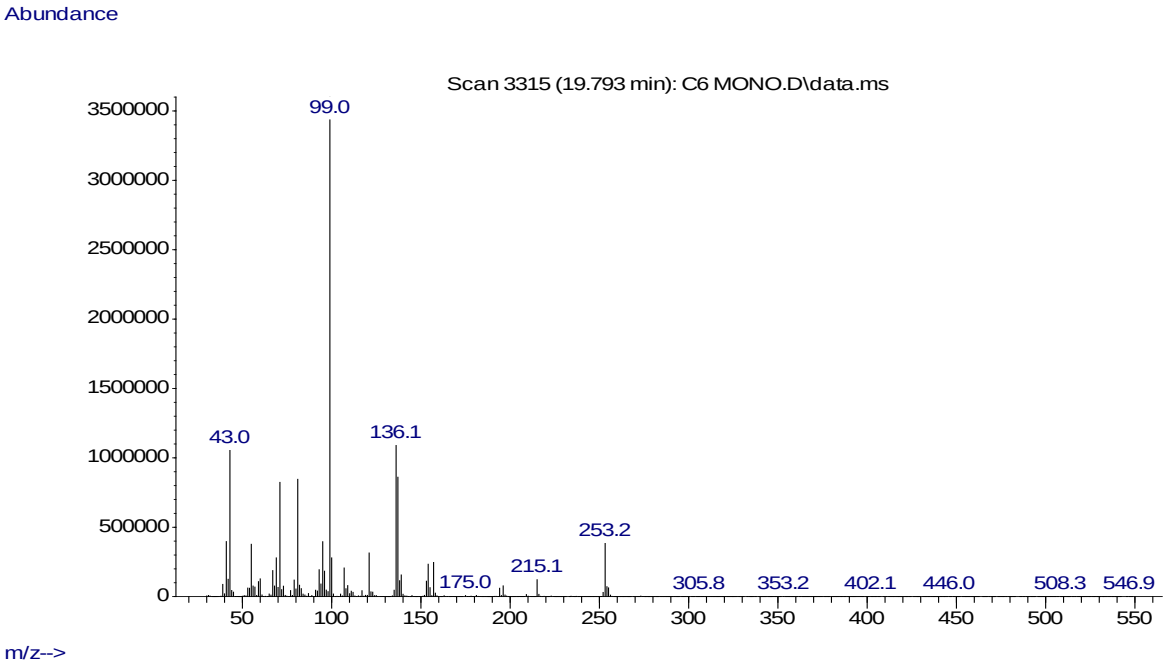

GC-MS spectrum for Mono-hexanoate

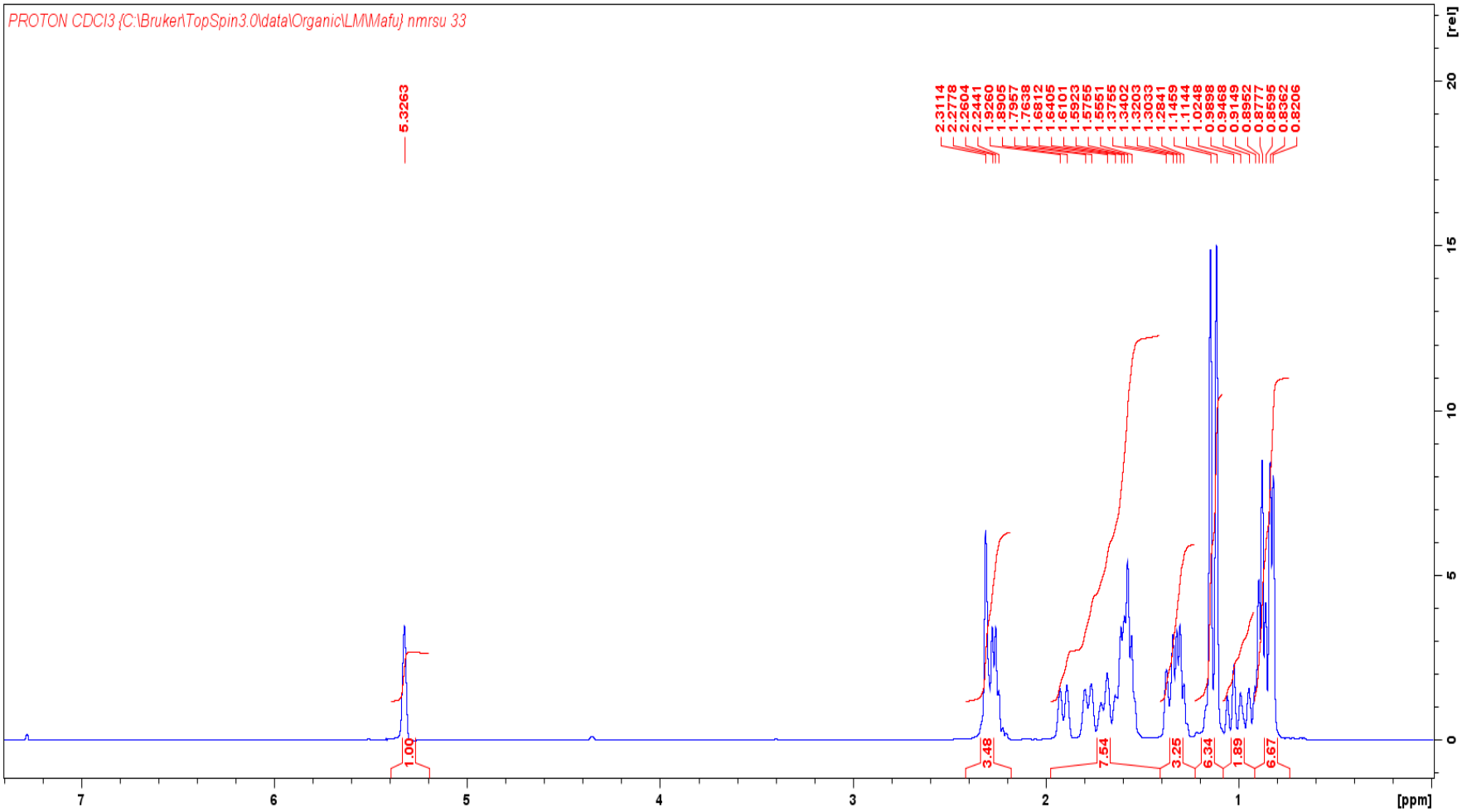

^{1}H-NMR spectrum for Mono-hexanoate

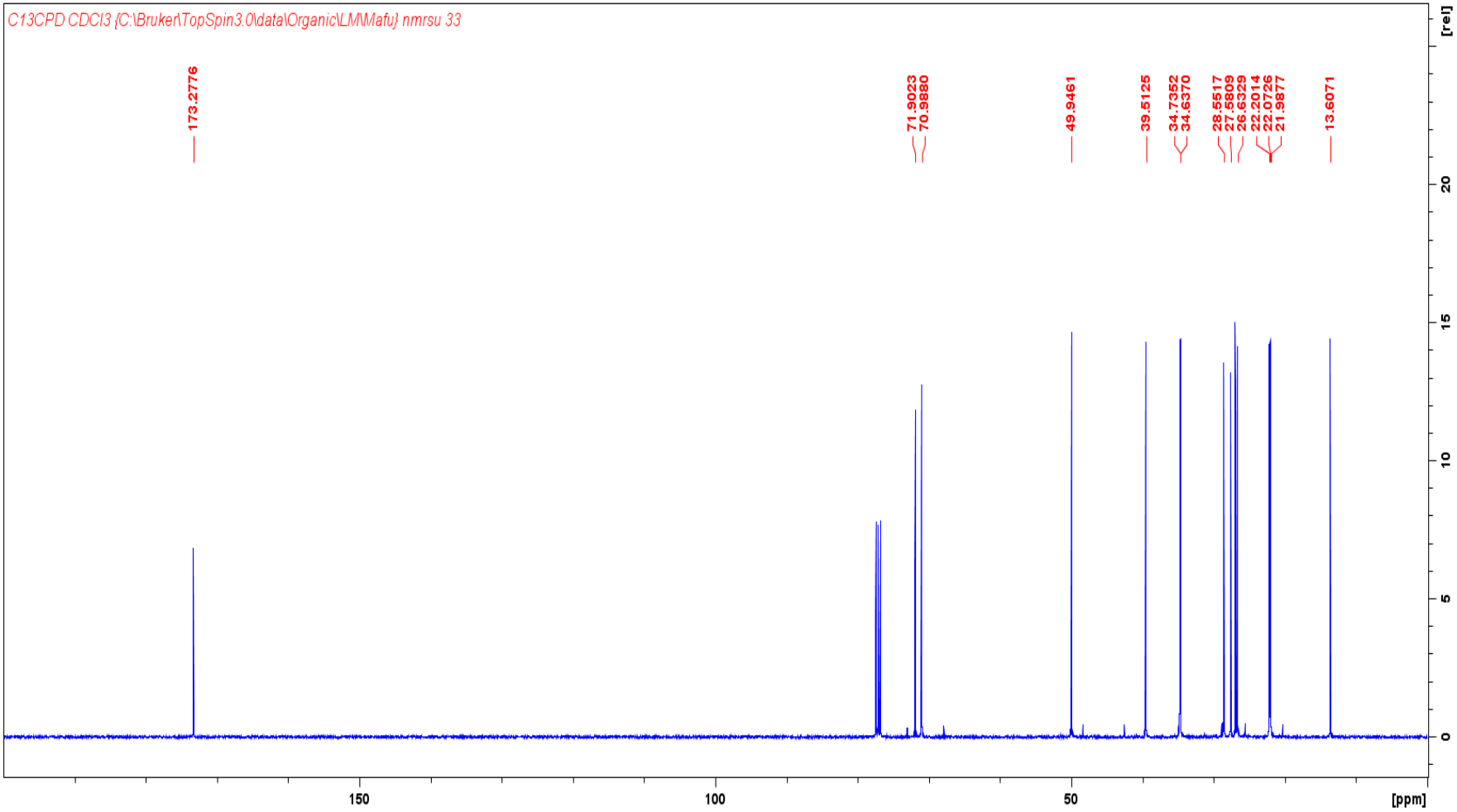

^{13}C-NMR spectrum for Mono-hexanoate

4.8. Di-hexanoate

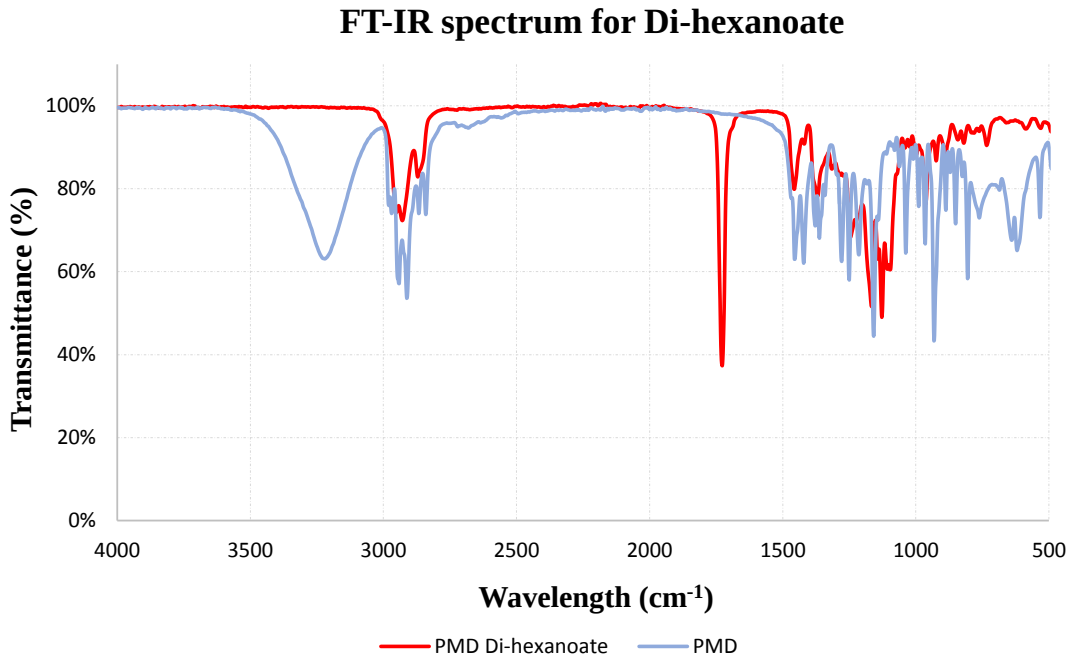

FT-IR spectrum for Di-hexanoate

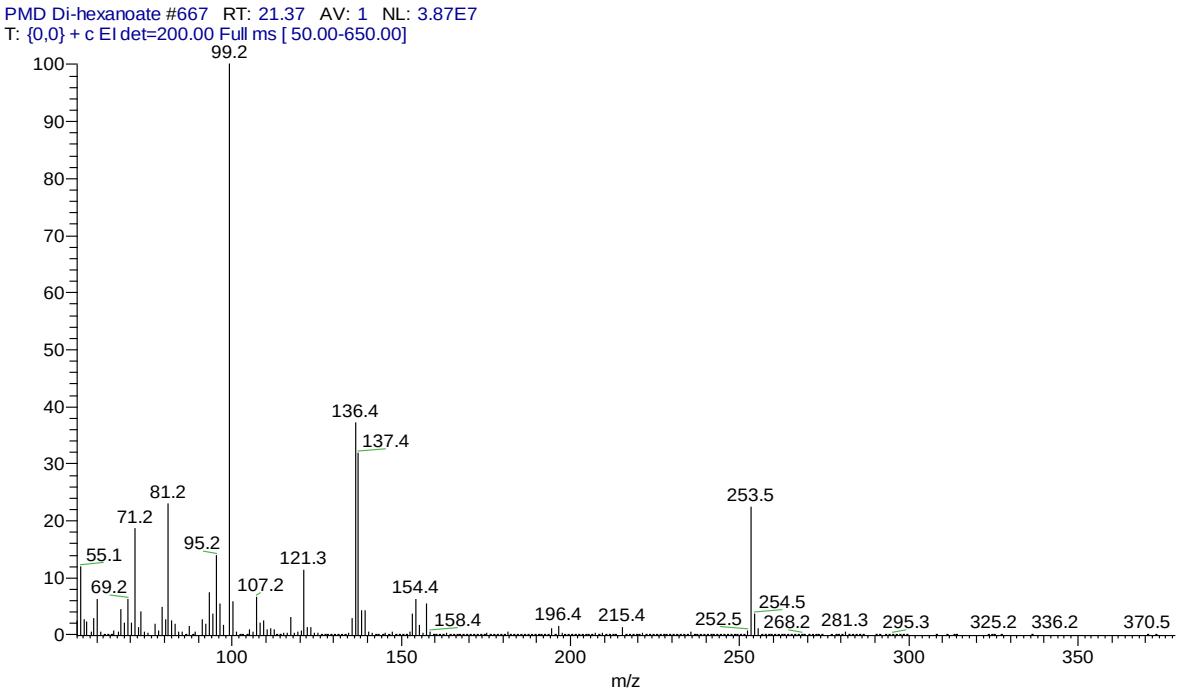

GC-MS spectrum for Di-hexanoate

4.9. Di-hexanoate

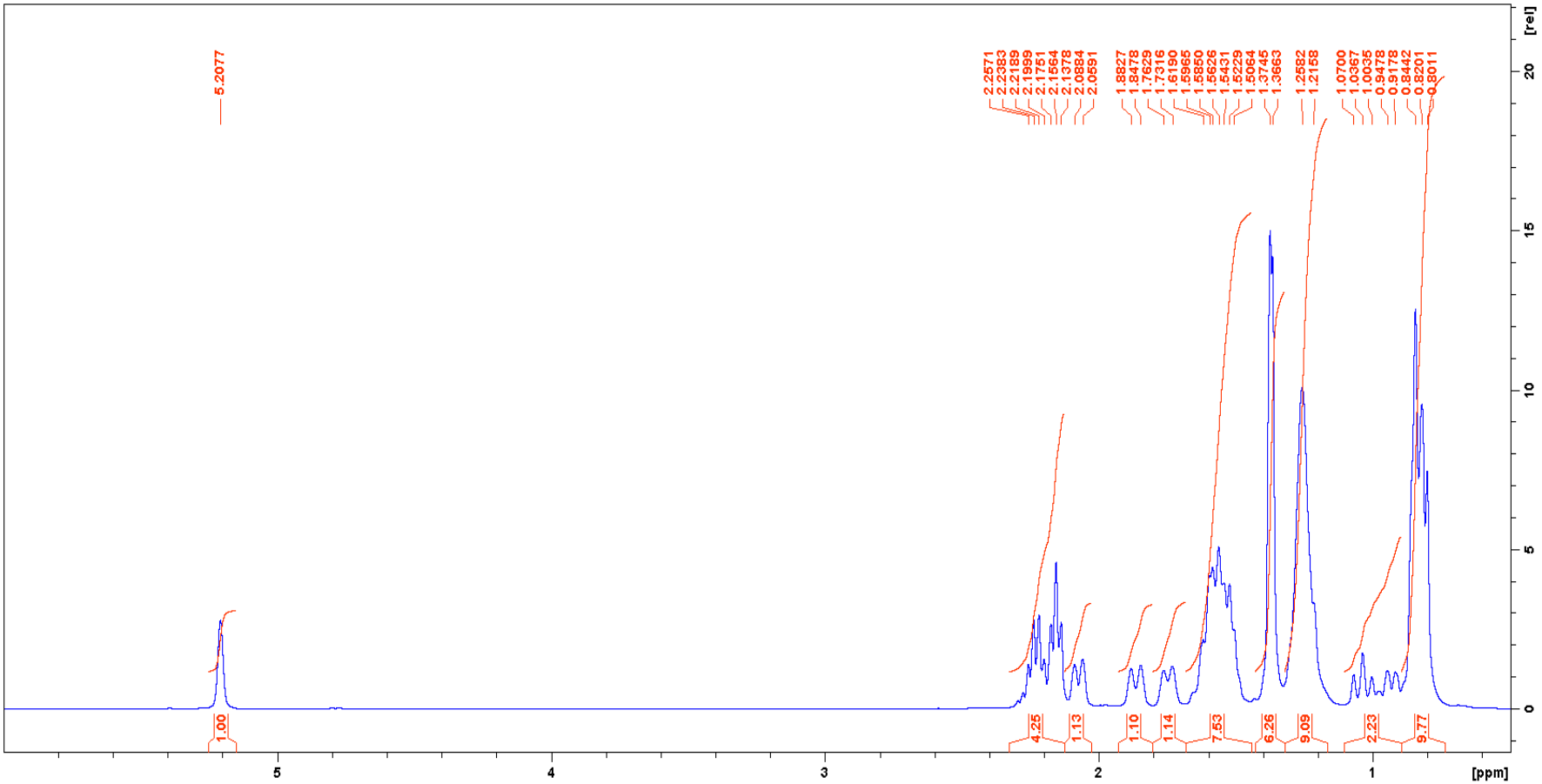

^{1}H-NMR spectrum for Di-hexanoate

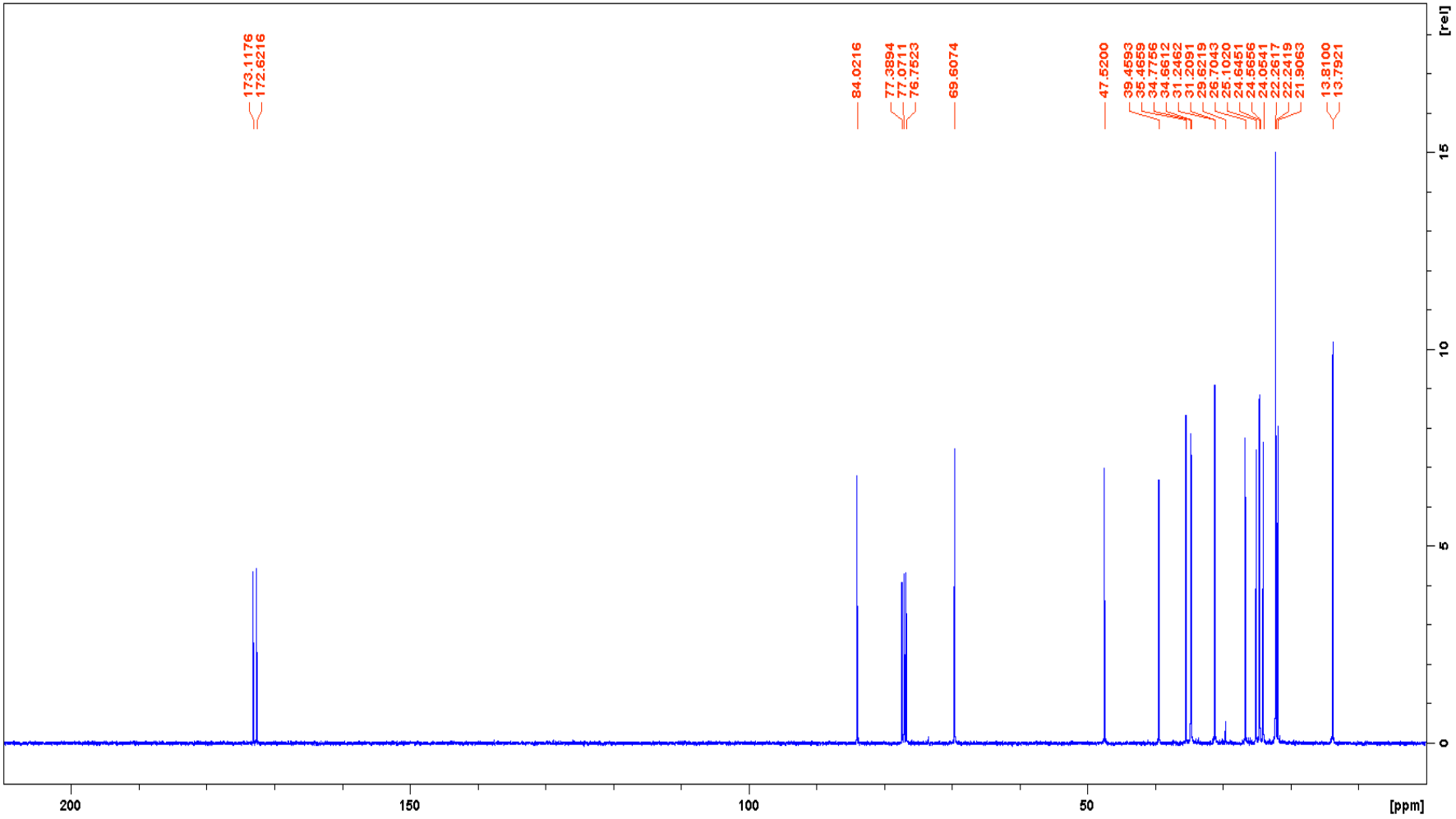

^{13}C-NMR spectrum for Di-hexanoate

Appendix C:

5. Physical properties of *para*-menthane-3,8-esters

Table 2.5: Physical properties of *p*-Menthane-3,8-ester derivatives

Properties	54	50	55	51	56	52	57	53
Molecular formula	$C_{12}H_{22}O_3$	$C_{14}H_{24}O_4$	$C_{13}H_{24}O_3$	$C_{16}H_{28}O_4$	$C_{15}H_{28}O_3$	$C_{18}H_{36}O_4$	$C_{16}H_{30}O_3$	$C_{20}H_{40}O_4$
Molecular Mass (g/mol)	214.30	256.17	228.33	284.4	256.38	340.26	270.41	368.55
Density @20 ^{0}C g/cm^3	0.9761	1.0018	0.9795	1.0034	0.9803	1.052	0.9845	1.091
Viscosity @ 20 ^{0}C mm^2/s	110.2	134.3	112.1	135.3	115.4	137.1	117.2	139.2
Boiling point (^{0}C) @ 760 mmHg	275	288	282	319	290	363	297	395
Flash point (^{0}C)	115.3	122.1	118.4	129.1	121.9	147.2	125.6	150.1
Physical state	Oily	Oily	Oily	Oily	Oily	Oily	Oily	Oily
Colour	Colourless	Colourless	Colourless	colourless	Colourless	colourless	Colourless	Colourless
Polar solvent	Partial soluble	Insoluble	Partial soluble	Insoluble	Partial soluble	Insoluble	Partial soluble	Insoluble
Non-polar solvent	Partial soluble	Soluble	Partial soluble	Soluble	Partial soluble	Soluble	Partial soluble	Soluble